MONASH University

Photoresponsive Self-Assembled Nanomaterials for On-Demand Drug Delivery

A thesis submitted for the degree of
DOCTOR OF PHILOSOPHY in Pharmacy
from the
Monash Institute of Pharmaceutical Sciences
Monash University

by

Wye Khay Fong

B. Form Sci (Hons)

March 2013

Drug Delivery, Disposition and Dynamics
Monash Institute of Pharmaceutical Sciences
Monash University (Parkville Campus)
381 Royal Parade, Parkville
Victoria, 3052, Australia

For my parents, Chee Weng and Lee Kim Fong

Table of contents

Abstract

On-demand drug delivery systems have the potential to optimise drug delivery by allowing drug administration as required. Lipid-based liquid crystalline matrices (LC) are increasingly explored as a means of controlled release drug delivery due to their biocompatibility and ability to incorporate and control the release drugs of a wide ranging size and polarity. The rate at which drug is released is ultimately determined by the mesophase nanostructure. This inbuilt 'on-off' switch for drug release affords the opportunity to manipulate drug delivery by influencing lipid packing by e.g. changing temperature. The utilisation of advanced synchrotron SAXS has allowed for the understanding of mechanisms by which transformations between lipid self-assembled structures take place. Understanding these interactions is essential in the development of self-assembled matrices for many bioapplications.

Light-activated drug delivery systems have potential to provide a selective and non-invasive approach to accessing tissues that are not amenable to direct treatment. This thesis presents LC matrices which have been rendered light responsive by incorporation of additives that alter lipid packing upon irradiation and the effect of manipulating nanostructure on the release of drug from these matrices. Two approaches have been taken:

1. **Photothermal**

Gold nanorods were incorporated into LC matrices and irradiation with near infrared laser light induced reversible thermotropic phase transitions via a photothermal effect.

2. **Photochromic**

Photochromic compounds that undergo isomerisation in response to irradiation were incorporated into liquid crystalline systems where UV light induced a steric disturbance in the liquid crystalline nanostructure.

The potential of these optically addressable nanostructures as reversible 'on-demand' drug delivery systems will translate into novel treatments for diseases such as macular degeneration.

Declaration of Authorship

In accordance with Monash University Doctorate Regulation 17/ Doctor of Philosophy and Master of Philosophy (MPhil) regulations the following declarations are made:

I hereby declare that this thesis contains no material which has been accepted for the award of any other degree or diploma at any university or equivalent institution and that, to the best of my knowledge and belief, this thesis contains no material previously published or written by another person, except where due reference is made in the text of the thesis.

This thesis includes text and figures from 3 original papers published in peer reviewed journals and 3 unpublished publications. The inclusion of co-authors in the published papers reflects the fact that this work came from active collaborations. I have renumbered sections of submitted or published papers in order to generate a consistent presentation within the thesis.

The core theme of the thesis is photo responsive matrices for on-demand drug delivery. The ideas, development and authorship of all the papers in the thesis were the principal responsibility of myself, the candidate, working within the Monash Institute of Pharmaceutical Sciences under the supervision of Ben J. Boyd.

Wye Khay Fong

March 2013

Copyright Notices

Publications

First Author

1. Fong W-K, Hanley T, Boyd BJ. Stimuli responsive liquid crystals provide 'on-demand' drug delivery in vitro and in vivo. J Contr Release 2009; 135(3):218-26.
2. Fong W-K, Hanley TL, Thierry B, Kirby N, Boyd BJ. Plasmonic Nanorods Provide Reversible Control over Nanostructure of Self-Assembled Drug Delivery Materials. Langmuir 2010; 26(9):6136-9.
3. Fong W-K, Malic N, Evans R, Hawley A, Boyd B, Hanley T. Alkylation of Spiropyran Moiety Provides Reversible Photo-Control over Nanostructured Soft Materials. Biointerphases 2012; 7(1):1-5.

Second Author

1. Phan S, Fong W-K, Kirby N, Hanley T, Boyd BJ. Evaluating the link between self-assembled mesophase structure and drug release. Int J Pharm 2011; 421(1):176-82.
2. Tangso KJ, Fong W-K, Darwish T, Kirby N, Boyd BJ, Hanley T. Novel Spiropyran Derivatives and their Application as Light Responsive Liquid Crystalline Components Soft Matter. 2013; Submitted.

Manuscripts in Preparation

1. Fong W-K, Hanley TL, Thierry B, Kirby N, Waddington LJ, Boyd BJ. Nanostructure switching in liquid crystalline hybrid nanomaterials by laser irradiation. Journal Article. Intended for submission to Soft Matter.
2. Fong W-K, Hanley TL, & Boyd BJ. Liquid crystalline nanostructure manipulation by the addition of selected lipids. Journal Article. Intended for submission to Langmuir.
3. Fong W-K, Hanley TL, & Boyd BJ. Rich polymorphism in biological tissue as revealed by SAXS. Journal communication. Intended for submission to Soft Matter.

Communications

1. Fong W.-K., Hanley T.L. & Boyd B.J.; 2009; Photoresponsive additives in lyotropic liquid crystals; abstract in the 16th AINSE Conference on Nuclear and Complementary Techniques of Analysis; Lucas Heights; November 2009. Oral presentation p. 14.
2. Fong W.-K., Hanley T.L., Thierry B., Kirby N., Boyd B.J.; (2010) Lyotropic Liquid Crystals Responsive to Light Stimuli; abstract in the 27th Australian Colloid & Surface Science Student Conference. Poster presentation P15.
3. Fong W.-K., Hanley T.L., Thierry B., Kirby N., Boyd B.J.; (2010) Using Gold Nanorods as a Switch for Photo-Responsive Lyotropic Liquid Crystal Drug Delivery Systems; poster abstract in FIP PSWC/AAPS Annual Meeting & Exposition and the PSWC 2010 Congress for Students and Postdoctoral Fellows.
4. Fong W.-K., Hanley T.L., Boyd B.J.; (2010) Light Responsive Nanostructured Matrices for Pulsatile Drug Delivery; poster abstract in the 4th Annual Meeting of the Australian Chapter of the Controlled Release Society.

5. Fong W.-K., Hanley T.L., Boyd B.J.; (2010) Light Responsive Nanostructured Matrices for Pulsatile Drug Delivery; oral abstract in the 9th AINSE / ANBUG Neutron Scattering Symposium. Oral Presentation p. 17.
6. Fong, WK; Hanley TL; Boyd, BJ. (2011) Light Responsive Nanostructured Matrices for Pulsatile Drug Delivery; oral abstract in the 5th Biennial Australian Colloid & Interface Symposium. Oral presentation number: OC314
7. Fong, WK; Hanley TL; Boyd, BJ. (2011) Light Responsive Nanostructured Matrices for Pulsatile Drug Delivery: Photochromics. Poster abstract in the 38th Annual Meeting and Exposition of the Controlled Release Society. Poster number: 223
8. Fong W.-K., Hanley T.L., Thierry B., Kirby N., Boyd B.J.; (2012) Light Responsive Liquid Crystalline Nanostructures as Externally Triggerable Drug Delivery Systems. Oral abstract in the 28th Australian Colloid and Surface Science Student Conference. Oral Presentation number O17.
9. Fong W.-K., Hanley T.L., Thierry B., Kirby N., Boyd B.J.; (2012) Light Responsive Liquid Crystalline Nanostructures as On-Demand Drug Delivery Systems. Oral abstract in the International Small Angle Scattering Conference SAS2012. Oral presentation number: C1.2.
10. W.-K. Fong, T.L. Hanley, K. J. Tangso, N. Malic, R.A. Evans, N. Kirby, B. Graham & B.J. Boyd (2012) Light Responsive Liquid Crystalline Nanostructures as On-Demand Drug Delivery Systems. Poster abstract in Drug Delivery Australia 2012. Poster number: P21.

Acknowledgements

Firstly, to my advisors:

Ben J. Boyd – for the freedom to run riot with our ideas, for the encouragement, discussions and the teaching;

Tracey Hanley – for the on-call consultations and your boundless expertise at the synchrotron & ANSTO.

To our collaborators:

Nigel Kirby, Adrian Hawley and Steven Mudie (SAXS/WAXS, Australian Synchrotron) – for being on call at all hours of the day and night during our beamtimes,

Benjamin Thierry (UniSA) – for the synthesis of gold nanorods,

Richard Evans and Nino Malic (CSIRO) – for the synthesis of the spiropyran laurate derivative,

Bim Graham and Jose Selano (MIPS) – for the synthesis of the upconverting nanoparticles

Tamim Darwish (ANSTO) – for the NMR assistance and synthesis of other spiropyran derivatives

Lyn Waterhouse (Adelaide Microscopy) – for assistance with cryoFESEM

The Australian Postgraduate Award and AINSE PGRA are acknowledged for financial support.

To my colleagues at MIPS:

The Boyd group past and present: Kristian, Josie, Adam, Charlie, Stephs Phan and Parker, Xav, Jason, Aurelia, Kathy, Tri, Scott (now PE-DSC specialist) & Danielle – thanks for the teaching and the learning, the shared pain and most of all, your friendship.

The members of the Pharmaceutics department and everyone involved with the Parkville Postgraduate Association. Thanks for the laughs.

To my family and friends: Chun, Theng and my Glennies. Thanks for putting up with my “Khay-nalities”.

And finally, to Sarah who captured my imagination, thank you for being my muse.

List of Abbreviations

AMD	Age-related macular degeneration
AZO	Azobenzene
CA	Cinnamic Acid
Ch	Cholesterol
$CHCl_3$	Chloroform
CNV	Choroidal neovascularisation
CPLM	Cross Polarised Light Microscopy
CPP	Critical packing parameter
cryoFESEM	Cryogenic Field Emission Scanning Electron Microscopy
cryoTEM	Cryogenic Transmission Electron Microscopy
CTAB	Cetyltrimethylammonium bromide
DOPC	1,2-dioleoyl-sn-glycero-3-phosphocholine
DOPE	1,2-dioleoyl-sn-glycero-3-phosphoethanolamine
DOPS	Dioleoylphosphatidylserine
DPhPC	1,2-diphytanoyl-sn-glycero-3-phosphocholine
DPhPE	1-Palmitoyl-2-oleoyl-sn-glycero-3-phosphoethanolamine
DSC	Differential Scanning Calorimetry
EMF	Electromagnetic field
EPR	Enhanced permeation and retention
GMO	Glyceryl monooleate
GNP	Gold nanoparticles
GNR	Gold nanorods
GNR660	Gold nanorods with a LSPR of 660 nm
GNR810	Gold nanorods with a LSPR of 810 nm
H_2	Reversed hexagonal phase
HFU	High frequency ultrasound
$k_{app\ 3\text{-}5}$	Apparent absorption rate constant
L_2	Reversed micellar phase
L_3	Sponge phase
LC	Lipid based liquid crystalline materials
LFU	Low frequency ultrasound
LSPR	Local surface plasmon resonance wavelength
LTD	Light-targeted drug delivery
lysoPC	1-oleoyl-2-hydroxy-*sn*-glycero-3-phosphocholine
L_α	Lamellar phase
MC	Merocyanine
ME	Monoelaidin
NIR	Near infrared
OA	Oleic Acid
PBS	Phosphate buffered saline
PDT	Photodynamic therapy

PEG	Polyethylene glycol
PEG-SH	A thiol-terminated polyethylene glycol
PEO	Polyethylene oxide
PHYT	Phytantriol
PHYT-GNR	Hydrated phytantriol + gold nanorod liquid crystalline matrix
POPE	1-palmitoyl-2-oleoyl-*sn*-glycero-3-phosphoethanolamine
RES	Reticuloendothelial system
S.D.	Standard deviation
SA	Selachyl alcohol
SAXS	Small Angle X-Ray Scattering
SEM	Standard error of the mean
SOX	Spirooxazine
SP	Spiropyran/Spirobenzopyran
SPL	Spiropyran laurate
SSAXS	Synchrotron SAXS
Tapp	Apparent Temperature
THF	Tetrahydrofuran
UCNP	Upconverting nanoparticles
UV	Ultraviolet
V_2	Bicontinuous cubic phase
$V_{2\ D}$, $V_{2\ Pn3m}$	Bicontinuous cubic phase with double diamond crystallographic spacing
$V_{2\ G}$, $V_{2\ Ia3d}$	Bicontinuous cubic phase with gyroid crystallographic spacing
$V_{2\ P}$, $V_{2\ Im3m}$	Bicontinuous cubic phase with primitive crystallographic spacing
VitEA	Vitamin E acetate

Chapter 1 – Introduction

1. Introduction

1.1. Declaration for Chapter 1

Most of this introduction has been published as: Boyd BJ, Fong W-K. Stimuli-Responsive Lipid-Based Self-Assembled Systems. In: Garti N, Somasundaran P, Mezzenga R, editors. Self-Assembled Supramolecular Architectures. Surface and Interfacial Chemistry. Hoboken, New Jersey: John Wiley & Sons, Inc.; 2012. p. 257-88.

1.2. A Statement of the Problem

Over the past 30 years, there has been intensive research and development into effective drug delivery systems in order to resolve issues that come hand in hand with pharmaceutical treatments. These issues include systemic toxicity, drug instability and patient compliance. Much of this research has resulted in the evolution of nanomedicines which matches innovative technologies from different scientific disciplines to create drug delivery systems with a practical, well-designed function. These hybrid nanomaterials have the potential to provide a specific, non-invasive approach to pharmaceutical treatments thereby revolutionising the way in which therapies are administered.

Towards this objective, many natural and synthesised matrices have been rendered stimuli responsive through the incorporation of novel materials, including the use of self-assembled systems such as lipid based liquid crystalline materials. These materials have been shown to provide sustained release of actives in food and pharmaceutical applications, where the drug release rate is determined by the nanostructure formed. The dynamic manipulation of the lipid packing in these systems using temperature has been shown to alter drug release rate. However, as the use of temperature as a stimulus has practical issues in real-life applications, a non-invasive means of nanostructure manipulation is envisaged. Light stimuli provide an ideal alternative as it

can be easily applied externally, and certain wavelengths can safely penetrate through biological tissues. Thus, this thesis focuses on the creation of light responsive liquid crystalline matrices for on demand drug delivery.

1.3. The Application and Benefits of Self-assembled Systems in Drug Delivery

The use of self-assembled systems based on lipids and surfactants in drug delivery applications is predicated on three primary features.

1. Enhanced solubilisation: Self-assembly provides an internal hydrophobic environment for enhanced solubilisation of drug molecules that are otherwise poorly water soluble which limits the administrable dose. Emulsions, micelles and liposomes have all been utilised for this purpose in a range of pharmaceutical products already on the market. While micelles have a disadvantage of potential loss of solubilisation capacity on dilution beyond the critical micelle concentration of the surfactant, other self-assembled systems such as emulsions and liposomes do not.

2. Manipulate pharmacokinetic behaviour: Side effects due to drug administration are most often associated with high blood concentrations immediately after administration. Incorporation of drug into a carrier system can slow down the bioavailability of drug, thus reducing side effects without reducing the total dose of drug administered.

3. Targeting drug to particular tissues: The functionalisation of micelles and liposomes has been utilised to direct the carrier to the desired tissue site, either by passive or active targeting. Passive targeting involves surface coverage with polyethylene glycol (PEG) chains to prevent non-specific removal from the circulatory system, leading to preferential deposition in tumour tissues and sites of inflammation. Active targeting involves functionalising the surface of the particle with a tissue specific moiety such as an antibody or antigen, to encourage specific interaction with

diseased tissues that differentially express the complementary entity to the functional group, compared to healthy tissues.

As will be discussed later in this Introduction, there are many types of stimuli that can be introduced into the lipid-based self-assembled matrix in order to induce phase transitions in these systems. However, most studies have revolved around imparting responsiveness into liposomes. Other self-assembled nanostructures, such as non-lamellar liquid crystals, have received much less attention despite the potential for reversibility of structural changes that could permit repeated on-demand administration of drug with a single injection. Such non-lamellar structures are discussed in the next section.

1.3.1. Self-Assembled Nanostructures for Drug Delivery

Self-assembled systems hold promise as stimuli responsive systems as outlined in the earlier sections, where both lipid-based and polymeric systems have potential in such applications. Polymeric materials have been heavily investigated in order to enhance different aspects of drug delivery. They have a narrow size distribution and provide great versatility as easy modifications can be made to their structure. For example, changes in molecular weight and geometry and addition of covalently bonded ligands which can provide protection against physical and physiological factors[1]. However, as functionalised polymers are synthesised materials, some potential issues exist. These include polymer toxicity, immunogenicity, non-specific biodistribution, *in vivo* circulation instability, low drug carrying capacity, rapid drug release and manufacturing challenges. Stimuli-sensitive hydrogels, made of natural gums and polymers, are an alternative to synthetic polymeric systems; however, their major drawback is a slow response time[2]. The easiest way to achieve fast-acting responsiveness is to develop thinner and smaller hydrogels which, in turn, bring about fragility and loss of mechanical strength in the polymer

network and the hydrogel device itself[2]. A possible alternative to polymeric materials and hydrogels are self-assembling amphiphilic lipid-based liquid crystals.

Lipid-based liquid crystalline matrices have an unrealised potential in providing external control over drug delivery, through manipulation of self-assembled structure and hence optimisation of drug release, disposition and bioavailability[3-5]. The thermodynamic stability of self-assembled lipid systems is a distinct advantage over e.g. polymer based systems, as in theory, the self-assembly mode may be infinitely reversibly changed from one structure to another to modify drug release; in effect acting as an inbuilt 'on-off switch' for drug release.

1.3.2. Lipid Self-Assembly and Transitions between Self-Assembled Structures

Amphiphilic lipids and surfactants self-assemble in aqueous environments to form a variety of possible structures which depend on the solubility and effective geometry of the assembling amphiphiles. These structures form spontaneously and in the absence of physical or chemical changes to the system are thermodynamically stable. The structures formed are discrete phases within the binary lipid-water phase diagram. The phases which can most often be formed by amphiphilic lipids are shown in Figure 1.1. Not all lipids can form each of the displayed phase structures. The phases formed by the lipid-water systems can be understood using a concept known as the critical packing parameter (CPP), which describes how the amphiphiles will aggregate according to the geometry of the molecule, based on theory by Israelachvili[6]. CPP is defined by Equation (1)

$$CPP = \frac{v}{a\,l} \qquad (1)$$

where v is effective volume, a is head group area and l is chain length. For values of CPP < 1, a normal phase forms (where hydrophobic chains face inwards, towards the core of the

structure), for values CPP > 1, an inverse or reverse phase forms (where hydrophobic chains face outwards, away from the aqueous core).

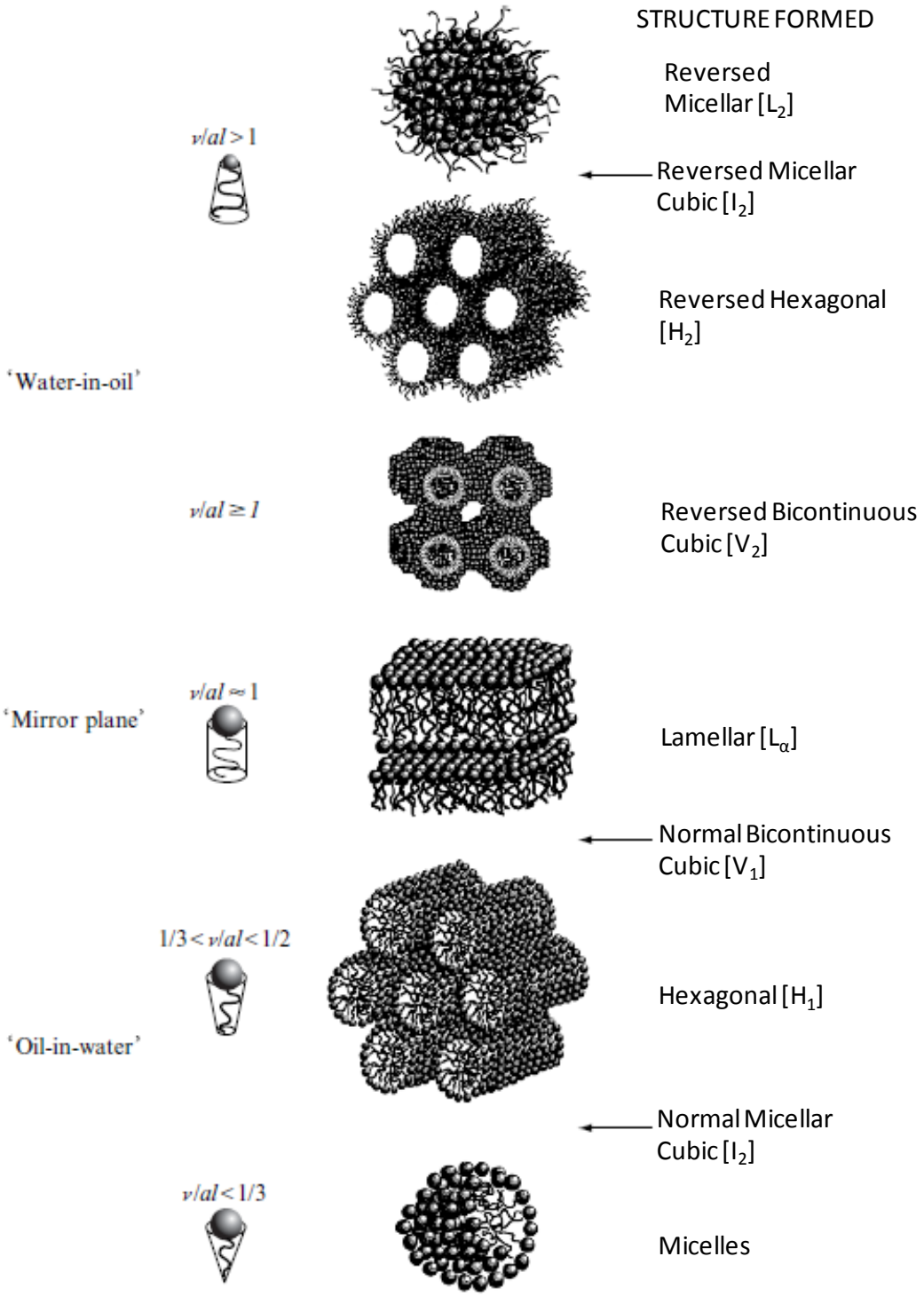

Figure 1.1 – Self-assembled phases of surfactant molecules and their preferred aggregate structures for geometrical packing reasons. Common abbreviations for each phase type and their CPP (given as v/al) are also listed. Adapted from [7].

Micelles are the simplest geometry and in their 'normal' configuration they are denoted as an L_1 phase. They typically occur at relatively high hydration. However, for relatively hydrophobic lipids and surfactants, the addition of water to surfactant sometimes does not induce the formation of the normal L_1 micellar phase. If the matrix has a finite capacity to incorporate additional water, the extra water may coexist as a separate phase. Such systems form the basis of bilayer structures that coexist in excess water, as in the case of cellular membranes and liposomes. Such systems, described below, are typically formed by lipids such as phospholipids, which have an inherent cylindrical shape suitable for the formation of bilayer structures.

The mesophases of current interest for drug delivery are the lamellar (L_α), the inverse hexagonal (H_2), the inverse bicontinuous cubic (V_2) and the inverse micellar (L_2) phases. L_α is the simplest of the liquid crystalline phases, consisting of flat lipid bilayers stacked on top of each other periodically. The addition of excess water to poorly water-soluble amphiphilic lipids can also result in the formation of the finite swelling inverse non-lamellar geometries; the H_2 and V_2 phases. The V_2 and H_2 phases are considered potential matrices for controlled release drug delivery. The V_2 phases appear as macroscopically stiff, optically isotopic gels which display three-dimensional cubic periodicity. Microscopically, they consist of two rod-like pipes, mutually interwoven, enantiomeric and unconnected, whose 3D structure has been well studied[8, 9]. Types of V_2 phases observed in lipid based liquid crystals include the double-diamond (space group Pn3m, Q^{224}), primitive (Im3m, Q^{229}) and gyroid (Ia3d, Q^{230}) phases. The H_2 phase consists of aggregates of closed reverse micellar cylinders, arranged in a 2D hexagonal lattice[10]. The L_2 phase, also known as the fluid isotropic phase, is comprised of inverse micelles, and although is technically not a liquid crystalline structure, is often observed on melting of the inverse hexagonal and cubic structures.

Thus lipid and surfactant self-assembly not only provides access to a range of thermodynamically stable structures, but also provides systems with very different classes of

behaviour that can be translated into different applications. In addition to their thermodynamically stable long range order, they also possess excellent biocompatibility due to their composition – lipid and water. The unique nanostructures formed by these lipids dictate their use, whether it be to control the rate of release of actives from within the well-defined geometric structures[11], as a template for matrix guided synthesis[12], or more classical surfactant applications such as wetting and detergency applications.

1.3.3. Drug Release from Liquid Crystalline Mesophases

In controlled release applications, drug release from V_2 and H_2 phases has been well established. The escape of drugs from the tortuous water channels of different liquid crystalline matrices is diffusion controlled as indicated by Higuchi's square root of time release kinetics[11, 13-15], shown in Equation 2:

$$Q = \sqrt{D_m C_d (2A - C_d) t} \qquad (2)^{16}$$

where Q is the amount of drug released per unit area of matrix, D_m is the diffusion coefficient of the drug in the matrix, A is the initial amount of drug in unit volume of matrix, C_d is the solubility of drug in matrix and t is time. The ability to switch between V_2 and H_2 structures and consequently control the release of model hydrophilic drugs using temperature as a stimulus *in vivo* and *in vitro*[17] has been reported, as has the *in vitro* use of pH in a similar manner[18].

1.3.4. Lyotropic Liquid Crystal Forming Lipids

There are many reported amphiphilic lipids that form liquid crystalline phases, and those that form non-lamellar phases have been reviewed by Kaasgaard et al.[19] Further, the liquid crystalline phases formed by phosphatidylcholines have been reviewed by Koynova et al.[20]. Some lipids of

interest in this thesis are discussed in more detail below and their molecular structures are shown in Figure 1.2.

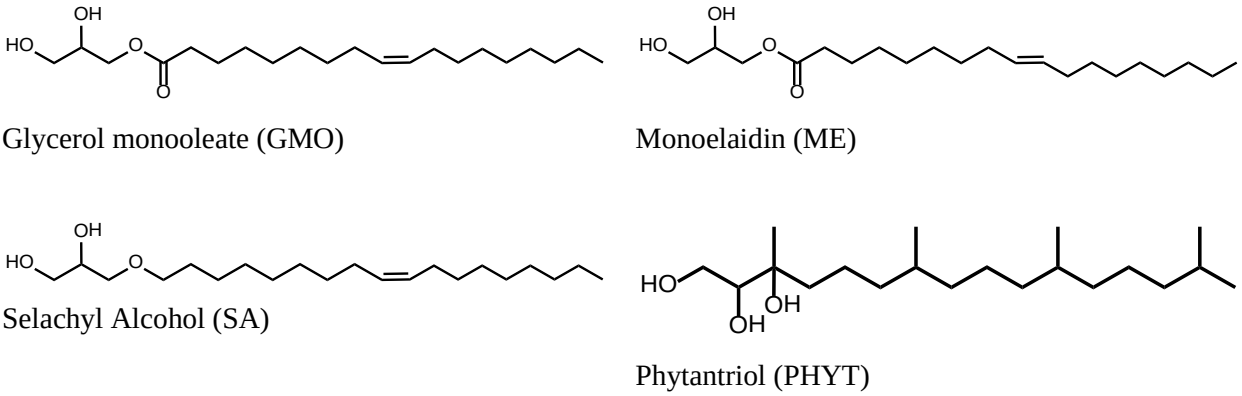

Figure 1.2 – Molecular structures of some lipids which form non-lamellar liquid crystalline nanostructures.

Glyceryl monooleate (GMO) and monoelaidin (ME) are neutral monoacylglycerides which are widely used in the food industry and are found in the body as intermediates of fat digestion and metabolism. Both are food additives and pharmaceutical excipients with oral GRAS status[21]. They have the same molecular formula, but GMO has a *cis* double bond at the 9,10 position of the acyl chain, whereas ME has a *trans* double bond.

GMO has received the most attention with regards to its utility as a liquid crystalline based drug delivery system. It is an attractive material as the GMO/water system forms L_α, V_2 and H_2 phases in an accessible temperature range and it is readily available at a low cost. Commercially produced sources of these lipids such as Myverol 18-99K (Kerry) and RyloMG (Danisco), are often complex mixtures of amphiphilic substances varying in chain length and purity level, which may make their behaviour somewhat difficult to characterise and control. In addition to this, the ester-based structure of this lipid may limit its practical application due to hydrolysis of the ester bond and the consequent chemical instability and disruption of the liquid crystalline structure.

ME has not been investigated as intensively as GMO as its phase transitions are much more complex and so have been thought less useful than GMO. Several of the polymorphs and mesophases have been found to be metastable and transform to more stable states isothermally and/or in the course of thermal cycling[22-25]. In addition to this, the solid lipid does not form a liquid crystalline phase and so it does not imbibe water below 38°C [23, 24]. Chang et al. compared liquid crystalline structure in ME and GMO dispersions, attributing the difference in phase behaviour to the *trans* double bond of ME increasing the length of the hydrophobic chains and as such giving the molecule a more cylindrical shape. This, in turn, makes the CPP of the ME molecule closer to 1 and so is more likely to form L_α phase[22]. The effect of salts on ME mesophases has also been studied[26].

Phytantriol (PHYT) is a precursor of vitamin E acetate, derived from chlorophyll, which is used as a cosmetic excipient in skin care and hair conditioning products[27, 28]. PHYT has been suggested as a practical alternative to the glyceride lipids. Its structure comprises of a highly branched phytanyl tail with a tri-hydroxyl head group and, most importantly, its structure does not include an ester functional group. Phytantriol is also commercially available in relative pure form.

Although very different in structure, PHYT and GMO show similar phase progressions. At room temperature, the phases formed upon increasing the water concentration occur in the sequence: reversed micellar, lamellar and then cubic phase. With both lipids, the cubic phase is the dominant phase formed in excess water. With an increase in temperature, the cubic phases formed by GMO and phytantriol in excess water have been reported to transform into a reversed hexagonal phase and reversed micellar phase. These phase transitions occur at higher temperatures in GMO (>80°C)[29, 30] than for phytantriol (>40°C)[31, 32].

Selachyl Alcohol (SA), also known as glyceryl monooleyl ether, is another lipid known to form inverse liquid crystalline phases in excess water. SA forms H_2 phase at room temperature,

and forms L_2 phase at higher temperatures in excess water. The bulk and dispersed systems of SA have been characterised in the literature[33, 34].

1.3.5. Dispersed Liquid Crystalline Matrices: Cubosomes and Hexosomes

Bulk liquid crystal systems are regarded as soft nanostructured materials and have been proposed for use as controlled release drug delivery depots amongst other potential applications[35]. When lipid-based liquid crystalline phases can co-exist in equilibrium with an excess of water, kinetically stable colloidal dispersions such as cubosomes and hexosomes can be formed where the colloidal material retains the internal 'parent' phase structure of cubic and hexagonal phases respectively.

In order to provide colloidal stability, the presence of a stabiliser is required. The most commonly used stabiliser is the triblock PEO-PPO-PEO copolymer, Pluronic F-127[36]. More recently, Pluronic F-108[37] has been proposed as an alternative stabiliser for cubosomes. Cryogenic transmission electron microscopy (cryo-TEM) and cryogenic field emission scanning electron microscopy (cryo-FESEM) images of cubosomes are shown in Figure 1.3. A dispersion, as opposed to a bulk phase, may have benefits in drug delivery as they are nano-sized and so are more easily injected than the bulk phase. They have potential to be injected systemically and locally[38] with faster drug release kinetics than depot systems. However, previous studies with dispersed systems finds only burst release of a range of hydrophilic and hydrophobic from cubosomes in aqueous media[39, 40]. Additionally, the particles have been found to be unstable in plasma[41]. Nevertheless, Nguyen et al. found that under some circumstances cubosomes can provide a sustained release formulation for a poorly water soluble drug on oral administration[42, 43]. Release kinetics from cubosomes has been improved by altering charge, viscosity and structure[44-

[46]; however controlling responsiveness of the nanostructure of dispersed liquid crystalline matrices e.g. from L_α to V_2 may be a more effective way to control the release of actives from the particles.

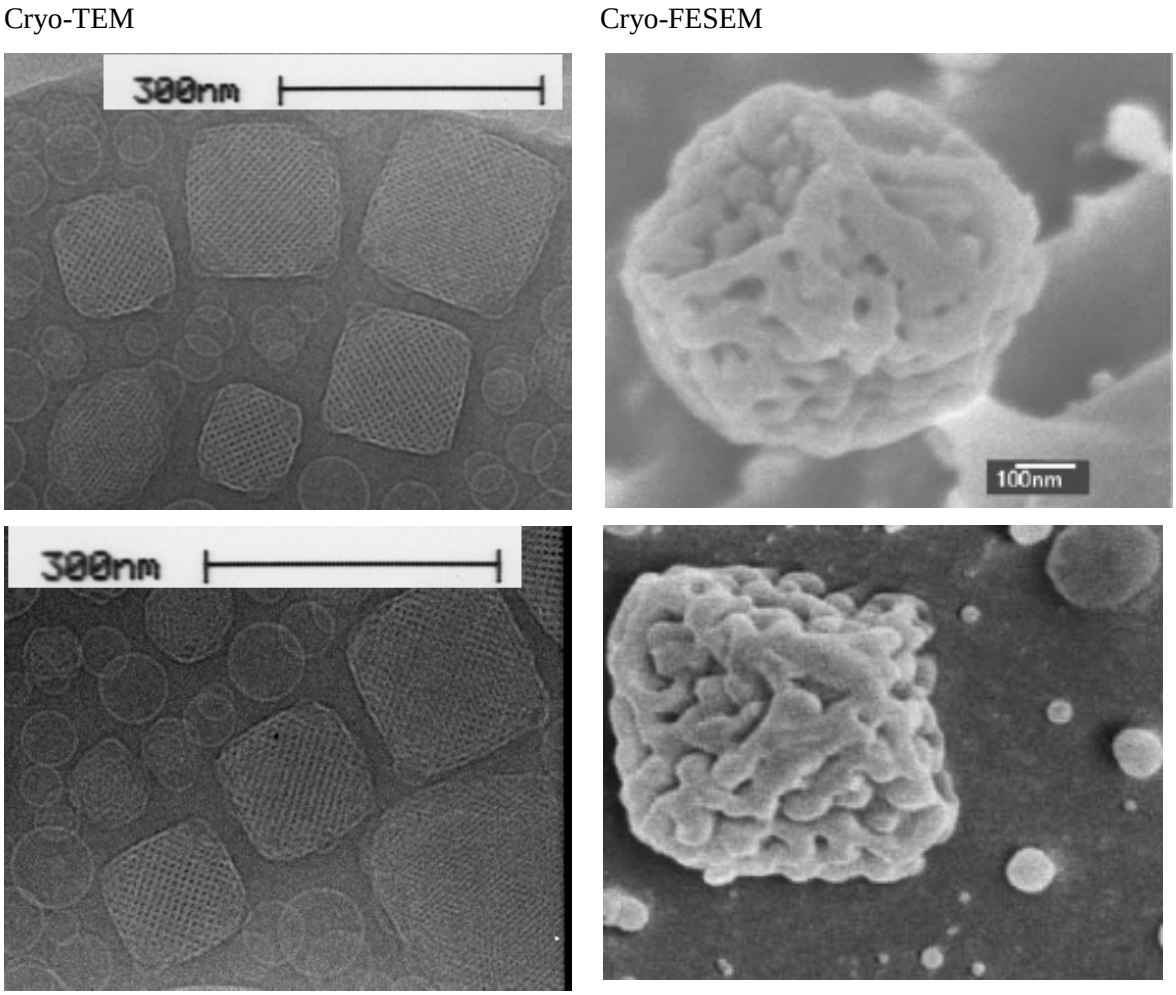

Figure 1.3 – Cryo-TEM and cryo-FESEM images of cubosomes. Cryo-TEM (left panel) images show 2D particle morphology and cryo-FESEM (right panel) show 3D particle morphology. Adapted from[47, 48].

1.3.6. Transitions between Self-Assembled Structures

Transitions between different self-assembled geometries for lipids in aqueous environments are ubiquitous in nature and have received a huge amount of attention in biophysical chemistry research[49, 50]. The formation and structure of cellular membranes, membrane fusion and some cellular uptake mechanisms all involve manipulation of lipid self-assembly at the molecular and meso-length scales. The rich diversity of structures that lipids may adopt lends itself as the basis of complex biological functions. There is potential to utilise the reversible phase transitions in lipid

systems to impart responsiveness into materials. With the advent of advanced synchrotron and neutron scattering facilities, we are only now fully understanding the mechanisms by which transformations between lipid self-assembled structures takes place[51, 52]. Harnessing this information is key to utilising the transformation between lipid systems.

It is notable that no drug delivery products have yet made it to market based on stimuli responsive systems. A heat sensitive liposome system containing doxorubicin for heat selective tumour delivery (Thermodox® owned by Celsion) has entered clinical trials; however, the potential for accidental activation of the delivery system needs to be carefully controlled to avoid inadvertent activation in non-target tissues. Consequently, it might be expected that alternative means of activation such as an optical stimuli, will ultimately be viewed as a safer approach to on-demand delivery systems. The major hurdle to progress in light activated delivery systems is the need to include light responsive elements that may themselves be prohibitively toxic and require their own highly costly preclinical and clinical toxicological evaluation. Hence, there is a need to expand the range of materials available to the formulator to identify the ideal selective responsive drug delivery system that meets the demands of functionality, safety and toxicity.

The self-assembly of lipids can be manipulated by factors such as the presence of additives, solution conditions e.g. pH and environmental conditions such as temperature and pressure. The interplay between lipid packing, nanostructure and drug release rate is shown in Figure 1.4 whereby the alteration of packing at the intramolecular scale can ultimately result in a change in the drug release rate from the matrix. The addition of known amounts of specific additives can result in quantifiable modifications in phase behaviour – e.g. cholesterol in liposomes effects bilayer fluidity[53], oleic acid in GMO[54, 55] and vitamin E acetate in phytantriol[56] causes the reduction of the V_2 to H_2 to L_2 phase transition temperatures; allowing for the ability to fine tune the desired properties of lipid based systems. These parameters, and hence lipid packing, can be manipulated providing specific stimuli. For example, in the case of liquid crystalline structure, an

increase in temperature will tend to induce a higher degree of chain splay, therefore increasing the spontaneous mean curvature of the monolayer and forcing the structure to switch to a more energetically favourable phase with potential to thereby manipulate drug release[57].

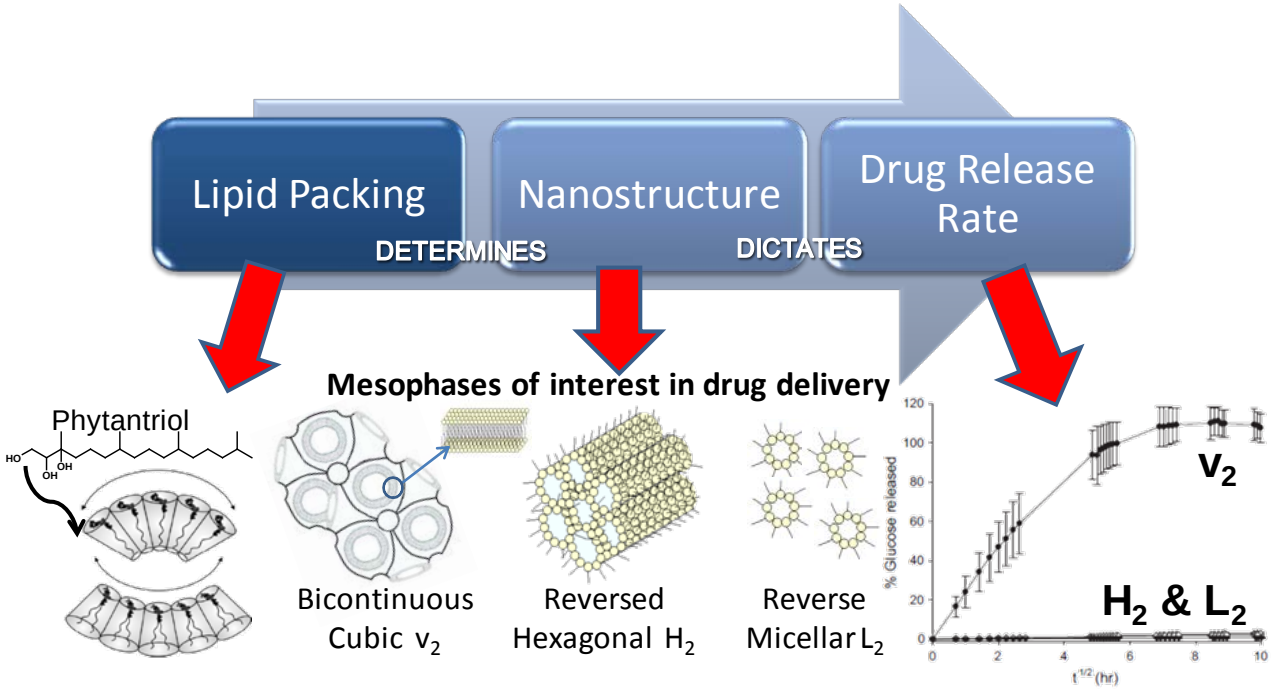

Figure 1.4 – Schematic diagram showing the interplay between lipid packing, nanostructure and drug release rate of self-assembled liquid crystalline systems.

1.4. Drug Delivery, On-Demand

Research into modern pharmacological treatments for diseases is focussed on coupling pharmaceuticals with nanotechnology to not only achieve increased bioavailability and sustained release, but to also achieve site specific delivery and drug release on-demand[58-62]. In particular, external control over release of incorporated agents to overcome unmet therapeutic needs is desired. The potential to improve the delivery of actives is also recognised in the cosmetics and personal care industry[63, 64] as well as in functional foods[5, 65-67] and environmental protection[68]. Hence, there a number of therapeutic scenarios in which external control over drug release may be beneficial including:

- **Frequently injected compounds with short half-lives** – The frequency of administration of drugs that require multiple injections may be replaced by the application of an external stimulus. For example, in hormone treatments a depot injection can be administered in the morning with external activation resulting in the release of drug as required[69].
- **Theranostics (imaging guided therapy)** – The development of novel carriers which deliver both imaging contrast agents and active compounds, so that imaging reveals the ideal location for remote activation of drug delivery[58, 70].
- **Chronically administered compounds with high risk of complications from administration –** for example, the necessity for frequent intravitreal injection of steroids or anti-VEGF compounds for macular degeneration is associated with high risk of infection and retinal detachment[71-73].
- **Symptom responsive drug release –** the ability to rapidly administer a dose of drug on development of symptoms without going through an administration procedure. This could be achieved through the administration of a prior injected dose form, from which drug release is sparked by the onset of symptoms[74].

- **Sequential delivery of therapeutic agents** – drug-drug interactions can cause problems especially for patients on multiple treatments. A delivery system which can release drugs dosed at the same time at different spatial or temporal locations could reduce side effects and make dosing less complicated[75].

This Introduction will provide a view of the landscape of stimuli responsive self-assembled systems with a focus on surfactants and lipids, particularly for drug delivery applications. It is proposed that there are three main categories of stimuli responsive systems for drug delivery applications, namely Active Targeting, Endogenous Stimuli and External Stimuli. The specific stimuli responsive mechanisms and matrices in each category are summarised in Table 1.1. The general aspects of each of these stimuli responsive areas will be discussed.

Table 1.1 – An overview of some of the proposed endogenous and external stimuli and different classes of self-assembled drug delivery systems reported in literature.

Endogenous Stimuli	External Stimuli	Active Targeting	Depot Systems
• pH changes • Redox sensitivity • Ionic changes • Changes in osmotic pressure • Increased expression & activity of proteins	• Temperature • Light • Electromagnetic Field • Ultrasound	• Antibody-Antigen • Enzymes • Receptors e.g. folate, growth factors • Aptamers • Integrins	• Lipid based soft materials • Hydrogels • Polymeric cages, membranes and self-assembled nanoparticles

For application in drug delivery, the obvious aim is to control the availability of drug from the carrier to the general circulation if systemic availability is desired or to the intended site of action for localised delivery. It is therefore useful to briefly discuss drug release mechanisms so that subsequent discussion of stimuli responsiveness can be understood in terms of the particular mechanism at play. Release of drug from delivery systems is recognised as being via three means:

(i) **Passive diffusion** relies on a chemical potential gradient to drive the drug from the self-assembled system into the bulk liquid into which it is introduced, such as the blood stream. Drug is maintained inside the self-assembled system prior to administration purely by partitioning or equivalence of concentration in the internal and external aqueous compartments – dilution is the trigger by which drug is released by reducing the concentration of drug in the external surrounding fluid.

(ii) **Non-specific degradation of the carrier** through normal physiological processes such as phagocytic uptake and/or hydrolytic destruction. Degradation is the usual mechanism controlling release from solid matrices made from e.g. biodegradable polymer or solid lipid nanoparticles, in which hydrolysis induces chemical degradation of the polymer structure and erosion of the particle.

(iii) **Covalent drug release** is usually achieved through incorporation of a functional linker within the self-assembled system that is cleaved in the particular environment of the target tissue. The cleavage of these systems is often achieved through pH sensitive functional groups that decouple drug from the carrier in hypoxic environments, or in enzymatically activated systems.

1.4.1. Endogenous Stimuli

The 'holy grail' of therapy is for there to be no intervention in the management and treatment of disease where the development of biochemical markers or symptoms that are not noticeable to the patient would trigger drug release automatically in response to some measured indicator[74]. Such systems are already in use for the treatment of diabetes to much success, where the implantable mechanical pumps release insulin in response to falling glucose levels in the blood[76]. Hence, drug delivery systems that are responsive to variation in physiological conditions are sought after. The use of physiological triggers in drug delivery to date, particularly in

polymers, has largely exploited the difference in physiological conditions between pathological and normal tissues in conditions such as cancer and inflammatory diseases[77]. The ability to induce variation in lipid-based systems (rather than mechanical-based systems) using physiological stimuli has not been used to such great advantage, particularly in consideration of the vast capability of cellular structures to utilise changes in lipid assembly to modulate function.

1.4.1.1. Targeted Drug Delivery

For some cases, an ideal drug delivery system could be dosed systematically and accumulate at a desired site where it can release drug on contact with a local phenomenon or on demand via an external stimulus as previously outlined. Many factors affect the ability of a drug to get to its intended target at an effective concentration. The main non-cellular mechanism affecting the circulation of colloids in the body is their rapid opsonisation by phagocytic cells and consequent rapid clearance from the blood; a phenomenon known as the reticuloendothelial defence system (RES). In addition, cellular-based defence mechanisms, drug distribution, biotransformation and clearance also hinder accumulation of carrier in specific tissues[78].

In order to counter these physiological effects and so deliver actives to target specific tissues several methods have been reported. This has somewhat been dominated by the approach of preparation of nanoparticles to an optimum size and sterically stabilising them through PEGylation[79]. PEGylation refers to covering the particle with PEO chains and so provide a ‘cloud’ of hydrophilic chains which act as a steric barrier and so repel plasma proteins. This increases blood circulation time of nanoparticles[80] as well as reduces *in vivo* degradation[81].

Active targeting refers to the attachment of ligands which bind to specific receptors or antigens by molecular recognition to the surface of nanoparticles, with the aim to increase accumulation and penetration into desired sites. Numerous nanocarriers have been developed in

order to target the physiological differences between healthy and diseased tissues such as cancer[4] and inflammation. The literature on actively-targeted lipid-based self-assembled systems has focussed primarily on liposomes[59]. These nanoparticles are coupled to specific antibodies or coated with aptamers or ligands through the functionalisation of the amphiphilic lipid head group or the terminus of a PEG polymer[82]. The ligand must also be attached at an optimum length so that it extends outside the steric PEG barrier in order to maximise interaction with the target[83]. Particles can be targeted to particular tissues as outlined in Table 1.2; however, some are likely to partition into non-target tissues and so cause potential toxicity issues. Therefore, it would be more desirable to have particles that are activated only in target tissues.

Table 1.2 – Some examples of targeted functionalised liposomes.

Target	Functional moiety	References
Folate receptors of actively growing tumour cells	Folate	83, 84
Epidemal growth factor receptors	Epidemal growth factor	84
Surface glycoprotein receptor (gp112)	IgG monoclonal antibody	85
Integrins, receptors expressed in neo-vasculature of tumours during angiogenesis	Small peptides	86, 87
Ischaemically damaged cardiomyocytes	Anti-cardiac myosin monoclonal antibodies	88-90
Solid tumours and B-cell lymphoma	Antibody fragments scFv or Fab'	91, 92
CD19 and CD20 epitopes	CD19 and CD20 antigens	93
Biotin-rich optically clear nuclei in tumours	avidin/biotinylated complexes	94, 95

1.4.1.2. pH Variation

Differences between the pH in tissue and cellular components in pathological conditions provide points of potential exploitation. Normal pH gradients exist naturally throughout the body, for instance, inside some parts of the gastrointestinal tract and cellular components differ from the extracellular pH of 7.4. This is commonly utilised to enhance oral drug bioavailability through the

formulation of drug molecules as salts of base forms. In drug delivery it is utilised in selective drug release through preparation of enteric coatings for tablets, which protect drug from the harsh acidic environment of the stomach, allowing drug to be released at a more acceptable pH in the intestines.

Abnormal pH gradients exist between normal tissues and those affected by conditions such as cancer, inflammation and infection. Sites of infection and inflammation, metastasised tumours and primary tumours have a significantly lower pH to normal tissues[96]. For example, 60 min after an inflammatory infection, the pH at the site of inflammation drops to 6.5. These disease states have been the target of many lipid-based self-assembly systems. As such, pH-sensitive systems have been extensively investigated since the early 1980s as a means of increasing drug delivery to tumours. Many examples of pH-sensitive systems found in the literature are based on polymeric and lipid-based liposomes and hydrogel systems which can be synthetically altered to provided highly specific structural changes under differing pH conditions. Hydrogels have a unique pH-dependent swelling–deswelling behaviour where the deswelling of the gel results in encapsulated drug release[97, 98]. More recently, Negrini *et al*. reversibly manipulated the phase transition of a monoolein-based lyotropic liquid crystal in order to modulate drug release *in vitro*[18].

Liposomal systems have been designed to be systemically administered and accumulate in tumours where they release their contents under mildly acidic conditions[99-101]. The liposomes are made responsive by the inclusion of a modified lipid as a sensitiser and the mechanisms of release have been suggested to be one or a mixture of the following:

- The pH change triggers a change in morphology from the lamellar lipid bilayer (L_α) to e.g. micellar or hexagonal phase[102]. The liposome contains negatively-charged lipids e.g. lipids with a carboxyl group which neutralise in acidic pH and so causes the collapse of L_α into a hexagonal phase. This concept is exploited in the enteric coating of pharmaceuticals to protect

them from degradation in the stomach at low pH, where the carboxylate groups of the coating polymer are protonated imparting low solubility, but ionise in the small intestine to allow polymer dissolution. In self-assembled systems this concept has been rarely employed, but has recently been demonstrated in lyotropic liquid crystalline systems prepared using monoglycerides doped with fatty acid to induce a morphology change from the hexagonal phase to the bicontinuous cubic phase[103]. The hexagonal phase present under simulated gastric conditions at low pH released the model drug probucol slowly, compared to the cubic phase structure present at intestinal pH.

- The pH change causes the ionisation of bilayer surfactants. Cholesterol hemisuccinate[104-106] and oleic acid[107, 108] are two mildly acidic amphiphiles which become protonated when in acidic conditions. When exposed to the acidic environment, a decrease in hydration of the lipid headgroups results and as a consequence, formation of a non-bilayer structure which can fuse with the endosome membrane and so release contents into the cytoplasm[109].
- The pH change results in acid-catalysed hydrolysis of specifically engineered lipids resulting in the formation of detergents or fusion. Acid-labile PEG-conjugated vinyl ether lipids have been used by Thompson *et al*. to stabilise liposomes. At pH <5, hydrolysis of the ether bond results in the removal of the PEG moiety and consequently allowing the liposome to become fusogenic[110, 111]. Other groups have employed acid-labile and ester[112, 113] linkages in order to render liposomes pH-sensitive.
- The pH change leads to the destabilisation of the bilayer through lysis, phase separation, pore formation or fusion. This can be achieved in vesicles with incorporated pH-sensitive polymers such as poly(2-ethylacrylic acid)[114] and poly(glycidol)s[115].

However, three limiting issues exist for the application of pH-sensitive liposomes in tumour treatment. Firstly, the narrow pH window of between pH 7.4 in normal tissues and tumour pH which is typically at a minimum at 6.5, provides only a narrow range over which the stimuli must

be tuned to occur. Secondly, the region of highest acidity in the tumour is in the tumour interstitium which is not close to the vasculature, thereby limiting their effectiveness. In light of the issues of application to tumour treatment, the focus on potential clinical applications of pH-sensitive liposomes has somewhat shifted to the control of drug release in cellular components such as endosomes and lysosomes where the pH may be lower than 5. In some cases, however, some liposomes lose their pH sensitivity or become unstable in the presence of serum[116, 117]. This has been somewhat overcome through the use of a sterically stabilising PEG coating, which is removable (i.e. dePEGylation) in order to maximise release response on encountering a low pH.

1.4.1.3. Redox, Ionic & Osmotic Variation

Drug delivery systems have been designed to take advantage of cellular reduction potential at different locations within and around cells[118, 119]. Disulfide linkages (-S-S-) exist most commonly in cellular material as oxidised sulfhydryl (SH) groups of cysteine moieties in peptides and proteins. They are unique in that they form reversible covalent bonds, a property which has been manipulated in drug delivery to the cytosolic space, cellular components such as endosomes, lysosomes, endoplasmic reticulum and mitochondria, and tumours. The reduction of disulfide linkages can also be a consequence of exposure to a reductase enzyme. Entry of molecules to these compartments is limited to small molecules; however techniques have been developed to overcome this, including the use of liposomes.

In liposomal drug delivery strategies, disulfides act as linkers for targeting conjugates[105, 106, 120] or as disulfide-bridged lipids[121, 122] which are critical to liposome stability. Kirpotin *et al.* synthesised a disulfide-linked PEG conjugate which had two functions in two different approaches with these materials; firstly, thiolytic cleavage led to destabilisation of the vesicle and release of its content, and second provided pH sensitivity in the system[105]. Annapragada and co-workers have

made cross-linked liposomes towards creating a drug delivery system suitable for nebulisation for inhalation delivery. These modified liposomes are cleavable on exposure to cysteine thereby altering the size distribution and consequently stimulating drug release[122].

Lipid self-assembled systems with responsiveness to ionic or osmotic variation to stimulate changes in self-assembly, thus leading to control over drug release have not been commonly reported. These two stimuli present an interesting option for controlling self-assembled systems as pressure and ionic strengths are known to affect the packing of amphiphiles[123-126]. A possible application of pressure dependence of a drug delivery system could arise in the treatment of eye conditions such as glaucoma, where the 'intelligent' drug delivery system could act as a sensor to changes in intraocular pressure and so automatically adjust the release of encapsulated drug. The pressure is elevated inside tumour tissues due to compromised lymphatic drainage which also presents an limited opportunity for using variation to homeostatic pressure as a trigger for drug release from such systems[127].

Addition of specific ions or change in counter ions has been reported as a means by which to manipulate lipid self-assembly and hence could be used as a drug release trigger. Shen *et al*. reported that the self-assembly of an amphiphilic ionic liquid that forms micelles in water was disrupted on exchange of the bromide counter ion with hexafluorophosphate, with subsequent dye release[128]. Yaghmur *et al*. have demonstrated a direct vesicle to inverted hexagonal phase transition for mixtures of glyceryl monooleate and dioleyl phosphatidyl glycerol when exposed to increasing concentration of calcium ions[129]. The divalent counter ion reduced the apparent area of the headgroup, leading to a change in molecular packing and subsequent phase transition. Although not resulting in a change in self-assembly behaviour, the release of a cationic ruthenium complex from the cubic phase on addition of sodium chloride to the aqueous compartment was demonstrated when the glyceryl monooleate cubic phase contained a small amount of oleic acid[130]. The shielding of the electrostatic interaction between the cationic compound and the negatively

charged acid provided the trigger for release, highlighting the potential for specific salt effects to provide triggers for changes in self-assembly and or release in lipid based systems.

1.4.1.4. Increased Expression & Activity of Proteins

The upregulation of proteins in tumours and inflammation, and specificity of protein location throughout tissues in the body, has afforded a tissue-specific target for drug release. This has already been exploited in polymeric systems for selective delivery in tumour tissues. Due to their rapid and abnormal growth, tumours often over express macromolecules, in particular enzymes, which can recognise and cleave specific linker groups between drug and carrier, or within the carrier structure itself. Inflammatory conditions such as cystic fibrosis, rheumatoid arthritis and emphysema are accompanied by an increase in the release of elastase from phagocytic cells into extracellular compartments.

Enzymatically-activated drug delivery from liposomes has been investigated and reviewed[131]. Liposomes have been designed to be activated by many different macromolecules resulting in the collapse of the liposome or to induce membrane fusion under the action of the enzyme. A common strategy is to incorporate an enzymatically-sensitive lipid to facilitate conversion of the lipid to a fusogenic derivative, such as dioleylphosphatidylethanolamine (DOPE), or to otherwise disrupt the bilayer structure of the liposome. Phospholipids are natural substrates for phospholipase enzymes – with phospholipase A_2[3, 132, 133] and phospholipase C[134-136] having been investigated for liposome destabilisation. A more common and specific strategy is to build a custom phospholipid or lipopeptide with a molecular feature that is a substrate for specific enzymes over-expressed in diseased tissues. Lipids sensitive to elastase were prepared by incorporation of the *N*-Ac-Ala-Ala sequence into the headgroup[137, 138]. Similarly, matrix metalloproteinase (MMP-9), often over expressed in tumours, was found to cleave lipopeptides

containing the specific motif sensitive to this gelatinase enzyme, resulting in release of the liposome cargo[139, 140]. With a view to activation by quinone reductase, Ong *et al*. have reported the reductive cleavage of quinone headgroups from phospholipid derivatives to reveal DOPE, leading to release of incorporated model drug molecules from the liposomes[141]. An alternative approach has been to sensitise liposomes through the use of cholesterol esters that are sensitive to alkaline phosphatase[142]. Incorporation of transmembrane proteins into DOPE particles has been known for decades to induce bilayer formation, providing liposomes stabilised by incorporated proteins. The degradation of the protein by trypsin has been long proposed as a means of inducing liposome destabilisation[143].

The clinical advantage of physiological triggers to induce phase changes in materials, and thus stimulate drug release, centres on the simplicity and specificity of the process. The problem with this approach, however, is the potential for non-specific activation and release of material in tissues other than the target tissues.

Accidental release may occur, for example, in inflamed tissues when targeting tumours, or normal tissues where enzymes are expressed at much lower levels than the target tissues, which may lead to side effects. Having specific temporal and spatial control over exactly where the delivery system is activated overcomes these concerns, although it introduces increased complexity and likely requires intervention by health professionals. Hence systems that are responsive to external stimuli that can be controlled in a non-invasive manner have attracted significant attention in the literature.

1.4.2. External Stimuli

A number of different external stimuli for inducing drug release from self-assembled systems are listed in Table 1.2 and are discussed in more detail in this section.

1.4.2.1. Electromagnetic Field

Electromagnetic fields (EMF) can be used in therapeutically for two main purposes; to focus delivery to a target[144-146] e.g. tumour site where the system can cause cell death through intracellular hyperthermia[147], or to selectively release drug or imaging agents[148]. Carrier particles can be made magnetically-sensitive by encapsulating magnetic nanoparticles within the membrane or in the aqueous interior of polymers or liposomes. These systems have been dubbed 'magnetoliposomes'. After local or systemic administration of magnetoliposomes, the tumour-affected area can either be placed between two poles of a magnet[149-151], or the magnet imbedded within the tumour[152] where the application of an EMF for a specific period of time results in the increased accumulation of drug concentration in the tumour; the drug is released from the liposome by diffusion or by heating of the bilayer by the EMF. The use of low frequency magnetic fields to disrupt liposomes loaded with magnetic nanoparticles in an aqueous chamber has also been investigated[153] where magnetic nanoparticle motion causes disruptions in the bilayer and consequently drug release is achieved. EMF-sensitive polymeric hydrogels[154] and vesicles[155] have also been reported.

1.4.2.2. Ultrasound

Ultrasound is an attractive local physical stimulus as it can be easily focused in the body and is able to penetrate into deep tissue[156]. Low frequency (LFU) and high frequency (HFU) ultrasound have been employed to release drugs from acoustically-active systems such as polymeric micelles and matrices[61, 157], and more recently liposomes[158-161]. It is proposed that the presence of microbubbles in the structure affords the liposome sensitivity to ultrasound. Insonation of acoustically-active systems results in the cavitation of nanoparticles and consequently the leakage of the vesicle contents into the surrounding environment. Heating of the tissues through ultrasound may also play a role in triggering drug release.

Research into creating ultrasound-triggered, lipid-based systems has focussed on forming LFU responsive liposomes as contrast agents or for drug delivery as LFU responsive systems have been found to be more effective in releasing contents from liposomes than HFU[162, 163]. However, the potential clinical applications of ultrasound-activated liposomes may be more compatible with HFU as they may integrate with readily available instruments.

In lipid-based self-assembled systems, it is well established that insonation and sonication of sufficient intensity can be employed to destabilise self-assembled systems and so make multilamellar liposomes into unilamellar ones[164, 165] and viscous cubic phase gels into cubosomes[166, 167]. As ultrasound has the ability to disrupt self-assembled bilayers, ultrasound can also penetrate through cell membranes which can result in cell death[168, 169]. This must be accounted for in ultrasound responsive systems for use in drug delivery applications. Lin *et al*. achieved selectivity for liposomes over cell membranes through the incorporation of PEG-lipids and oligo(ethylene glycol) surfactants[158] thereby tuning the liposome to be more sensitive to insonation than cell membranes. Huang *et al*. have formulated liposomes with different lipids which increase their sensitivity to LFU [162]. Most recently, Anna *et al*. has demonstrated the *in vivo* ultrasound mediated intracellular delivery of an otherwise impermeable compound[170].

1.4.2.3. Temperature

Temperature has been the most popular trigger mechanism in order to control the structure of self-assembled systems as the assembly of molecules is inherently affected by changes in temperature, largely by inducing chain splay and mobility in lipid tails or by disruption of headgroup hydration. Additionally, temperature is a very accessible trigger for many therapeutic applications. Hyperthermic conditions have been used to induce cytotoxicity[171] and can augment some treatments by increasing blood perfusion and permeability[172]. The primary means of

inducing the hyperthermic environment are summarised in Table 1.3. Laser heating using a near infrared laser is commonly reported. An electromagnetic field is also reportedly able to induce localised heating and release of contents from 'magnetoliposomes'. The simple application of heat pack or cool pack to manipulate self-assembled structure and modulate drug release has also been reported. Hence, there are a variety of potential approaches available to induce drug release using hyperthemia as the common trigger.

Table 1.3 – Primary means of inducing a hyperthermic environment and some examples of their use in drug delivery.

Heat source	**Formulation & Dosing method**	**Location & References**
Laser	Liposome, Systemic	Subcutaneous: [173]
	Liposome, Systemic	Tumour: [174-177]
	Liposome, IV	Ocular: [178]
	Liposome, Systemic	Liver: [179]
Electromagnetic Field	Liposome incorporating dextran magnetite or colloid iron oxide, Systemic	Also promotes increased accumulation at tumour site [151, 180, 181]
Water Bath	Liposome, IV	Tumour [182]
Heat/cool pack	Bulk liquid crystal, Subcutaneous	Subcutaneous[17]

Thermoliposomes

As is the case for enzymatically-activated systems, liposomal systems sensitive to temperature have received most attention in the literature compared to other self-assembled structures. The application of hyperthermia takes advantage of the acyl-chain melting phase transition in phospholipids which results in an increase in permeability across the lipid bilayer, and consequent drug release. The transition temperature of the lipids, and heat applied is tuned to be just above physiological temperature, but low enough so as to not perturb cell function in

surrounding tissues. The first systems were reported by Yatvin *et al.*[174, 183] who designed liposomes to release drug in this narrow temperature range. More recently, liposome formulations have been modified with polymers, most commonly poly(N-isopropylacrylamide) or a derivative thereof, which become water insoluble above a critical solution temperature (CST) and so destabilise the liposome bilayer[184-188]. Interestingly, Regan and co-workers have created pore-forming amphiphiles comprised of cholic acid, lysine and spermine which act as thermal gates when heat melts the liposome bilayer thereby changing the release rate of glucose *in vitro*[189, 190].

Other Thermoresponsive Structures

Reversibility of the system, i.e. the ability of the system to return to its original state on removal of the stimulus, is an important attribute in order to provide pulsatile release for the repeated treatment of chronic conditions. Reversible activation may reduce the required frequency of administration by providing repeat doses of drug on activation, and switch drug release off when the stimulus is removed.

Non-lamellar liquid crystalline systems are gaining increasing attention as potential reversible responsive materials, as the specific geometries adopted by the lipids are thermodynamically stable and transitions between structures are generally reversible[191]. This is in contrast to most liposomal or polymer systems where drug release behaviour is often irreversible. The complexity of potential structures that may be adopted also provides control over drug release rates through selection of specific amphiphile/phase structure combinations[11]. The reversibility of the transition between the bicontinuous cubic (V_2) and inverse hexagonal phase (H_2) structures exhibited by a phytantriol + vitamin E acetate liquid crystal system was previously investigated in my undergraduate degree. The possibility to switch drug release between fast and slow release rates respectively by changing between self-assembled structures was demonstrated *in vitro* and *in vivo*[17]. Figure 1.5 shows the *in vitro* release of glucose and use of change in temperature to reversibly modify drug release rates from the matrix through control of nanostructure.

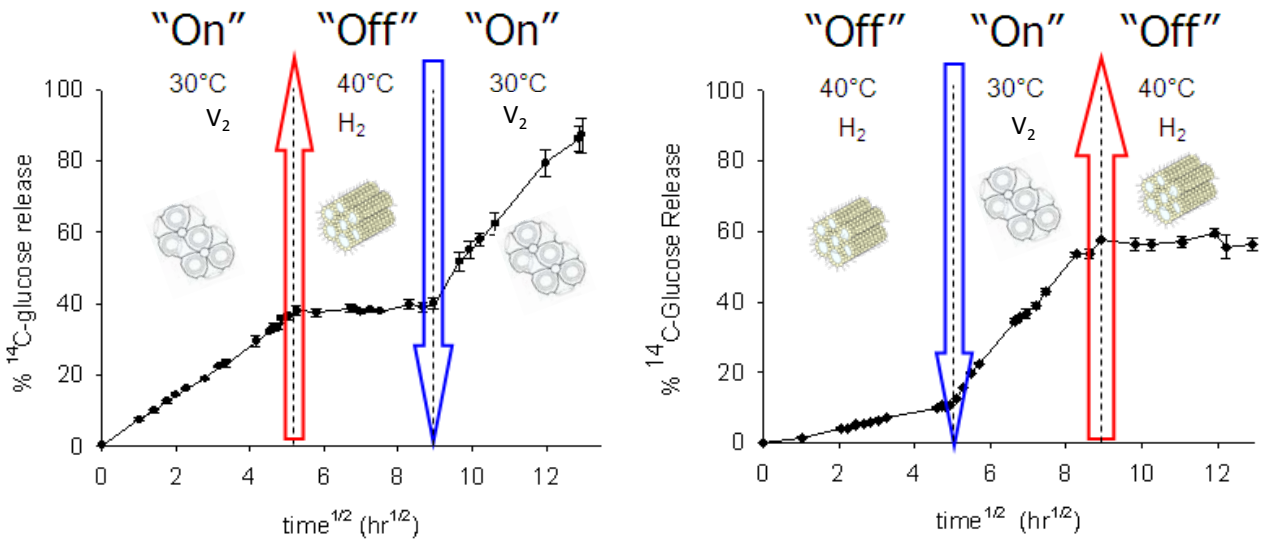

Figure 1.5 – Release of glucose from liquid crystalline matrix prepared from phytantriol containing 3% vitamin E acetate in response to temperature-induced changes in nanostructure. Modified from[17].

The responsive phytantriol + vitamin E acetate system was taken into a proof of concept *in vivo* study in rats. The subcutaneous injection of the liquid crystal matrix and subsequent application of a heat or cool pack to the site of injection provided control over the matrix nanostructure which consequently modified drug absorption from the implanted delivery system *in vivo*. Along similar lines, the phase transformation of vesicles to non-lamellar phase structures has also been proposed as a means to stimulate drug release from self-assembled lipid systems. One such system is monoelaidin, as it is known to undergo a lamellar to cubic phase transition at physiological temperatures[24].

However, practicalities of using direct heat as the stimulus will likely limit the ultimate development of such a system as the basis of an actual product. The use of temperature as a stimulus would be limited to applications where the site of required treatment is readily accessible and amenable to direct heating or cooling, essentially limiting applicability to subcutaneous depot application. Further problems arise when one considers that the body encounters local temperature changes in everyday situations, such as a hot shower, leaning against cold surfaces, etc., with

potential to lead to accidental activation. Hence more selective means of inducing hyperthermic conditions are desirable.

1.4.2.4. Light

Light responsive systems have the advantage of being non-invasive and provide a broad range of adjustable parameters such as wavelength, duration and intensity that can be optimised as required. Light-sensitive self-assembling systems have been reviewed recently[192, 193] as have light activated drug delivery systems[194, 195]. Photosensitivity has been imparted into self-assembled systems through the incorporation of specific chemical moieties and/or light sensitive nanoparticles incorporated into the matrix. The photo-activation mechanism in self-assembled systems can be distributed into three categories: irreversible photo-activation, photochromics and photothermal, each of which is discussed below.

Irreversible Light-Activated Systems

Light induced polymerisation, fragmentation and oxidation are irreversible processes which disrupt the integrity of the lipid structure. As the reactions of the photosensitive components discussed in this section are irreversible, the use of these in drug delivery systems is effective for single use but not pulsatile release.

Photo-induced oxidation utilises the reaction of a photosensitiser to a specific wavelength of light with oxygen which generates free radicals and singlet oxygen ($^1O_2$) to mediate their effects. Photodynamic therapy (PDT) uses these free radicals to cause cell death. These radical oxygen species cause localised oxidative damage to the surrounding tissue[196, 197]. The consequent physiological effect depends on the type of photosensitiser and where it is applied and activated. Current PDTs are focussed on treating tumours by either targeting the tumour microvasculature,

tumour cells or the inflammatory and immune host system. However, PTD is limited by the need to keep doses of the photosensitiser and light low enough to avoid collateral damage. The formation of free radicals has also been employed to induce drug release from vesicles such as liposomes. The free radicals cause membrane destabilisation through lipid hydrolysis. Thompson and co-workers have manipulated the effects of plasmalogen photo-oxidation on membrane permeability in order to release drug from liposomes. The photooxidation of light sensitive components promotes bilayer fusion and release of contents [102, 198, 199], such as aluminium phthalocyanine disulfonic acid[200].

Systems have also been synthesised which undergo photo-fragmentation or polymerisation of the stabilising element upon exposure to light. Photocleavable lipid derivatives in conjunction with a lipid e.g. dioleoylphosphatidyl ethanolamine (DOPE) have been used to form liposomes. On exposure to UV irradiation, the fragmentation of the modified lipid destabilises the bilayer and contents release ensues. Zhang *et al*. achieved 50% calcein release from liposomes through the photo-fragmentation of NVOC-DOPE[201]. Activation of photo-polymerising components in self-assembled systems has also been used to cause drug release. Polymerisation of these components condenses a portion of the interface, resulting in the formation of pores. For example, Spratt *et al*. achieved 28 000 fold increase in liposome bilayer permeability on activation of a synthesised photoreactive lipid bis-SorbPC$_{17,17}$[202].

Photochromic Systems

Photochromic molecules reversibly isomerise upon exposure to a light source in the UV-visible range. When incorporated into a self-assembled system, the activation and deactivation of photochromics can cause a steric disturbance in the packing in the self-assembled structures resulting in a change in e.g. drug release. The response of the lipid system can be manipulated by

composition of the lipid host and photochromic concentration[53, 203]. Research into photochromic self-assembled systems include azobenzene[204], spiropyran[205], stilbene[206] and retinal[207] moieties amongst others[192]. In some cases, photoisomerisation does not compromise interface integrity, thus pulsatile delivery may be achieved[208-210].

Azobenzene

Aromatic azo compounds are a group of molecules whose photochemistry is determined by an azobenzene moiety; an azo group -N=N- in conjugation with two phenyl substituents. Upon UV-irradiation, the azobenzene moiety undergoes a considerable change in length with the distance between the 4- and 4' carbons decreasing from 9.0 Å in the *trans* form to 5.5 Å in the *cis* form[211]. The azobenzene photoisomers also differ in polarity; the *cis* isomer is more hydrophilic than the *trans*. The N=N isomerisation between *trans* and *cis* azobenzene isomers is shown in Figure 1.6, Panel A. The extent of *trans* to *cis* isomerisation is dependent on strength and time of irradiation, solvent effects, and is slightly affected by the nature of substituents[212].

The main uses of azobenzene are as yellow/orange synthetic dyes, however molecules and surfactants containing an azobenzene moiety and have also been used to impart control over membrane permeability in aggregates such as: emulsions[210, 213-215], Langmuir-Blodgett films[216-219], liposomes and vesicular membranes[220-227], polymeric vesicles[208, 228], hydrogels[229], silica materials[230] and liquid crystals[231-234]. The isomerisation of the azo-moiety is sufficient to destabilise the surrounding area and as a consequence, induce a phase transformation or disruption of the bilayer as schematically demonstrated in Figure 1.6, panel B.

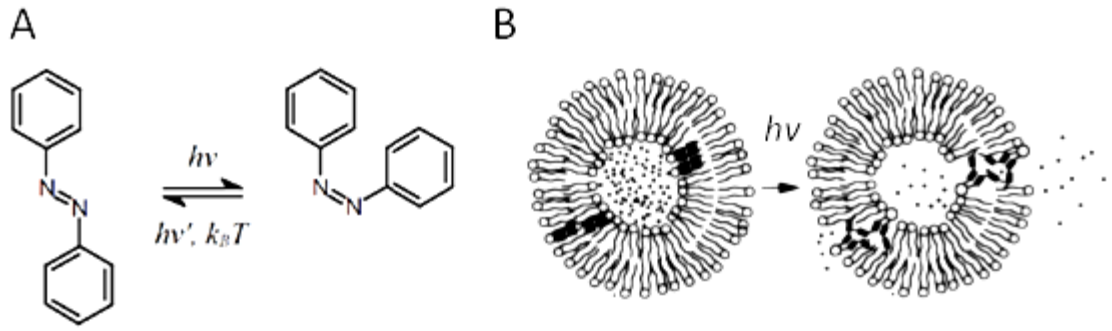

Figure 1.6 – Azobenzene photoisomerisation. Panel A shows the reversible *trans* to *cis* isomerisation upon exposure to an appropriate wavelength of UV light. Panel B shows a diagrammatic representation of the disruption of a liposome through the activation of the AZO moiety with UV light and subsequent drug release. Adapted from [226].

Spiropyrans

The structure of spiropyran is shown in Figure 1.7. Upon exposure to UV light, spiropyrans undergo a heterocyclic ring cleavage that produces the relatively hydrophilic, open cationic merocyanine form. The spiropyran form (hydrophobic, closed) is colourless, whereas the merocyanine structure (hydrophilic, open) has a strong absorption in the visible region and so is purple in colour. The photoisomerisation of the spiropyran moiety is shown in Figure 1.7. The irradiation of spiropyran doped systems has been used as a trigger to alter the packing of amphiphiles in bilayer membranes[235, 236], surfactant films and vesicles[237-239] and micelles[240], thus modifying the permeation of solutes through the interface.

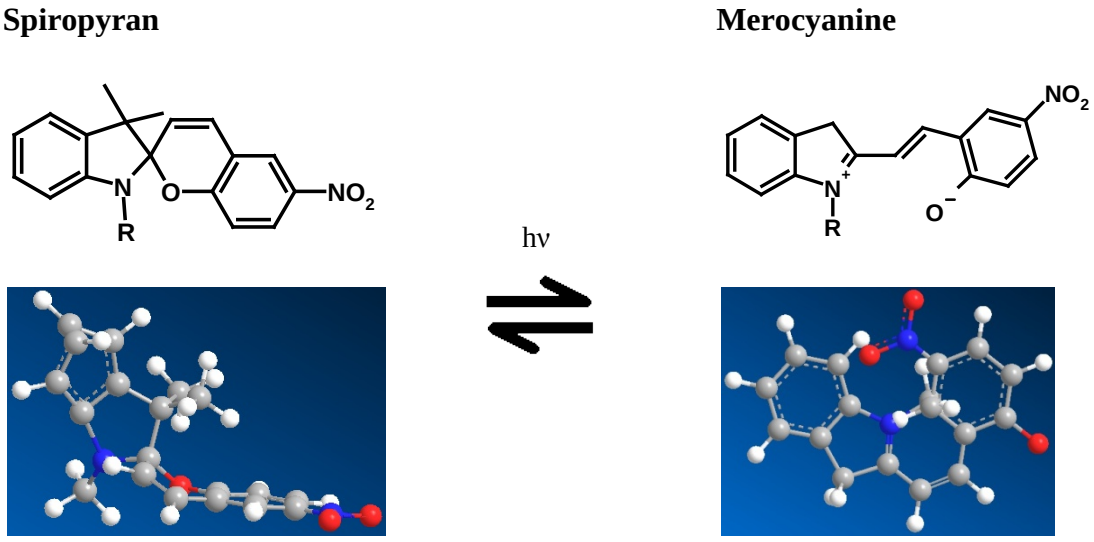

Figure 1.7 – The isomerisation of benzospiropyran to merocyanine on exposure to UV light, demonstrating its change in state of ionisation and molecular shape.

Cinnamic acid (CA)

Cinnamic acid and its derivatives undergo a trans/cis isomerisation upon exposure to UV light. These photoisomers are also ionisable with a change in pH. As yet, there has been no light switchable CA-based drug delivery systems reported, however, CA has been used to impart photosensitivity to self-assembled systems. Baglioni et al. have reported that the *trans* to *cis* isomerisation of *o*-methoxyCA modifies the molecular packing of a surfactant and, as a consequence, induces a reduction in fluid viscosity[241]. Although, not strictly a self-assembled biomaterial of interest, Lendlein et al. grafted CA into the backbone of hydroxyethyl acrylate hydrogels and when exposed to ultraviolet radiation of >260 nm, the CA molecules underwent a reversible cycloaddition which added new crosslinks into the material. The crosslinking process was reversed upon exposure to light <260 nm[242].

Photothermal Systems

Light can be used to impart heat into systems in two ways. Firstly, light can be used as a source of gentle heat. There is a particular focus on light in the near infrared (NIR) region as it has sufficient penetration through tissue for utility in an *in vivo* setting[243]. A major focus of the application of photothermal systems concentrates on drug delivery to the posterior section of the eye, especially the retina and choroid, in order to treat degenerative conditions such as choroidal neovascularisation, a cause of age-related macular degeneration (AMD). Current methods of drug delivery for AMD treatments are based on topical, periorbital, intravitreal and systemic administration. These are problematic as low penetration is gained through topical and periorbital administration, periorbital and intravitreal administration are invasive, and systemic administration of the drugs present toxicity issues as the whole body is exposed to large concentrations of drug in order to get a therapeutic amount into the target tissue. An interesting method developed by Zeimer et al., called light-targeted drug delivery (LTD), uses a non-invasive laser source to gently heat liposomes and so trigger drug release[196, 244]; the intended target of this system being the posterior section of the eye. The method involves the intravenous administration of drug encapsulated in a heat-sensitive liposome, and release of its contents at the target tissue by gently warming up the target tissue to 41°C with a directed laser light pulse. LTD, like PTD is limited by the need to keep doses of the photosensitiser and light sufficiently low to avoid collateral damage.

Secondly, light can be used to activate metallic nanoparticles (NPs) which are able to act as ‘nanoheaters’ on a highly localised scale. The unique optical, chemical and biological properties of these materials have led to their development in biological applications including drug delivery[245] and biosensors[246]. The evolved heat can induce bond cleavage, phase transitions or mechanical damage to biological systems. In recent times, there has been a flurry of research into the optical properties and potential applications of metallic nanoparticles. Metallic nanoparticles (mainly gold, but also silver and copper) are of interest as, on exposure to radiation of a specific

wavelength and intensity, they can heat to their vaporisation point within femtoseconds due to the activation of surface plasmon resonances, a phenomenon demonstrated in Figure 1.8[247, 248]. When these metallic NPs are illuminated at the appropriate optical frequencies, the conduction band electrons in the gold are excited, resulting in a resonant, coherent oscillation of these electrons. Wavelengths at which the NPs absorb are tuneable according to their size, shape, composition and state of aggregation[249-251]. Metallic NP have been synthesised as spheres, rods and shells, where the shape of the NP also plays a role in its ability to absorb photons[252]. In addition to their specific dimensions, metallic nanoparticles can also be functionalised and made more biocompatible through the facile binding of various types of biomolecules e.g. phosphatidylcholine[253]. Gold nanorods, are of particular interest as their properties allow them to absorb NIR light in the optimum range for imaging and therapy, within the so-called 'water window' in the wavelengths 700 – 1200 nm[254, 255].

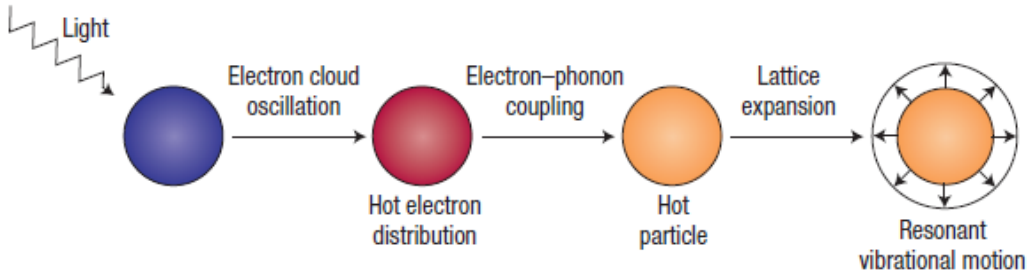

Figure 1.8 – The interaction of light with metallic nanoparticles. Light absorption heats the electrons of the particles which then equilibrate through electron-phonon coupling. This initiates coherent vibrational motion in the particles called surface plasmon resonance. The heat created can then be transferred to its surroundings through transduction. Adapted from [256].

Therapeutic applications of research into gold nanoparticles has focussed on the use of metallic nanoparticles to cause tumour cell death by localised heating of the tumour[257-260] or to elicit remote release of entrapped materials via photothermal conversion[261] from within liposomes[250, 262-265], polyelectrolyte capsules[266], hydrogels[267-269], polymer vesicles[270] or from a NP-

drug conjugate[271, 272]. Plasmon resonant heating has also been used to trigger phase transitions in self-assembled lipid systems, with a view to elucidate the mechanisms behind photothermal activated responses[273-275]. This phenomenon has been used to enact contents release *in vitro*[276, 277].

1.5. Light Activated Transitions between Self-Assembled Structures for On-Demand Drug Delivery

This introduction has highlighted the potential of light activated systems as one major promising method to provide on-demand drug delivery systems, with the potential to address unmet therapeutic needs. The properties of liquid crystalline systems, i.e. thermodynamic stability, versatility in structure, direct link between structure and drug release, and inherent biocompatibility therefore poses the research question of whether liquid crystalline systems can be designed to perform as an effective light responsive drug delivery systems.

1.6. Hypotheses

It is envisaged that lipid-based liquid crystals can be manipulated through the use of stimuli-responsive additives to act as a non-invasive, externally activated, reversible, multi-dosing drug delivery system.

1. That the internal nanostructure of bulk liquid crystal systems can be rendered light sensitive through inclusion of light sensitive materials into the matrix.
2. That light-activated changes in liquid crystalline nanostructure are reversible and depend on three main factors: the quantity and properties of additive incorporated in to the matrix, the interplay between the light responsive moiety and the liquid crystalline nanostructure, and thirdly, the nature of the irradiation source.

3. That dispersed particles of light responsive liquid crystalline materials exhibit similar photoresponsive behaviour to the bulk, non-dispersed material.
4. That bulk light-responsive liquid crystal systems act as a sustained release drug depot which can be switched on/off through external optical activation *in vitro* and *in vivo*.

1.7. Aims

1. To identify photoresponsive bulk and dispersed lipid-based liquid crystal systems.
    a. By determining whether the inclusion of plasmonic particles enables NIR Irradiation to trigger changes in phase structure via the photothermal heating effect.
    b. By investigating a range of photochromic systems including azobenzenes and spiropyran additives for their ability to disrupt lipid packing in response to UV irradiation, thus changing the effective packing parameter in the matrix, leading to phase changes.
2. To characterise and optimise light-responsive liquid crystals by understanding:
    a. the effect of irradiation on liquid crystals containing light responsive elements;
    b. the nature of the interaction between the lipid and light sensitive components, that is the influence of surface functionalisation of gold nanorods and the properties of photochromic components on the self-assembled lipid structure; and
    c. the influence of system variables (composition, lipid type, light responsive element properties, irradiation frequency and duration) on the response of the nanomaterials to irradiation.
3. To understand the influence of dispersion of the hybrid matrix into sub-micron sized particles on the response of the materials to irradiation.

4. To determine whether control over nanostructure in the hybrid materials can be translated into control over drug delivery behaviour *in vivo* though subcutaneous delivery of a light responsive matrix containing a model hydrophilic drug.

References

1. Fattal E, Bochot A. State of the art and perspectives for the delivery of antisense oligonucleotides and siRNA by polymeric nanocarriers. Int J Pharm. 2008;364(2):237-48.

2. Qiu Y, Park K. Environment-sensitive hydrogels for drug delivery. Advanced Drug Delivery Reviews. 2001 12/31/;53(3):321-39.

3. Andresen TL, Jensen SS, Jørgensen K. Advanced strategies in liposomal cancer therapy: Problems and prospects of active and tumor specific drug release. Progress in Lipid Research. 2005;44(1):68-97.

4. Kaasgaard T, Andresen TL. Liposomal cancer therapy: exploiting tumor characteristics. Expert Opinion on Drug Delivery 2010;7(2):225-43.

5. Garti N, Libster D, Aserin A. Lipid polymorphism in lyotropic liquid crystals for triggered release of bioactives. Food & Function. 2012;3(7):700-13.

6. Israelachvili JN, Mitchell DJ, Ninham BW. Theory of self-assembly of lipid bilayers and vesicles. Biochim Biophys Acta Biomembr. 1977;470(2):185-201.

7. Holmberg K, Jönsson B, Kronberg B, Lindman B. Surfactants and Polymers in Aqueous Solution. Chichester: John Wiley & Sons Ltd.; 2002.

8. Luzzati V, Delacroix H, Gulik A, Gulik-Krzywicki T, Mariani P, Vargas R, et al. The cubic phases of lipids. Studies in Surface Science and Catalysis. Volume 148: Elsevier; 2004. p. 17-40.

9. Hyde S. The Language of shape: the role of curvature in condensed matter--physics, chemistry, and biology. Amsterdam [Netherlands]; New York: Elsevier; 1997.

10. Seddon JM. Structure of the inverted hexagonal (HII) phase, and non-lamellar phase transitions of lipids. Biochim Biophys Acta Rev Biomembr. 1990;1031(1):1-69.

11. Lee KWY, Nguyen T-H, Hanley T, Boyd BJ. Nanostructure of liquid crystalline matrix determines in vitro sustained release and in vivo oral absorption kinetics for hydrophilic model drugs. Int J Pharm. 2009;365(1-2):190-9.

12. Hegmann T, Qi H, Marx V. Nanoparticles in Liquid Crystals: Synthesis, Self-Assembly, Defect Formation and Potential Applications. Journal of Inorganic and Organometallic Polymers and Materials. 2007;17(3):483-508.

13. Boyd BJ, Whittaker DV, Khoo S-M, Davey G. Lyotropic liquid crystalline phases formed from glycerate surfactants as sustained release drug delivery systems. Int J Pharm. 2006 Feb 17;309(1-2):218-26.

14. Boyd BJ, Khoo S-M, Whittaker DV, Davey G, Porter CJH. A lipid-based liquid crystalline matrix that provides sustained release and enhanced oral bioavailability for a model poorly water soluble drug in rats. Int J Pharm. 2007;340(1-2):52-60.

15. Phan S, Fong W-K, Kirby N, Hanley T, Boyd BJ. Evaluating the link between self-assembled mesophase structure and drug release. Int J Pharm. 2011;421(1):176-82.

16. Higuchi WI. Diffusional models useful in biopharmaceutics. Drug release rate processes. J Pharm Sci. 1967;56(3):315-24.

17. Fong W-K, Hanley T, Boyd BJ. Stimuli responsive liquid crystals provide 'on-demand' drug delivery *in vitro* and *in vivo*. J Contr Release. 2009;135(3):218-26.

18. Negrini R, Mezzenga R. pH-Responsive Lyotropic Liquid Crystals for Controlled Drug Delivery. Langmuir. 2011:null-null.

19. Kaasgaard T, Drummond CJ. Ordered 2-D and 3-D nanostructured amphiphile self-assembly materials stable in excess solvent. Phys Chem Chem Phys. 2006;8(43):4957-75.

20. Koynova R, Caffrey M. Phases and phase transitions of the phosphatidylcholines. Biochimica et Biophysica Acta (BBA) - Reviews on Biomembranes. 1998;1376(1):91-145.

21. Engström S. Cubic phases as drug delivery systems. Polym Preprint. 1990;31:2.

22. Chang CM, Bodmeier R. Swelling of and drug release from monoglyceride-based drug delivery systems. J Pharm Sci. 1997;86(6):747-52.

23. Chung H, Caffrey M. Polymorphism, mesomorphism, and metastability of monoelaidin in excess water. Biophys J. 1995 Nov;69(5):1951-63.

24. Yaghmur A, Laggner P, Almgren M, Rappolt M. Self-Assembly in Monoelaidin Aqueous Dispersions: Direct Vesicles to Cubosomes Transition. PLoS ONE. 2008;3(11):e3747.

25. Yaghmur A, Sartori B, Rappolt M. Self-Assembled Nanostructures of Fully Hydrated Monoelaidin-Elaidic Acid and Monoelaidin-Oleic Acid Systems. Langmuir. 2012 2012/07/03;28(26):10105-19.

26. Takahashi H, Matsuo A, Hatta I. Effects of salt on the lamellar and bicontinuous cubic phases of fully hydrated monoacylglycerol (monoelaidin). Phys Chem Chem Phys. 2002;4(11):2365-70.

27. Phytantriol Technical Information: BASF Aktiengesellschaft; 2003 [cited 2007 14 October]. Available from: http://www.basf.com/businesses/consumer/cosmeticingredients/docs/phytantriol_ti.pdf.

28. Final Report on the Safety Assessment of Phytantriol. International Journal of Toxicology 2007 January 1, 2007;26 (suppl. 1):107-14.

29. Hyde ST, Andersson S, Ericsson B, Larsson Kr. A cubic structure consisting of a lipid bilayer forming an infinite periodic minimum surface of the gyroid type in the glycerolmonooleat-water system. Z Krist. 1984 2011/03/28;168(1-4):213-9.

30. Kulkarni CV, Wachter W, Iglesias-Salto G, Engelskirchen S, Ahualli S. Monoolein: a magic lipid? Phys Chem Chem Phys. 2011;13(8):3004-21.

31. Barauskas J, Landh T. Phase Behavior of the Phytantriol/Water System. Langmuir. 2003;19(23):9562-5.

32. Dong Y-D, Larson I, Hanley T, Boyd BJ. Bulk and Dispersed Aqueous Phase Behavior of Phytantriol: Effect of Vitamin E Acetate and F127 Polymer on Liquid Crystal Nanostructure. Langmuir. 2006 August 14, 2006;22:7.

33. Barauskas J, Svedaite I, Butkus E, Razumas V, Larsson K, Tiberg F. Synthesis and aqueous phase behavior of 1-glyceryl monooleyl ether. Colloids Surf, B. 2005;41(1):49-53.

34. Popescu G, Barauskas J, Nylander T, Tiberg F. Liquid Crystalline Phases and Their Dispersions in Aqueous Mixtures of Glycerol Monooleate and Glyceryl Monooleyl Ether. Langmuir. 2006;23(2):496-503.

35. Yaghmur A, Glatter O. Characterization and potential applications of nanostructured aqueous dispersions. Advances in Colloid and Interface Science. 2009;147-148:333-42.

36. Gustafsson J, Ljusberg-Wahren H, Almgren M, Larsson Kr. Submicron Particles of Reversed Lipid Phases in Water Stabilized by a Nonionic Amphiphilic Polymer. Langmuir. 1997;13(26):6964-71.

37. Chong JYT, Mulet X, Waddington LJ, Boyd BJ, Drummond CJ. Steric stabilisation of self-assembled cubic lyotropic liquid crystalline nanoparticles: high throughput evaluation of triblock polyethylene oxide-polypropylene oxide-polyethylene oxide copolymers. Soft Matter. 2011;7(10):4768-77.

38. Gan L, Han S, Shen J, Zhu J, Zhu C, Zhang X, et al. Self-assembled liquid crystalline nanoparticles as a novel ophthalmic delivery system for dexamethasone: Improving preocular retention and ocular bioavailability. Int J Pharm. 2010;396(1-2):179-87.

39. Boyd BJ. Characterisation of drug release from cubosomes using the pressure ultrafiltration method. Int J Pharm. 2003 Jul;260(2):239-47.

40. Boyd BJ. Controlled release from cubic liquid-crystalline particles. In: Lynch ML, Spicer PT, editors. Bicontinuous liquid crystals 2005. p. 285–306.

41. Leesajakul W, Nakano M, Taniguchi A, Handa T. Interaction of cubosomes with plasma components resulting in the destabilization of cubosomes in plasma. Colloids Surf, B. 2004;34(4):253-8.

42. Nguyen T-H, Hanley T, Porter CJH, Boyd BJ. Nanostructured liquid crystalline particles provide long duration sustained-release effect for a poorly water soluble drug after oral administration. J Contr Release. 2011;153(2):180-6.

43. Nguyen TH, Hanley T, Porter CJH, Larson I, Boyd BJ. Phytantriol and glyceryl monooleate cubic liquid crystalline phases as sustained-release oral drug delivery systems for poorly water-soluble drugs II. In-vivo evaluation. Journal of Pharmacy and Pharmacology. 2010;62(7):856-65.

44. Lynch ML, Ofori-Boateng A, Hippe A, Kochvar K, Spicer PT. Enhanced loading of water-soluble actives into bicontinuous cubic phase liquid crystals using cationic surfactants. Journal of Colloid and Interface Science. 2003;260(2):404-13.

45. Lindell K, Engblom J, Engström S, Jonströmer M, Carlsson A. Influence of a charged phospholipid on the release pattern of timolol maleate from cubic liquid crystalline phases. 1998. p. 111-8.

46. Clogston J, Craciun G, Hart DJ, Caffrey M. Controlling release from the lipidic cubic phase by selective alkylation. Journal of Controlled Release. 2005;102(2):441-61.

47. Rizwan SB, Dong YD, Boyd BJ, Rades T, Hook S. Characterisation of bicontinuous cubic liquid crystalline systems of phytantriol and water using cryo field emission scanning electron microscopy (cryo FESEM). Micron. 2007;38(5):478-85.

48. Boyd BJ, Rizwan SB, Dong Y-D, Hook S, Rades T. Self-Assembled Geometric Liquid-Crystalline Nanoparticles Imaged in Three Dimensions: Hexosomes Are Not Necessarily Flat Hexagonal Prisms. Langmuir. 2007;23(25):12461-4.

49. Conn CE, Ces O, Mulet X, Finet S, Winter R, Seddon JM, et al. Dynamics of structural transformations between lamellar and inverse bicontinuous cubic lyotropic phases. Physical Review Letters. 2006;96(10).

50. Brink-van der Laan EV, Killian JA, de Kruijff B. Nonbilayer lipids affect peripheral and integral membrane proteins via changes in the lateral pressure profile. Biochimica Et Biophysica Acta-Biomembranes. 2004;1666(1-2):275-88.

51. Kriechbaum M, Laggner P. States of phase transitions in biological structures. Progress in Surface Science. 1996;51(3):233-61.

52. Rappolt M, Hickel A, Bringezu F, Lohner K. Mechanism of the Lamellar/Inverse Hexagonal Phase Transition Examined by High Resolution X-Ray Diffraction. 2003;84:3111-22.

53. Bisby RH, Mead C, Morgan CG. Photosensitive liposomes as 'cages' for laser-triggered solute delivery: the effect of bilayer cholesterol on kinetics of solute release. FEBS Letters 1999;463(1-2):165-8.

54. Aota-Nakano Y, Li SJ, Yamazaki M. Effects of electrostatic interaction on the phase stability and structures of cubic phases of monoolein/oleic acid mixture membranes. Biochim Biophys Acta Biomembr. 1999;1461(1):96-102.

55. Borne J, Nylander T, Khan A. Phase Behavior and Aggregate Formation for the Aqueous Monoolein System Mixed with Sodium Oleate and Oleic Acid. Langmuir. 2001;17(25):7742-51.

56. Dong Y-D, Larson I, Hanley T, Boyd BJ. Bulk and Dispersed Aqueous Phase Behavior of Phytantriol: Effect of Vitamin E Acetate and F127 Polymer on Liquid Crystal Nanostructure. Langmuir 2006;22(23):9512-8.

57. Kulkarni CV, Tang T-Y, Seddon AM, Seddon JM, Ces O, Templer RH. Engineering bicontinuous cubic structures at the nanoscale-the role of chain splay. Soft Matter. 2010;6(14):3191-4.

58. Bayer CL, Peppas NA. Advances in recognitive, conductive and responsive delivery systems J Contr Release. 2008;132(3):216-21.

59. Couvreur P, Vauthier C. Nanotechnology: Intelligent design to treat complex disease. Pharm Res. 2006 Jul;23(7):1417-50.

60. Torchilin V. Multifunctional and stimuli-sensitive pharmaceutical nanocarriers. European Journal of Pharmaceutics and Biopharmaceutics. 2009;71(3):431-44.

61. Kost J, Langer R. Responsive polymeric delivery systems. Adv Drug Deliv Rev. 2001;46(1-3):125-48.

62. Li WJ, Szoka FC. Lipid-based nanoparticles for nucleic acid delivery. Pharm Res. 2007 Mar;24(3):438-49.

63. Perrier E, Hart J. Smart Vectorization. In: Rosen MR, editor. Delivery System Handbook for Personal Care and Cosmetic Products - Technology, Applications and Formulations: William Andrew Publishing; 2005. p. 797-816.

64. Rosen MR, editor. Delivery System Handbook for Personal Care and Cosmetic Products - Technology, Applications and Formulations: William Andrew Publishing; 2005.

65. Mezzenga R, Schurtenberger P, Burbidge A, Michel M. Understanding foods as soft materials. Nat Mater. 2005;4(10):729-40.

66. Leser ME, Sagalowicz L, Michel M, Watzke HJ. Self-assembly of polar food lipids. Advances in Colloid and Interface Science. 2006;123-126:125-36.

67. Amar-Yuli I, Libster D, Aserin A, Garti N. Solubilization of food bioactives within lyotropic liquid crystalline mesophases. Curr Opin Colloid Interface Sci. 2009;14(1):21-32.

68. Garti N, Yaghmur A, Aserin A, Spernath A, Elfakess R, Ezrahi S. Solubilization of active molecules in microemulsions for improved environmental protection. Colloid Surface Physicochem Eng Aspect. 2003;230(1-3):183-90.

69. Chung H, Kim J, Um JY, Kwon IC, Jeong SY. Self-assembled "nanocubicle" as a carrier for peroral insulin delivery. Diabetologia. 2002;45(3):448-51.

70. Kelkar SS, Reineke TM. Theranostics: Combining Imaging and Therapy. Bioconjugate Chemistry. 2011 2011/10/19;22(10):1879-903.

71. Hsu J. Drug delivery methods for posterior segment disease. Current Opinion in Opthalmology. 2007;18(3):235-9.

72. Janoria KG, Gunda S, Boddu SH, Mitra AK. Novel approaches to retinal drug delivery. Expert Opinion on Drug Delivery. 2007 Jul;4(4):371-88.

73. Thrimawithana TR, Young S, Bunt CR, Green C, Alany RG. Drug delivery to the posterior segment of the eye. Drug Discovery Today. 2010;16(5-6):270-7.

74. Wanakule P, Roy K. Disease-Responsive Drug Delivery: The Next Generation of Smart Delivery Devices. Current Drug Metabolism. 2012;13(1):42-9.

75. Carregal-Romero S, Ochs M, Rivera-Gil P, Ganas C, Pavlov AM, Sukhorukov GB, et al. NIR-light triggered delivery of macromolecules into the cytosol. J Contr Release. 2012;159(1):120-7.

76. Oates TW, Huynh-Ba G, Vargas A, Alexander P, Feine J. A critical review of diabetes, glycemic control, and dental implant therapy. Clinical Oral Implants Research. 2013;24(2):117-27.

77. Bajpai AK, Shukla SK, Bhanu S, Kankane S. Responsive polymers in controlled drug delivery. Progress in Polymer Science. 2008;33(11):1088-118.

78. Kaminskas L, Boyd B. Nanosized Drug Delivery Vectors and the Reticuloendothelial System. In: Prokop A, editor. Intracellular Delivery. Fundamental Biomedical Technologies. 5: Springer Netherlands; 2011. p. 155-78.

79. Moghimi SM, Szebeni J. Stealth liposomes and long circulating nanoparticles: critical issues in pharmacokinetics, opsonization and protein-binding properties. Progress in Lipid Research. 2003;42(6):463-78.

80. Jeon SI, Lee JH, Andrade JD, Degennes PG. Protein surface interactions in the presence of polyethylene oxide.1. Simplified theory. J Colloid Interface Sci. 1991;142(1):149-58.

81. Davis FF. The origin of pegnology. Adv Drug Deliv Rev. 2002; 54(4):457-8.

82. Gabizon A, Catane R, Uziely B, Kaufman B, Safra T, Cohen R, et al. Prolonged Circulation Time and Enhanced Accumulation in Malignant Exudates of Doxorubicin Encapsulated in Polyethylene-glycol Coated Liposomes. Cancer Res. 1994 February 15, 1994;54(4):987-92.

83. Lee RJ, Low PS. Delivery of Liposomes into Cultured KB Cells via Folate Receptor-Mediated Endocytosis. J Biol Chem. 1994 Feb;269(5):3198-204.

84. Saul JM, Annapragada AV, Bellamkonda RV. A dual-ligand approach for enhancing targeting selectivity of therapeutic nanocarriers. J Contr Release. 2006;114(3):277-87.

85. Maruyama K, Ishida O, Takizawa T, Moribe K. Possibility of active targeting to tumor tissues with liposomes. Adv Drug Deliv Rev. 1999;40(1-2):89-102.

86. Hood JD, Bednarski M, Frausto R, Guccione S, Reisfeld RA, Xiang R, et al. Tumor regression by targeted gene delivery to the neovasculature. Science. 2002 Jun;296(5577):2404-7.

87. Schiffelers RM, Koning GA, ten Hagen TLM, Fens MHAM, Schraa AJ, Janssen APCA, et al. Anti-tumor efficacy of tumor vasculature-targeted liposomal doxorubicin. J Contr Release. 2003;91(1-2):115-22.

88. Torchilin V, Klibanov A, Huang L, O'Donnell S, Nossiff N, Khaw B. Targeted accumulation of polyethylene glycol-coated immunoliposomes in infarcted rabbit myocardium. FASEB J. 1992 June 1, 1992;6(9):2716-9.

89. Khaw BA, Torchilin VP, Vural I, Narula J. Plug and Seal - Prevention of Hypoxic Cardiocyte Death by Sealing Membrane Lesions with Antimyosin-Liposomes. Nat Med. 1995 Nov;1(11):1195-8.

90. Khudairi T, Khaw B-A. Preservation of ischemic myocardial function and integrity with targeted cytoskeleton-specific immunoliposomes. J Am Coll Cardiol. 2004 May 5, 2004;43(9):1683-9.

91. Maruyama K, Takahashi N, Tagawa T, Nagaike K, Iwatsuru M. Immunoliposomes bearing polyethyleneglycol-coupled Fab' fragment show prolonged circulation time and high extravasation into targeted solid tumors in vivo. FEBS Letters. 1997;413(1):177-80.

92. Cheng WWK, Allen TM. Targeted delivery of anti-CD19 liposomal doxorubicin in B-cell lymphoma: A comparison of whole monoclonal antibody, Fab' fragments and single chain Fv. J Contr Release. 2008;126(1):50-8.

93. Laginha K, Mumbengegwi D, Allen T. Liposomes targeted via two different antibodies: Assay, B-cell binding and cytotoxicity. Biochim Biophys Acta Biomembr. 2005;1711(1):25-32.

94. Moro M, Pelagi M, Fulci G, Paganelli G, Dellabona P, Casorati G, et al. Tumor cell targeting with antibody-avidin complexes and biotinylated tumor necrosis factor alpha. Cancer Res. 1997 May;57(10):1922-8.

95. Jayanna PK, Torchilin VP, Petrenko VA. Liposomes targeted by fusion phage proteins. Nanomedicine: Nanotechnology, Biology and Medicine. 2009;5(1):83-9.

96. Gerweck LE, Seetharaman K. Cellular pH Gradient in Tumor versus Normal Tissue: Potential Exploitation for the Treatment of Cancer. Cancer Res. 1996 March 15, 1996;56(6):1194-8.

97. Kopecek J, Yang J. Hydrogels as smart biomaterials. Polymer International. 2007;56(9):1078-98.

98. Oh JK, Lee DI, Park JM. Biopolymer-based microgels/nanogels for drug delivery applications. Progress in Polymer Science. 2009;In Press, Corrected Proof.

99. Yatvin M, Kreutz W, Horwitz B, Shinitzky M. pH-sensitive liposomes: possible clinical implications. Science. 1980 December 12, 1980;210(4475):1253-5.

100. Guo X, Szoka FC. Chemical Approaches to Triggerable Lipid Vesicles for Drug and Gene Delivery. Accounts Chem Res 2003;36(5):335-41.

101. Drummond DC, Zignani M, Leroux J-C. Current status of pH-sensitive liposomes in drug delivery. Progress in Lipid Research. 2000;39(5):409-60.

102. Gerasimov OV, Boomer JA, Qualls MM, Thompson DH. Cytosolic drug delivery using pH- and light-sensitive liposomes. Adv Drug Deliv Rev. 1999;38(3):317-38.

103. Negrini R, Mezzenga R. pH-Responsive Lyotropic Liquid Crystals for Controlled Drug Delivery. Langmuir. 2011 May;27(9):5296-303.

104. Slepushkin VA, SimÃµes S, Dazin P, Newman MS, Guo LS, De Lima MCP, et al. Sterically stabilized pH-sensitive liposomes. Intracellular delivery of aqueous contents and prolonged circulation in vivo. J Biol Chem. 1997;272(4):2382-8.

105. Kirpotin D, Hong K, Mullah N, Papahadjopoulos D, Zalipsky S. Liposomes with detachable polymer coating: destabilization and fusion of dioleoylphosphatidylethanolamine vesicles triggered by cleavage of surface-grafted poly(ethylene glycol). FEBS Letters. 1996;388(2-3):115-8.

106. Zhang JX, Zalipsky S, Mullah N, Pechar M, Allen TM. Pharmaco attributes of dioleoylphosphatidylethanolamine/cholesterylhemisuccinate liposomes containing different types of cleavable lipopolymers. Pharmacological Research. 2004;49(2):185-98.

107. Hong MS, Lim SJ, Oh YK, Kim CK. pH-sensitive, serum-stable and long-circulating liposomes as a new drug delivery system. Journal of Pharmacy and Pharmacology. 2002;54:51-8.

108. Torchilin VP, Lukyanov AN, Klibanov AL, Omelyanenko VG. Interaction between oleic acid-containing pH-sensitive and plain liposomes Fluorescent spectroscopy studies. FEBS Letters. 1992;305(3):185-8.

109. Chernomordik L. Non-bilayer lipids and biological fusion intermediates. Chemistry and Physics of Lipids. 1996;81(2):203-13.

110. Shin J, Shum P, Thompson DH. Acid-triggered release via dePEGylation of DOPE liposomes containing acid-labile vinyl ether PEG-lipids. J Contr Release. 2003;91(1-2):187-200.

111. Boomer JA, Inerowicz HD, Zhang Z-Y, Bergstrand N, Edwards K, Kim J-M, et al. Acid-Triggered Release from Sterically Stabilized Fusogenic Liposomes via a Hydrolytic DePEGylation Strategyâ€ Langmuir. 2003;19(16):6408-15.

112. Guo X, Szoka FC. Steric Stabilization of Fusogenic Liposomes by a Low-pH Sensitive PEG-Diortho Ester-Lipid Conjugate. Bioconjugate Chemistry 2001;12(2):291-300.

113. Heller J, Himmelstein KJ, Kenneth JW, Ralph G. Poly(ortho ester) biodegradable polymer systems. Methods in Enzymology. Volume 112: Academic Press; 1985. p. 422-36.

114. Mills JK, Eichenbaum G, Needham D. Effect of Bilayer Cholesterol and Surface Grafted Poly(Ethylene Glycol) on pH-Induced Release of Contents from Liposomes by Poly(2-Ethylacrylic Acid). Journal of Liposome Research 1999;9(2):275-90.

115. Yuba E, Harada A, Sakanishi Y, Kono K. Carboxylated hyperbranched poly(glycidol)s for preparation of pH-sensitive liposomes. J Contr Release. 2010;149(1):72-80.

116. Roux E, Lafleur M, Lataste E, Moreau P, Leroux JC. On the characterization of pH-sensitive liposome/polymer complexes. Biomacromolecules. 2003 Mar-Apr;4(2):240-8.

117. Collins D, Litzinger DC, Huang L. Structural and Functional Comparisons of pH-Sensitive Liposomes Composed of Phosphatidylethanolamine and 3 Different Diacylsuccinylglycerols. Biochimica Et Biophysica Acta. 1990 Jun;1025(2):234-42.

118. Saito G, Swanson JA, Lee K-D. Drug delivery strategy utilizing conjugation via reversible disulfide linkages: role and site of cellular reducing activities. Adv Drug Deliv Rev. 2003;55(2):199-215.

119. West KR, Otto S. Reversible Covalent Chemistry in Drug Delivery. Current Drug Discovery Technologies. 2005;2:123-60.

120. Ishida T, Kirchmeier MJ, Moase EH, Zalipsky S, Allen TM. Targeted delivery and triggered release of liposomal doxorubicin enhances cytotoxicity against human B lymphoma cells. Biochim Biophys Acta Biomembr. 2001;1515(2):144-58.

121. Bhavane R, Karathanasis E, Annapragada AV. Agglomerated vesicle technology: a new class of particles for controlled and modulated pulmonary drug delivery. J Contr Release. 2003;93(1):15-28.

122. Karathanasis E, Ayyagari AL, Bhavane R, Bellamkonda RV, Annapragada AV. Preparation of in vivo cleavable agglomerated liposomes suitable for modulated pulmonary drug delivery. J Contr Release. 2005;103(1):159-75.

123. Greaves TL, Drummond CJ. Ionic liquids as amphiphile self-assembly media. Chem Soc Rev. 2008;37(8):1709-26.

124. Czeslik C, Winter R, Rapp G, Bartels K. Temperature- and pressure-dependent phase behavior of monoacylglycerides monoolein and monoelaidin. Biophys J. 1995;68(4):1423-9.

125. Winter R, Erbes J, Templer RH, Seddon JM, Syrykh A, Warrender NA, et al. Inverse bicontinuous cubic phases in fatty acid/phosphatidylcholine mixtures: the effects of pressure and lipid composition. Phys Chem Chem Phys. 1999 Mar;1(5):887-93.

126. Yaghmur A, Kriechbaum M, Amenitsch H, Steinhart M, Laggner P, Rappolt M. Effects of Pressure and Temperature on the Self-Assembled Fully Hydrated Nanostructures of Monoolein-Oil Systems. Langmuir. 2009;26(2):1177-85.

127. Baxter LT, Jain RK. Transport of fluid and macromolecules in tumors. II. Role of heterogeneous perfusion and lymphatics. Microvascular Research. 1990 9//;40(2):246-63.

128. Shen Y, Zhang Y, Kuehner D, Yang G, Yuan F, Niu L. Ion-Responsive Behavior of Ionic-Liquid Surfactant Aggregates with Applications in Controlled Release and Emulsification. ChemPhysChem. 2008;9(15):2198-202.

129. Yaghmur A, Laggner P, Sartori B, Rappolt M. Calcium Triggered L-alpha-H-2 Phase Transition Monitored by Combined Rapid Mixing and Time-Resolved Synchrotron SAXS. PLoS ONE. 2008 Apr;3(4):11.

130. Clogston J, Caffrey M. Controlling release from the lipidic cubic phase. Amino acids, peptides, proteins and nucleic acids. J Contr Release. 2005;107(1):97-111.

131. Meers P. Enzyme-activated targeting of liposomes. Adv Drug Deliv Rev. 2001;53(3):265-72.

132. Davidsen J, Jørgensen K, Andresen TL, Mouritsen OG. Secreted phospholipase A2 as a new enzymatic trigger mechanism for localised liposomal drug release and absorption in diseased tissue. Biochim Biophys Acta Biomembr. 2003;1609(1):95-101.

133. Davidsen J, Vermehren C, Frokjaer S, Mouritsen OG, Jørgensen K. Drug delivery by phospholipase A2 degradable liposomes. Int J Pharm. 2001;214(1-2):67-9.

134. Montes LR, Goni FM, Johnston NC, Goldfine H, Alonso A. Membrane Fusion Induced by the Catalytic Activity of a Phospholipase C/Sphingomyelinase from Listeria monocytogenesâ€ Biochemistry. 2004;43(12):3688-95.

135. Nieva JL, Goni FM, Alonso A. Liposome fusion catalytically induced by phospholipase C. Biochemistry. 1989;28(18):7364-7.

136. Ruiz-Arguello MB, Goni FM, Alonso A. Phospholipase C Hydrolysis of Phospholipids in Bilayers of Mixed Lipid Compositions. Biochemistry. 1998;37(33):11621-8.

137. Pak CC, Ali S, Janoff AS, Meers P. Triggerable liposomal fusion by enzyme cleavage of a novel peptide-lipid conjugate. Biochim Biophys Acta Biomembr. 1998;1372(1):13-27.

138. Pak CC, Erukulla RK, Ahl PL, Janoff AS, Meers P. Elastase activated liposomal delivery to nucleated cells. Biochim Biophys Acta Biomembr. 1999;1419(2):111-26.

139. Sarkar NR, Rosendahl T, Krueger AB, Banerjee AL, Benton K, Mallik S, et al. "Uncorking" of liposomes by matrix metalloproteinase-9. Chem Comm. 2005 (8):999-1001.

140. Terada T, Iwai M, Kawakami S, Yamashita F, Hashida M. Novel PEG-matrix metalloproteinase-2 cleavable peptide-lipid containing galactosylated liposomes for hepatocellular carcinoma-selective targeting. J Contr Release. 2006;111(3):333-42.

141. Ong W, Yang Y, Cruciano AC, McCarley RL. Redox-Triggered Contents Release from Liposomes. J Am Chem Soc. 2008;130(44):14739-44.

142. Davis SC, Szoka FC. Cholesterol Phosphate Derivatives: Synthesis and Incorporation into a Phosphatase and Calcium-Sensitive Triggered Release Liposome. Bioconjugate Chemistry. 1998;9(6):783-92.

143. Lan-rong H, Ho RJY, Huang L. Trypsin induced destabilization of liposomes composed of dioleoylphosphatidylethanolamine and glycophorin. Biochem Biophys Res Comm. 1986;141(3):973-8.

144. Arruebo M, Fernández-Pacheco R, Ibarra MR, Santamaría J. Magnetic nanoparticles for drug delivery. Nano Today. 2007;2(3):22-32.

145. Blasi P, Giovagnoli S, Schoubben A, Ricci M, Rossi C. Solid lipid nanoparticles for targeted brain drug delivery. Adv Drug Deliv Rev. 2007;59(6):454-77.

146. Jain TK, Richey J, Strand M, Leslie-Pelecky DL, Flask CA, Labhasetwar V. Magnetic nanoparticles with dual functional properties: Drug delivery and magnetic resonance imaging. Biomaterials. 2008;29(29):4012-21.

147. Yanase M, Shinkai M, Honda H, Wakabayashi T, Yoshida J, Kobayashi T. Intracellular Hyperthermia for Cancer Using Magnetite Cationic Liposomes: Ex vivo Study. Cancer Science. 1997;88(7):630-2.

148. Kumar A, Jena PK, Behera S, Lockey RF, Mohapatra S, Mohapatra S. Multifunctional magnetic nanoparticles for targeted delivery. Nanomedicine: Nanotechnology, Biology and Medicine 2009;6(1):64-9.

149. Viroonchatapan E, Sato H, Ueno M, Adachi I, Tazawa K, Horikoshi I. Magnetic targeting of thermosensittve magnetoliposomes to mouse livers in an in situ on-line perfusion system. Life Sciences. 1996;58(24):2251-61.

150. Nobuto H, Sugita T, Kubo T, Shimose S, Yasunaga Y, Murakami T, et al. Evaluation of systemic chemotherapy with magnetic liposomal doxorubicin and a dipole external electromagnet. International Journal of Cancer. 2004;109(4):627-35.

151. Zhu L, Huo ZL, Wang LL, Tong X, Xiao Y, Ni KY. Targeted delivery of methotrexate to skeletal muscular tissue by thermosensitive magnetoliposomes. Int J Pharm. 2009 Mar;370(1-2):136-43.

152. Kubo T, Sugita T, Shimose S, Nitta Y, Ikuta Y, Murakami T. Targeted delivery of anticancer drugs with intravenously administered magnetic liposomes in osteosarcoma-bearing hamsters. Int J Oncol. 2000 Aug;17(2):309-15.

153. Nappini S, Bombelli FB, Bonini M, Norden B, Baglioni P. Magnetoliposomes for controlled drug release in the presence of low-frequency magnetic field. Soft Matter. 2010;6(1):154-62.

154. Satarkar NS, Hilt JZ. Magnetic hydrogel nanocomposites for remote controlled pulsatile drug release. J Contr Release. 2008;130(3):246-51.

155. Krack M, Hohenberg H, Kornowski A, Lindner P, Weller H, FoÌˆrster S. Nanoparticle-Loaded Magnetophoretic Vesicles. J Am Chem Soc. 2008;130(23):7315-20.

156. Wu J, Nyborg WL. Ultrasound, cavitation bubbles and their interaction with cells. Adv Drug Deliv Rev. 2008;60(10):1103-16.

157. Husseini GA, Myrup GD, Pitt WG, Christensen DA, Rapoport NY. Factors affecting acoustically triggered release of drugs from polymeric micelles. J Contr Release. 2000;69(1):43-52.

158. Lin H-Y, Thomas JL. PEG-Lipids and Oligo(ethylene glycol) Surfactants Enhance the Ultrasonic Permeabilizability of Liposomes. Langmuir. 2003;19(4):1098-105.

159. Schroeder A, Avnir Y, Weisman S, Najajreh Y, Gabizon A, Talmon Y, et al. Controlling Liposomal Drug Release with Low Frequency Ultrasound: Mechanism and Feasibility. Langmuir 2007;23(7):4019-25.

160. Schroeder A, Kost J, Barenholz Y. Ultrasound, Liposomes, and Drug Delivery: Principles for Using Ultrasound to Control the Release of Drugs from Liposomes. Chemistry and Physics of Lipids. 2009;162(1-2):1-16.

161. Chen D, Wu J. An in vitro feasibility study of controlled drug release from encapsulated nanometer liposomes using high intensity focused ultrasound. Ultrasonics. 2010;In Press, Uncorrected Proof.

162. Huang S-L, MacDonald RC. Acoustically active liposomes for drug encapsulation and ultrasound-triggered release. Biochim Biophys Acta Biomembr. 2004;1665(1-2):134-41.

163. Liu Y, Miyoshi H, Nakamura M. Encapsulated ultrasound microbubbles: Therapeutic application in drug/gene delivery. J Contr Release. 2006;114(1):89-99.

164. Zasadzinski JA. Transmission electron microscopy observations of sonication-induced changes in liposome structure. Biophys J. 1986;49(6):1119-30.

165. Huang C-H. Phosphatidylcholine vesicles. Formation and physical characteristics. Biochemistry. 1969;8(1):344-52.

166. Ljusberg-Wahern H, Nyberg L, Larsson K. Dispersion of the cubic liquid crystalline phase - Structure preparation and functionality aspects. Chimica Oggi-Chemistry Today. 1996 Jun;14(6):40-3.

167. Landh T, Larsson K, inventors; GS Biochem AB, assignee. Particles, method of preparing said particles and uses thereof patent 5531925 1993.

168. Clarke PR, Hill CR. Physical and Chemical Aspects of Ultrasonic Disruption of Cells. The Journal of the Acoustical Society of America. 1970;47(2B):649-53.

169. Liu J, Lewis TN, Prausnitz MR. Non-Invasive Assessment and Control of Ultrasound-Mediated Membrane Permeabilization. Pharm Res. 1998;15(6):918-24.

170. Anna Y, Matthieu L-C, Mariska DS, Sander L, Holger G, Chrit M. In vivo temperature controlled ultrasound-mediated intracellular delivery of cell-impermeable compounds. J Contr Release. 2012;161(1):90-7.

171. Dewhirst MW, Prosnitz L, Thrall D, Prescott D, Clegg S, Charles C, et al. Hyperthermic treatment of malignant diseases: Current status and a view toward the future. Seminars in Oncology. 1997 Dec;24(6):616-25.

172. Hettinga JVE, Konings AWT, Kampinga HH. Reduction of cellular cisplatin resistance by hyperthermia - a review. International Journal of Hyperthermia. 1997;13(5):439-57.

173. Mackanos MA, Larabi M, Shinde R, Simanovskii DM, Guccione S, Contag CH. Laser-induced disruption of systemically administered liposomes for targeted drug delivery. J Biomed Opt. 2009 Jul-Aug;14(4):8.

174. Weinstein JN, Magin RL, Yatvin MB, Zaharko DS. Liposomes and Local Hyperthermia - Selective Delivery of Methotrexate to Heated Tumors. Science. 1979;204(4389):188-91.

175. Ponce AM, Vujaskovic Z, Yuan F, Needham D, Dewhirst MW. Hyperthermia mediated liposomal drug delivery. International Journal of Hyperthermia. 2006;22(3):205-13.

176. Gaber MH. Modulation of Doxorubicin Resistance in Multidrug-resistance Cells by Targeted Liposomes Combined with Hyperthermia. Journal of Biochemistry, MolBiol& Biophys. 2002;6(5):309 - 14.

177. Gaber MH, Wu NZ, Hong KL, Huang SK, Dewhirst MW, Papahadjopoulos D. Thermosensitive liposomes: Extravasation and release of contents in tumor microvascular networks. Int J Radiat Oncol Biol Phys. 1996 Dec;36(5):1177-87.

178. Desmettre TJ, Soulie-Begu S, Devoisselle JM, Mordon SR. Diode laser-induced thermal damage evaluation on the retina with a liposome dye system. Lasers in Surgery and Medicine. 1999;24(1):61-8.

179. Mordon S, Desmettre T, Devoisselle JM, Soulie S. Fluorescence measurement of 805 nm laser-induced release of 5,6-CF from DSPC liposomes for real-time monitoring of temperature: An in vivo study in rat liver using indocyanine green potentiation. Lasers in Surgery and Medicine. 1996;18(3):265-70.

180. Viroonchatapan E, Sato H, Ueno M, Adachi I, Tazawa K, Horikoshi I. Release of 5-fluorouracil from thermosensitive magnetoliposomes induced by an electromagnetic field. J Contr Release. 1997;46(3):263-71.

181. Babincová M, Cicmanec P, Altanerová V, Altaner C, Babinec P. AC-magnetic field controlled drug release from magnetoliposomes: design of a method for site-specific chemotherapy. Bioelectrochemistry 2002;55(1-2):17-9.

182. Needham D, Anyarambhatla G, Kong G, Dewhirst MW. A New Temperature-sensitive Liposome for Use with Mild Hyperthermia: Characterization and Testing in a Human Tumor Xenograft Model. Cancer Res. 2000 March 1, 2000;60(5):1197-201.

183. Yatvin MB, Weinstein JN, Dennis WH, Blumenthal R. Design of Liposomes for Enhanced Local Release of Drugs by Hyperthermia. Science. 1978; 202(4374):1290-3.

184. Kono K, Nakai R, Morimoto K, Takagishi T. Thermosensitive polymer-modified liposomes that release contents around physiological temperature. Biochim Biophys Acta Biomembr. 1999;1416(1-2):239-50.

185. Kono K. Thermosensitive polymer-modified liposomes. Adv Drug Deliv Rev. 2001 Dec;53(3):307-19.

186. Kono K, Murakami T, Yoshida T, Haba Y, Kanaoka S, Takagishi T, et al. Temperature Sensitization of Liposomes by use of thermosensitive block copolymers synthesized by living cationic polymerization: Effect of copolymer chain length. Bioconjugate Chemistry. 2005 Nov-Dec;16(6):1367-74.

187. Kono K, Yoshino K, Takagishi T. Effect of poly(ethylene glycol) grafts on temperature-sensitivity of thermosensitive polymer-modified liposomes. J Contr Release. 2002 Apr;80(1-3):321-32.

188. Yoshino K, Kadowaki A, Takagishi T, Kono K. Temperature sensitization of liposomes by use of N-isopropylacrylamide copolymers with varying transition endotherms. Bioconjugate Chemistry. 2004 Sep-Oct;15(5):1102-9.

189. Petrov RR, Chen WH, Regen SL. Thermally Gated Liposomes: A Closer Look. Bioconjugate Chemistry. 2009 May;20(5):1037-43.

190. Chen W-H, Regen SL. Thermally Gated Liposomes. J Am Chem Soc. 2005;127(18):6538-9.

191. de Campo L, Yaghmur A, Sagalowicz L, Leser ME, Watzke H, Glatter O. Reversible Phase Transitions in Emulsified Nanostructured Lipid Systems. Langmuir. 2004;20(13):5254-61.

192. Eastoe J, Vesperinas A. Self-assembly of light-sensitive surfactants. Soft Matter. 2005;1(5):338-47.

193. Katz JS, Burdick JA. Light-Responsive Biomaterials: Development and Applications. Macromolecular Bioscience. 2010;10(4):339-48.

194. Shum P, Kim J-M, Thompson DH. Phototriggering of liposomal drug delivery systems. Adv Drug Deliv Rev 2001;53(3):273-84.

195. Alvarez-Lorenzo C, Bromberg L, Concheiro A. Light-sensitive Intelligent Drug Delivery Systems Photochem Photobiol. 2009;85(4):848-60.

196. Zeimer R, Goldberg MF. Novel ophthalmic therapeutic modalities based on noninvasive light-targeted drug delivery to the posterior pole of the eye. Adv Drug Deliv Rev. 2001;52(1):49-61.

197. Dolmans DEJGJ, Fukumura D, Jain RK. Photodynamic therapy for cancer. Nat Rev Cancer. 2003;3(5):380-7.

198. Anderson VC, Thompson DH. Triggered release of hydrophilic agents from plasmologen liposomes using visible light or acid. Biochim Biophys Acta Biomembr. 1992;1109(1):33-42.

199. Collier JH, Hu BH, Ruberti JW, Zhang J, Shum P, Thompson DH, et al. Thermally and Photochemically Triggered Self-Assembly of Peptide Hydrogels. J Am Chem Soc. 2001;123(38):9463-4.

200. Randles EG, Bergethon PR. A Photodependent Switch of Liposome Stability and Permeability. Langmuir. 2013.

201. Zhang ZY, Smith BD. Synthesis and characterization of NVOC-DOPE, a caged photoactivatable derivative of dioleoylphosphatidylethanolamine. Bioconjugate Chem. 1999 Nov-Dec;10(6):1150-2.

202. Spratt T, Bondurant B, O'Brien DF. Rapid release of liposomal contents upon photoinitiated destabilization with UV exposure. Biochim Biophys Acta Biomembr. 2003;1611(1-2):35-43.

203. Bisby RH, Mead C, Mitchell AC, Morgan CG. Fast Laser-Induced Solute Release from Liposomes Sensitized with Photochromic Lipid: Effects of Temperature, Lipid Host, and Sensitizer Concentration. Biochem Biophys Res Comm. 1999;262(2):406-10.

204. Liu Y-C, Le Ny A-LM, Schmidt J, Talmon Y, Chmelka BF, Lee CT. Photo-Assisted Gene Delivery Using Light-Responsive Catanionic Vesicles. Langmuir. 2009 2009/05/19;25(10):5713-24.

205. Lee H-i, Wu W, Oh JK, Mueller L, Sherwood G, Peteanu L, et al. Light-Induced Reversible Formation of Polymeric Micelles. Angewandte Chemie International Edition. 2007;46(14):2453-7.

206. Eastoe J, Dominguez MS, Wyatt P, Beeby A, Heenan RK. Properties of a Stilbene-Containing Gemini Photosurfactant: Light-Triggered Changes in Surface Tension and Aggregation. Langmuir. 2002 2002/10/01;18(21):7837-44.

207. Sun Z, Qin G, Xia X, Cronin-Golomb M, Omenetto FG, Kaplan DL. Photoresponsive retinal-modified silk-elastin copolymer. Journal of the American Chemical Society. 2013.

208. Tong X, Wang G, Soldera A, Zhao Y. How Can Azobenzene Block Copolymer Vesicles Be Dissociated and Reformed by Light? J Phys Chem B. 2005;109(43):20281-7.

209. Zhang J, Wang S-C, Lee CT. Photoreversible Conformational Changes in Membrane Proteins Using Light-Responsive Surfactants. J Phys Chem B. 2009;113(25):8569-80.

210. Khoukh S, Perrin P, Berc FBd, Tribet C. Reversible Light-Triggered Control of Emulsion Type and Stability. ChemPhysChem. 2005;6(10):2009-12.

211. Natansohn A, Rochon P. Photoinduced motions in azo-containing polymers. Chem Rev. 2002 Nov;102(11):4139-75.

212. Knoll H. Photoisomerism of Azobenzenes. In: Horspool WM, Lenci F, editors. CRC handbook of organic Photochem Photobiol. 2nd ed: CRC Press LLC; 2004.

213. Bufe M, Wolff T. Reversible Switching of Electrical Conductivity in an AOT-Isooctane-Water Microemulsion via Photoisomerization of Azobenzene. Langmuir. 2009;25(14):7927–31.

214. Cicciarelli BA, Elia JA, Hatton TA, Smith KA. Temperature Dependence of Aggregation and Dynamic Surface Tension in a Photoresponsive Surfactant System. Langmuir. 2007;23(16):8323-30.

215. Han M, Hara M. Intense Fluorescence from Light-Driven Self-Assembled Aggregates of Nonionic Azobenzene Derivative. J Am Chem Soc. 2005;127(31):10951-5.

216. Sorensen TJ, Kjaer K, Breiby DW, Laursen BW. Synthesis of Novel Amphiphilic Azobenzenes and X-ray Scattering Studies of Their Langmuir Monolayers. Langmuir. 2008;24(7):3223-7.

217. Haruta O, Matsuo Y, Ijiro K. Photo-induced fluorescence emission enhancement of azobenzene thin films. Colloid Surface Physicochem Eng Aspect. 2008;313-314:595-9.

218. Kumar B, Prajapati AK, Varia MC, Suresh KA. Novel Mesogenic Azobenzene Dimer at Air-Water and Air-Solid Interfaces. Langmuir. 2009;25(2):839-44.

219. Oki K, Nagasaka Y. Measurements of anisotropic surface properties of liquid films of azobenzene derivatives. Colloid Surface Physicochem Eng Aspect. 2009;333(1-3):182-6.

220. Song X, Perlstein J, Whitten DG. Photoreactive Supramolecular Assemblies: Aggregation and Photoisomerization of Azobenzene Phospholipids in Aqueous Bilayers. J Am Chem Soc. 1995;117(29):7816-7.

221. Eastoe J, Zou A, Espidel Y, Glatter O, Grillo I. Photo-labile lamellar phases. Soft Matter. 2008;4(6):1215-8.

222. Kuiper JM, Engberts JBFN. H-Aggregation of Azobenzene-Substituted Amphiphiles in Vesicular Membranes. Langmuir. 2004;20(4):1152-60.

223. Kuiper JM, Stuart MCA, Engberts JBFN. Photochemically Induced Disturbance of the Alkyl Chain Packing in Vesicular Membranes. Langmuir. 2008;24(2):426-32.

224. Lei Y, Hurst JK. Photoregulated Potassium Ion Permeation through Dihexadecyl Phosphate Bilayers Containing Azobenzene and Stilbene Surfactants. Langmuir. 1999;15(10):3424-9.

225. Zou A, Eastoe J, Mutch K, Wyatt P, Scherf G, Glatter O, et al. Light-sensitive lamellar phases. J Colloid Interface Sci. 2008;322(2):611-6.

226. Morgan CG, Bisby RH, Johnson SA, Mitchell AC. Fast solute release from photosensitive liposomes: an alternative to 'caged' reagents for use in biological systems. FEBS Letters. 1995;375(1-2):113-6.

227. Liu X-M, Yang B, Wang Y-L, Wang J-Y. Photoisomerisable cholesterol derivatives as photo-trigger of liposomes: Effect of lipid polarity, temperature, incorporation ratio, and cholesterol. Biochim Biophys Acta Biomembr. 2005;1720(1-2):28-34.

228. Liu J, He Y, Wang X. Azo Polymer Colloidal Spheres Containing Different Amounts of Functional Groups and Their Photoinduced Deformation Behavior. Langmuir. 2008;24(3):678-82.

229. Zhao Y-L, Stoddart JF. Azobenzene-Based Light-Responsive Hydrogel System. Langmuir. 2009;25(15):8442-6.

230. Tanaka T, Ogino H, Iwamoto M. Photochange in Pore Diameters of Azobenzene-Planted Mesoporous Silica Materials. Langmuir. 2007;23(23):11417-20.

231. Yamamoto T, Tabe Y, Yokoyama H. Photochemical transformation of topological defects formed around colloidal droplets dispersed in azobenzene-containing liquid crystals. Colloid Surface Physicochem Eng Aspect. 2009;334(1-3):155-9.

232. Corvazier L, Zhao Y. Induction of Liquid Crystal Orientation through Azobenzene-Containing Polymer Networks. Macromolecules. 1999;32(10):3195-200.

233. Yamamoto T, Tabe Y, Yokoyama H. Photonic manipulation of topological defects in liquid-crystal emulsions doped with azobenzene derivatives. Thin Solid Films. 2006;509(1-2):81-4.

234. Yi Y, Farrow MJ, Korblova E, Walba DM, Furtak TE. High-Sensitivity Aminoazobenzene Chemisorbed Monolayers for Photoalignment of Liquid Crystals. Langmuir. 2009;25(2):997-1003.

235. Khairutdinov RF, Hurst JK. Photocontrol of Ion Permeation through Bilayer Membranes Using an Amphiphilic Spiropyran. Langmuir. 2001;17(22):6881-6.

236. Wohl CJ, Kuciauskas D. Isomerization Dynamics of Photochromic Spiropyran Molecular Switches in Phospholipid Bilayers. J Phys Chem B. 2005;109(46):21893-9.

237. Drummond CJ, Furlong DN, Georgaklis G. Comparison of the photochromism of a spirobenzopyran derivative in unilamellar surfactant vesicles and solvent-cast surfactant films. Journal of the Chemical Society, Faraday Transactions. 1990;86(23).

238. Drummond CJ, Albers S, Furlong DN, Wells D. Photocontrol of surface activity and self-assembly with a spirobenzopyran surfactant. Langmuir. 1991 2012/02/19;7(10):2409-11.

239. Drummond CJ, Furlong DN. Photochromism of a surface-active spirobenzopyran moiety in dioxane-water mixtures and self-assembled surfactant aggregates. Journal of the Chemical Society, Faraday Transactions. 1990;86(21).

240. Takumi K, Sakamoto H, Uda RM, Sakurai Y, Kume H, Kimura K. Photocontrol of anionic micelles containing lipophilic crowned spirobenzopyran. Colloid Surface Physicochem Eng Aspect. 2007;301(1-3):100-5.

241. Baglioni P, Braccalenti E, Carretti E, Germani R, Goracci L, Savelli G, et al. Surfactant-Based Photorheological Fluids: Effect of the Surfactant Structure. Langmuir. 2009 19th May 2009;25(10):5467-75.

242. Lendlein A, Jiang H, Junger O, Langer R. Light-induced shape-memory polymers. Nature. 2005 04/14/print;434(7035):879-82.

243. Weissleder R. A clearer vision for in vivo imaging. Nat Biotech. 2001;19(4):316-7.

244. Zeimer R, Khoobehi B, Niesman M, Magin R. A potential method for local drug and dye delivery in the ocular vasculature. Invest Ophthalmol Vis Sci. 1988 July 1, 1988;29(7):1179-83.

245. Pissuwan D, Niidome T, Cortie MB. The forthcoming applications of gold nanoparticles in drug and gene delivery systems. J Controlled Release. 2011 1/5/;149(1):65-71.

246. Saha K, Agasti SS, Kim C, Li X, Rotello VM. Gold Nanoparticles in Chemical and Biological Sensing. Chemical Reviews. 2012 2012/05/09;112(5):2739-79.

247. Govorov AO, Richardson HH. Generating heat with metal nanoparticles. Nano Today. 2007;2(1):30-8.

248. Murray WA, Barnes WL. Plasmonic Materials. Advanced Materials. 2007;19(22):3771-82.

249. Jain PK, Lee KS, El-Sayed IH, El-Sayed MA. Calculated Absorption and Scattering Properties of Gold Nanoparticles of Different Size, Shape, and Composition: Applications in Biological Imaging and Biomedicine. J Phys Chem B. 2006;110(14):7238-48.

250. Volodkin Dmitry V, Skirtach Andre G, Möhwald H. Near-IR Remote Release from Assemblies of Liposomes and Nanoparticles. Angewandte Chemie International Edition. 2009;48(10):1807-9.

251. Zhang JZ. Optical properties and spectroscopy of nanomaterials. Hackensack, N.J.: World Scientific; 2009. xvi, 383 p. p.

252. Harris N, Ford MJ, Mulvaney P, Cortie MB. Tunable infrared absorption by meta nanoparticles: The case for gold rods and shells. Gold Bulletin. 2008;41(1):5-14.

253. Takahashi H, Niidome Y, Niidome T, Kaneko K, Kawasaki H, Yamada S. Modification of Gold Nanorods Using Phosphatidylcholine to Reduce Cytotoxicity. Langmuir. 2006;22(1):2-5.

254. Alkilany AM, Thompson LB, Boulos SP, Sisco PN, Murphy CJ. Gold nanorods: Their potential for photothermal therapeutics and drug delivery, tempered by the complexity of their biological interactions. Adv Drug Deliv Rev. 2012;64(2):190-9.

255. Daniel M-C, Astruc D. Gold Nanoparticles: Assembly, Supramolecular Chemistry, Quantum-Size-Related Properties, and Applications toward Biology, Catalysis, and Nanotechnology. Chem Rev. 2003;104(1):293-346.

256. Hartland GV. Is perfect better? Nat Mater. 2007 Oct;6(10):716-8.

257. Dickerson EB, Dreaden EC, Huang X, El-Sayed IH, Chu H, Pushpanketh S, et al. Gold nanorod assisted near-infrared plasmonic photothermal therapy (PPTT) of squamous cell carcinoma in mice. Cancer Letters. 2008;269(1):57-66.

258. Lee SE, Liu GL, Kim F, Lee LP. Remote Optical Switch for Localized and Selective Control of Gene Interference Nano Letters 2009;9(2):562-70.

259. Maeda H, Fang J, Inutsuka T, Kitamoto Y. Vascular permeability enhancement in solid tumor: various factors, mechanisms involved and its implications. International Immunopharmacology. 2003;3(3):319-28.

260. Tong L, Zhao Y, Huff TB, Hansen MN, Wei A, Cheng J-X. Gold Nanorods Mediate Tumor Cell Death by Compromising Membrane Integrity. Advanced Materials. 2007;19(20):3136-41.

261. Skirtach AG, Dejugnat C, Braun D, Susha AS, Rogach AL, Parak WJ, et al. The Role of Metal Nanoparticles in Remote Release of Encapsulated Materials. Nano Letters. 2005;5(7):1371-7.

262. Paasonen L, Laaksonen T, Johans C, Yliperttula M, Kontturi K, Urtti A. Gold nanoparticles enable selective light-induced contents release from liposomes. J Contr Release. 2007;122(1):86-93.

263. Park S-H, Oh S-G, Mun J-Y, Han S-S. Loading of gold nanoparticles inside the DPPC bilayers of liposome and their effects on membrane fluidities. Colloids Surf, B 2006 48 (2):112-8

264. Wu G, Mikhailovsky A, Khant HA, Fu C, Chiu W, Zasadzinski JA. Remotely Triggered Liposome Release by Near-Infrared Light Absorption via Hollow Gold Nanoshells. J Am Chem Soc. 2008;130(26):8175-7.

265. Troutman TS, Leung SJ, Romanowski M. Light-Induced Content Release from Plasmon-Resonant Liposomes. Advanced Materials. 2009;21(22):2334-8.

266. Munoz JA, del Pino P, Bedard MF, Ho D, Skirtach AG, Sukhorukov GB, et al. Photoactivated Release of Cargo from the Cavity of Polyelectrolyte Capsules to the Cytosol of Cells. Langmuir. 2008;24(21):12517-20.

267. Das M, Mordoukhovski L, Kumacheva E. Sequestering Gold Nanorods by Polymer Microgels. Advanced Materials. 2008;20(12):2371-5.

268. Das M, Sanson N, Fava D, Kumacheva E. Microgels Loaded with Gold Nanorods: Photothermally Triggered Volume Transitions under Physiological Conditions. Langmuir. 2007;23(1):196-201.

269. Kim J-H, Lee TR. Discrete thermally responsive hydrogel-coated gold nanoparticles for use as drug-delivery vehicles. Drug Development Research. 2006;67(1):61-9.

270. Murphy CJ, Orendorff CJ. Alignment of Gold Nanorods in Polymer Composites and on Polymer Surfaces. Advanced Materials. 2005;17(18):2173-7.

271. Agasti SS, Chompoosor A, You C-C, Ghosh P, Kim CK, Rotello VM. Photoregulated Release of Caged Anticancer Drugs from Gold Nanoparticles. J Am Chem Soc. 2009;131(16):5728-9.

272. Barhoumi A, Huschka R, Bardhan R, Knight MW, Halasa NJ. Light-induced release of DNA from plasmon-resonant nanoparticles: towards light-controlled gene therapy. Chemical Physics Letters. 2009;In Press, Accepted Manuscript.

273. Orendorff CJ, Alam TM, Sasaki DY, Bunker BC, Voigt JA. Phospholipid-Gold Nanorod Composites. ACS Nano. 2009;3(4):971-83.

274. Urban AS, Fedoruk M, Horton MR, Radler JO, Stefani FD, Feldmann J. Controlled Nanometric Phase Transitions of Phospholipid Membranes by Plasmonic Heating of Single Gold Nanoparticles. Nano Letters. 2009;9(8):2903-8.

275. Yaghmur A, Paasonen L, Yliperttula M, Urtti A, Rappolt M. Structural Elucidation of Light Activated Vesicles. J Phys Chem Letters. 2010;1:962-6.

276. An X, Zhan F, Zhu Y. Smart Photothermal-Triggered Bilayer Phase Transition in AuNPs–Liposomes to Release Drug. Langmuir. 2013.

277. Paasonen L, Sipilä T, Subrizi A, Laurinmäki P, Butcher SJ, Rappolt M, et al. Gold-embedded photosensitive liposomes for drug delivery: Triggering mechanism and intracellular release. J Contr Release. 2010;147(1):136-43.

Chapter 2 – General Materials and Methods

2. General Materials and Methods

2.1.Formulation

2.1.1. Materials

Lipids: Phytantriol (3,7,11,15-tetramethyl-1,2,3-hexadecanetriol) was a gift from DSM (Basel, Switzerland). Vitamin E acetate, cholesterol and Pluronic® F-127 were purchased from Sigma Aldrich (St. Louis, MO, USA). Rylo MG90 was a gift from Danisco (Botany, NSW, Australia). The main constituent of Rylo MG90 is glyceryl monooleate and all subsequent references to GMO will refer to this product. Monoelaidin was purchased from TCI (Kuraray, Tokyo, Japan). Selachyl alcohol was a gift from Cee Chemicals (Blacktown, NSW, Australia). Phospholipon 90G (DOPC) was a gift from Lipoid GmbH (Ludwigshafen, Germany); 1-palmitoyl-2-oleoyl-sn-glycero-3-phosphoethanolamine (POPE), 1,2-diphytanoyl-sn-glycero-3-phosphoethanolamine (DPhPE) and 1-oleoyl-2-hydroxy-sn-glycero-3-phosphocholine (LysoPC) was purchased from Avanti Polar Lipids (Alabaster, AL, USA); Oleic Acid was purchased from Sigma Aldrich (St. Louis, MO, USA).

General Materials: Sodium chloride and di-sodium hydrogen phosphate were purchased from Chemsupply (Port Adelaide, SA, Australia); potassium dihydrogen phosphate was purchased from BDH AnalaR, Merck Pty. Ltd (Kilsyth, VIC, Australia). These salts were used to prepare phosphate buffered saline (PBS). PBS was prepared as a representative media for physiological subcutaneous conditions according to British Pharmacopoeial Appendix XI [1]. It comprises of 2.38 g disodium hydrogen orthophosphate, 0.19 g potassium dihydrogen orthophosphate and 8.0 g sodium chloride per litre MilliQ water. Milli-Q grade water (0.05 μS cm^{-1} at 25°C) purified through a Millipore system (Sydney, Australia) was used for the preparation of all samples. The pH was then adjusted to using 0.1 M hydrochloric acid or sodium hydroxide. Hydrochloric acid 1 N was purchased from AVS Merck Pty. Ltd. (Kilsyth, Victoria, Australia).

Chloroauric acid ($HAuCl_4.3H_2O$), sodium borohydride ($NaBH_4$), silver nitrate, ascorbic acid, cetyltrimethylammonium bromide (CTAB) and dodecanethiol were obtained from Sigma-Aldrich (St Louis, MO) and used as received. Polyethyleneglycol thiol (PEG-SH, Fw 5000) was obtained from Rapp Polymere (Tübingen, Germany). Acetonitrile isocratic grade for liquid chromatography (LiChrosolv®) was purchased from Merck Chemicals (Darmstadt, Germany).

2.1.2. Photosensitive Elements

The photo-responsive materials used were classified as either photothermal or photochromic.

2.1.2.1. Photothermal: Gold Nanorods

Photothermal systems incorporated hydrophobised plasmonic gold nanorods (GNR). The GNR were prepared by B. Thierry (Uni SA) using the standard seed-mediated growth methodology in presence of cetyltrimethylammonium bromide (CTAB). GNR were synthesised with longitudinal surface plasmon resonances (LSPR) at 810 nm and 660 nm and will be referred to as GNR810 and GNR660 respectively. The aspect ratio of the GNR was controlled through control of the silver nitrate concentration as previously described[2]. GNR were hydrophobised using dodecanethiol in a two-step ligand exchange procedure as previously described[3]. Briefly, the 'as synthesised' GNR were first purified to remove the excess CTAB molecules and an intermediate steric barrier was introduced using a thiol-terminated polyethylene glycol (PEG-SH). The second step of the process involved the removal of the residual CTAB bilayer and the ligand exchange of the PEG-SH molecules by dodecanethiol. The hydrophobised GNR were readily redispersed in non-polar solvent (e.g. chloroform ($CHCl_3$), tetrahydrofuran (THF)) and remained stable for several hours. The UV-vis absorption spectra of the as synthesised and hydrophobised GNR suspensions with a LSPR at 810 nm are presented in the Figure 2.1.

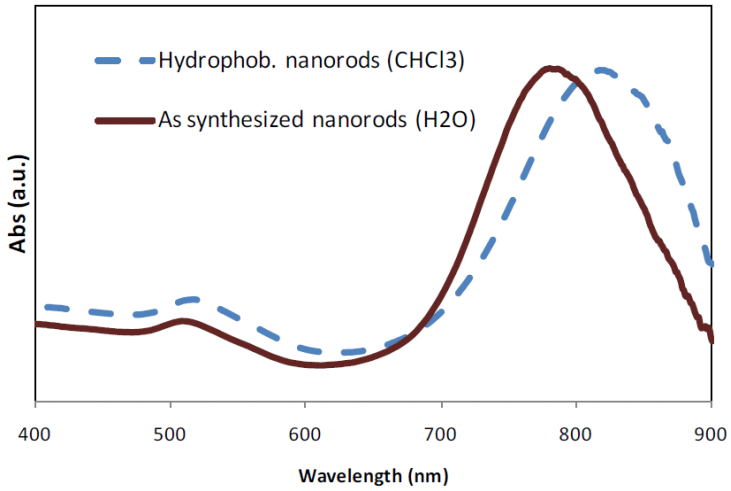

Figure 2.1 – Normalised absorption spectra of the 'as synthesised' gold nanorods. Solid line represents CTAB capping in H_2O and dashed line the hydrophobised dodecanethiol GNR in $CHCl_3$.

No broadening of the absorption spectra was observed for the GNR redispersed in non-polar solvents, confirming the absence of significant aggregation during the ligand exchange procedure. Although the GNR polydispersity index has not been directly calculated in this study, the dispersity of the sample was in good agreement with previously published GNR dispersions prepared using the standard CTAB–seed-mediated growth methodology as indicated by transmission electron microscopy (TEM) size measurements and width of the LSPR absorption spectrum. GNR810 had an average aspect ratio: 3.3 (length: 55.5 ± 9.5 nm, width: 16 ± 2.5 nm) and GNR660 had an average aspect ratio of 2.6 (length: 41 ± 7 nm, width: 15 ± 2.1 nm).

2.1.2.2. Photochromics

The photochromic systems investigated contained additives that had UV sensitive functional groups, namely azobenzene and spiropyran. Cinnamic acid was also investigated as an additive; however, the photochromic was not soluble in the lipid and consequently could not be further investigated. In the first instance, additives were purchased "off the shelf", then an alkylated spiropyran moiety was synthesised for further investigation, as spiropyran was found to have the

greater photochromic effect with the least toxicity issues[4]. The photochromics used are reported in more detail in Chapter 5.

2.1.3. Formulation of Photosensitive Matrices

Both bulk and dispersed liquid crystalline matrices were evaluated. The photoresponsive moiety was incorporated into the lipid before the aqueous phase was added. As the GNR were dispersed in THF, the suspension was rinsed and redispersed in THF to a concentration of 2.5 x 10^{-9} M. Different volumes of the GNR suspension were added to the lipids and the solvent removed *in vacuo* (48 hr) and gently heated under a stream of N_2 (4 hr). Photochromic moieties were dissolved in the bulk lipid upon gentle heating, thoroughly vortexed and allowed to equilibrate on rollers overnight before the addition of the aqueous phase to prepare either the bulk or dispersed particulate systems.

Bulk systems: To the photothermal systems, an equal weight of MilliQ water was added unless otherwise specified. To the photochromic systems an equal weight of phosphate buffered saline (PBS), pH 7.4 100 mM, was added to the lipid mixture unless otherwise specified. Mixing of the bulk systems was then achieved by heating to 70°C momentarily to reduce viscosity and allow vortex mixing. This was repeated three times. The mixture was then centrifuged and allowed to equilibrate for >24 hr on rollers in a 37°C incubator prior to investigation.

Dispersed systems: Cubosome (phyt, GMO) and hexosome (phyt + 5% VitEA, SA) dispersions were prepared by injecting 0.2 g molten lipid (containing the photosensitive component) in 2 mL of a 1.0% w/v Pluronic® F-127 solution. The coarse dispersion was then subjected to 20 min of pulsed ultrasonication (1 s on, 1 s off) using a Misonix S-4000 Ultrasonic Liquid Processor (NY, USA) fitted with a microtip, at 30% power.

2.2.Liquid Crystalline Matrix Characterisation Methods

Several techniques have been employed in the literature to identify phase structures and thermal behaviour of liquid crystals. These include small angle X-ray scattering (SAXS), cross polarised light microscopy (CPLM), differential scanning calorimetry (DSC), nuclear magnetic resonance (NMR), cryogenic transmission electron microscopy (cryoTEM), neutron diffraction, Raman spectroscopy, Fourier transform infrared spectroscopy (FTIR), and time resolved fluorescence[5]. Many of these techniques are used as complementary methods to SAXS or cryoTEM methods. Only the methods relevant to this project are detailed below, namely CPLM, SAXS, cryoTEM and cryogenic field emission scanning electron microscopy (cryoFESEM).

2.2.1. Cross Polarised Light Microscopy (CPLM)

CPLM is the most common and convenient method of phase determination, and so was the first technique employed to determine the solubility and optimal percentage of additive in the bulk lipid. In CPLM, samples are viewed on a microscope under crossed polarised light. Sample temperatures are controlled by a heating stage. Using this method, phase changes are indicated by changes in birefringence and viscosity of the sample. Three liquid crystal phases were identified in this study via CPLM[6]. The V_2 phase is highly viscous, non-birefringent material; H_2 is a birefringent and highly viscous material which shows an angular fan-like texture and L_2 (inverse micellar phase) is isotropic and has a low viscosity. Lamellar phase can also be identified using crossed polarised microscopy as it appears birefringent with a number of different possible textures but are very different to hexagonal phase. CPLM was used as a preliminary means to identify the liquid crystal phase formed using either pre-formed systems, or as composition 'penetration' scans where a drop of the anhydrous matrix is added to a slide and the aqueous phase introduced from the side to induce a gradient of aqueous phase through the sample. The appearance of bands of characteristic birefringence or viscosity allows identification of phases that

will exist in the phase diagram. Temperature can then be increased to determine transition temperatures. The short fall of CPLM is that it does not provide any information on structure dimensions or compositions.

2.2.2. Small Angle X-ray Scattering (SAXS)

X-ray scattering is one of the most common techniques used to probe soft matter, including lyotropic liquid crystalline structures. When the X-ray beam, of radiation of wavelength, λ, enters the sample, the X-rays are scattered by electrons within the crystal structure as if they were reflected by a family of parallel planes. The average intensity of the X-ray scattering is taken over time, where the recorded scattering pattern directly probes the structure and dynamics of a sample in reciprocal space (q-space). The basic set up of a SAXS instrument is shown in Figure 2.2.

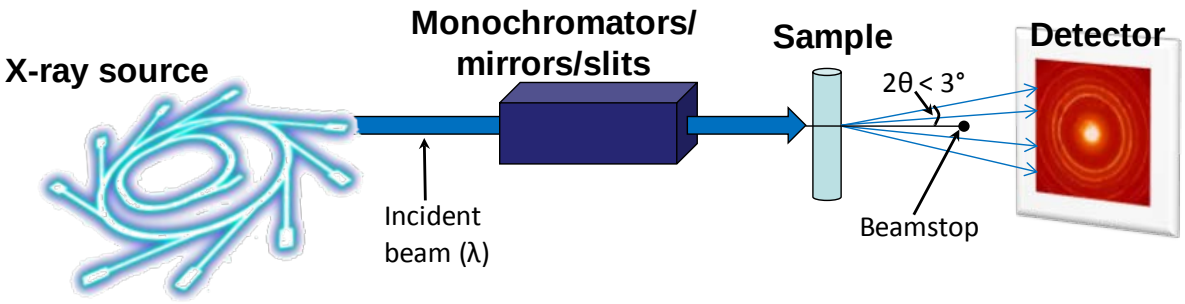

Figure 2.2 – SAXS instrument set up showing the incident beam (of wavelength, λ) and scattering angle (2θ).

The variation of the intensity as a function of the scattering angle, 2θ, is measured as a scattering pattern, examples of which are in Figure 2.3. This scattering pattern and its relation to atoms arranged in a crystal lattice (or planes of symmetry in the case of liquid crystalline materials) can be described by Bragg's Law; Equation 1:

$$2d \sin\theta = n\lambda \quad (1)$$

where *d* represents the interplanar spacing. The data are usually converted from a 2D scattering pattern to a one dimensional plot of intensity versus scattering vector, q, according to Equation 2:

$$q = \frac{4\pi}{\lambda} \sin\theta / 2 \quad (2)$$

Reflection laws have been previously documented[7] for the indexation of peaks of the different mesophases. Thus, from the relative location of the peaks, the symmetry of the structure can be assigned. The scattering vector at which the peaks occur is then used to calculate the interplanar spacing, *d*, between two reflecting planes of the liquid crystal phase. *d* is calculated by Equation 3:

$$d = 2\pi/q \quad (3)$$

The calculation of *d* and the absolute location of the peaks allows for the calculation of the mean lattice parameter, a, of the crystal unit cell, amongst other parameters, from the corresponding reciprocal spacings[8, 9]. The q values of the visible peaks are correlated with Miller indices for known phases and used to identify the mesophase formed and calculate the mean lattice parameter of the systems. The reduction of acquired SAXS patterns of interest is schematically shown in Figure 2.3. The mean lattice parameter, a, was deduced from the corresponding set of observed interplanar spacings, d, using the appropriate scattering law for the phase structure as shown in Table 2.1. For the bicontinuous cubic phases, $a = d(h^2+k^2+l^2)^{1/2}$, while for H_2 phase, $a=4d/3(h^2+k^2)^{1/2}$, where h, k and l are the Miller indices for the particular structure present. For the L_2 phase, which shows only one broad peak, d is termed the characteristic distance.

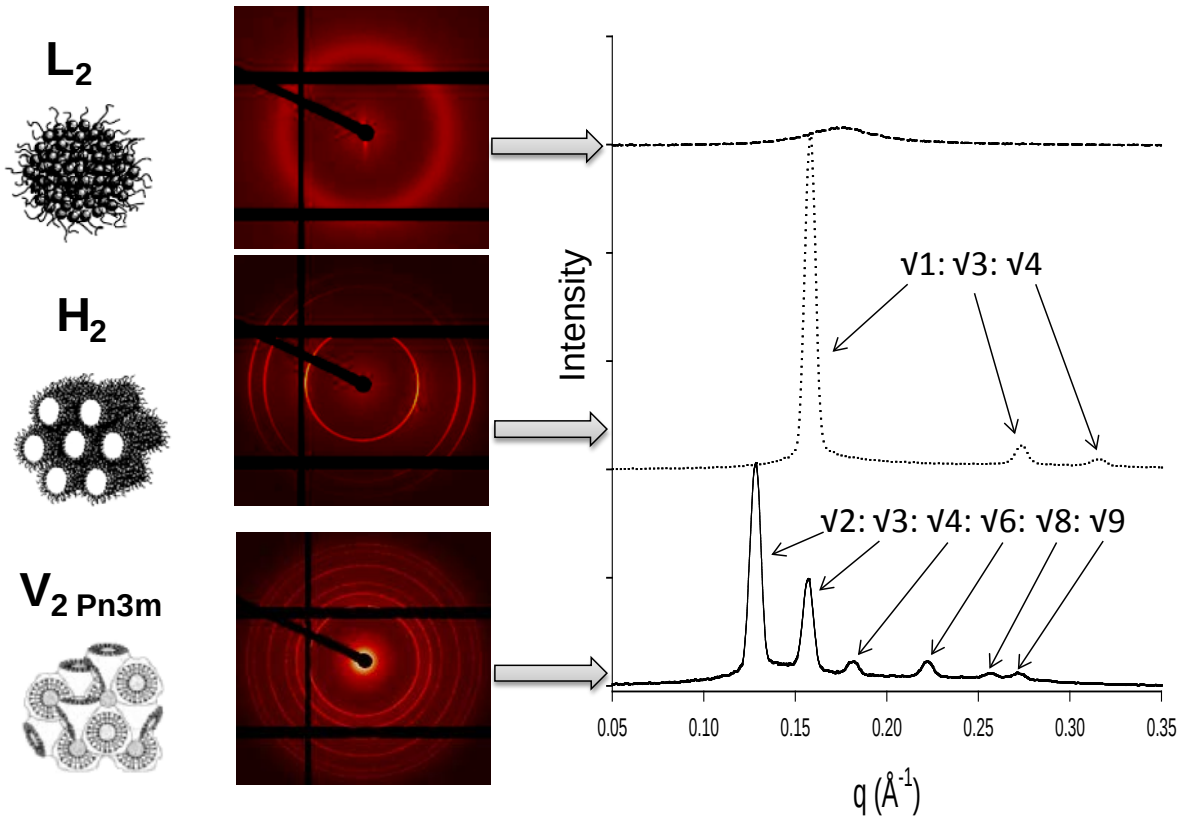

Figure 2.3 – Some phase structures of interest (left) with measured 2D SAXS patterns (middle) and their corresponding intensity vs. q plot (right). Note that the L_2 phase is a fluid isotropic phase which is identified by a characteristic broad peak.

Table 2.1 – SAXS reflection laws of liquid crystal mesophases formed by amphiphiles investigated.

Name		Space group (number)	Characteristic SAXS peak ratios
Lamellar		L_α	1:2:3:4….
Bicontinuous cubic (V_2)	Double diamond (D)	Pn3m (V^{224})	√2:√3:√4:√6:√8:√9:√10:√11…
	Gyroid (G)	Ia3d (V^{230})	√6:√8:√14:√16:√20:√22:√24…
	Primitive (P)	Im3m (V^{229})	√2:√4:√6:√8:√10:√12:√14…
Inverse hexagonal (H_2)		P6m	√1:√3:√4:√7:√9:√12:√13…

Equilibrium temperature scan SAXS experiments, where synchrotron X-rays were not necessary, were performed at ANSTO, NSW, Australia, on a Bruker Nanostar SAXS camera, with pinhole collimation for point focus geometry. Samples were loaded into 2 mm or 1.5 mm internal diameter quartz capillaries sealed with capillary wax and mounted on a temperature controlled stage. The instrument source was a copper rotating anode (0.3 mm filament) operating at 45 kV and 110 mA, fitted with cross-coupled Montel mirrors, resulting in CuKα radiation with wavelength of 1.54 Å. The temperature range investigated was 25 -80°C at 2°C or 5°C intervals with 15 min equilibration time after each temperature change.

Due to the high flux available with synchrotron X-ray sources, synchrotron SAXS has been increasingly employed to elucidate rapid structural transitions in self-assembled systems in real time[10-12]. In this thesis, synchrotron SAXS was the primary technique for studying the kinetics of phase transitions in photoresponsive systems, and to elucidate structural detail via lattice parameter calculations not obtainable using CPLM. Dynamic SAXS data were collected on the SAXS/WAXS beamline at the Australian Synchrotron. Bulk photothermal samples (50 mg) were sandwiched in Kapton tape or loaded into 2 mm internal diameter quartz capillaries and dispersions were loaded into 1.5 mm internal diameter quartz capillaries. Bulk photochromic samples were enclosed in a custom made HDPE/mylar/kapton cylindrical sample holder; diameter 6 mm, thickness 0.5 mm. Samples were then mounted on a hot stage where they were held at 27°C for irradiation studies. An X-ray beam with a wavelength of 0.83 Å (15 keV) was selected. The 2D SAXS patterns were collected using a Pilatus 200k detector (active area 169 × 33 mm^2 with a pixel size of 172 μm) which was located 966 mm from the sample position. The total q range for the instrument configuration outlined above was $0.02 < q < 1.06$ $Å^{-1}$. 2D SAXS patterns were collected for 100 ms over 30 s; the computer software SAXS15ID[131313], Fit2D[14] and Scatterbrain were used to acquire and reduce 2D patterns to 1D intensity v q profiles.

2.2.2.1. Calculation of the Apparent Temperature (T_{app})

In order to further interrogate and compare photothermal systems, the 'apparent temperature' (T_{app}) of the matrix was determined at each time point. The T_{app} indicates a level of disruption of the matrix that would occur under direct heating, photothermal heating or steric disruption using photochromic compounds. In order to determine T_{app}, lattice parameter vs. temperature profiles obtained from the equilibrium temperature scans were used as calibration curves (as shown in Figure 2.4) to convert the dynamic lattice parameter versus time profiles into apparent temperature versus time profiles.

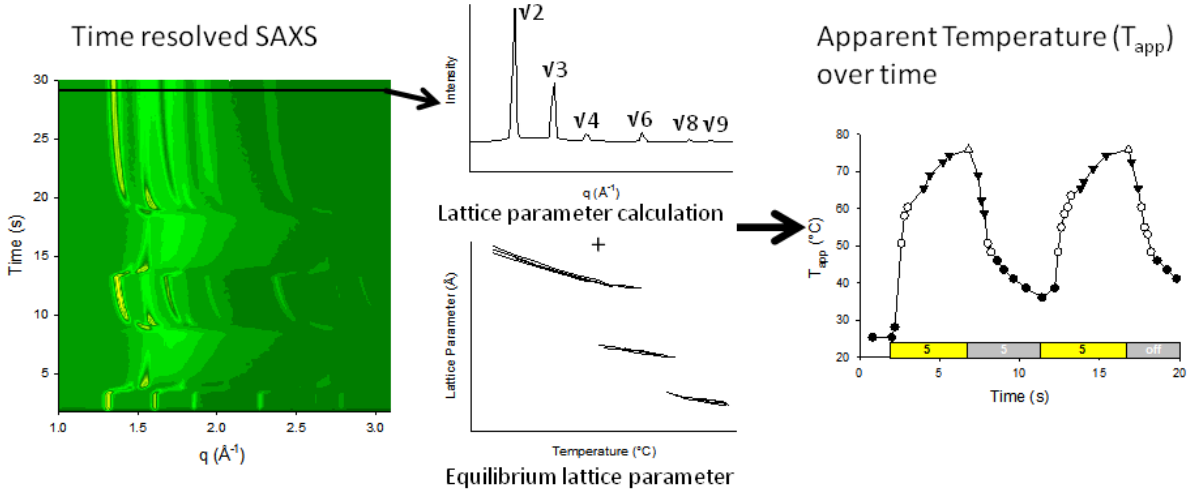

Figure 2.4 – Schematic for the conversion of lattice parameters obtained from time resolved SAXS (figure left) to apparent temperature (T_{app}) (figure right) over time. Integration of individual frames were used to calculate lattice parameters over time. Equilibrium lattice parameter vs temperature values were then used as a calibration curve to convert this value to T_{app}.

2.2.3. Cryogenic Transmission Electron Microscopy (cryo-TEM) and Cryogenic Field Emission Scanning Electron Microscopy (cryo-FESEM)

CryoTEM and cryo-FESEM were used to visualise the nanostructure formed and allow for the determination of the morphology and quality of the liquid crystal matrix with a resolution down to 2 – 3 nm. The visualisation of self-assembled systems via TEM and SEM techniques is becoming increasingly common. The use of imaging techniques such as these have been used

quantitatively in situations where SAXS cannot differentiate between some crystallographic space groups, e.g. the discontinuous inverse micellar cubic phases Fd3m vs Fd3[15].

These imaging techniques allowed for the observation of the disposition of GNR within the bulk and dispersed liquid crystal systems. Cryogenic methods are to be used in favour of normal TEM as it avoids likely artifacts introduced during TEM sample preparation, where water needs to be removed because the sample is under vacuum. In cryo-EM samples are frozen in liquid ethane and viewed with low electron doses to prevent sample thawing[16].

CryoTEM was used to characterise cubosomes and hexosomes. A 4 − 5 μL aliquot of sample solution was applied to a 300-mesh copper TEM grid coated with a lacey carbon film (ProSciTech, Thuringowa Qld, Australia) and allowed to settle for 30 s. The grid was manually blotted for 10 − 15 s, and the resulting thin film was then vitrified by plunging into liquid ethane. Grids were stored in liquid nitrogen before transferring into a Gatan 626-DH Cryo-holder where samples were maintained at -180 °C during imaging. Imaging was carried out using an FEI Tecnai 12 TEM (120 kV), equipped with a MegaView III CCD camera and AnalySis imaging software (Olympus Soft Imaging Solutions).

CryoFESEM was used to image GNR disposition within the bulk liquid crystalline phase. Samples were transferred onto brass stubs in ambient conditions, then plunge frozen in liquid ethane slurry. The sample was subsequently transferred under vacuum to the cryoFESEM sample preparation chamber where the sample was maintained at -120 °C and fractured with a cold scalpel blade. The sample was sublimed for 2 min at -93 °C, then sputter coated with platinum at -110 °C. Samples were viewed on a Philips XL30 Field Emission Scanning Electron Microscope, equipped with a Gatan CT1500 HF Cryo Stage, at -120 °C with an accelerating voltage of 5 kV and a working distance of 9.4 – 11.7 mm. Samples viewed in backscatter mode were viewed using an accelerating voltage of 20 kV, and spot analysis was used to identify the element(s) present.

2.3.Light Sources

2.3.1. Near Infrared Lasers – 808 nm

Two different near infrared (NIR) lasers were used for the photothermal activation studies. For the pulsed laser kinetic experiments at the Australian synchrotron, a Class IIIB diode pen laser with the output λ = 808 ± 3 nm and peak power <400 mW (Changchun New Industries, China). Samples were illuminated by computer controlled pulses with an unmodified laser beam at a distance of 1.2 cm with a spot size of 4 mm^2. As the beam was well collimated, at this distance, the samples received a 390 mW dose, corresponding to 975 mW cm^{-2}.

Longer irradiation times used for in vivo studies were achieved using a continuous wave Class IIIB diode-pumped solid-state (DPSS) fibre optic coupled laser with the output λ = 808 nm and variable power output (Changchun New Industries, China).

2.3.2. UV Light Sources

The light source used during the time resolved UV kinetic studies was an EXFO Acticure 4000 (Phoenix, AZ, USA) set at 350 nm and 60 mW power.

The UV light source used for SPL characterisation was 3 x NSHU551B UV LED with a radiant flux rank = 6 (Nichia Chemical PTE LTD, Japan). The white light source used was 4 x Ultrabright Nichia White LED (Blackburn, IL, USA).

2.3.3. Near Infrared Laser – 980 nm

Class IIIB diode pen laser with the output λ = 980 nm and laser power of 150 mW (Changchun New Industries, China).

2.3.4. Optical Power Meter

Laser power was recorded using a Thorlabs Optical Power Meter PM 100D (Thorlabs, NJ, USA).

References

1. The British pharmacopœia. London: Published for the General Medical Council by Constable & Co.,; 2007.

2. Nikoobakht B, El-Sayed MA. Preparation and Growth Mechanism of Gold Nanorods (NRs) Using Seed-Mediated Growth Method. Chem Mater. 2003;15(10):1957-62.

3. Thierry B, Ng J, Krieg T, Griesser HJ. A robust procedure for the functionalization of gold nanorods and noble metal nanoparticles. Chem Comm. 2009 (13):1724-6.

4. Movia D, Prina-Mello A, Volkov Y, Giordani S. Determination of Spiropyran Cytotoxicity by High Content Screening and Analysis for Safe Application in Bionanosensing. Chem Res Toxicol. 2010;23(9):1459-66.

5. Sagalowicz L, Mezzenga R, Leser ME. Investigating reversed liquid crystalline mesophases. Curr Opin Colloid Interface Sci. 2006;11(4):224-9.

6. Rosevear F. The microscopy of the liquid crystalline neat and middle phases of soaps and synthetic detergents. J Am Oil Chem Soc. 1954; 31 (12):628-39.

7. de Campo L, Yaghmur A, Sagalowicz L, Leser ME, Watzke H, Glatter O. Reversible Phase Transitions in Emulsified Nanostructured Lipid Systems. Langmuir. 2004;20(13):5254-61.

8. Andersson S, Hyde ST, Larsson K, Lidin S. Minimal surfaces and structures: from inorganic and metal crystals to cell membranes and biopolymers. Chemical Reviews. 1988;88(1):221-42.

9. Kulkarni CV, Wachter W, Iglesias-Salto G, Engelskirchen S, Ahualli S. Monoolein: a magic lipid? Phys Chem Chem Phys. 2011;13(8):3004-21.

10. Fong W-K, Hanley TL, Thierry B, Kirby N, Boyd BJ. Plasmonic Nanorods Provide Reversible Control over Nanostructure of Self-Assembled Drug Delivery Materials. Langmuir. 2010.

11. Yaghmur A, Laggner P, Almgren M, Rappolt M. Self-Assembly in Monoelaidin Aqueous Dispersions: Direct Vesicles to Cubosomes Transition. PLoS ONE. 2008;3(11):e3747.

12. Yaghmur A, Paasonen L, Yliperttula M, Urtti A, Rappolt M. Structural Elucidation of Light Activated Vesicles. J Phys Chem Letters. 2010;1:962-6.

13. SAXS / WAXS Data & Analysis. Available from: http://www.synchrotron.org.au/index.php/aussyncbeamlines/saxswaxs/saxs-data-a-processing

14. Hammersley AP. ESRF Internal Report, ESRF98HA01T 1998. FIT2D V9129 , Reference Manual V31.

15. Delacroix H, Gulik-Krzywicki T, Seddon JM. Freeze Fracture Electron Microscopy of Lyotropic Lipid Systems: Quantitative Analysis of the Inverse Micellar Cubic Phase of Space Group Fd3m (Q^{227}). Journal of Molecular Biology. 1996;258(1):88-103.

16. Adrian M, Dubochet J, Lepault J, McDowall AW. Cryo-electron microscopy of viruses. Nature. 1984; 308(5954):32-6.

Chapter 3 – Photothermal Control of Nanostructure within Gold Nanorod-Liquid Crystalline Hybrid Materials

3. Photothermal Control of Nanostructure within Gold Nanorod-Liquid Crystalline Hybrid Materials

3.1. Declaration for Chapter 3

Some of the research presented this chapter have been published as:

- Fong W-K, Hanley TL, Thierry B, Kirby N, Boyd BJ. Plasmonic Nanorods Provide Reversible Control over Nanostructure of Self-Assembled Drug Delivery Materials. Langmuir. 2010; 26(9):6136-9
- Fong W-K, Hanley TL, Thierry B, Kirby N, Waddington LJ, Boyd BJ. Controlling the Nanostructure of Gold Nanorod-Lyotropic Liquid-Crystalline Hybrid Materials Using Near-Infrared Laser Irradiation. Langmuir. 2012; 28(40):14450-60.

3.2. Introduction

Soft materials that are responsive to external stimuli are of interest for many bioapplications including the optimisation of pharmaceutical and diagnostic therapies. Light responsive matrices are of particular interest due to the non-invasive and penetrating nature of light. A range of different light-responsive elements have been incorporated into liposomes, hydrogels and nanocomposites and other drug delivery systems[1, 2]. Near infrared (NIR) light (700 – 1000 nm) is potentially the most useful modality for triggering on-demand release of drug, as skin and tissue minimally absorb radiation at these wavelengths, allowing relatively deep penetration of NIR light[3], and reduced cellular damage[4, 5].

Gold nanoparticles can be tuned to efficiently absorb light in the NIR range, converting most of this absorbed light energy into thermal energy within picoseconds via activation of their surface plasmon resonances[6, 7]. Because of this photothermal property, gold nanoparticles have been

proposed for use in pharmaceutical applications such as thermal ablative therapy[8], diagnostics[9] and stimuli-responsive drug delivery[10, 11]. They have also been incorporated into matrices, such as silica gels[12] and microcapsules[13], in order to impart functionality.

Of increasing interest in bioapplications and drug delivery is the use of ordered nanostructured lyotropic liquid crystalline mesophases, formed by some lipidic amphiphiles. The interest in these materials stems from biocompatibility, the ability to solubilise hydrophobic and hydrophilic active drugs[14], thermodynamic stability which allows for dispersion of lipids into nanoparticles which retain the internal nanostructure[15], and most importantly, the potential to control the release of active drugs through control in nanostructure[16]. Transitions between different self-assembled geometries for lipids in aqueous environments are ubiquitous in nature, and some form the basis of complex biological functions, for instance, the formation and structure of cellular membranes, membrane fusion, and some cellular uptake mechanisms[17]. These transitions all involve manipulation of lipid self-assembly by altering lipid packing geometry[18] which can be reversibly achieved through environmental changes, amongst other variables. Thus, there is the potential to tune, manipulate and therefore utilise these reversible phase transitions in lipid systems to impart responsiveness into materials[19]. Given the earlier stated applications of plasmonic heating in soft matter, it is of direct interest to determine whether the particles can be utilised to control thermal transformation in liquid crystalline materials to remotely control drug release.

This Chapter firstly explores the use of phytantriol (PHYT)-gold nanorod (GNR) nanohybrid matrices as light sensitive materials (Section 3.5), where the ability to photosensitise these matrices are discussed in terms of GNR, laser and matrix properties. GNR were incorporated into the PHYT matrix to identify the effect the GNR and laser properties have on the PHYT matrix. Additionally, in order to investigate the influence of the 'starting phase' on the matrix response, a H_2 sample was prepared by the addition of vitamin E acetate at 5%, which induces a $V_{2\,D}$ to H_2

transition at room temp[20]. On completion of the studies focussing on PHYT-GNR matrices which address the major hypothesis for this chapter, analogous studies were performed with a number of alternative lipids in order to understand the influence of the matrix composition on the photothermal response of the systems (Section 3.6). These systems contained lipids of more immediate relevance to on-demand drug delivery. Specifically, the dynamic photoresponsive transition behaviour on irradiation of GNR containing mesophases was studied for the bicontinuous cubic phase formed by glyceryl monooleate (GMO) in excess water[21, 22], the hexagonal phase formed using selachyl alcohol (SA) in excess water[23] and the lamellar phase formed by monoelaidin (ME) in excess water[24]. The molecular structures and literature phase behaviours of the lipids of interest are shown in Figure 3.1. GMO, SA and ME are very closely structurally related, enabling comparison of the influence of starting mesophase with minimal influence of molecular amphiphile structure. Some of the PHYT results are reproduced in this section to enable direct comparison.

A. Phytantriol (PHYT)

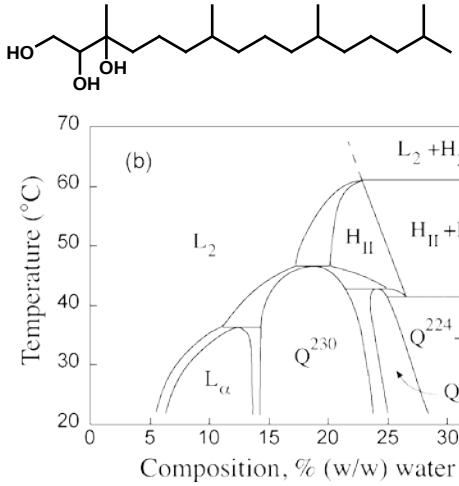

B. Glycerol Monooleate

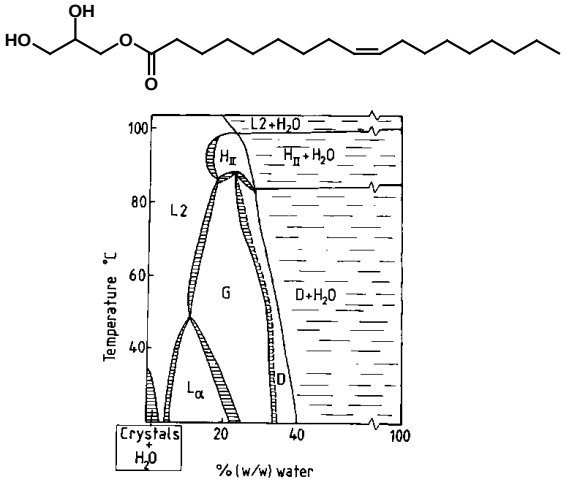

C. Selachyl Alcohol

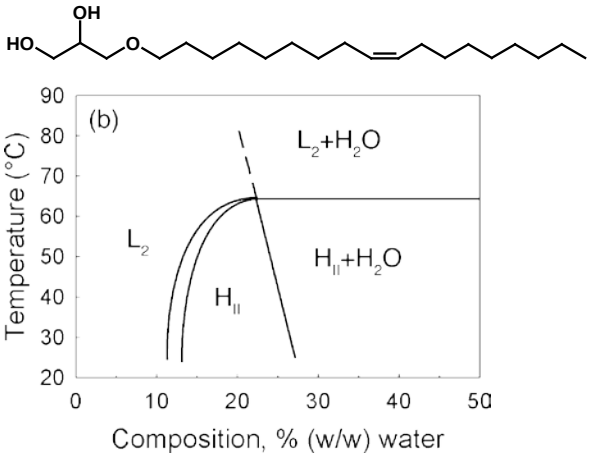

D. Monoelaidin

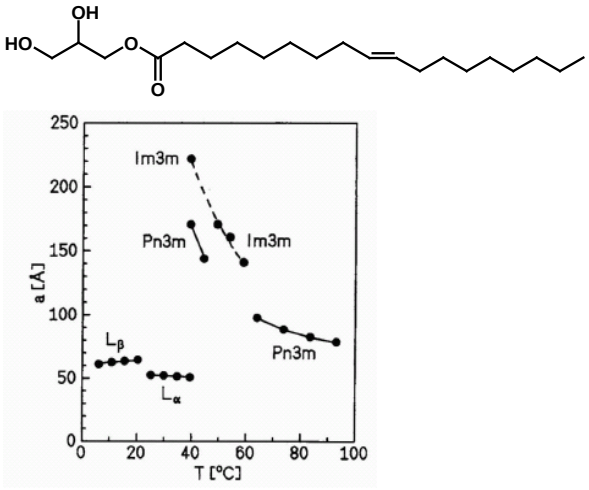

Figure 3.1 – The molecular structures and the reported thermal phase behaviours of the lipids of interest in this Chapter. Adapted from [21, 23-25]

3.3. Hypotheses and Aims

Hypothesis 1

That the NIR laser activation of gold nanorods incorporated into lipid bilayers will alter lipid packing in self-assembled systems by introducing photothermally generated heat at a local level.

In order to investigate these hypotheses, the following aims will be achieved:

1. To determine the potential of gold nanorods as photosensitisers in phytantriol liquid crystalline matrices using SAXS by understanding the effects of the following on the matrix response:
    a. The effect of different matrix nanostructures.
    b. The effect of GNR aspect ratio.
    c. The effect of laser irradiation duration, intensity and wavelength.
    d. The effect of dispersion of the matrix.
2. To determine the influence of the matrix composition on the photothermal response of the system.

3.4.Materials and Methods

The general materials and methods employed in this chapter are detailed in Chapter 2.

3.4.1. Differential Scanning Calorimetry

Differential Scanning Calorimetry (DSC) was used to identify the heat capacity of the different liquid crystalline phases. Heat capacity measurements were performed on a Perkin-Elmer DSC 8500 with an integrated cooling system (Intracooler III). The measurements were carried out under a nitrogen purge gas at a flow rate of 60 mL/min. The instrument was calibrated for temperature and heat flow using indium as a standard. A baseline for an empty pan was established for the heating rate. An empty aluminium pan was used as a reference. Approximately 20 mg of

the samples were sealed in aluminium pans and step scan measurements were taken under static air over a temperature range of 20 – 70°C in 5°C steps at a heating rate of 5 °C/min, with a 1 min isothermal at each temperature step. Heat capacity (C_p) was then calculated using the Perkin Elmer Pyris software. To convert to C_p units, the baseline heat flow data was subtracted from the sample curve heat flow data in milliwatts (mW) which is then converted to specific heat using Equation (1).

$$C_p = \frac{Q}{\Delta T.m} \qquad (1)$$

Where C is the specific heat in J $g^{-1}°C^{-1}$, Q is heat flow in mW, ΔT is the heating rate in °C s^{-1} and m is mass in g. The result is a specific heat data curve as a function of temperature. Note that the molar heat capacity was not calculated due to inaccuracies associated with calculating the amount in mole of the lipid-water liquid crystalline phase.

3.5.Results – Phytantriol Matrices

3.5.1. Bulk, Non-Dispersed Systems

The equilibrium pseudo-binary phase diagrams for the PHYT and PHYT + 5% Vitamin E acetate (VitEA) bulk matrices in excess water in the presence of increasing concentration of GNR810 and GNR660 are shown in Figure 3.2 PHYT and PHYT + 5% VitEA without GNR formed the $V_{2\ D}$ and H_2 phases respectively at ambient temperature. The hydrophobised GNR incorporated into the unactivated $V_{2\ D}$ and H_2 matrices had some minor effects on the phase transition temperatures but did not disrupt or substantially modify the equilibrium phase behaviour. GNR incorporation into the $V_{2\ D}$ liquid crystal matrix caused a slight but insignificant (~1 Å) reduction in the lattice parameters in the $V_{2\ D}$ phase (Figure 3.2, Panel A). The presence of GNRs also changed the V_2 to H_2 phase transition temperature, dependent on the GNR

concentration. There was generally an insignificant effect of GNR concentration on the equilibrium phase behaviour with temperature, except for a slight suppression of the V_2 to H_2 transition at high GNR concentration (Figure 3.2, Panel A), which was also apparent for the H_2 to L_2 transition in the PHYT + 5% VitEA matrix (Figure 3.2, Panel C).

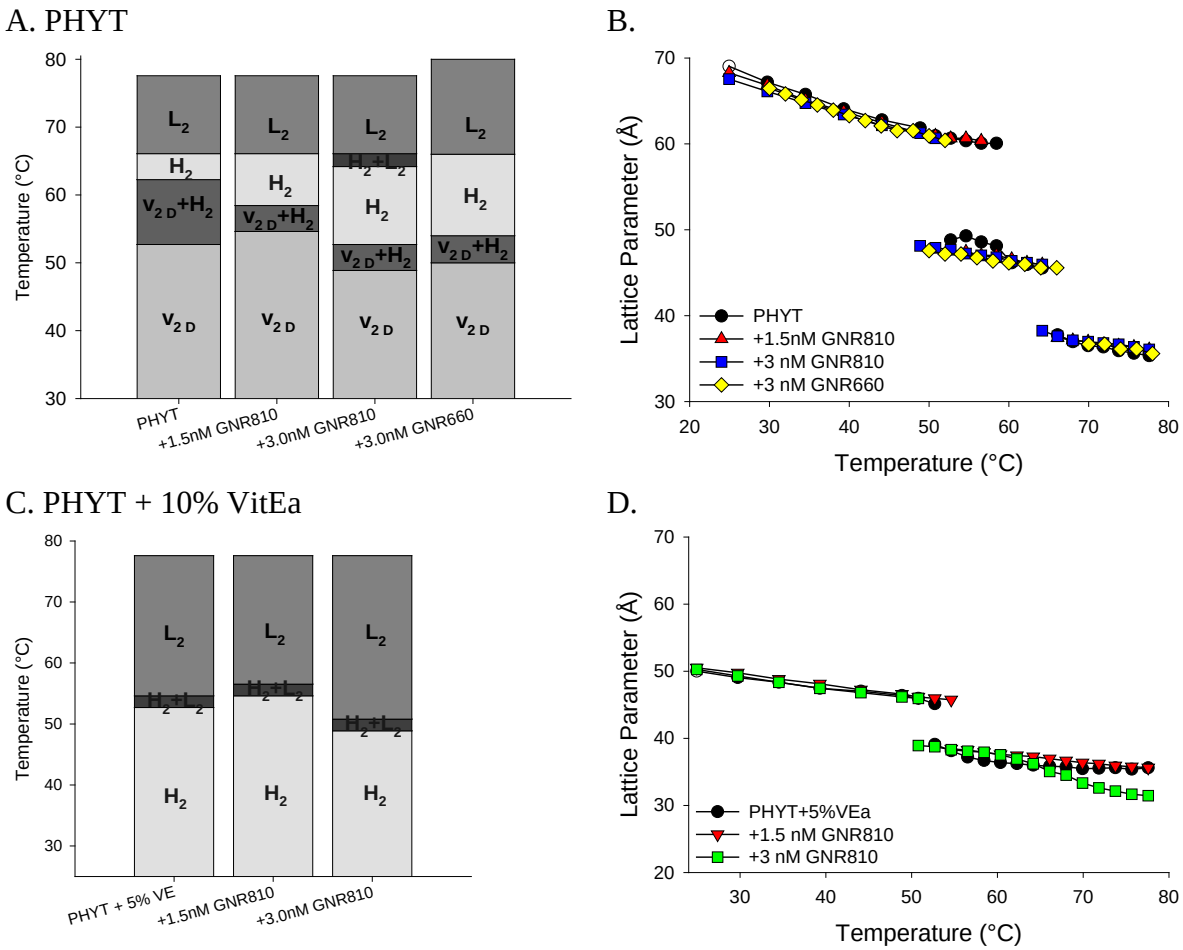

Figure 3.2 – Equilibrium temperature scans and lattice parameters for cubic and hexagonal phases containing increasing concentrations of GNR. Panels A. & B. PHYT-water cubic phase + increasing concentrations of GNR. Panels C. & D. PHYT + 5% VitEA-water hexagonal phase + different concentrations of GNR. All matrices are in excess water. GNR810 refers to gold nanorods with a LSPR of 810 nm, GNR660 refers to gold nanorods with an LSPR of 660 nm.

3.5.2. The Effect of Gold Nanorod Concentration

Figure 3.3 displays the SAXS profiles of NIR laser irradiation of PHYT matrices containing increasing concentrations of GNR. Irradiation of PHYT matrix did not induce a matrix response (Panel A). Irradiation of the 0.3nM matrix (Panel B.), did not induce a change in phase structure away from the $V_{2\,D}$ phase however, the pulsed laser irradiation resulted in the contraction and expansion of the lattice on photothermal heating and consequent cooling. The structure relaxed back to the original positionwhen the laser was off. The contraction and expansion of the lattice has been termed the " breathing mode" by de Campo, as it is accompanied by concurrent expulsion and uptake of water from the matrix to satisfy the changes in lattice dimension[26]. Thus, the photothermal heating effect is both reversible and reproducible, but the 0.3 nM GNR concentration was not sufficient to convert the phase nanostructure to the H_2 or L_2 phases.

In the case of higher concentrations of GNR, the 5 s NIR pulse induced a phase change to the H_2 and L_2 structures in both the 1.5 nM (Panel C.) and 3 nM (Panel D.) systems. At 3 nM, complete transformation to the L_2 phase occurred by the end of the 5 s irradiation, while the lower 1.5 nM concentration resulted in a mixed H_2 + L_2 phase, indicating a reduced heating effect. Again, on cessation of irradiation, the system ultimately returned to the initial $V_{2\,D}$ structure. Interestingly, on reversion from the L_2 or H_2 + L_2 state back to the $V_{2\,D}$ structure, the gyroid bicontinuous cubic phase with Ia3d space group ($V_{2\,G}$) was encountered. The $V_{2\,G}$ phase initially coexisted with the H_2 phase and then with the $V_{2\,D}$ phase for approximately 5 – 6 s after the laser was switched off. This is highly unusual as the samples are present in excess water and the $V_{2\,G}$ phase only exists at equilibrium in dehydrated liquid crystalline structures for the PHYT + water matrix[20]. The $V_{2\,G}$ phase was not observed during the heating phase of the cycle.

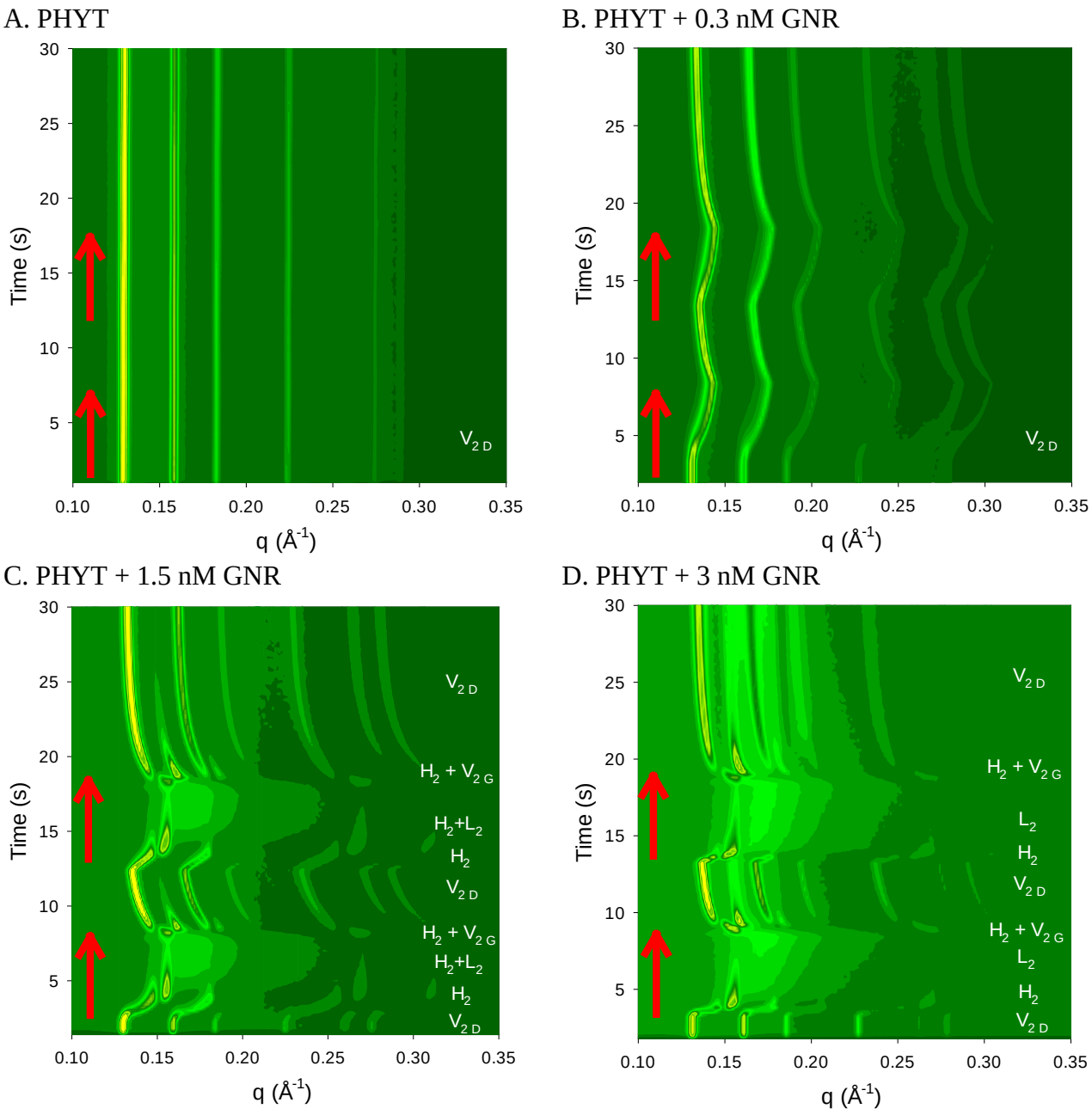

Figure 3.3 – Time resolved SAXS profiles of PHYT liquid crystalline matrices with and without 810GNR upon NIR laser activation with increasing concentrations of GNR. Panels A. PHYT, B. PHYT + 0.3 nM GNR, C. PHYT + 1.5 nM GNR, D. PHYT + 3 nM GNR. All samples were in excess water. Red arrows indicate the duration of laser exposure, in this case two repeat cycles of 5 s on, 5 s off. Increased colour intensity towards bright yellow indicates increased intensity of signal at that q-value. Annotated phase structures on the right were determined from indexing peaks in intensity vs. q profiles from individual frames.

The lattice parameters at each temperature were converted to apparent sample temperature (T_{app}) using the calibration curves in Figure 3.2, and the resulting plot of T_{app} vs. time is illustrated in Figure 3.4. In the case where no GNRs were added to the matrix, there was no significant change in lattice parameter and thus T_{app} upon laser irradiation. The reversibility of the heating effect in the presence of the GNR is evident from the T_{app} profiles for the three samples containing the nanorods. The sample containing 0.3 nM GNR heated to approximately 50 ºC, just below the transition above which coexisting H_2 phase occurs.

Increasing the nanorod concentration to 1.5 nM induces heating to a T_{app} of approx 70 ºC, while 3 nM GNR heated the matrix to an apparent temperature of 75 ºC. The repeat irradiation provided the same peak temperature within 1 – 2 ºC and reproducible kinetics of heating and cooling. The phase structures observed at the calculated T_{app} values closely agreed with the equilibrium structures apparent from the calibration plots at those temperatures, although H_2 + L_2 coexisting phases were observed for a number of samples in Figure 3.4 (squares) at 65 – 75 ºC which was not apparent in the equilibrium behavior in Figure 3.2. The L_2 phase coexists in the 1.5 and 3 nM systems on cooling below the equilibrium heating transition temperatures as indicated by the dotted lines, indicating a kinetic supercooling effect.

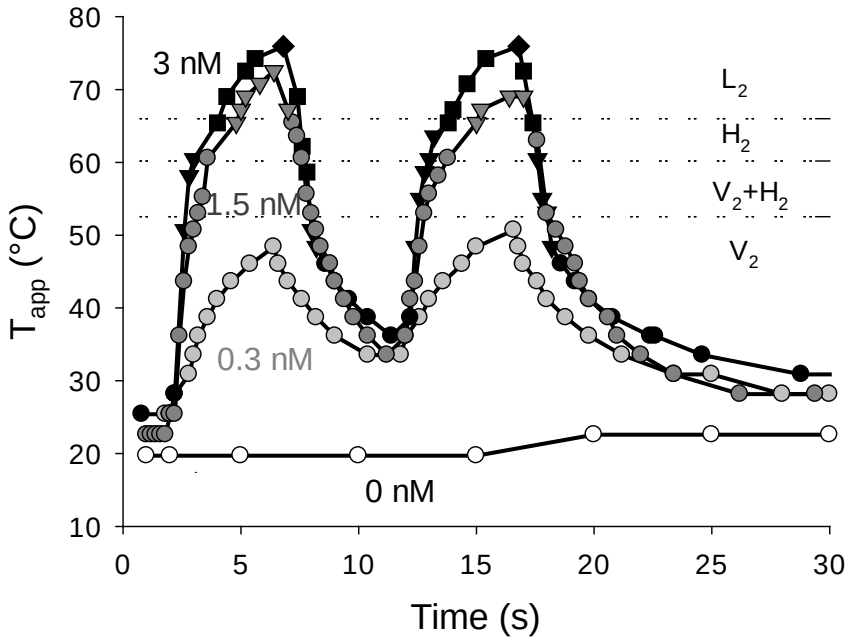

Figure 3.4 – Effect of laser irradiation on apparent temperature (T_{app}) of the PHYT + water matrix with change in GNR concentration. T_{app} was derived from lattice dimensions in Figure 3.2, using the calibration data from Figure 2. [GNR] = 0 nM white symbols, 0.3 nM grey symbols, 1.5 nM dark grey symbols, and 3 nM black symbols. Circles indicate $V_{2\ D}$, triangles indicate $V_{2\ D}$ + H_2, squares indicate H_2 + L_2, and diamonds indicate L_2. The horizontal lines indicate the typical equilibrium phase boundaries derived from the data in Figure 3.2.

3.5.3. The Effect of Initial Phase Nanostructure

The photothermal effect on the $V_{2\ D}$ PHYT matrix (Figure 3.3, Panels A. and D.) is compared to the H_2 PHYT + 5% VitEA system (Figure 3.5). Only the lipid systems containing 810GNR exhibit a phase transition upon NIR laser irradiation. The PHYT + 3 nM GNR matrix (Panel D.) initially exhibited a $V_{2\ D}$ and upon NIR exposure, transitioned to H_2 to L_2 and returns to $V_{2\ D}$ when the stimuli is removed. The PHYT + 5% VitEA system begins in the H_2 nanostructure and transitions to the L_2 phase upon a shorter irradiation time than the PHYT + 3 nM GNR matrix. The PHYT + 5% VitEA system returns to the starting nanostructure, however the process takes a

longer time than in the PHYT + 3 nM GNR cubic phase matrix. A supercooling effect was observed in both systems before returning to the starting phase of $V_{2\,D}$ and H_2 in the PHYT and PHYT + 5% VitEA systems respectively. Figure 3.6 displays the T_{app} over time for 3 nM 810GNR in both PHYT cubic phase (Panel A, 2 cycles shown) and PHYT + 5% VitEA matrices H_2 phase (Panel B, 1 cycle shown). The PHYT + 5% VitEA matrix does not reach a T_{app} value as high as the PHYT matrix.

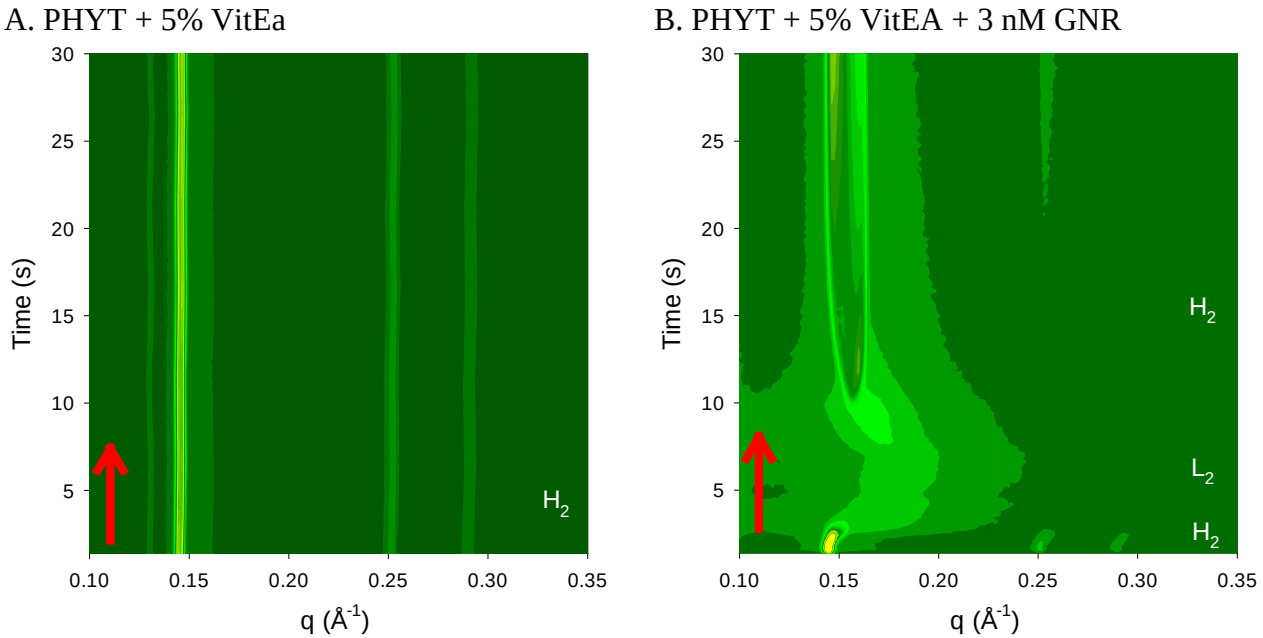

Figure 3.5 – Time resolved SAXS profiles of PHYT + 5% VitEA liquid crystalline matrices with and without 810GNR upon NIR laser activation with varying laser power. Panel A. PHYT + 5% VitEa, B. PHYT + 5% VitEA + 3 nM GNR. All samples were in excess water. Red arrows indicate the duration of laser exposure (5 s). Increased colour intensity towards bright yellow indicates increased intensity of signal at that q-value. Annotated phase structures on the right were determined from indexing peaks in intensity vs. q profiles from individual frames.

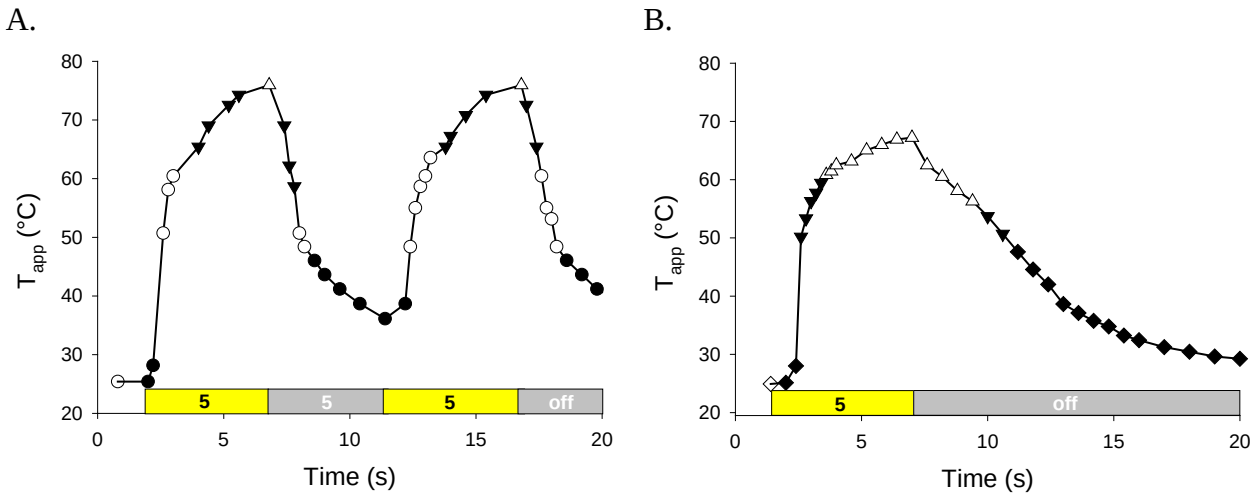

Figure 3.6 – The effect of starting nanostructure on apparent temperature (T_{app}) over time after laser irradiation. Liquid crystalline matrices of PHYT (Panel A) and PHYT + 5% VitEA (Panel B) contained 3 nM GNR810 in excess water. T_{app} was derived from lattice dimensions of the individual frames using the calibration data from static temperature scans of the different systems in Figure 3.2. Symbols represent: ● $V_{2\ D}$, ○ $V_{2\ D}$+H_2, ◆ H_2, ▼ H_2+L_2, and △ L_2.

3.5.4. The Effect of Laser Pulse Time

The apparent temperatures of the matrix (T_{app}) achieved with increasing laser pulse time for PHYT + 1.5 nM GNR810 system is shown in Figure 3.7. Longer laser exposure times resulted in an increase in the maximum T_{app} experienced by the matrix. Increasing the duration of laser exposure resulted in an increased amount of radiation being absorbed by the GNRs and consequently converted into local heat within the liquid crystalline phase. Exposure for 2 s was sufficient to provide a heating effect of over 30°C, resulting in a T_{app} of 60°C and the appearance of coexisting $V_{2\ D}$ + H_2 phases. This is consistent with the coexisting phases in the equilibrium diagram in Figure 3.2, Panel A. The increase in laser exposure time resulted in a concomitant increase in T_{app} achieved in the liquid crystal matrix. A laser exposure time of 5 s was required for the liquid crystalline phase to transition from the $V_{2\ D}$ through to a mixed phase of H_2 and L_2 nanostructure. This represented a heating effect of greater than 40 °C, with a maximum T_{app} of 70°C when irradiated for 5s.

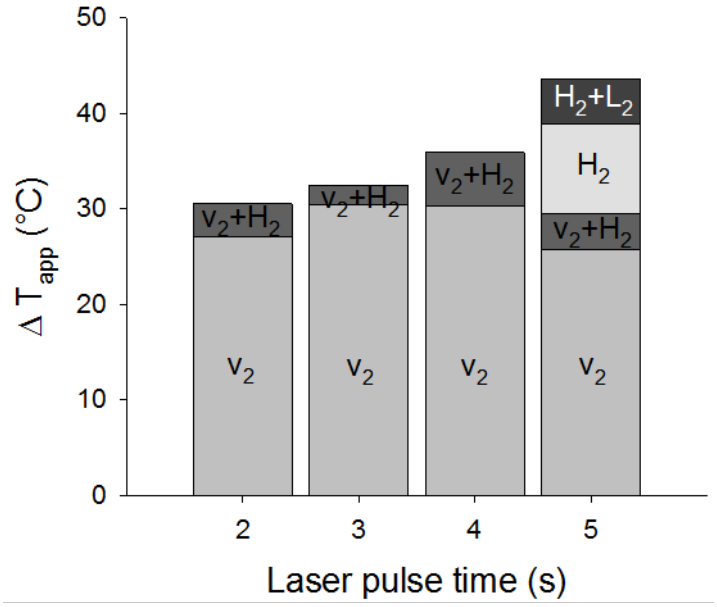

Figure 3.7 – Effect of laser pulse time on heating of a phytantriol cubic phase matrix containing GNR810 at 1.5 nM. The phases were identified by indexing peaks from the individual SAXS frames and are annotated on the bar stacks.

3.5.5. The Effect of Laser Power

A continuous wave variable-power laser was used to investigate the effect of variation in laser power on the GNR-PHYT matrix. Samples were placed at a distance of 1.2 cm from the laser source, corresponding to a spot size of 9 mm^2, and the phase transition kinetics of the LC sample followed using SAXS in Figure 3.8. All samples are initially in $V_{2\ D}$ nanostructure and only the samples which contain GNR (Panels A. – C.) exhibit a phase transition upon NIR irradiation; Panel D did not contain GNR and no change in phase or lattice parameter was observed even on extended heating at the highest power. At low laser power (25.7 mW, Panel A.), the matrix displayed a slight right shift in the q value of the $V_{2\ D}$ peaks consistent with a small heating effect, but no phase transition was observed. At 120.1 mW (Panel B.) the transitions to the H_2 phase and with increased laser power to 215.2 mW the phase transitions through the H_2 phase to the L_2 phase and returns to V_2 on cessation of irradiation.

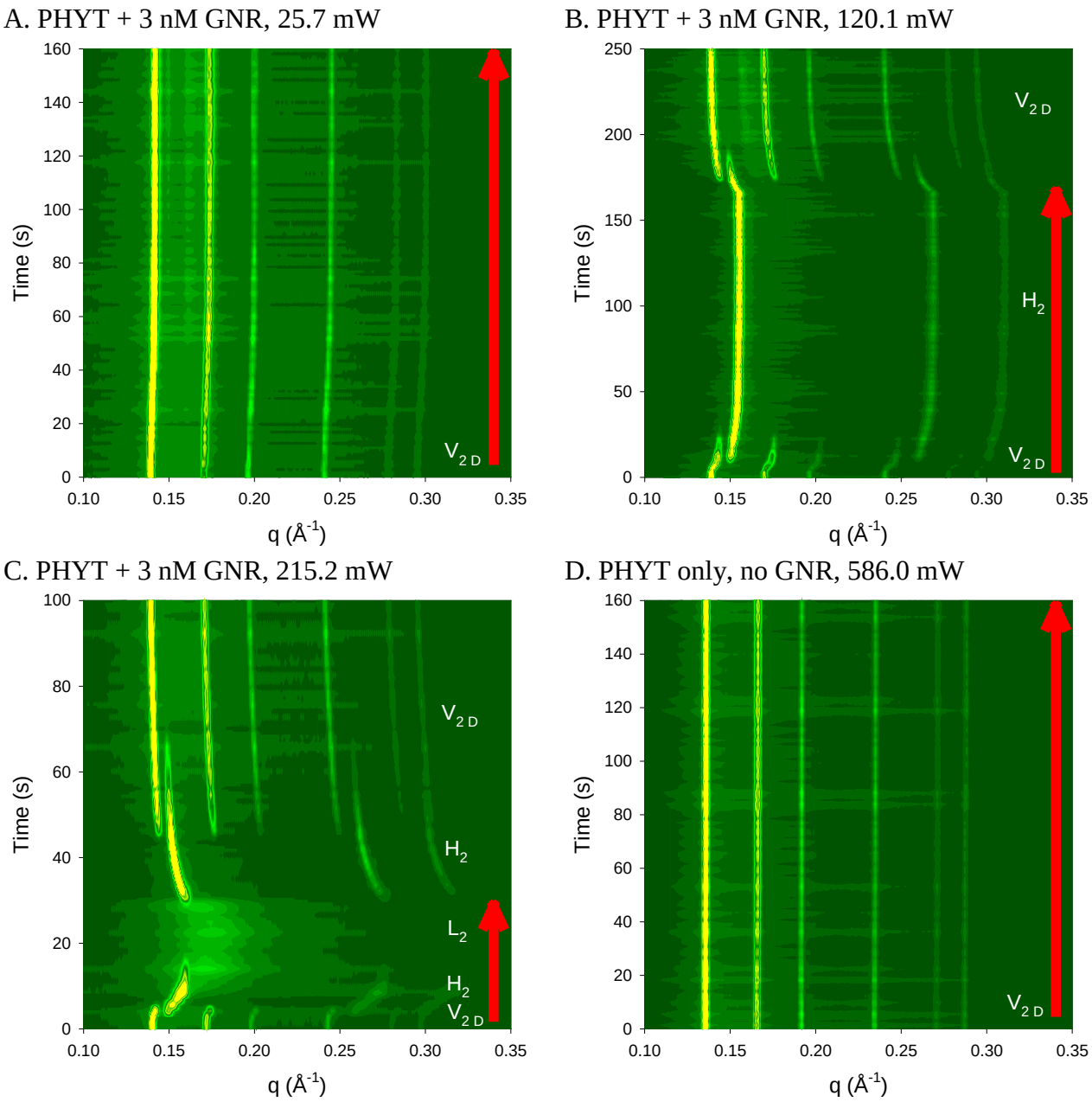

Figure 3.8 – Time resolved SAXS profiles of PHYT liquid crystalline matrices upon NIR laser activation with varying laser power. Panels A. – C. PHYT + 3nM 810GNR, Panel D. PHYT only. All samples were in excess water. Red arrows indicate the duration of laser exposure. Increased colour intensity towards bright yellow indicates increased intensity of signal at that q-value. Annotated phase structures on the right were determined from indexing peaks in intensity vs. q profiles from individual frames.

Figure 3.9 and Table 3.1 detail the irradiation time required to achieve the change in apparent temperature ΔT_{app}. There appears to be an approximately linear relationship between laser power and the maximum T_{app} achieved, as well as the irradiation time taken to reach T_{app}; the higher the laser power, the higher the T_{app} achieved in a shorter amount of time.

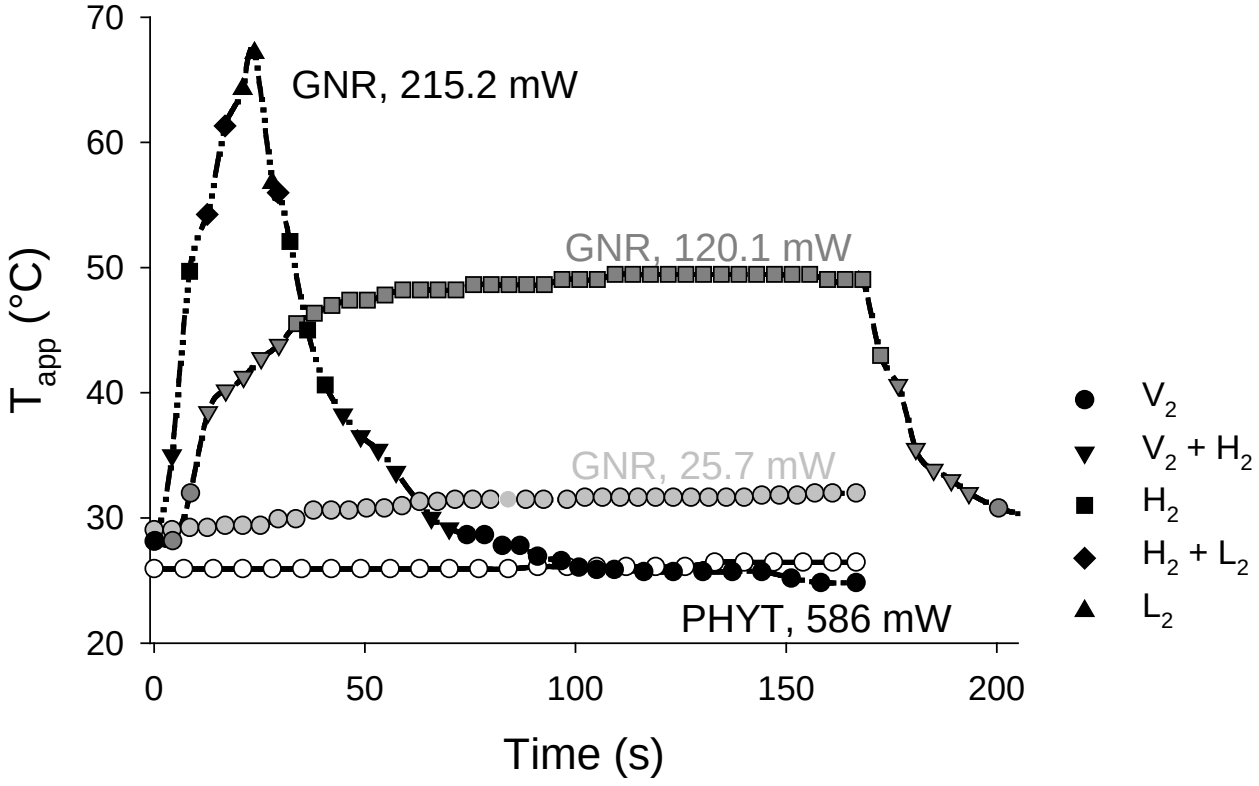

Figure 3.9 – Effect of laser power on apparent temperature (T_{app}) over time. "GNR" corresponds to a liquid crystalline matrix containing PHYT + 3 nM GNR810, and "PHYT" contains phytantriol only. Both formulations are in excess water. T_{app} was derived from lattice dimensions of the individual frames using the calibration data from static temperature scans of the different systems in Figures 3.2.

Table 3.1 – The effect of different laser powers on the irradiation time taken to achieve the maximum T_{app} and the change in T_{app} (ΔT_{app}) observed.

Laser setting	Laser Power (mW)	Irradiation Time to max T_{app} (s)	ΔT_{app} (°C)
0.4	25.7	160.0	2.9
0.5	120.1	96.8	20.9
0.6	215.2	23.8	39.0

3.5.6. Dispersed Liquid Crystalline Systems

The equilibrium phase behaviour of PHYT cubosomes and PHYT + 5% VitEA hexosomes with addition of GNR are shown in Figure 3.10, analogous to the bulk phase data in Figure 3.2.

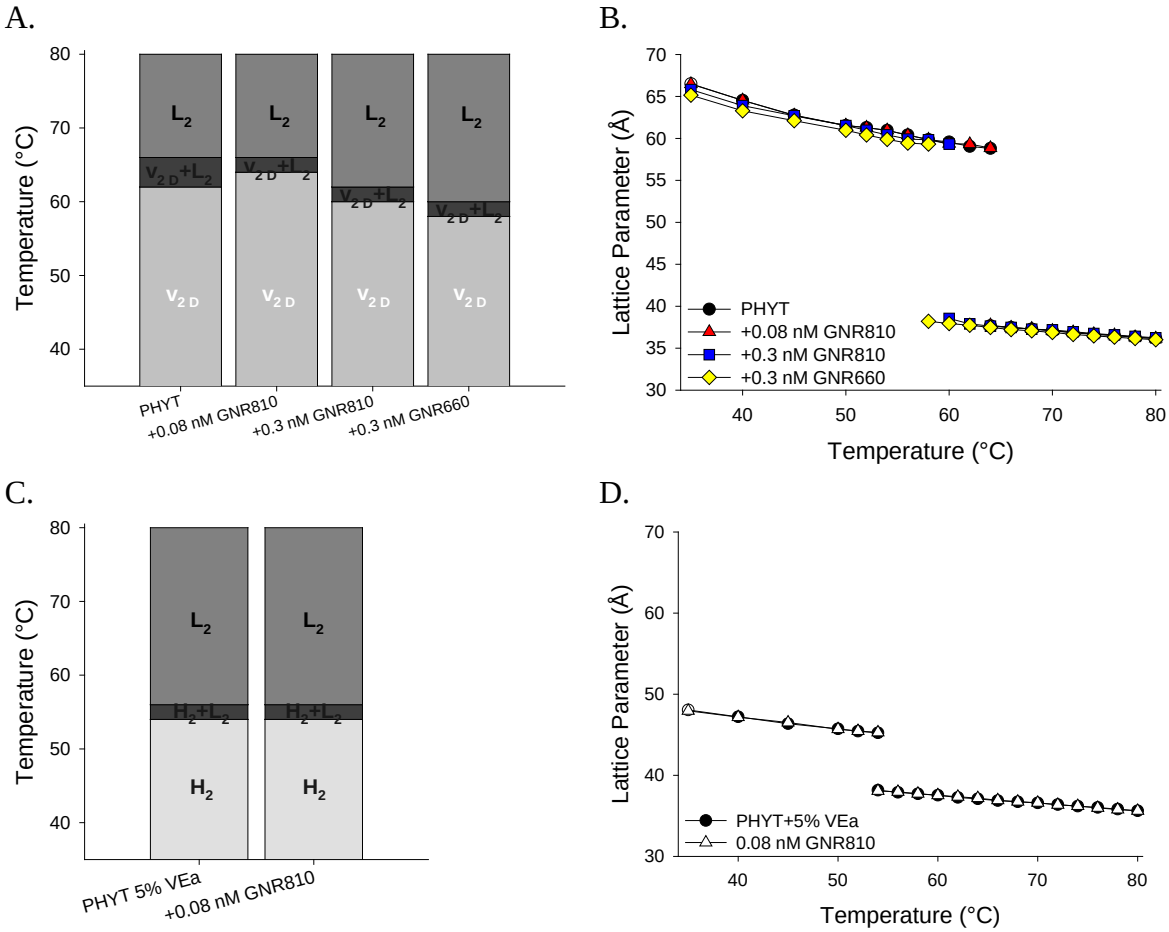

Figure 3.10 – Static temperature scans and lattice parameters of dispersed PHYT cubosomes (Panels A and B), and PHYT + 5% VitEA hexosomes (Panels C and D) with increasing concentrations of GNR. GNR810 refers to gold nanorods with a LSPR of 810 nm, GNR660 refers to gold nanorods with an LSPR of 660 nm.

The hydrophobised GNR incorporated into cubosomes and hexosomes had some minor effects on the liquid crystalline nanostructure but did not disrupt or substantially modify the equilibrium phase behaviour, consistent with the bulk phases. On direct heating, the PHYT cubosomes transitioned from $V_{2\ D}$ to L_2 as shown in Panels A. and B. The H_2 phase was not

observed, in accordance with previous reports[20]. The effect of incorporation of GNR into the dispersed $V_{2\ D}$ phase was similar to that of the bulk phase as the incorporation of GNR caused a reduction of the $V_{2\ D}$ to L_2 temperature. The H_2 to L_2 phase transition temperatures of the PHYT + 5% VitEA hexosomes are shown in Panels C and D. The addition of 0.08 nM GNR810 did not affect the H_2 to L_2 phase transition temperature of the hexosomes (Panel C.) and caused only a minor reduction in the lattice parameters of the matrix (Panel D.).

3.5.7. The Effect of Dispersion of Mesophase on the Photothermal Effect

Laser activation of GNR embedded into dispersed liquid crystal nanoparticles was investigated and the effect on scattering from the liquid crystalline particles is shown in Figure 3.11. Cubosomes containing GNR810 in concentrations at or less than 0.08 nM did not exert a heating effect on the nanostructure upon laser activation. Increasing the concentration of GNR to 0.3 nM (Panel C) resulted in a reversible phase transition from the $V_{2\ D}$ to a mixed $V_{2\ D}$ + L_2 phase on laser activation. The photothermal effect and resulting phase behaviour in this system was reversible and repeatable.

Laser activation of PHYT + 5% VitEA + 0.08 nM GNR hexosomes is shown in Figure 3.11, Panel D. A slight decrease and increase in the H_2 lattice was observed with each application of the laser, however laser activation of the GNR was not sufficient to produce sufficient plasmonic heat in order to stimulate a phase transition.

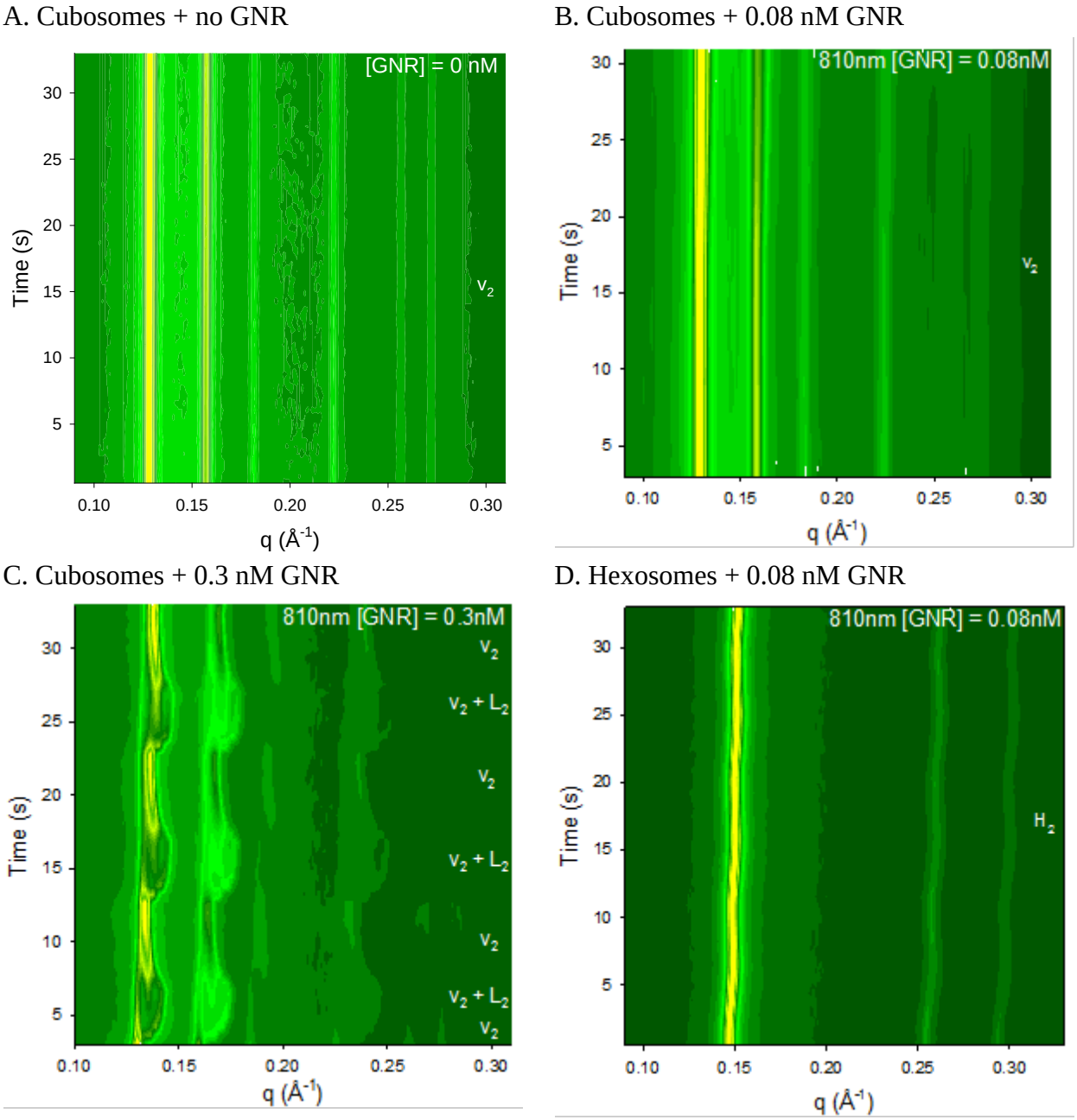

Figure 3.11 – Time resolved SAXS profiles of laser activation of GNR in dispersed liquid crystalline matrices. Panel A. PHYT cubosomes, B. PHYT + 0.08 nM GNR810, C. GNR PHYT + 0.3 nM GNR810, and D. PHYT 5% VitEA + 0.08nM GNR810. Laser application in Panels A. to D. is three repeat cycles of 5 s on, 5 s off. Increased colour intensity towards bright yellow indicates increased intensity of signal at that q-value. Annotated phase structures on the right were determined from indexing peaks in intensity vs. q profiles from individual frames.

3.5.8. The Effect of Aspect Ratio of GNRs and Irradiation Wavelength

Gold nanoparticles can be tuned to respond to specific wavelengths of light according to size, aspect ratio, geometry and composition[27]. Even the smallest change in aspect ratio can result in substantial changes to their optical properties[28, 29]. This is advantageous for photoactivated formulations, as the wavelength specificity can be finely tuned to avoid accidental activation of drug release. The wavelength specificity of GNR with different aspect ratios was investigated by comparing the behaviour of GNR with LSPRs of 810 nm (GNR810) and 660 nm (GNR660) irradiated at 808 nm under the hypothesis that the effect would be substantially attenuated for the 660 nm-responsive particles. A comparison of the T_{app} profiles for the PHYT liquid crystalline matrices upon 5 s of laser irradiation at 808 nm is shown in Figure 3.12. In the bulk phase (Panel A), the photothermal effect on the system containing the GNR660 was approximately half as effective as that of the GNR810 matrix. In the dispersed phase (Panel B), there was a negligible response from the cubosomes containing the GNR660, whereas the cubosomes containing the GNR810 achieved a T_{app} of 45 °C.

In comparison with the attenuation observed in Figure 3.12 where the plasmonic particles are mismatched to the laser frequency, GNR synthesised to optimally respond to 810 nm did not respond optimally to different wavelengths of NIR irradiation. Figure 3.13 exhibits the response of the PHYT + 3 nM 810GNR liquid crystalline matrix irradiated with a 980 nm NIR laser. There was no change in peak positions observed using SAXS (Panel A.), and consequently no change in the calculated T_{app} (Panel B.)

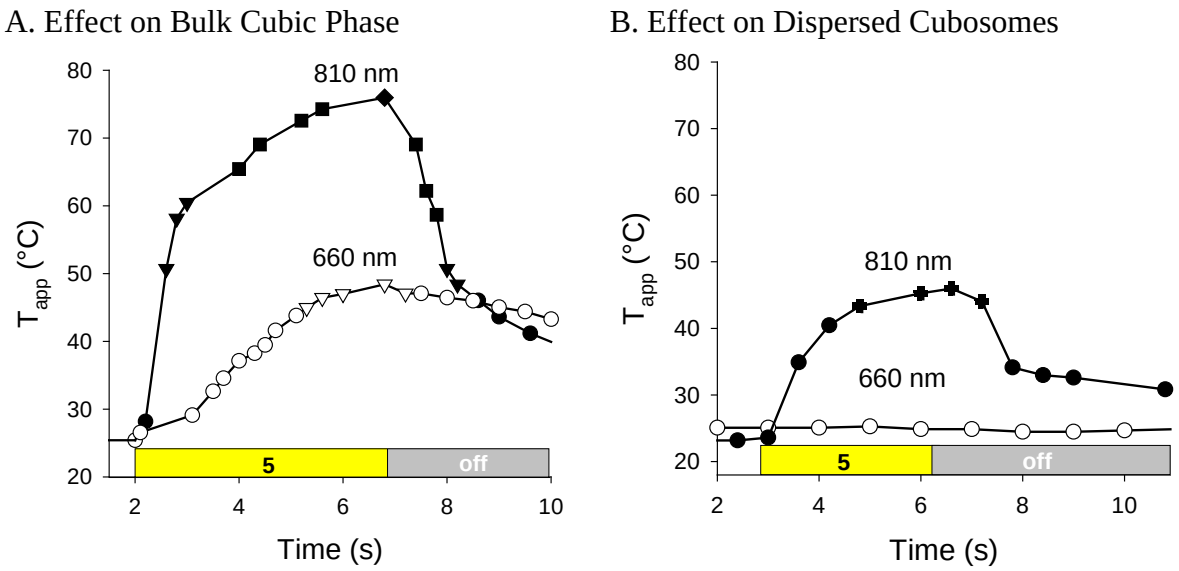

Figure 3.12 – The GNR aspect ratio effects on plasmonic heating in bulk and dipsersed systems with 5 s laser pulse: A. bulk PHYT phase + 3 nM of GNR810 (solid symbols) or GNR660 (open symbols), B. PHYT cubosomes + 0.3 nM of GNR810 (solid symbols) or GNR660 (open symbols). Circles indicate $V_{2\,D}$, triangles $V_{2\,D}$ +H_2, squares indicate H_2 + L_2, diamonds indicate L_2 and crosses indicate $V_{2\,D}$ + L_2.

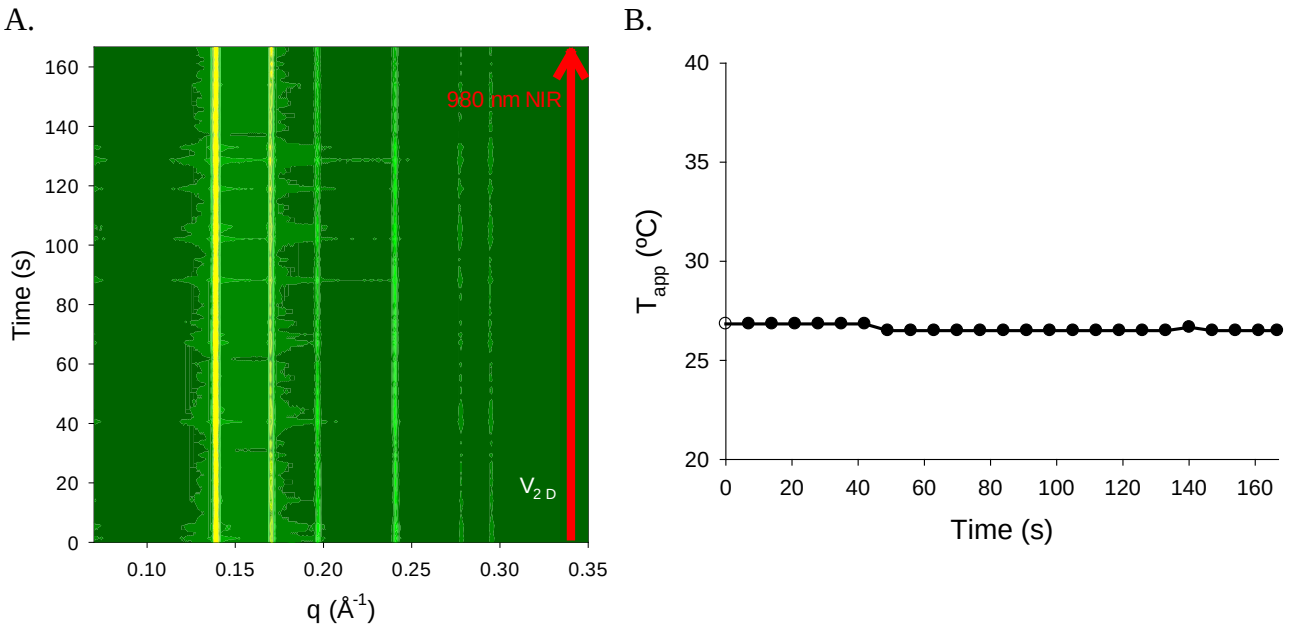

Figure 3.13 – Panel A. Time resolved SAXS profile; Panel B. apparent temperature (T_{app}) of a PHYT + 3 nM GNR liquid crystalline matrix irradiated for 160 s with a continuous wave 980 nm laser.

3.6. Photosensitisation of Self-Assembled Lipid Matrices

3.6.1. Equilibrium Behaviour of Bulk GNR-Lipid Hybrid Nanomaterials

The molecular structures, along with the literature temperature-dependent equilibrium phase structures and lattice parameters of four different lipids, phyt, GMO, SA and ME in excess water are shown in Figure 3.1. The temperature-dependent equilibrium phase structures and lattice parameters of four different lipids as determined by SAXS are shown in Figure 3.14. The presence of 3 nM GNR in the PHYT and GMO materials caused a slight reduction in the phase transition temperature and lattice parameter, as has been previously observed in these systems upon the addition of hydrophobic moieties[20, 30].

The lattice parameters of the SA matrix were unaffected by the presence of GNR, and the H_2 to L_2 phase transition of SA was not observed in the temperature range investigated. This phase transition temperature has been reported to be 63 °C[23], but was not observed in this system and is attributed to the use of a different source of material.

The phase behaviour of bulk ME in excess water was similar to previous reports, where the H_2 phase was observed during the equilibrium and dynamic studies of the ME phases, with and without GNR[31]. The phase behaviour of the ME + 3 nM GNR hybrid matrix differed from the blank ME matrix at temperatures between 62 – 72 °C. Several unresolved broad reflections appeared in the scattering profiles in this temperature range, and the $V_{2\,D}$ phase was not observed. Whilst these phase transitions at higher temperatures are of interest, it is the phase transition from the L_α to the $V_{2\,P}$ phase at ~40 °C that is of the most interest for drug delivery applications.

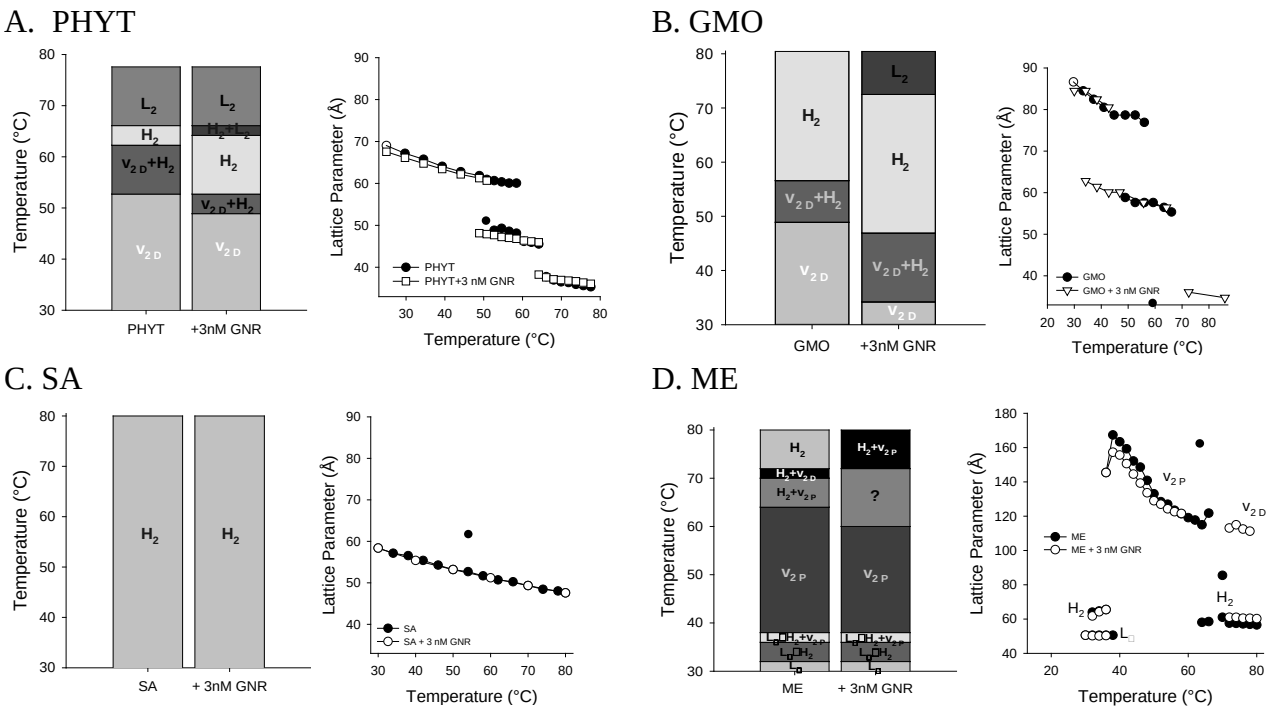

Figure 3.14 – Equilibrium phase behaviour of the four lipids and lipids + 3 nM GNR in excess water as determined by SAXS: A. phytantriol (PHYT), B. glyceryl monooleate (GMO), C. selachyl alcohol (SA) and D. monoelaidin (ME). The phases formed are annotated on the bar charts.

3.6.2. The Effect of Laser Activation on the Different Liquid Crystalline Phases

Laser activation of the GNR-lipid-water hybrid nanomaterials was employed to cause phase transitions in the liquid crystals via photothermal heating. Time-resolved SAXS patterns obtained during and after laser activation of the different systems are shown in Figure 3.15. As previously reported, the phyt-GNR matrix transitioned from the $V_{2\ D}$ to H_2 to L_2 nanostructures within 5 s on laser irradiation. On cessation of laser exposure, the system exhibited the non-equilibrium gyroid cubic phase, $V_{2\ G}$, before relaxing to the original $V_{2\ D}$ phase (Panel A.).

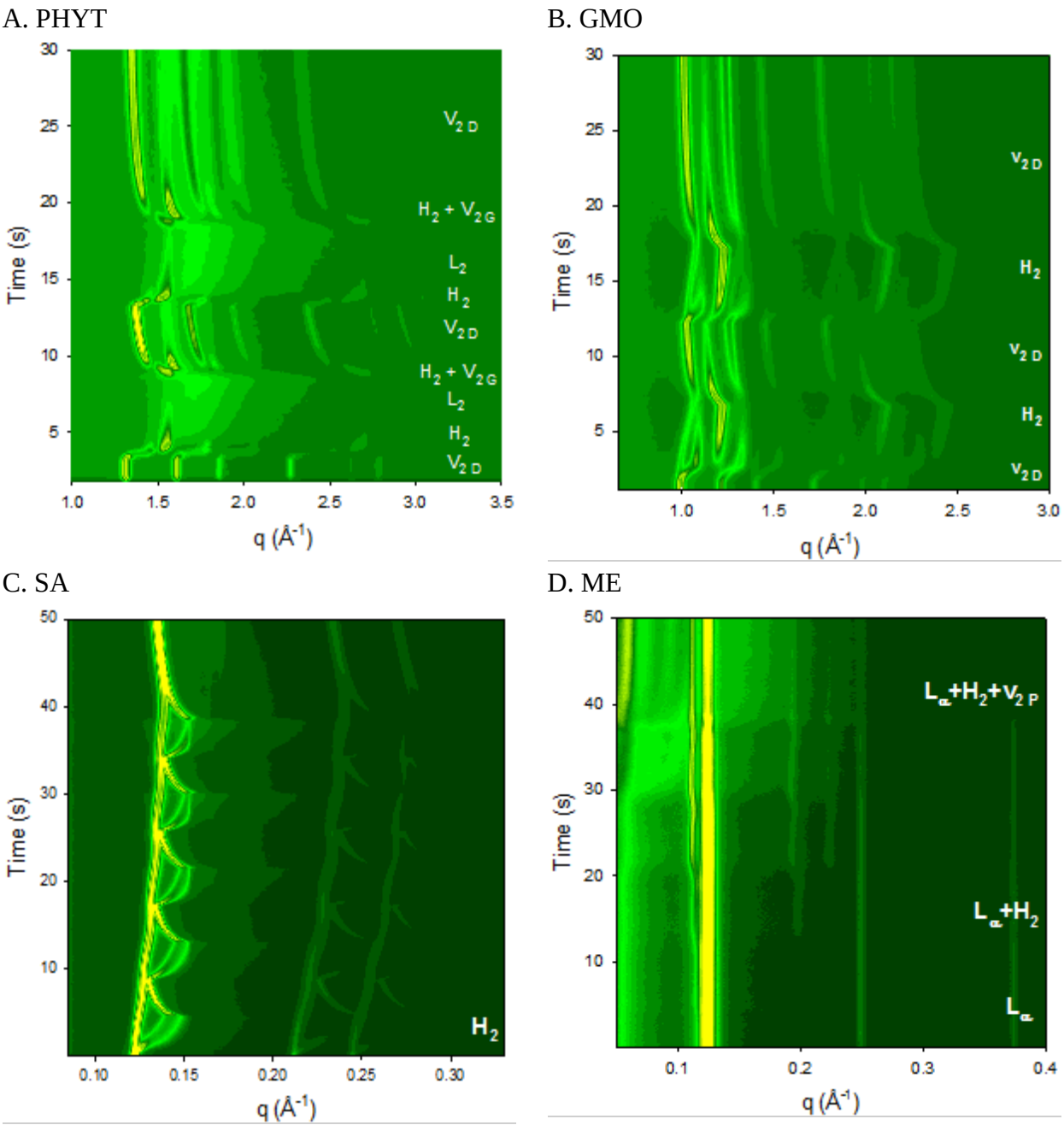

Figure 3.15 – Time resolved SAXS patterns of bulk liquid crystal phases formed with different lipids with 3 nM GNR in excess water: Panel A. PHYT, B. GMO, C. SA and D. ME. Laser application in Panels A and B was 5 s on, 5 s off x 2 and in Panels C and D, 5 s on, 5 s off x 5. Increased colour intensity towards bright yellow indicates increased intensity of signal at that q-value. Annotated phase structures on the right were determined from indexing peaks in intensity vs. q profiles from individual frames.

Laser activation of the GMO-GNR matrix caused a phase transition from the $V_{2\ D}$ to H_2 phase within 5 s of laser activation (Panel B). The amount of plasmonic heat produced was not sufficient to induce the transition to the L_2 phase seen in the case of the bulk PHYT system.

No phase transitions were observed in the SA and ME systems after an initial 5 s pulse, therefore additional 5 s laser pulses were applied. The SA-GNR matrix did not transition from H_2 to the L_2 phase, but the lattice parameter contracted and expanded, appearing to 'breathe' (Panel C). There appeared to be two independent hexagonal phases with differing lattice parameters which contracted and expanded at different rates with the laser activation and removal. Laser activation of the colloidal SA + GNR dispersion also caused the H_2 lattice to 'breathe' with each laser pulse (Figure 3.16) consistent with the behaviour of the bulk phase, however, in the dispersion, only one lattice dimension was present.

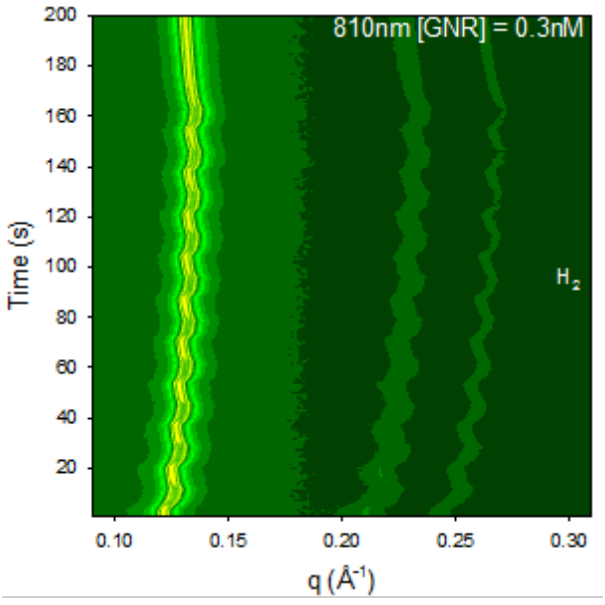

Figure 3.16 – Time-resolved SAXS patterns of laser activation of GNR in selachyl alcohol hexosomes. Laser is applied for 5 s on, 5 s off for 10 repetitions. Increased colour intensity towards bright yellow indicates an increased intensity of signal at that specific q-value. The annotated phase structure on the right was determined from indexing peaks in intensity vs. q profiles from individual frames

Repeated activation of the ME-GNR matrix (Panel D) resulted in the gradual reduction of the L_α symmetry with the concurrent formation of the H_2 and $V_{2\,P}$ phases, but no reversal of the transition during the laser 'off' time was observed. In general, the phase transitions of the GMO, ME and SA liquid crystalline matrices upon laser activation agreed with the equilibrium thermal phase behaviour shown in Figure 3.14.

The thermal phase transitions and the corresponding lattice parameters are indicative of the amount of heat transferred to the matrix on GNR activation[32, 33] and thus were used to quantify the T_{app} of the systems. The T_{app} of the liquid crystal matrices over time are shown in Figure 3.17. The non-linear behaviour of these systems was consistent with previously observed thermo-optical properties of gold nanoparticle heat transfer into the surrounding environment[34]. The maximal T_{app} achieved for the GMO, SA and ME matrices on laser activation was insufficient to cause the complete phase transitions observed in the equilibrium temperature scans.

As observed with the PHYT matrix, supercooling behaviour was observed in the GMO-GNR matrix. The H_2 phase was seen to coexist with the $V_{2\,D}$ phase down to 25 °C on cooling, well below the equilibrium transition temperature of 48 °C seen on the first heating cycle and in the temperature scan (Figure 3.17, Panel B.).

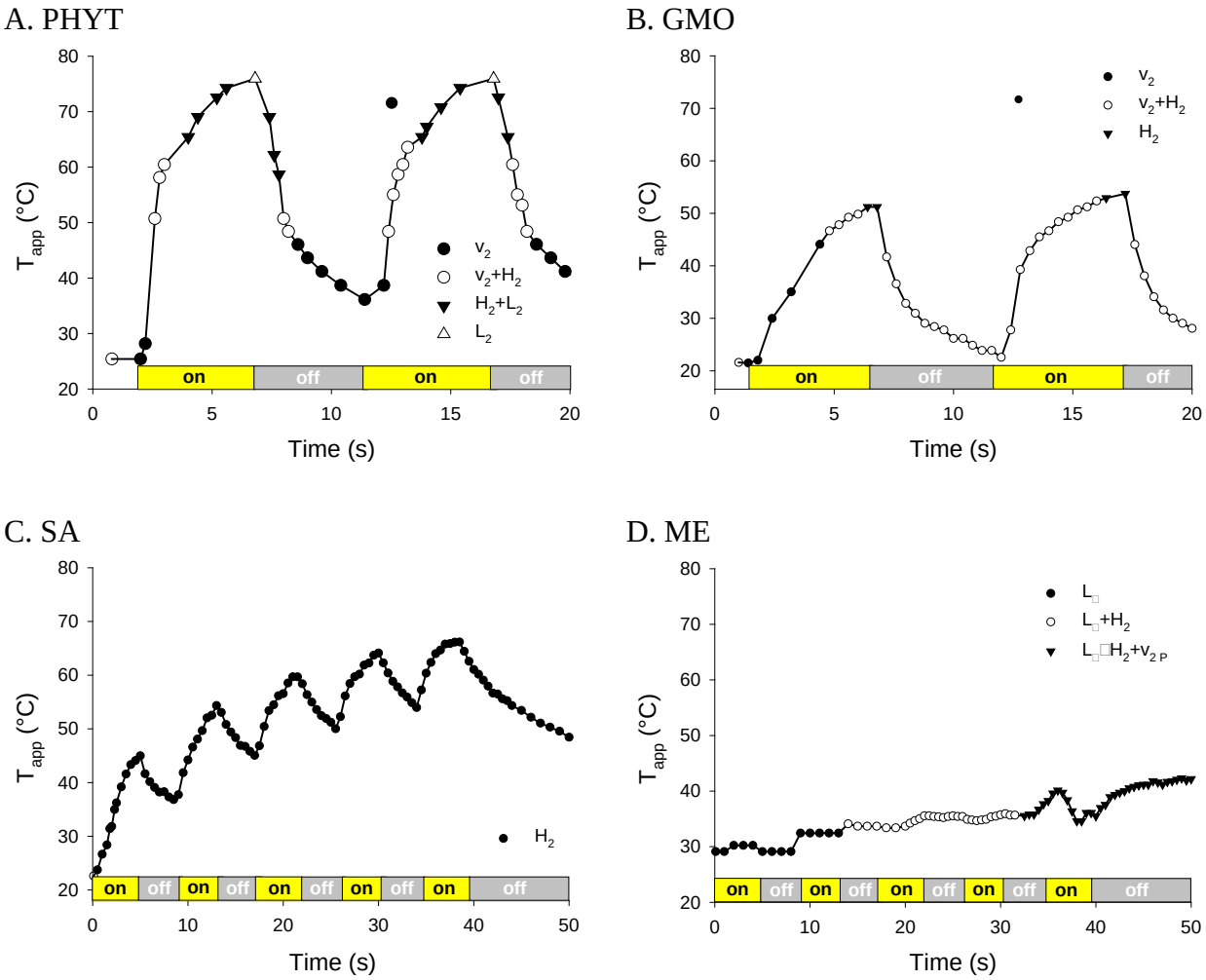

Figure 3.17 – Effect of laser irradiation on nanostructure in terms of apparent temperature (T_{app}) over time. Liquid crystalline matrices contain 3 nM GNR in excess water where the lipids are: Panel A. PHYT, B. GMO, C. SA and D. ME. T_{app} were derived from lattice dimensions of the individual frames using the calibration data from static temperature scans of the different systems.

3.6.3. Specific Heat Capacity of the Liquid Crystalline Matrices

The specific heat capacity (C_p) of the liquid crystalline matrices and their corresponding equilibrium phase behaviours are shown in Figure 3.18. The widths of the broad peaks observed in the C_p profiles for PHYT, GMO and ME liquid crystalline systems match the broad thermal phase transition events determined by SAXS. The C_p of the PHYT (Panel A.) and GMO systems (Panel B.) increased with an increase in temperature, with the appearance of each new phase resulting in a higher gradient of increase in the C_p. The appearance of L_2 in the PHYT matrix caused the steepest

increase in gradient. The C_p of SA (Panel C.) also increased with increased temperature however, as no phase transitions were observed in this phase, there was a linear increase in C_p observed. The C_p of ME (Panel D.) differed to the others as there was no linear increase observed, but fluctuated with the appearance of each phase in the fully hydrated phase. Both the initial L_α to H_2 to V_{2P} phase transition and the final V_2 to H_2 phase transitions required a large input of energy, which was represented by the sharp increases in C_p at these temperatures.

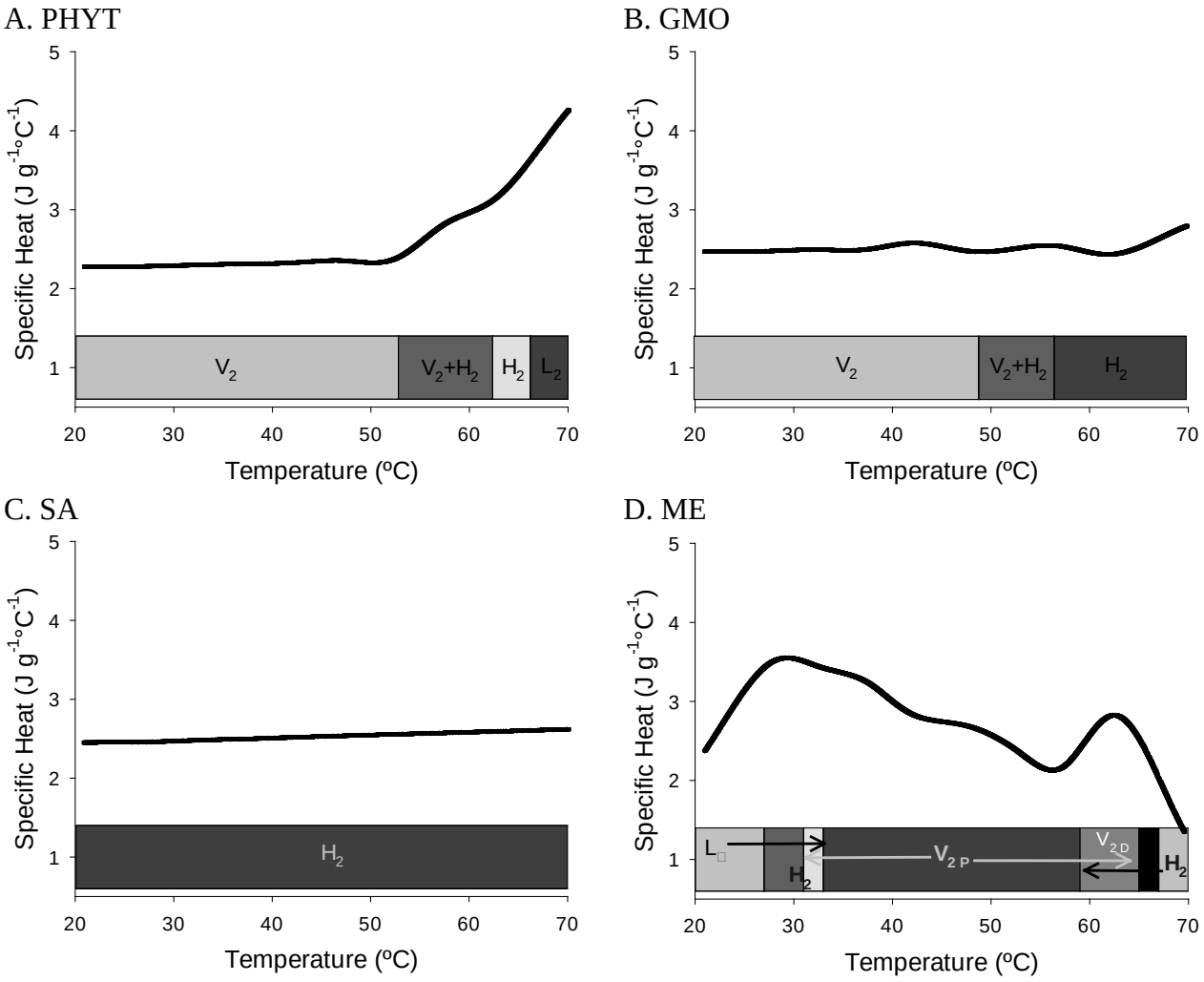

Figure 3.18 – The specific heat capacity (C_p) of A. PHYT, B. GMO, C. SA and D. ME with their equilibrium phase behaviours (horizontal stacked bars) as determined by SAXS.

3.6.4. Disposition of GNR within the Bicontinuous Cubic Nanostructure

Bulk PHYT samples were viewed using cryoFESEM in order to visualise both the effect of GNR incorporation into the liquid crystal nanostructure and the dispersity of the GNR throughout the bulk phase. The dispersity of the GNR throughout the matrix is important as gold nanoparticle aggregation can also have substantial effects on the optical properties of the system by effectively modifying the local surface plasmon resonance wavelength (LSPR) at which the particles respond[35].

The intricate nanostructure of the PHYT $V_{2\ D}$ bulk phase[36] is shown in Figure 3.19. The nodular appearance of the surface closely resembles that of the mathematical models proposed by Angelov *et al.* for the bulk phase[37] and Andersson *et al.* for cubosomes[38]. Panel B. viewed the samples using a secondary electron detector. This mode of imaging provides a contrast mechanism based on atomic number (elemental) distribution where elements of lower atomic number appear darker, and elements of higher atomic number (e.g. gold) appear as bright spots in the image. Backscattered electron analysis of the image identified the bright spots, which appear to sit within the nodes of the cubic phase, to be gold in composition. The sizes of these spots approximately matched the dimensions of the GNRs, albeit within the limitations of the spatial resolution of the imaging technique. The presence of the GNR did not alter the appearance of the liquid crystal nanostructure, and the GNR appear to be evenly distributed through the matrix.

Cubosomes with incorporated GNRs were viewed using cryoTEM. The GNRs were found to be in close proximity or incorporated into the cubosomes and hexosomes as shown in Figure 3.20. As these images are two dimensional, it is impossible to confirm whether they are incorporated into the matrix or whether they sit adjacent to the nanoparticles. However, it can be confirmed that the GNRs used were sphero-capped cylinders and do not appear to affect the internal nanostructure

of the liquid crystal particles. The different aspect ratios between GNR810 and GNR660 can be seen in the rod shapes in Figure 3.20, where GNR660 (Panel B.) were found to be significantly shorter in length than GNR810 (Panel A.).

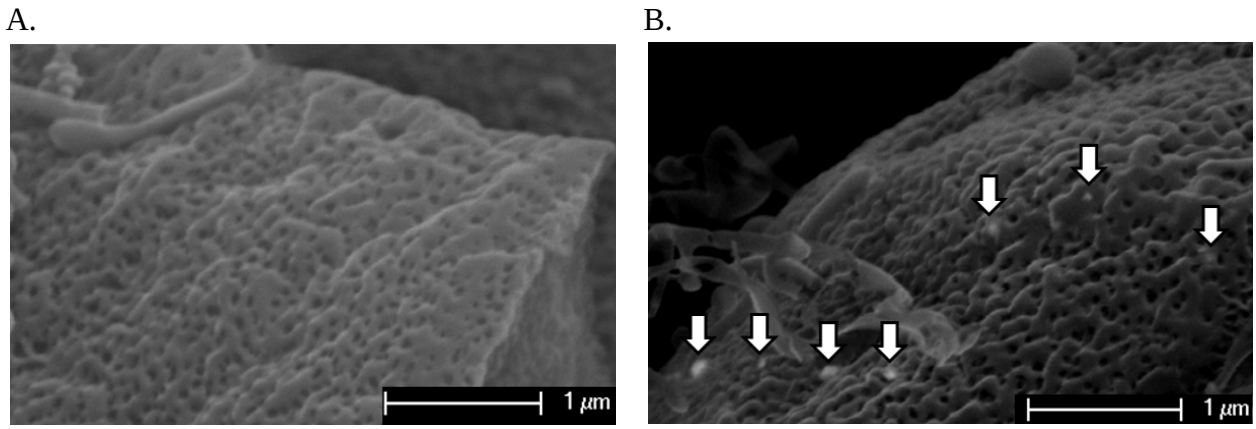

Figure 3.19 – cryoFESEM images of bulk phytantriol V_{2D} liquid crystal phase containing 3 nM GNR810. Panel A is viewed using a secondary electron detector. Panel B is viewed using a backscattered electron detector where the gold nanorods are indicated by white arrows.

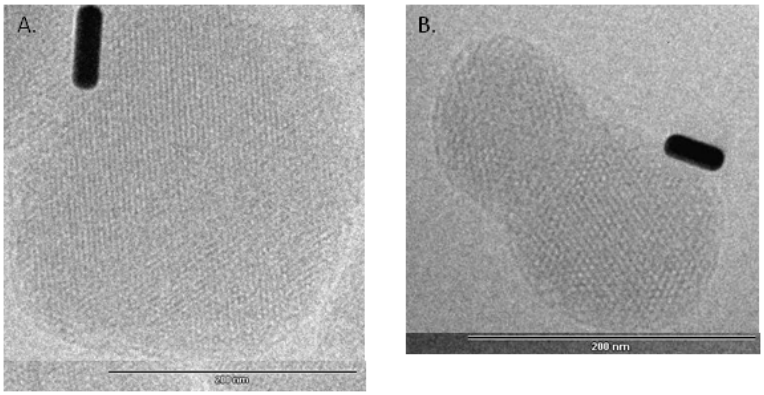

Figure 3.20 – Representative cryoTEM images of dispersed GNR-LC particles. Panel A. PHYT + 0.3 nM 810 nm GNR cubosomes and Panel B. PHYT + 0.3 nM 660 nm GNR cubosomes. Scale bar = 200 nm in each panel.

3.6.5. Disposition of GNR within the Reverse Hexagonal Nanostructure

Bulk SA samples were viewed using cryoFESEM in order to visualise both the effect of GNR incorporation into the H_2 nanostructure and the dispersity of the GNR throughout the phase. The intricate texture of the SA H_2 bulk phase is shown in Figure 3.21. This is the first known report of a cryoFESEM image of a bulk SA H_2 phase. Striations common to the inverse micellar rods of H_2 phase[39] are not observed as the magnification dimensions do not match the previously reported matrix. The image does, however, show angular faceting at 120° that is consistent with the H_2 structure[40] as indicated by the lines drawn across Panel A. Backscattered electron analyses of the images in Panel B show bright spots scattered uniformly through the liquid crystal, indicative of gold particles. The sizes of the spots are broadly consistent with the dimensions of the GNR. The circled area appears to contain aggregated GNR, which has the potential to modify the LSPR of the nanorods.

A. B.

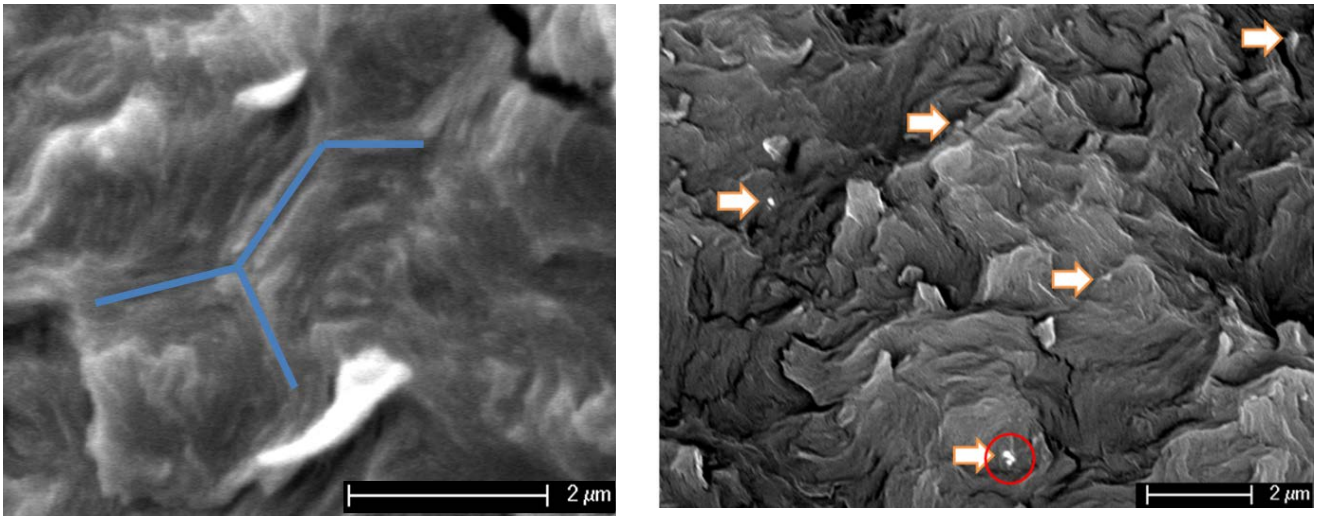

Figure 3.21 – cryoFESEM images of bulk selachyl alcohol H_2 phase. Panel A is viewed using a secondary electron detector. Panel B is viewed using a backscattered electron detector where analysis of the bright spots revealed these spots to be gold. The circled area indicates a GNR aggregate.

CryoTEM images show the GNR in close proximity or incorporated into hexosomes in both the PHYT + 10% VitEa and SA dispersions. The infinitely long hexagonal tubes and curved striations often observed for hexosomes can be clearly seen (Figure 3.22)[41]. As the cryoTEM images are two dimensional, it is impossible to determine whether the GNR are actually incorporated into the matrix or whether they are positioned adjacent to the hexosomes. However, it can be confirmed that the GNRs used are sphero-capped cylinders and again do not appear to affect the nanostructure of the hexosomes.

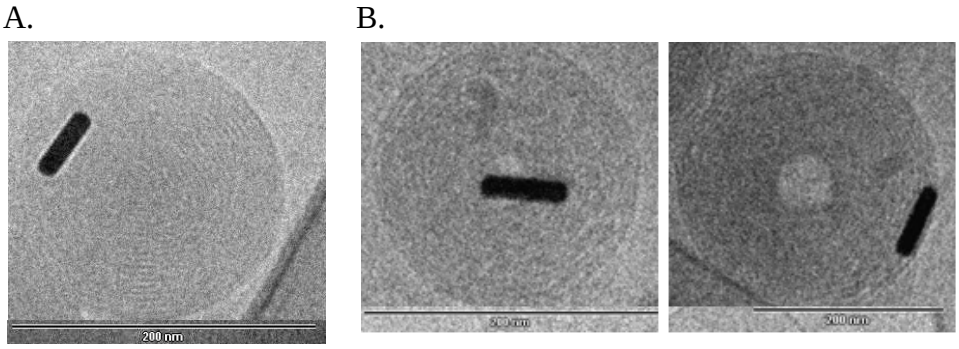

Figure 3.22 – Panel C. PHYT H_2 + 0.3 nM 810 nm GNR hexosomes. Panel B. cryoTEM images of SA + 0.3 nM 810 nm GNR hexosomes. Scale bar = 200 nm in each panel.

3.7. Discussion

3.7.1. Phytantriol Matrices

The incorporation of nanoparticles to control the phase behaviour of self-assembled systems has become an increasingly popular method for the creation of stimuli-responsive nanocomposites. It has evolved from the discovery and functionalisation of many novel materials such as metallic nanoparticles. It is important to understand the effect of additives within self-assembled systems, as it is the nanostructure of these matrices which affords their unique properties. Many groups have studied the addition of aqueous and lipid soluble components such as sugars[42] and phospholipids[43] into the cubic phase; however the effect of colloids is less well known. The response of the PHYT matrix was found to be dependent on the lipid composition of the liquid crystalline matrix, GNR concentration and aspect ratio, as well as NIR laser power wavelength and irradiation time. The effect of NIR irradiation of GNR doped PHYT matrices is summarised in Figure 3.23.

The hydrophobised GNR incorporated into the $V_{2\,D}$ matrix did not substantially modify the equilibrium phase behaviour of the liquid crystalline nanostructure. The dimensions of the GNRs are too large to interact with the nanostructure of the liquid crystal directly and instead may form occlusions in the matrix, around which the $V_{2\,D}$ unit cells can nucleate. Hydrophobic gold nanoparticles have been shown to strongly associate with the lipid bilayers in liposomes whereby heat is more efficiently conducted into the liquid crystalline nanostructure[44, 45]. It can be reasonably presumed that the hydrophobic GNR preferentially interact with lipid bilayers of the cubosome where they are able to transfer heat created by plasmon activation most efficiently. Their position is crucial as there is a very steep temperature gradient away from the surface of an activated gold nanoparticle. Activation of the surface plasmon resonance has been shown to heat a thin shell of water approximately 5 nm thick surrounding the particle[46]. A global change in

temperature was not observed in these experiments and so it appears that a global temperature change is not required to cause a global phase change. Instead, laser activation of the GNRs creates a nucleus from which a phase change propagates within the irradiated area. If this did not occur, a $V_{2\,D}$ phase present in the bulk would be observed to coexist with the H_2 or L_2 phase generated adjacent to the particle throughout the duration of laser activation.

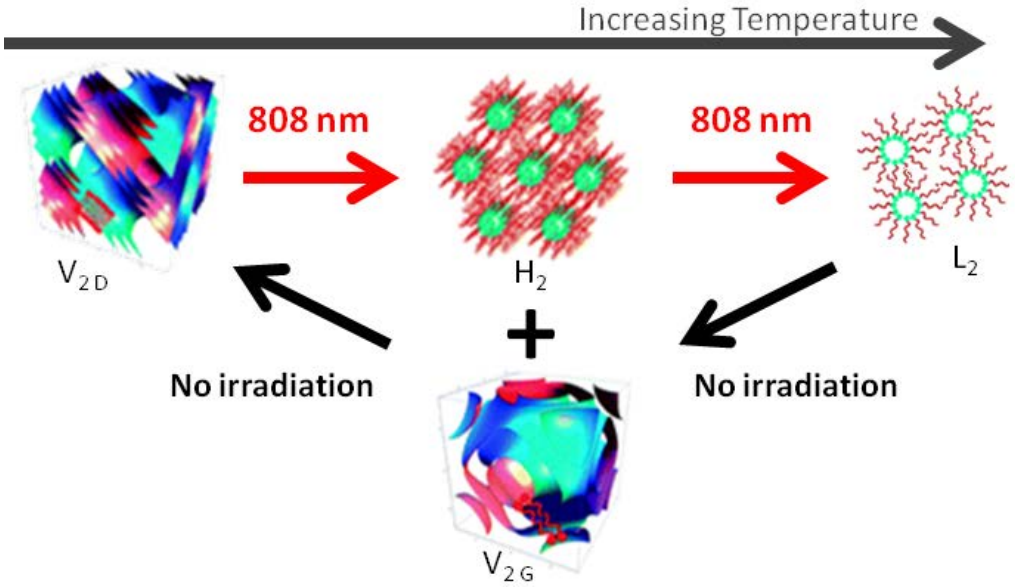

Figure 3.23 – In excess water, PHYT transitions from the double diamond bicontinuous cubic phase ($V_{2\,D}$), to the inverse hexagonal phase (H_2), then the fluid isotropic inverse micellar phase (L_2) with increasing temperature. The observed phase transition of the phyt-GNR liquid crystal upon laser irradiation. On irradition, the phyt-GNR liquid crystal transitioned from $V_{2\,D}$ to H_2 to L_2, and on cessation transtioned back from L_2 to H_2 + the non equilbrium gyroid bicontinuous cubic phase, $V_2\,G$, before returning to $V_{2\,D}$. Adapted from[47].

The addition of more than one component into self-assembled-structures tends to complicate their phase behaviour, for example, by the creation of lattice deformations thus causing bilayer distortions/disruptions and membrane curvature inhomogenicity[48]. The phase transitions within pure lipid-aqueous systems have been shown to nucleate and grow more readily than

multicomponent systems[49]. This behaviour was observed by the addition of a second additive, VitEA into the phyt+GNR matrix. Laser activation of the PHYT + GNR matrix achieved a T_{app} 10°C higher than the PHYT + 5% VitEA + GNR matrix (Figure 3.6). Both matrices were exposed to the same heat input from the activated GNR, but the more complex matrix was not able to attain the same T_{app} as the single lipid system.

The use of synchrotron SAXS has made it possible to detail the rapid reversible phase change kinetics of these self-assembled systems. The laser activated phase transitions were reversible and repeatable, and were controllable through changes in laser power and irradiation time, matrix composition and GNR properties. This indicated that the plasmonic heating of the liquid crystal did not compromise the integrity of the lipid molecules in any of the mesophases.

Nonequilibrium behaviour – Systems which exhibited phase transitions on laser irradiation also exhibited supercooling upon the cessation of irradiation the matrix before reverting back to the original phase. Non-equilibrium structures not observed on heating were observed on cooling. For example, when the laser stimulus was removed and cooling allowed for the PHYT matrix in Figure 3.4, the non-equilibrium gyroid cubic phase, $V_{2\,G}$, was observed. The H_2 phase was also seen to persist to a lower T_{app} (45°C), compared to the temperature that H_2 appears upon heating (51°C). The L_2 phase in the PHYT + 5% VitEA matrix also persisted to a lower T_{app} during cooling than during heating. The observation of supercooling in the PHYT matrices is consistent with previous studies using direct heat[50, 51], where it was hypothesised that the contraction of the lattice structure traps the system in a temporarily dehydrated state, which requires water flux back into the matrix to re-establish the equilibrium $V_{2\,D}$ structure.

Application of light activated systems to drug delivery – Colloidal dispersions of the liquid crystalline matrix are preferred for many applications like drug delivery, as these possess the same internal nanostructure as the parent phase but have much lower viscosity and higher payload

delivery attributed to their higher surface area. Preparation as a dispersion enables their deployment as injectable delivery systems. NIR activation of injectable systems may find application in the treatment of macular degeneration, where the injected nanoparticles can act as a depot in the vitreous and drug release activated through the application of the laser through the eye as required. This would minimise the frequency of injection and potentially reduce side effects associated with multiple intravitreal injections such as infection and blindness. Activation of GNR in cubosomes resulted in the formation of a mixed $V_{2\,D}$ + L_2 phase upon laser irradiation. Unlike the bulk phase, the dispersed matrix did not transition through the H_2 phase, as this phase is not observed in the equilibrium behaviour. To our knowledge this is the first report of light activated non-lamellar lipid based liquid crystalline phase transitions in nanostructured bulk and colloidal matrices. These externally triggered reversible phase transitions may provide a novel and practical solution for on-demand drug delivery.

In this study, the bulk matrices experienced heating up to T_{app} of ~75°C, although inclusion of a thermocouple registered bulk heating of the matrix of less than 2 °C. This indicates that the heat generated is rapidly dissipated and is localised close to the GNR surface as previously discussed. This finding has important implications for the *in vivo* use of these materials as the localised heating of adjacent tissue structures is unlikely, reducing the likelihood of collateral tissue damage. This novel method of drug delivery activation differs from photoablative therapy. Photoablative therapy involves the penetration of plasmonic nanoparticles into tumours, where illumination by near infrared light kills cancerous tissue by overheating [52]. However, this method of treatment is limited by the selectivity of the nanoparticles for cancerous tissue and the ability of non-spherical particles, which are more responsive to NIR light, to enter cells. Instead, the GNR-liquid crystal nanohybrid provides a potential avenue for the delivery of anti-cancer drugs to tumor sites, where the illumination of GNR promotes drug release from within the matrix.

The *in vivo* fate of gold nanoparticles is also an important issue in clinical applications due to recent interest in their application in therapeutics. Literature regarding gold nanoparticle toxicity has been reviewed; however, many unanswered questions still remain[53-55]. What is known, however, is that the toxicity and disposition of gold nanoparticles are attributed to nanoparticle size[56] and surface groups, where the surface groups of the particle can be modified to minimise cellular disruption and immune response[57-59]. Additionally, colloidal gold has been historically used for the treatment of rheumatoid arthritis[60] and thus is widely regarded as biocompatible. Gold nanoparticles have been shown to be cleared by via hepatobilary excretion, however, depending on the properties of the particle, their degradation and excretion it may take months[61]. Although there is concern regarding the safety of gold nanoparticles, the ability to functionalise their surfaces provides the ability to control the uptake and toxicity of these materials and thus control their *in vivo* safety. Dodecanethiol functionalised GNRs were used in this study to establish the proof of concept and effect of a range of experimental variables; translation to an actual product would likely require investigation into a more biocompatible coating. Further, the hydrophobic coating was used for easy preparation of the matrix; hydrophilic coatings such as PEG may work as effectively and will be investigated in future studies.

The inverse liquid crystalline phases are ideal candidates as drug delivery matrices as they control the release of drug by their tortuous nanostructure. As the V_2 phase releases drug at a faster rate than the other inverse phases[16, 62], the ideal phase transition for the system to function as a reversible pulsatile release system would be from a slow releasing phase, such as the H_2 phase, to a V_2 phase. We have demonstrated reversible phase transitions from V_2 to H_2 and L_2 and from H_2 to L_2, which are not ideal in this regard. However, the purpose of this initial study was to establish the concept of light activated liquid crystalline matrices and the effect of different variables. Systems which can reversibly transition from the lamellar phase (L_α) to the V_2 phase with an increase in temperature, such as monoelaidin[24, 63, 64], may provide an alternative system where the

bilayers of the L_α matrix can be controllably and reversibly converted to the highly porous V_2 phase with the application and removal of plasmonic heat, thus allowing for multiple activation of the drug delivery depot. Control of liquid crystalline nanostructure is key to controlling drug release from these matrices as these systems behave in a predictable fashion *in vivo*, with release behaviour being predictable when there is control over the phase formed[65, 66]. It has been previously demonstrated that by externally manipulating the temperature of a PHYT PHYT-based matrix using a heat/cool pack, it was possible to reversibly control drug release *in vitro* and *in vivo*[19]. It is anticipated that by controlling the nanostructure through laser activation of the GNR-liquid crystalline hybrid materials, a parallel effect can be achieved.

3.7.2. The Photosensitisation of Alternative Lipids

The ability of GNR to reversibly modify the phase behaviour of bulk and dispersed liquid crystal matrices prepared using alternative lipids to phytantriol has been investigated in terms of lipid composition and nanostructure of the matrix. In section 3.5, it was established that phyt-GNR matrices reversibly transition from V_2 to H_2 to L_2 phases on laser activation depending on GNR concentration, aspect ratio, laser power and pulse times. The effect of the PHYT liquid crystalline nanostructures was discussed.

The optical and dielectric properties of the matrix – It is equally as important to understand the effect that the matrix has on the photothermal conversion efficiency of the GNR[67]. The optical and dielectric properties of the liquid crystalline matrix play an important role in the photo activation of the GNR and consequent plasmonic heat transfer[28, 68]. It is these properties that afford them great potential in chemical and biological sensing[69]. The optical properties of the liquid crystal phase may cause non-specific scattering or absorption of the NIR irradiation, as they may act as a converging or diverging lens in nanocomposite material[70]. The V_2 phases are optically isotropic, whereas H_2 and L_α are optically anisotropic and translucent in appearance[71].

The turbidity of the H_2 phase of SA and L_α of ME may lead to suboptimal irradiation of the GNR and may therefore contribute to the reduced response of the matrix to irradiation. In addition, GNR are sensitive to their dielectric environments, where the GNR peak wavelength has been shown to increase linearly with local refractive index[72, 73]. The refractive indices for SA and ME (1.474 and 1.478 respectively) are higher than that of GMO and PHYT (1.463 and 1.467 respectively). The different refractive indices of the lipids suggest the modification of the LSPR of the GNR in the different liquid crystalline matrices. In addition to molecular features, dielectric properties of lipid membranes are dependent on molecular orientation[74] and environmental properties such as temperature and ion concentration[75], which could result in the fluctuation of GNR response over time. Further investigation into the effect of the changing dielectric nature of the matrix on the GNR LSPR would progress the development of these systems.

PHYT, GMO and SA – Phase transition temperatures and heat capacity of the different hybrid nanomaterials were indicative of their susceptibility to transition to a different phase upon plasmonic activation of the GNR. The GMO and SA systems had similar phase behaviour to PHYT at higher temperatures, where GMO exhibited the V_2 to H_2 to L_2 phase transitions and SA is reported to undergo the H_2 to L_2 phase transition[23]. As ME displays different phase transitions, it will be considered separately. The phase transition temperatures of GMO and SA occur at temperatures[21, 23], much higher than that of PHYT[25, 76]. As such, more plasmonic heat is required to enact a phase change in these lipids compared to PHYT. This was seen in both the maximum changes in T_{app} (ΔT_{app}) and C_p of the systems. The ΔT_{app} achieved upon 5 s of laser activation in the PHYT, GMO and SA systems are 50°C, 32°C and 23°C respectively. This was reflected in the C_p of the different systems detailed in Table 3.2. At 25°C, more energy is required to increase the matrix temperature in the H_2 phase of SA, than the V_2 phase of GMO, then the V_2 phase of PHYT. The rate increase of C_p in the SA system was higher, which may further retard the increase in matrix temperature and thus the consequent prevention of a phase change. The high temperatures

required to cause a phase transition to the L_2 phase could not be achieved within the GMO and SA liquid crystal matrices upon laser activation at the experimental variables employed in terms GNR concentration and laser pulse times. Thus, the same amount of plasmonic heat generated within these systems could not as efficiently affect the matrices with higher phase transition temperatures.

The two different rates of lattice reduction observed in the SA + 3 nM GNR matrix on laser application has been attributed to GNR aggregation. The lower viscosity of the H_2 phase[77, 78] may have allowed the GNR to aggregate, resulting in the modification of their optical properties[35]. Particle aggregation alters the aspect ratio of the GNR and consequently the LSPR. As such, aggregated GNR will not respond as effectively to the 810 nm irradiation in comparison to the unaggregated particles within the liquid crystal matrix, resulting in two rates of heating. Consequently only the H_2 matrix showing the greater response expected for dispersed GNR is shown in Figure 3.17, Panel C. The dual rate of heating was not observed in SA-GNR hexosomes and is attributed to a more even dispersion of the GNR throughout the sample.

Table 3.2 – The C_p and ΔT_{app} after 5s of NIR irradiation of all liquid crystalline matrices and the rate of increase in C_p with an increase in temperature in the PHYT, GMO and SA. The increase in C_p of PHYT, GMO and SA has been calculated between the temperatures 20 – 40°C as it was linear over this range.

Lipid	**Phase**	**C_p at 25°C (J °C^{-1} g^{-1})**	**Slope (C_p/°C)**	ΔT_{app} at 5s NIR
PHYT	V_2	2.281	2.468 x 10^{-3}	50°C
GMO	V_2	2.471	2.693 x 10^{-3}	32°C
SA	H_2	2.454	3.230 x 10^{-3}	23°C
ME	L_α	3.144	-	3°C

Monoelaidin – ME is a structural analogue of GMO with quite different phase behaviour to the other lipids, and as such, it is discussed separately to PHYT, GMO and SA. The restricted conformations in the *trans*-form of ME determines its phase behaviour[79], and allows for its rich

polymorphism in both bulk and dispersed matrices[31, 64, 80]. The ME-GNR system was investigated primarily because of the relevance of the L_α to V_2 phase transition in drug delivery applications. The higher C_p of the different phase transitions found in the ME phase affected its responsiveness to plasmonic activation. The amount of heat generated by the plasmonic activation of the GNR was not able to overcome the initial energy requirement (3.144 J $°C^{-1}$ g^{-1}) to cause the formation of the $V_{2\,P}$ phase until the fifth pulse. In previous studies, the L_α to V_2 phase transition in a monoolein matrix (4 cal g^{-1})[22] was found to be an order of magnitude larger than that of the V_2 to H_2 phase transition in PHYT PHYT (0.2 cal g^{-1})[76], further highlighting the significant difference in the thermal input required to enact a phase change from the L_α phase.

In addition, the ME system was not able to return to equilibrium as quickly as the PHYT and GMO matrices. Temperature and pressure jumps have been used to force the L_α to V_2 phase transition in dispersed ME[81] and GMO[82] formulations where the phase transition has been attributed to stalk formation. Stalks form where local lipidic connections between proximal contacting monolayers of the fusing membranes meet[83], a complex, time-consuming process that involves the growth of a well ordered structure through the simultaneous flow of both lipid and water. Thus, the lack of phase reversal within the 5 s laser off time is attributed to the formation of long living intermediates in L_α to V_2 phase transition and as such, reversal of the matrix is not as rapid or as easily achieved as in the case of the V_2 to H_2 transitions[49]. On the contrary, the V_2 to H_2 phase transition is described by a modified stalk theory, where the transition proceeds via the formation of discontinuous intermediate cubic structures which then morph into the characteristic inverse micellar rods of the H_2 phase, in a process that takes 40 ns[84].

3.8. Conclusions

The ability to externally manipulate non-lamellar liquid crystalline phase transitions by the application of near infra-red laser light by the incorporation of gold nanorods within bulk and dispersed phytantriol liquid crystal matrices has been demonstrated. The matrix response was determined by the properties of:

- the gold nanorods – aspect ratio and concentration;
- the laser – plasmon illumination time and power; and
- the liquid crystalline matrix – optical and thermodynamic properties.

The gold nanorod and laser variables can be manipulated in order to control the amount of plasmonic heat introduced into the liquid crystal matrix, and the composition of the liquid crystal matrix can be tuned for its intended purpose, for instance, the release rate of active from within the matrix. The ability to control and quantify gold nanoparticle heating behaviour in these GNR-liquid crystal nanocomposite matrices using laser light as an external stimulus has the potential for use in the creation of biosensors as well as being employed as a trigger mechanism for on-demand drug delivery. Application of some of the concepts learned in this Chapter is translated into an *in vivo* proof of concept study reported in Chapter 5.

References

1. Alvarez-Lorenzo C, Bromberg L, Concheiro A. Light-sensitive Intelligent Drug Delivery Systems Photochem Photobiol. 2009;85(4):848-60.

2. Bayer CL, Peppas NA. Advances in recognitive, conductive and responsive delivery systems J Contr Release. 2008;132(3):216-21.

3. Simpson CR, et al. Near-infrared optical properties of ex vivo human skin and subcutaneous tissues measured using the Monte Carlo inversion technique. Phys Med Biol. 1998;43(9):2465.

4. Hirsch LR, Stafford RJ, Bankson JA, Sershen SR, Rivera B, Price RE, et al. Nanoshell-mediated near-infrared thermal therapy of tumors under magnetic resonance guidance. Proc Natl Acad Sci USA 2003 November 11, 2003;100(23):13549-54.

5. Huang X, Jain PK, El-Sayed IH, El-Sayed MA. Determination of the Minimum Temperature Required for Selective Photothermal Destruction of Cancer Cells with the Use of Immunotargeted Gold Nanoparticles. Photochem Photobiol. 2006;82:412-7.

6. Ahmadi TS, Logunov SL, El-Sayed MA. Picosecond Dynamics of Colloidal Gold Nanoparticles. J Phys Chem. 1996;100(20):8053-6.

7. Dulkeith E, Niedereichholz T, Klar TA, Feldmann J, von Plessen G, Gittins DI, et al. Plasmon emission in photoexcited gold nanoparticles. Phys Rev B. 2004;70(20):205424.

8. Schwartz JA, Shetty AM, Price RE, Stafford RJ, Wang JC, Uthamanthil RK, et al. Feasibility Study of Particle-Assisted Laser Ablation of Brain Tumors in Orthotopic Canine Model. Cancer Res. 2009 February 15, 2009;69(4):1659-67.

9. Stehr J, Hrelescu C, Sperling RA, Raschke G, Wunderlich M, Nichtl A, et al. Gold NanoStoves for Microsecond DNA Melting Analysis. Nano Letters. 2008;8(2):619-23.

10. Agasti SS, Chompoosor A, You C-C, Ghosh P, Kim CK, Rotello VM. Photoregulated Release of Caged Anticancer Drugs from Gold Nanoparticles. J Am Chem Soc. 2009;131(16):5728-9.

11. Paasonen L, Sipilä T, Subrizi A, Laurinmäki P, Butcher SJ, Rappolt M, et al. Gold-embedded photosensitive liposomes for drug delivery: Triggering mechanism and intracellular release. J Contr Release. 2010;147(1):136-43.

12. Pérez-Juste J, Correa-Duarte MA, Liz-Marzán LM. Silica gels with tailored, gold nanorod-driven optical functionalities. Appl Surf Sci. 2004;226(1-3):137-43.

13. Huang J, Jackson KS, Murphy CJ. Polyelectrolyte Wrapping Layers Control Rates of Photothermal Molecular Release from Gold Nanorods. Nano Letters. 2012 2012/05/24.

14. Drummond CJ, Fong C. Surfactant self-assembly objects as novel drug delivery vehicles. Curr Opin Colloid Interface Sci. 1999;4(6):449-56.

15. Larsson K. Cubic lipid-water phases: Structures and biomembrane aspects. J Phys Chem. 1989;93(21):7304-14.

16. Lee KWY, Nguyen T-H, Hanley T, Boyd BJ. Nanostructure of liquid crystalline matrix determines in vitro sustained release and in vivo oral absorption kinetics for hydrophilic model drugs. Int J Pharm. 2009;365(1-2):190-9.

17. Brink-van der Laan Evd, Antoinette Killian J, de Kruijff B. Nonbilayer lipids affect peripheral and integral membrane proteins via changes in the lateral pressure profile. Biochim Biophys Acta Biomembr. 2004;1666(1-2):275-88.

18. Israelachvili JN, Mitchell DJ, Ninham BW. Theory of self-assembly of lipid bilayers and vesicles. Biochim Biophys Acta Biomembr. 1977;470(2):185-201.

19. Fong W-K, Hanley T, Boyd BJ. Stimuli responsive liquid crystals provide 'on-demand' drug delivery *in vitro* and *in vivo*. J Contr Release. 2009;135(3):218-26.

20. Dong Y-D, Larson I, Hanley T, Boyd BJ. Bulk and Dispersed Aqueous Phase Behavior of Phytantriol: Effect of Vitamin E Acetate and F127 Polymer on Liquid Crystal Nanostructure. Langmuir 2006;22(23):9512-8.

21. Hyde ST, Andersson S, Ericsson B, Larsson Kr. A cubic structure consisting of a lipid bilayer forming an infinite periodic minimum surface of the gyroid type in the glycerolmonooleat-water system. Z Krist. 1984 2011/03/28;168(1-4):213-9.

22. Qiu H, Caffrey M. The phase diagram of the monoolein/water system: metastability and equilibrium aspects. Biomaterials. 2000;21(3):223-34.

23. Barauskas J, Svedaite I, Butkus E, Razumas V, Larsson K, Tiberg F. Synthesis and aqueous phase behavior of 1-glyceryl monooleyl ether. Colloids Surf, B. 2005;41(1):49-53.

24. Czeslik C, Winter R, Rapp G, Bartels K. Temperature- and pressure-dependent phase behavior of monoacylglycerides monoolein and monoelaidin. Biophys J. 1995;68(4):1423-9.

25. Barauskas J, Landh T. Phase Behavior of the Phytantriol/Water System. Langmuir. 2003;19(23):9562-5.

26. de Campo L, Yaghmur A, Sagalowicz L, Leser ME, Watzke H, Glatter O. Reversible Phase Transitions in Emulsified Nanostructured Lipid Systems. Langmuir. 2004;20(13):5254-61.

27. Lee K-S, El-Sayed MA. Gold and Silver Nanoparticles in Sensing and Imaging: Sensitivity of Plasmon Response to Size, Shape, and Metal Composition. J Phys Chem B. 2006;110(39):19220-5.

28. Pérez-Juste J, Pastoriza-Santos I, Liz-Marzán LM, Mulvaney P. Gold nanorods: Synthesis, characterization and applications. Coord Chem Rev. 2005;249(17-18):1870-901.

29. Link S, Burda C, Nikoobakht B, El-Sayed MA. Laser-Induced Shape Changes of Colloidal Gold Nanorods Using Femtosecond and Nanosecond Laser Pulses. J Phys Chem B. 2000;104(26):6152-63.

30. Borne J, Nylander T, Khan A. Phase Behavior and Aggregate Formation for the Aqueous Monoolein System Mixed with Sodium Oleate and Oleic Acid. Langmuir. 2001;17(25):7742-51.

31. Yaghmur A, Sartori B, Rappolt M. Self-Assembled Nanostructures of Fully Hydrated Monoelaidin-Elaidic Acid and Monoelaidin-Oleic Acid Systems. Langmuir. 2012 2012/07/03;28(26):10105-19.

32. Richardson HH, Hickman ZN, Govorov AO, Thomas AC, Zhang W, Kordesch ME. Thermooptical Properties of Gold Nanoparticles Embedded in Ice: Characterization of Heat Generation and Melting. Nano Letters. 2006 2012/04/29;6(4):783-8.

33. Bendix PM, Reihani SNS, Oddershede LB. Direct Measurements of Heating by Electromagnetically Trapped Gold Nanoparticles on Supported Lipid Bilayers. ACS Nano. 2010 2012/04/29;4(4):2256-62.

34. Pustovalov V, Astafyeva L. Nonlinear thermo-optical properties of two-layered spherical system of gold nanoparticle core and water vapor shell during initial stage of shell expansion. Nanoscale Res Lett. 2011;6(1):448.

35. Kim T, Lee K, Gong M-s, Joo S-W. Control of Gold Nanoparticle Aggregates by Manipulation of Interparticle Interaction. Langmuir. 2005 2012/05/09;21(21):9524-8.

36. Rizwan SB, Dong YD, Boyd BJ, Rades T, Hook S. Characterisation of bicontinuous cubic liquid crystalline systems of phytantriol and water using cryo field emission scanning electron microscopy (cryo FESEM). Micron. 2007;38(5):478-85.

37. Angelov B, Angelova A, Garamus VM, Lebas Gv, Lesieur S, Ollivon M, et al. Small-Angle Neutron and X-ray Scattering from Amphiphilic Stimuli-Responsive Diamond-Type Bicontinuous Cubic Phase. J Am Chem Soc. 2007;129(44):13474-9.

38. Andersson S, Jacob M, Lidin S, Larsson K. Structure of the cubosome - a closed lipid bilayer aggregate. Z Kristallogr. 1995;210:315-8.

39. Tan G, Xu P, John VT, He J, McPherson GL, Agarwal V, et al. Cryo-Field Emission Scanning Electron Microscopy Imaging of a Rigid Surfactant Mesophase. Langmuir. 2008 2011/12/05;24(19):10621-4.

40. Boyd BJ, Rizwan SB, Dong Y-D, Hook S, Rades T. Self-Assembled Geometric Liquid-Crystalline Nanoparticles Imaged in Three Dimensions: Hexosomes Are Not Necessarily Flat Hexagonal Prisms. Langmuir. 2007;23(25):12461-4.

41. Sagalowicz L, Michel M, Adrian M, Frossard P, Rouvet M, Watzke HJ, et al. Crystallography of dispersed liquid crystalline phases studied by cryo-transmission electron microscopy. Journal of Microscopy. 2006;221(2):110-21.

42. Mezzenga R, Grigorov M, Zhang Z, Servais C, Sagalowicz L, Romoscanu AI, et al. Polysaccharide-Induced Order-to-Order Transitions in Lyotropic Liquid Crystals. Langmuir. 2005;21(14):6165-9.

43. Mulet X, Templer RH, Woscholski R, Ces O. Evidence That Phosphatidylinositol Promotes Curved Membrane Interfaces. Langmuir. 2008 2012/04/23;24(16):8443-7.

44. Park S-H, Oh S-G, Mun J-Y, Han S-S. Loading of gold nanoparticles inside the DPPC bilayers of liposome and their effects on membrane fluidities. Colloids Surf, B 2006 48 (2):112-8

45. Paasonen L, Laaksonen T, Johans C, Yliperttula M, Kontturi K, Urtti A. Gold nanoparticles enable selective light-induced contents release from liposomes. J Contr Release. 2007;122(1):86-93.

46. Govorov A, Zhang W, Skeini T, Richardson H, Lee J, Kotov N. Gold nanoparticle ensembles as heaters and actuators: melting and collective plasmon resonances. Nanoscale Res Lett. 2006;1(1):84-90.

47. Fong C, Le T, Drummond CJ. Lyotropic liquid crystal engineering-ordered nanostructured small molecule amphiphile self-assembly materials by design. Chem Soc Rev. 2012;41(3):1297-322.

48. Leaver MS, Holmes MC. Intermediate Phases. In: Lynch ML, Spicer PT, editors. Bicontinuous Liquid Crystals. Surfactant Science: CRC Press; 2005. p. 15-40.

49. Angelov B, Angelova A, Vainio U, Garamus VM, Lesieur S, Willumeit R, et al. Long-Living Intermediates during a Lamellar to a Diamond-Cubic Lipid Phase Transition: A Small-Angle X-Ray Scattering Investigation. Langmuir. 2009;25(6):3734-42.

50. Dong Y-D, Tilley AJ, Larson I, Lawrence MJ, Amenitsch H, Rappolt M, et al. Nonequilibrium Effects in Self-Assembled Mesophase Materials: Unexpected Supercooling Effects for Cubosomes and Hexosomes. Langmuir. 2010;26(11):9000-10.

51. Muller F, Salonen A, Glatter O. Phase behavior of Phytantriol/water bicontinuous cubic Pn3m cubosomes stabilized by Laponite disc-like particles. J Colloid Interface Sci. 2010;342(2):392-8.

52. Orca S. Targeting Cancer Cells with Nanoparticles 2009 [cited 2012 2nd July]. Available from: http://hplusmagazine.com/2009/10/06/targeting-cancer-cells-nanoparticles/.

53. Alkilany AM, Murphy CJ. Toxicity and cellular uptake of gold nanoparticles: what we have learned so far? J Nanopart Res. 2010;12(7):2313-33.

54. Alkilany AM, Thompson LB, Boulos SP, Sisco PN, Murphy CJ. Gold nanorods: Their potential for photothermal therapeutics and drug delivery, tempered by the complexity of their biological interactions. Adv Drug Deliv Rev. 2012;64(2):190-9.

55. Murphy CJ, Gole AM, Stone JW, Sisco PN, Alkilany AM, Goldsmith EC, et al. Gold Nanoparticles in Biology: Beyond Toxicity to Cellular Imaging. Accounts Chem Res. 2008;41(12):1721-30.

56. Chen Y-S, Hung Y-C, Liau I, Huang G. Assessment of the In Vivo Toxicity of Gold Nanoparticles. Nanoscale Res Lett. 2009;4(8):858 - 64.

57. Alkilany AM, Nagaria PK, Hexel CR, Shaw TJ, Murphy CJ, Wyatt MD. Cellular Uptake and Cytotoxicity of Gold Nanorods: Molecular Origin of Cytotoxicity and Surface Effects. Small. 2009;5(6):701-8.

58. Takahashi H, Niidome Y, Niidome T, Kaneko K, Kawasaki H, Yamada S. Modification of Gold Nanorods Using Phosphatidylcholine to Reduce Cytotoxicity. Langmuir. 2006;22(1):2-5.

59. Hauck TS, Ghazani AA, Chan WCW. Assessing the Effect of Surface Chemistry on Gold Nanorod Uptake, Toxicity, and Gene Expression in Mammalian Cells. Small. 2008;4(1):153-9.

60. Thakor AS, Jokerst J, Zavaleta C, Massoud TF, Gambhir SS. Gold Nanoparticles: A Revival in Precious Metal Administration to Patients. Nano Letters. 2011 2011/10/12;11(10):4029-36.

61. Cho W-S, Cho M, Jeong J, Choi M, Han BS, Shin H-S, et al. Size-dependent tissue kinetics of PEG-coated gold nanoparticles. Toxicology and Applied Pharmacology. 2010 5/15/;245(1):116-23.

62. Phan S, Fong W-K, Kirby N, Hanley T, Boyd BJ. Evaluating the link between self-assembled mesophase structure and drug release. Int J Pharm. 2011;421(1):176-82.

63. Chung H, Caffrey M. Polymorphism, mesomorphism, and metastability of monoelaidin in excess water. Biophys J. 1995 Nov;69(5):1951-63.

64. Yaghmur A, Laggner P, Almgren M, Rappolt M. Self-Assembly in Monoelaidin Aqueous Dispersions: Direct Vesicles to Cubosomes Transition. PLoS ONE. 2008;3(11):e3747.

65. Nguyen TH, Hanley T, Porter CJH, Larson I, Boyd BJ. Phytantriol and glyceryl monooleate cubic liquid crystalline phases as sustained-release oral drug delivery systems for poorly water-soluble drugs II. In-vivo evaluation. Journal of Pharmacy and Pharmacology. 2010;62(7):856-65.

66. Nguyen T-H, Hanley T, Porter CJH, Boyd BJ. Nanostructured liquid crystalline particles provide long duration sustained-release effect for a poorly water soluble drug after oral administration. J Contr Release. 2011;153(2):180-6.

67. Chen H, Shao L, Ming T, Sun Z, Zhao C, Yang B, et al. Understanding the Photothermal Conversion Efficiency of Gold Nanocrystals. Small. 2010;6(20):2272-80.

68. Belotskii ED, Tomchuk PM. Surface electron-phonon energy exchange in small metallic particles. Int J Electron. 1992;73(5):955 - 7.

69. Saha K, Agasti SS, Kim C, Li X, Rotello VM. Gold Nanoparticles in Chemical and Biological Sensing. Chemical Reviews. 2012 2012/05/09;112(5):2739-79.

70. Guillet Y, Rashidi-Huyeh M, Prot D, Palpant B. Gold nanoparticle assemblies: interplay between thermal effects and optical response. Gold Bulletin. 2008;41(4):341-8.

71. Rosevear F. The microscopy of the liquid crystalline neat and middle phases of soaps and synthetic detergents. J Am Oil Chem Soc. 1954; 31 (12):628-39.

72. Miller MM, Lazarides AA. Sensitivity of Metal Nanoparticle Surface Plasmon Resonance to the Dielectric Environment. J Phys Chem B. 2005;109(46):21556-65.

73. Xu G, Tazawa M, Jin P, Nakao S, Yoshimura K. Wavelength tuning of surface plasmon resonance using dielectric layers on silver island films. Applied Physics Letters. 2003 06/02/;82(22):3811-3.

74. Ohki S. Dielectric constant and refractive index of lipid bilayers. Journal of Theoretical Biology. 1968 4//;19(1):97-115.

75. Kimura Y, Ikegami A. Local dielectric properties around polar region of lipid bilayer membranes. J Membrain Biol. 1985 1985/10/01;85(3):225-31.

76. Dong Y-D, Dong AW, Larson I, Rappolt M, Amenitsch H, Hanley T, et al. Impurities in Commercial Phytantriol Significantly Alter Its Lyotropic Liquid-Crystalline Phase Behavior. Langmuir. 2008;24(13):6998-7003.

77. Mezzenga R, Meyer C, Servais C, Romoscanu AI, Sagalowicz L, Hayward RC. Shear Rheology of Lyotropic Liquid Crystals: A Case Study. Langmuir. 2005;21(8):3322-33.

78. Amar-Yuli I, Wachtel E, Shalev DE, Aserin A, Garti N. Low Viscosity Reversed Hexagonal Mesophases Induced by Hydrophilic Additives. J Phys Chem B. 2008 2012/05/17;112(13):3971-82.

79. Yamamura Y, Saito K. Effect of Cis and Trans Double Bonds on Conformational Disordering of the Hydrocarbon Chain of Lipid, Unsaturated Monoacylglycerols, in the Lamellar Phase of a Binary System with Water. The Journal of Physical Chemistry B. 2011 2012/10/18;115(50):14963-8.

80. Kulkarni CV. Nanostructural Studies on Monoelaidinâ€“Water Systems at Low Temperatures. Langmuir. 2011 2012/10/18;27(19):11790-800.

81. Conn CE, Ces O, Mulet X, Finet S, Winter R, Seddon JM, et al. Dynamics of Structural Transformations between Lamellar and Inverse Bicontinuous Cubic Lyotropic Phases. Phys Rev Lett. 2006;96(10):108102.

82. Kraineva J, Narayanan RA, Kondrashkina E, Thiyagarajan P, Winter R. Kinetics of Lamellar-to-Cubic and Intercubic Phase Transitions of Pure and Cytochrome c Containing Monoolein Dispersions Monitored by Time-Resolved Small-Angle X-ray Diffraction. Langmuir. 2005;21(8):3559-71.

83. Kozlovsky Y, Kozlov MM. Stalk Model of Membrane Fusion: Solution of Energy Crisis. Biophys J. 2002;82(2):882-95.

84. Marrink SJ, Tieleman DP. Molecular dynamics simulation of spontaneous membrane fusion during a cubic-hexagonal phase transition. Biophys J. 2002 Nov;83(5):2386-92.

Chapter 4 – Photochromics for UV-Induced Steric Disturbance of Liquid Crystalline Nanostructure

4. Photochromics for UV-Induced Steric Disturbance of Liquid Crystalline Nanostructure

4.1.Declaration for Chapter 4

Part of the research presented in this chapter has been published as: Fong W-K, Malic N, Evans R, Hawley A, Boyd B, Hanley T. Alkylation of Spiropyran Moiety Provides Reversible Photo-Control over Nanostructured Soft Materials. Biointerphases. 2012; 7(1):1-5.

4.2. Introduction

Light sensitive materials based on organic photochromic molecules have been proposed for the next generation of optical, electronic and mechanical materials and devices for purposes ranging from memory devices and switches to on-demand drug delivery depots[1-3]. Photochromics have a molecular structure that can be reversibly and reliably modified in a controllable manner[4]. These molecules have been incorporated into a range of materials where the unique differences in properties between their isomers upon photoisomerisation have been utilised to manipulate their immediate environment. The most manipulated photoreaction is the ring-opening and ring closing of many photochromics, which can not only cause a steric change in molecular shape, but also can result in a change in conductivity due to the ionisation of the photochromic groups[5].

Towards the development of light responsive soft materials, photochromic additives have been used to impart photosensitivity into materials such as polymers and self-assembled structures[6-9]. When exposed to specific wavelengths of ultraviolet (UV) light, photochromics can reversibly switch between two isomeric forms of the chemical species. This feature has led to photochromic moieties, such as spiropyran and azobenzene, being incorporated into self-assembled systems to sensitise these matrices for light activated drug release[10, 11]. The use of UV light to trigger drug release has also been shown to improve intercellular penetration of drugs[12].

Consequently, photochromics were incorporated into lipid-based liquid crystal materials in order to impart photosensitivity upon these matrices as potential triggers for pulsatile active release. As described in previous chapters, some amphiphilic molecules form thermodynamically stable nanostructures, which control the rate of drug release from the material[13-15]. It was hypothesised that sufficient steric disturbance in the lipid packing, caused by the light-activated isomerisation of photochromic moieties in the lipid bilayer can cause a change in nanostructure and thus 'trigger' a change in drug release, analogous to that of a previously reported system which utilised temperature as a stimulus[16].

With the need for a non-invasive means of controlling drug release, this chapter reports the incorporation of photochromics into liquid crystalline systems and the effect of irradiation upon the nanostructure. Two main groups of photochromics, shown in Figure 4.1, were investigated for their compatibility in liquid crystalline materials. Azobenzenes are photochromic compounds that undergo a reversible *trans* to *cis* isomerisation upon exposure to UV irradiation in solution. UV light (320 – 375 nm) promotes the *trans* to *cis* conversion as it corresponds to the energy gap of the π-π* (S_2 state). Blue light (400 – 450 nm) causes the reversal of the isomerisation, as this wavelength of light is equivalent to the n-π* (S_1 state) transition. In addition, the *cis* isomer is less stable than the *trans* isomer due to its distorted configuration, thus the *cis* isomer will thermally relax back to the trans isomer[17]. The shortening in bond length between the 4- and 4' carbons and consequent conformational changes caused by photoisomerisation is the main feature of this photochrome which provides the molecular switch for responsive materials[18].

Spiro compounds, like azobenzenes, have been extensively studied over the past century[1, 4, 19, 20]. Spiropyrans isomerise between the colourless, non-ionic spiro and the coloured, charged merocyanine (MC) form when exposed to wavelengths of UV light (250 – 380 nm) (Figure 4.1). Spirooxazines are structurally related to spiropyrans, however do not ionise upon

photoisomerisation[2]. This family of photochromics has been well studied and been shown to induce changes in materials such as liquid crystal phase structure[21] and modifying the self-assembly of lipid and surfactant membranes[22-25]. Drummond *et al.* synthesised a series of spiropyran surfactants, where equilibrium photochemical and physicochemical behaviour was able to control both surface activity and self-assembly of structural change[26-28]. Spirooxazines are also commonly used as photosensitisers in polymeric ophthalmic lenses[29].

On the basis of this past literature, spiro compounds were therefore investigated in this Chapter for their ability to induce phase changes in LC matrices on irradiation with UV light. Further, we introduce a novel alkylated spiropyran derivative, spiropyran laurate (SPL), hypothesised to interact more strongly with the lipid matrix than non-derivatised photochromics.

Name	Molecular Structure	3D Structure
Azobenzene (AZO)	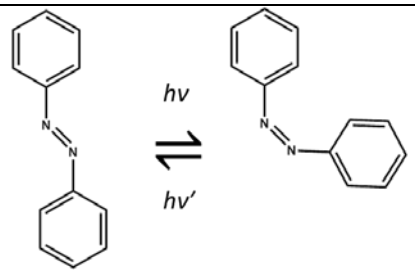	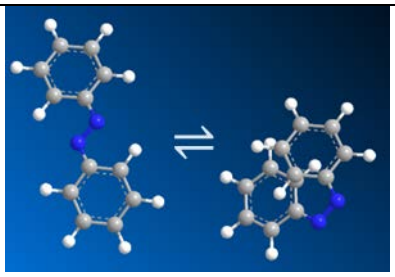
Spiropyran (SP)	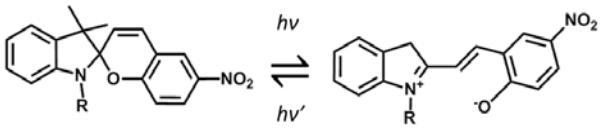	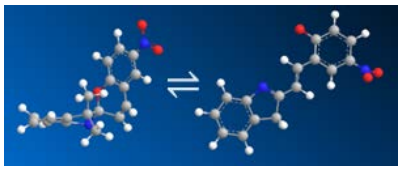
Spirooxazine (SOX)	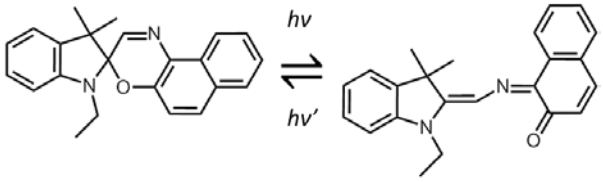	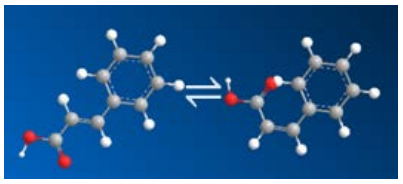

Figure 4.1 – The molecular structures of the photochromic groups of interest (middle panel). The 3D structures in the right panels demonstrate the differences in spatial conformation of the isomers of each photochromic group.

Although UV activation of photochromics has been promisingly employed as an effective trigger for drug release in responsive materials, the photochemistry of these organic molecules is limited by practical applications. This is due to the chromophores requiring high intensity UV and visible light to elicit photoisomerisation. Such high radiation levels in a biological setting can cause damage such as erythema, immune suppression and can be mutagenic[30] and the dose of UV light required to trigger isomerisation may exceed the recommended limits[31]. UV irradiation is intensely attenuated by biological tissues which results in minimal penetration of the UV light into the tissues, eliminating potential targets entrenched more than skin deep. In contrast to UV light, near infrared (NIR) wavelengths (650 – 900 nm) are not strongly absorbed by biological tissue[32] and present an alternative switch to control drug release.

In order to circumvent issues associated with the use of direct irradiation, a way of delivering the lower energy UV light deep into tissues has been proposed through the use of up-converting luminescent nanoparticles (UCNP)[33-35]. Up-conversion refers to non-linear optical processes in which the absorption of two or more photons leads to the emission of light at a shorter wavelength than the excitation wavelength. Thus, UCNPs are colloidal nanoparticles doped with rare-earth lanthanide ions such as Yb^{3+} and Er^{3+}which absorb light at higher energy NIR wavelengths and convert them to wavelengths of UV-visible light[33]. The dopants provide the luminescent centres, and the crystalline host lattice provides a matrix for the optimal positioning of the centres. Accordingly, the up-conversion efficiency and the absorbed and emitted wavelengths are dependent on the tuneable arrangement between the host lattice, dopant ions and concentration[36-38]. The surface of UCNPs can also be modified and functionalised to make them more biocompatible and/or suit their intended purpose[35]. They have been touted for use in bioimaging applications[39] and more importantly, for the triggered release of encapsulated compounds[40]. In recent times, UCNPs have been used to trigger the photoisomerisation of a spiropyran covalently grafted onto the surface of these particles[41, 42], a merocyanine doped particle

for photodynamic therapy[42, 43] as well as photoactivation of dithienylethene in solution[38]. A promising study by Yan *et al.* has employed the use of UCNP to trigger structural changes in photosensitive hydrogels using a continuous wave NIR laser[44]. Along these lines, the ability of UCNPs to act as an *in situ* switch within a photochromic doped liquid crystalline matrix was investigated.

4.3. Hypotheses and Aims

Hypothesis 1

That the UV activation of photochromics incorporated into lipid bilayers will alter lipid packing in self-assembled systems by acting as a steric disturbance at the lipid-water interface.

Hypothesis 2

That the NIR activation of upconverting nanoparticles embedded in UV responsive liquid crystalline matrices can act as an *in situ* UV light source and induce photoisomerism of spiropyran lipids in liquid crystalline phases.

In order to investigate these hypotheses, the following aims will be achieved:

1. To determine the potential of azobenzene and spiro compounds as photosensitisers in phytantriol liquid crystalline matrices using SAXS.
2. To characterise a novel alkylated spiropyran and determine its potential as a photosensitiser in phytantriol liquid crystalline matrices.
3. To assess the ability of up-converting nanoparticles to act as an *in situ* UV switch in photochromic doped liquid crystalline matrices.

4.4. Materials and Methods

General materials and methods used are detailed in Chapter 2.

The photochromic groups investigated in this study are detailed in Figure 4.1. Spiropyran (SP) (1′,3′-Dihydro-1′,3′,3′-trimethyl-6-nitrospiro[2H-1-benzopyran-2,2′-(2H)-indole]) and azobenzene (AZO) were purchased from Sigma-Aldrich. Oxford Blue (spirooxazine (SOX)) was purchased from James Robinson. Lauroyl chloride was purchased from Aldrich and used as supplied. Lauric acid (98% deuterated) was generously provided by the National Deuteration Facility (Lucas Heights, NSW, Australia). Please note that formulations of photochromics in liquid crystals are described in mol %, which refers to the concentration of photochromic in lipid prior to hydration or dispersion. Radiolabelled ^{14}C-glucose (262 mCi/mmol) was obtained from Moravek Biochemicals (Brea, California, USA). D-(+)-glucose was purchased from Sigma Aldrich (St. Louis, MO, USA).

4.4.1. Spiropyran Laurate Synthesis

A spiropyran derivative with a laurate tail, spiropyran laurate (SPL) was synthesised by N. Malic (CSIRO) according to: 2-(3’,3’-Dimethyl-6-nitro-3’H-spiro[chromen-2,2’-indol]-1’-yl)-ethanol (0.50 g, 1.42 mmol) was dissolved in dry dichloromethane (10 mL) together with triethylamine (0.39 mL, 2.84 mmol), under nitrogen. Lauroyl chloride (0.33 mL, 1.42 mmol) was then added via syringe at room temperature. After stirring for 10 min, the reaction mixture was passed through a plug of silica gel, the solvent evaporated *in vacuo*, and the residue purified by column chromatography (SiO2, EtOAc/hexanes, 1:3). SPL: ^{1}H NMR (400 MHz, d_6-acetone) δ8.15 (d, J = 2.8 Hz, 1H), 8.05 (dd, J = 8.9, 2.8 Hz, 1H), 7.21 (d, J = 10.4 Hz, 1H), 7.19-7.13 (m, 2H), 6.85 (m, 2H), 6.76 (d, J = 7.8 Hz, 1H), 6.09 (d, J = 10.4 Hz, 1H), 4.25 (m, 2H), 3.56 (m, 1H), 3.46 (m, 1H), 2.24 (td, J = 7.5, 2.1 Hz, 2H), 1.53 (m br, 2H), 1.27 (m, 21H), 1.18 (s, 3H), 0.88 (t br, 3H) ppm.

A similar procedure was used to synthesise a SPL moiety with a deuterated laurate tail (SPL-d) by Kristian J. Tangso (MIPS) for use in NMR studies and for future SANS studies. A solution of DCC was added drop-wise to an ice cooled solution of lauric acid, spiropyran alcohol and DMAP in dry dichloromethane and stirred under nitrogen. The mixture was allowed to warm up to room temperature and maintained under these conditions for a further 48 hr. The crude product was then filtered to remove solid white precipitate. The solvent was evaporated and the residue was passed through a silica column and eluted with a solvent system giving the greatest separation, 100% dichloromethane, confirmed by TLC. Fractions of eluent collected from flash column chromatography FCC containing the product (pale green solution) were combined, evaporated and dried under high vacuum overnight to remove residual solvent to yield the product. NMR was used to characterise and assess the purity of the compounds synthesised. *SP-L (d):* ^{1}H NMR (400 MHz, $CDCl_3$) δ 8.02 (m, 1H, Ph-*H*), 8.00 (m, 1H, Ph-*H*), 7.19 (t, 1H, Ph-*H*), 7.08 (d, 1H, Ph-*H*), 6.91 (d, 1H, -CH=C*H*-), 6.89 (t, 1H, Ph-*H*), 6.75 (d, 1H, Ph-*H*), 6.68 (d, 1H, Ph-*H*), 5.88 (d, 1H, -C*H*=CH-), 4.21 (m, 2H, -N-CH_2), 3.45 (m, 2H, N-CH_2-CH_2-O-CO), 1.29 (s, 3H, CH_3), 1.16 (s, 3H, CH_3) ppm; ^{2}H NMR (102.6 MHz, $CDCl_3$) δ 2.21 (s, 2D, O-CO-CD_2-CD_2), 1.51 (s, 2D, O-*C*O-CD_2-CD_2), 1.16 (s, 22D, $(CD_2)_{11}$), 0.80 (s, 3D, CD_2-CD_3) ppm; ^{13}C NMR (100.6 MHz, $CDCl_3$) δ 173.7, 159.4, 146.1, 141.0, 135.6, 128.2, 127.8, 125.9, 122.7, 121.8, 121.8, 119.9, 118.4, 115.5, 106.7, 106.7, 62.2, 52.8, 42.4, 28.3, 25.8, 19.8 ppm.

4.4.2. UV Spectral Characterisation of SPL

UV-visible absorption spectra were measured on a Cary-50 spectrometer from 200−800 nm at a scan rate of 600 nm s^{-1} and kinetic measurements at 540 nm. Representative scans are shown in Figure 4.5. The spectrometer was fitted with a Peltier temperature controlled cell. Solutions for UV−visible measurements were made at concentrations of 1 mg/mL in methanol and hexane.

This allowed for the determination of $k_{1\ obs}$ and $k_{2\ obs}$ (Table 4.1) by fitting the plots above, with the equations 1 and 2:

1. $y = y_0 - ae^{-k1obs\ x}$
2. $y = y_0 + ae^{-k2obs\ x}$

4.4.3. Photochromic and ^{14}C -Glucose Release Experiments

UV triggered *in vitro* release was investigated through the observation of the diffusion of a model drug, ^{14}C-Glucose, over time. In a similar way, the retention of SP and SPL in the bulk cubic phase matrix was tested using a pseudo-release/leaching experiment. These studies were performed in triplicate. In both cases, bulk phase (~200 mg) containing lipid, photochromic + 30% Milli-Q water were loaded into purpose built plastic mini-beakers (r = 3.75 mm), ensuring a well defined reproducible surface area for drug release, and suspended in 20 mL of phosphate buffered saline (PBS) in 20 mL glass scintillation vials. Continuous agitation of the buffer was achieved via a magnetic stirrer.

In the ^{14}C-Glucose release experiments, the sample matrix consisted of 1 mol% of SPL in PHYT + 30% aqueous component which contained both radiolabelled and cold glucose. The samples were irradiated with LED UV light between t = 6.25 – 5 h.

In the photochromic release experiments, the samples consisted of 0 and 1 mol% of SP and SPL in PHYT. The UV irradiated samples were exposed to 24 h of LED UV light at 350 nm, 30 mW (Nichia Chemical, Japan). Samples were then allowed to release for 6 additional days, the time at which the release medium was sampled and analysed using HPLC.

4.4.3.1. Quantification of Released SP and SPL

High Performance Liquid Chromatography (HPLC) was used to quantify the concentration of SP in the buffer. The HPLC system used was a Shimadzu Prominence UFLC (Tokyo, Japan)

with UV/Vis detection (SPD-20A Prominence UV-Vis detector-D2 lamp, 210 nm). The column (4.6 x 75 mm) was packed with Symmetry® $C_{18,}$ particle size 3.5 µm (Waters: Dublin, Ireland) and used at room temperature. The mobile phase (90% acetonitrile: 10% Milli-Q water) was prepared volumetrically. Sample injection volumes of 40 µL were used and the retention time ($t_{R,}$ ~ 11 min) were measured at room temperature at a flow rate of 1 mL/min using an isocratic elution system.

4.4.3.2. Quantification of Released ^{14}C-glucose

^{14}C-glucose samples were analysed by scintillation counting. The release medium was sampled (100 µL) from the release medium and replaced by 100 µL PBS at predetermined time points, and mixed with 2 mL of scintillation cocktail in a 6 mL scintillation vial for scintillation counting on a Tri-Carb 2800TR, Perkin Elmer Liquid Scintillation Analyser. Data were converted to percentage of ^{14}C-glucose released against time and standard deviation (n=3) or range (n=2) calculated for data at each time point. As previous studies have shown that liquid crystalline systems display diffusion controlled release, the data were plotted as drug release versus square root of time ($t^{½}$). A linear relationship between percent released and $t^{½}$ provided confirmation of first order diffusion controlled release. Experimental assistance from Kristian J. Tangso for the ^{14}C -glucose release experiments is gratefully acknowledged.

4.4.4. Nuclear Magnetic Resonance (NMR)

^{1}H NMR (400 MHz) and ^{2}H NMR (400 MHz) spectra were recorded on a Bruker 400 MHz instrument at ~25°C. In ^{1}H NMR spectra, chemical shifts (ppm) were referenced to residual solvent protons (7.26 ppm in $CDCl_3$). In ^{13}C NMR spectra, chemical shifts (ppm) were referenced to the carbon signal of the deuterated solvent (77.0 ppm in $CDCl_3$).

4.4.5. Synthesis of Up-Converting Nanoparticles

Synthesis of UCNPs was performed by B. Graham and J. Selano (MIPS). Mixtures of:

1. Bare UCNP: $Y(CH_3CO_2)_3$ (2.78 mmol), $Yb(CH_3CO_2)_3$ (1.20 mmol), $Tm(CH_3CO_2)_3$ (0.02 mmol), octadecene (60 mL); and
2. OA-UCNP: Mixture 1. + oleic acid (24 mL)

were heated to 120 °C under vacuum for 90 min, with constant magnetic stirring. The resulting pale yellow solution was then cooled to 50 °C and placed under a nitrogen atmosphere, before a methanolic solution (40 mL) of ammonium fluoride (16 mmol) and sodium hydroxide (10 mmol) was added. After 30 min of constant stirring, the temperature was raised to 70°C and the methanol distilled off from the reaction mixture by placing it under vacuum for 60 min. The vacuum was then removed and the temperature increased to 310 °C and maintained at this level for 120 min, whilst maintaining a nitrogen atmosphere. The resulting slightly turbid, pale brown reaction mixture was allowed to cool to room temperature. The UCNPs were then precipitated by adding absolute ethanol (300 mL) and isolated *via* centrifugation at 3400 rpm. The resulting oily pellet was dispersed in hexane (10 mL) and re-precipitated with absolute ethanol (100 mL).

Before incorporation into liquid crystalline phases, the UCNP were centrifuged at 3400 rpm and re-dispersed in 10 mL hexane (OA-UCNP) or 10 mL MilliQ water. OA-UCNPs were incorporated into the SPL-PHYT lipid so that the final concentrations were 50 or 100 mg/g liquid crystal before the evaporation of the solvent under vacuum overnight, and the hydration of the lipids with 50% (w/w) PBS. Bare-UCNP were dispersed in PBS and were used to hydrate the SPL-PHYT at a 1:1 ratio so that the final concentrations were 50 or 100 mg/g liquid crystal.

4.5. Results – Incorporation of Photochromics into Liquid Crystalline Matrices

4.5.1. Azobenzenes

The readily available azobenzene (AZO) compound (Figure 4.1, top panel) was added to a phytantriol-water liquid crystal matrix to assess its ability to manipulate lipid packing on irradiation. In the absence of irradiation, the transition temperatures between liquid crystalline phases were substantially altered (Figure 4.2, Panel A.), however the lattice dimensions of the phases were not significantly affected by the presence of the azobenzene additives as shown by the equilibrium phase behaviour in Figure 4.2, Panel B. A V_2+H_2 mixed phase was present at 25°C in the AZO doped phases, and the H_2 phase persisted over a greater temperature range, a phenomenon which has been previously observed upon addition of a hydrophobic moiety into the PHYT bilayer[45, 46].

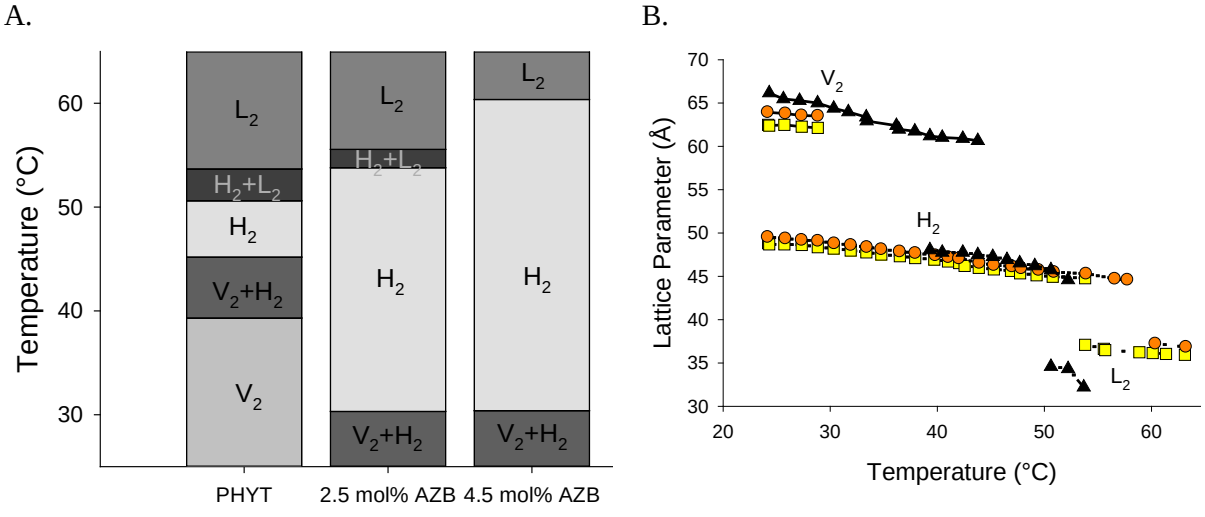

Figure 4.2 – Equilibrium phase behaviour of azobenzene-doped PHYT liquid crystalline matrices. All matrices are in excess water. Panel B. Black triangles = phyt, yellow squares = 2.5 mol% AZO & orange circles = 4.5 mol% AZB.

Kinetic phase behaviour of the AZO-PHYT matrices on irradiation with UV light were observed using time-resolved synchrotron SAXS. A PHYT matrix containing no photochromic displayed a slight shift in lattice parameter upon 60 s UV exposure (Figure 4.7, Panel A), but no phase transition was observed. AZO-doped matrices were exposed to 30 s of UV irradiation and the mesophase evolution is shown in Figure 4.3. Both 1% and 2% matrices were initially in the $V_{2\ Pn3m}$ phase (spacing ratios of √2: √3: √4: √6: √8: √9…[47]) and transition to the H_2 phase (peaks at spacing ratio 1: √3: √4) at 10.3 and 8.6 s respectively. Upon cessation of irradiation, the $V_{2\ Pn3m}$ phase reappeared, however, a mixed V_2+H_2 phase persisted until the end of the 60 s acquisition period. The mixed phase still persisted when phases were re-investigated at 4 h. The matrix with a higher concentration of AZO was able to achieve a phase transition in a shorter amount of time; however there was no other distinction between the two concentrations of AZO investigated.

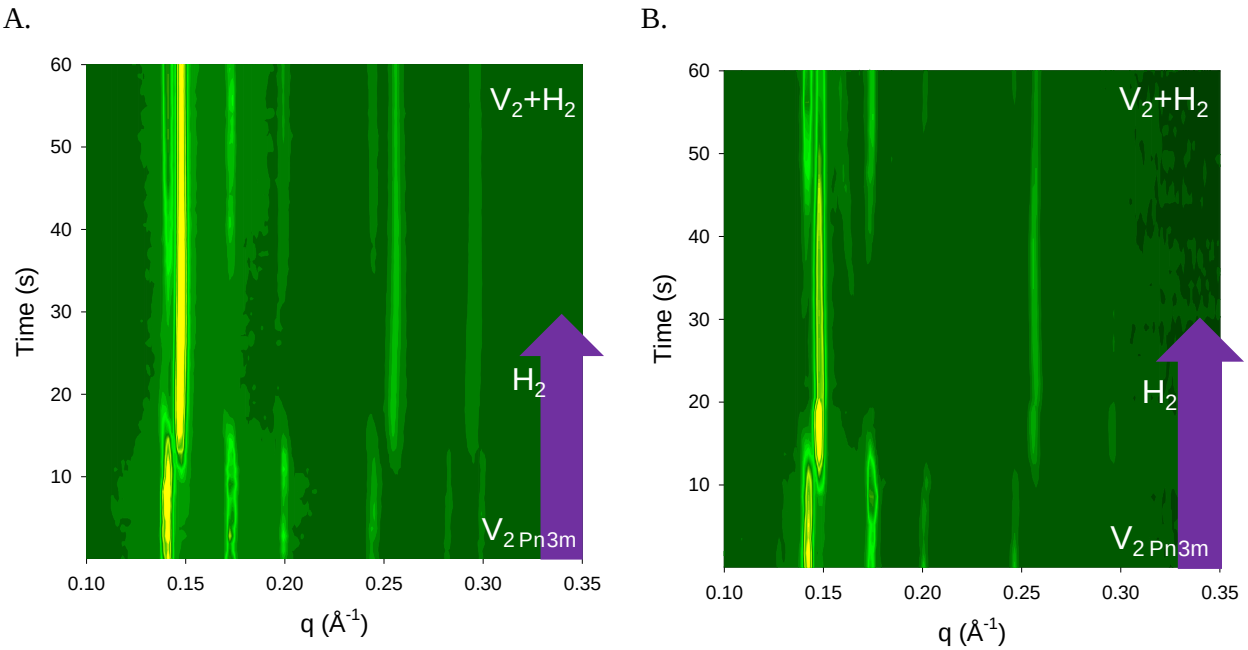

Figure 4.3 – Time resolved SAXS profiles showing the mesophase transitions upon UV irradiation of A. 2.5 mol% AZO in PHYT and B. 4.5 mol% AZO in PHYT liquid crystalline phases. All matrices are in excess water. UV irradiation was at 375 nm, 60 mW power and of 30 s duration as indicated by the purple arrow on the profiles.

4.5.2. Spiro-Compounds

4.5.2.1. UV Characterisation of Spiropyran Laurate, a Novel Photochromic

The UV-visible spectral characteristics were determined for the novel SPL compound. The UV-visible scan of SPL in methanol (Figure 4.4) shows that the molecule absorbs strongly at UV wavelengths. Exposure to UV light leads to the appearance of a peak at 540 nm, corresponding to the formation of the open MC form of the SPL, in accordance with previously reported behaviour for the non-alkylated spiropyran molecule[2, 48]. The rate of opening of the SPL spiropyran ring in methanol mirrors that of previously reported rate constants for SP, however, the observed rate constants (Table 4.1, fitted from profiles in Figure 4.5) indicate that in non-polar environments, the SPL preferentially adopts the closed spiropyran form due to the polarity of the solvent stabilising the closed spiropyran form[49, 50]. Consequently, the spiropyran moiety opens in such a miniscule proportion in hexane that it is almost impossible to detect the rate constant for MC ring closing. In comparison, when in a relatively polar environment such as methanol, the open MC form is partially stabilized and at equilibrium both the closed spiropyran form and a small percentage of the open MC form are both present.

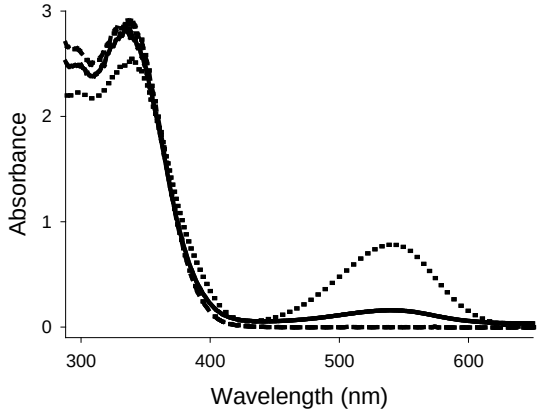

Figure 4.4 – UV-visible spectra of SPL in methanol (1.87×10^{-3} M, 298 K) with curves corresponding to equilibrium condition without light (——), after 10 min UV light exposure (·····) and after 10 min white light exposure (----). The peaks at 300-375 nm are assigned to the closed spiro form of the SPL and the peak at and 540 nm assigned to the open MC form of the SPL.

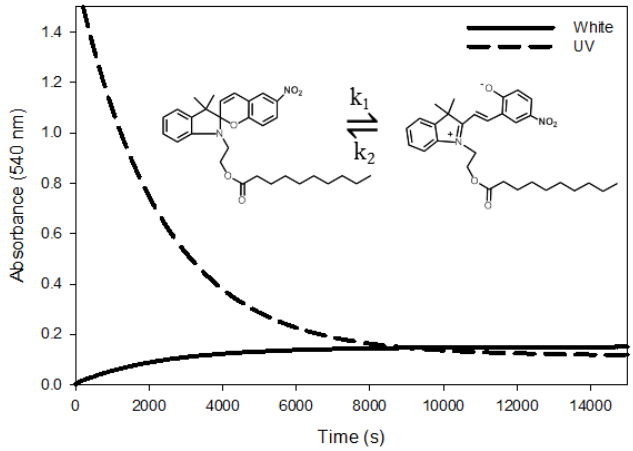

Figure 4.5 – Time dependence of the absorbance at 540 nm of a solution (1.87×10^{-3}M, MeOH, 298 K) of SPL in the dark after 10 min of irradiation by UV (dashed) and white (solid) light. This allowed for the determination of $k_{1\ obs}$ (spiro → mero) and $k_{2\ obs}$ (mero → spiro), presented in Table 4.1, by fitting the plots above, with the equations 1 & 2.

Table 4.1 – Observed rate constants for isomerisation of SPL in different solvents at 1 mg/mL. The value of k_{1obs} for SPL in hexane and phytantriol could not be determined due to the polarity of the solvent stabilizing the closed spiropyran form[49, 50].

Solvent	$k_{1\ obs}$ (after white light)	$k_{2\ obs}$ (after UV)
methanol	4.5×10^{-4} s^{-1}	4.0×10^{-4} s^{-1}
hexane	n/a	6.2×10^{-2} s^{-1}
phytantriol-water liquid crystal	n/a	1.1×10^{-3} s^{-1}

4.5.2.2. Spiro-Phytantriol Matrices

The three structurally related spiro compounds (SP, SPL, SOX) were added to a PHYT-water liquid crystal matrix and their effectiveness in disrupting lipid packing on irradiation was compared. In the absence of irradiation, the liquid crystal structure was not adversely affected significantly by the presence of the additives as shown by the equilibrium phase behaviour (Figure 4.6). As in the case for addition of AZO to the PHYT matrix, there was a reduction in the $V_{2\ Pn3m}$ to H_2 phase transition temperatures, which was also observed upon addition of hydrophobic

moieties into the PHYT liquid crystalline matrix in excess water[45]. There is also a stabilisation of the H_2 phase for SP and SOX where L_2 occurs at higher temperature.

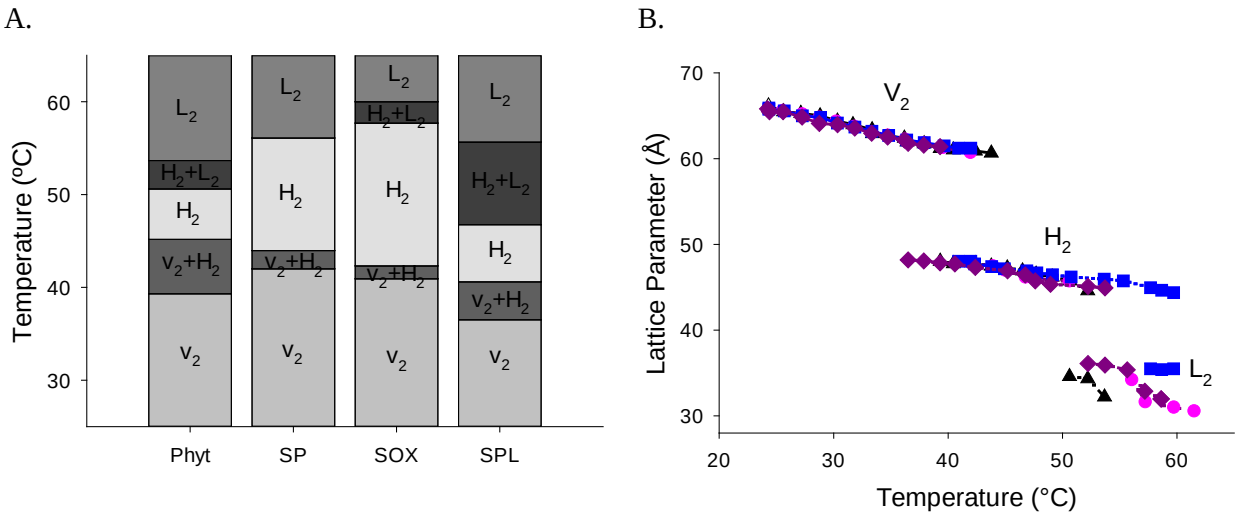

Figure 4.6 – Equilibrium phase behaviour of 1 mol% spiro-doped PHYT liquid crystalline matrices. All matrices are in excess water. Panel B. ▲PHYT, ●SP, ■ SOX and ♦ SPL.

4.5.2.3. UV Activation of Spiro-Phytantriol Matrices

Samples were irradiated with UV light (60 mW, 375 nm) for 60 s periods and the liquid crystal structure observed using synchrotron SAXS over this time. The acquired SAXS patterns showed that all matrices began in the V_2 phase with Pn3m spacegroup[47]. Over 60 s of UV irradiation, the SP and SOX systems exhibited some minor changes in lattice dimensions (Figure 4.7, Panel B. & C.), indicative of some disruption of lipid packing. However, the effect was not sufficient to induce a phase transition. In contrast, the SPL-containing system completely transitioned to the H_2 phase (peaks at spacing ratio 1: $\sqrt{3}$: $\sqrt{4}$[47]) after 20 s of UV exposure (Figure 4.7, Panel D.). The lattice parameter for the H_2 phase (48-49 Å, Figure 4.7 Panel B) is consistent with previous reports for the H_2 phase in PHYT-water systems[45, 51, 52]. This effect was found to reversible as shown in Figure 4.8, with the appearance of the non-equilibrium structure $V_{2\ Ia3d}$ transiently on the return of the system to the original phase. Unlike the AZO-PHYT matrix, the SPL-PHYT system returned to the original mesophase within 40 s.

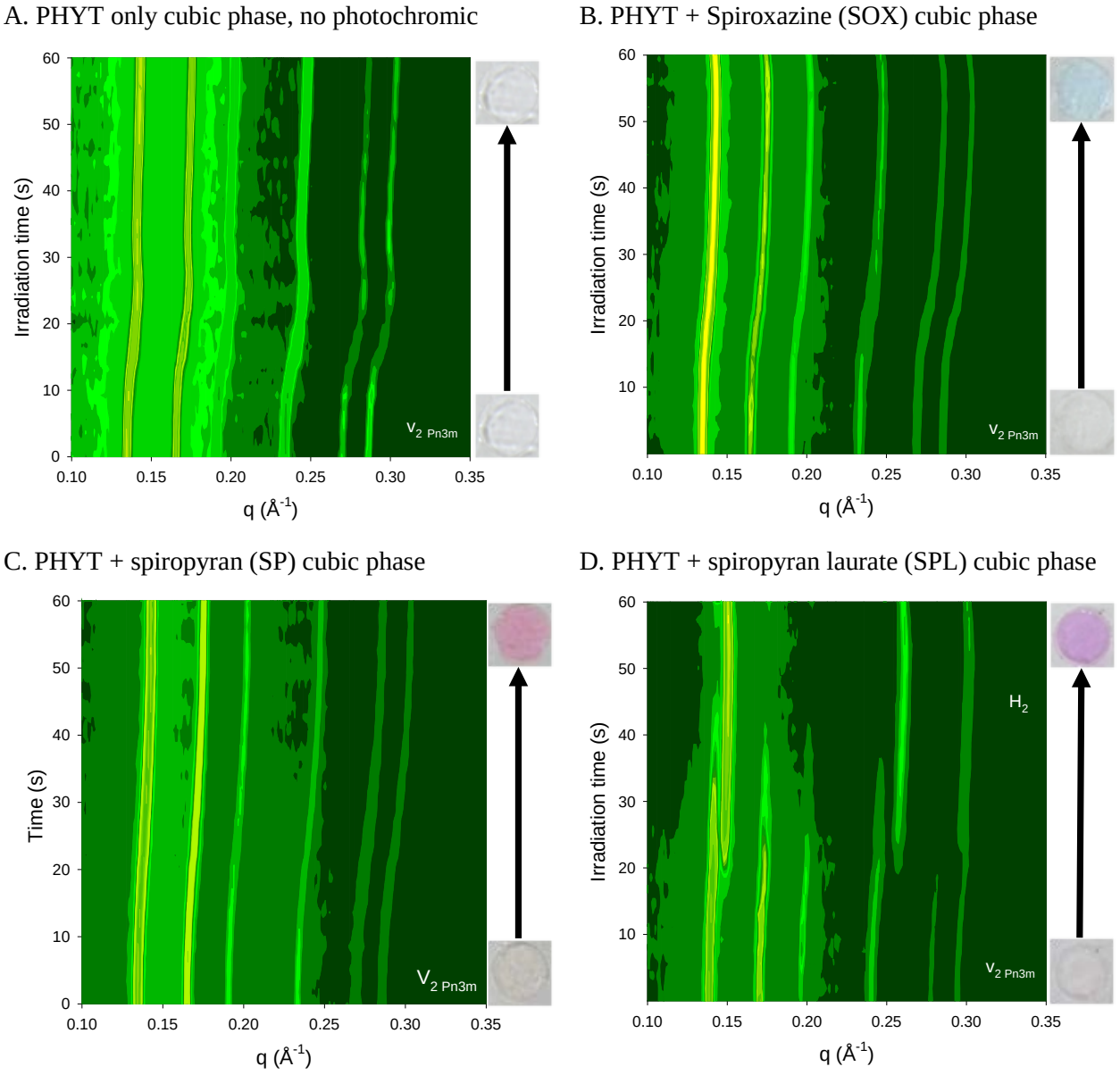

Figure 4.7 – Time resolved SAXS plots following the mesophase structure of phytantriol-water liquid crystal matrices containing A. no photochromic, B. 1 mol% SOX, C. 1 mol% SP and (D) 1 mol% SPL to 60 s of UV irradiation (375 nm, 60 mW). Brighter yellow shading indicates greater scattered intensity. The liquid crystal phase transitions are annotated on the right. The insets show the colour change of the matrices from clear to pinky-purple (SP), blue (SOX) or purple (SPL), before and after UV exposure due to the transition from the clear spiropyran form to the coloured MC form.

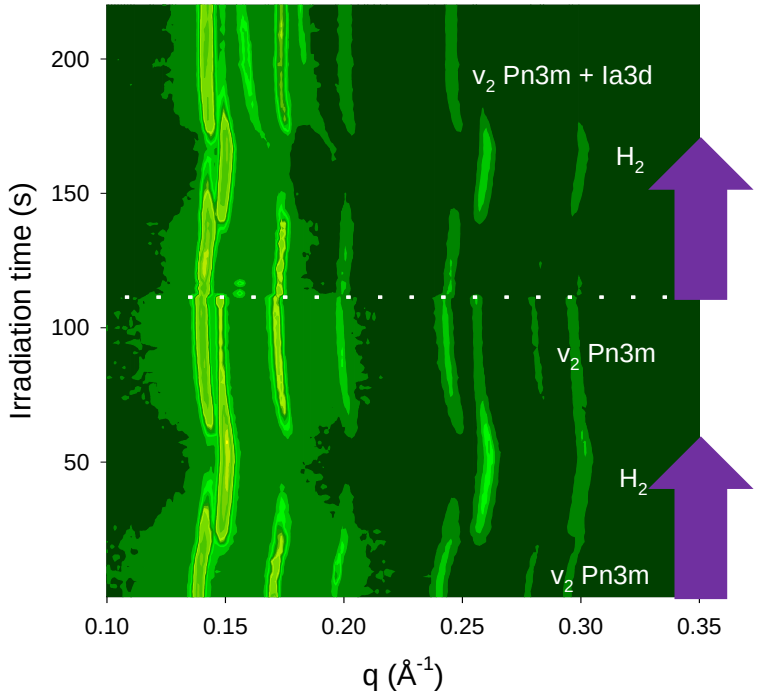

Figure 4.8 – Time resolved SAXS profile showing reversible phase transitions of the SPL-phytantriol liquid crystalline system. Brighter yellow shading indicates greater scattered intensity. Samples were exposed to UV light (375 nm, 60 mW) for two cycles of 60 s on, 40 s off as indicated by the purple arrows on the right. The white line indicates the start of the second cycle and a change in sample position. The liquid crystalline phase transitions are annotated on the right.

4.5.2.4. Spiropyran Release on Irradiation

As the SP matrix was not as effective in initiating a phase change, it was hypothesised that the photochromic leached out of the sample upon UV activation. Of the formulations investigated in Table 4.2, the only formulation where photochromic compound was released from the cubic phase on irradiation was the SP-PHYT matrix after 24 h of UV irradiation. The amount released corresponds to approximately 1% of the incorporated SP. This amount could be underrepresented as the buffer was visibly yellow, indicative of SP oxidation. No discolouration or photochromic was found in the buffer of other samples, including a non-irradiated SP sample. In addition to the appearance of the SP moiety in the buffer, the PBS was visibly yellow which is indicative of degradation of the spiropyran moiety. Degradation of spiropyrans occurs mainly through the

oxidation of the C–O bond in the open pyran ring in the MC form[53, 54] resulting in a yellowing of the system. The spiro form is very stable in comparison as no degradation of spiropyran occurs in the dark, where the photochromic exists mainly in the closed form[55].

Table 4.2 – Release of spiro compounds from the liquid crystal matrix at 7 days with and without UV irradiation (n=3). Only the sample containing SP with UV irradiation demonstrated evidence of release.

Liquid Crystal matrix	Photochromic released at t = 7 d, no irradiation (µg)	Photochromic released at t = 7 d, 24 h UV irradiation (375 nm, 30 mW) (µg)
PHYT	0	0
PHYT+1mol% SP	0	5.5 ± 0.08
PHYT+1mol% SPL	0	0

4.5.2.5. ^{1}H and ^{2}H NMR Studies on SP & SPL-PHYT Liquid Crystalline Matrices

NMR spectroscopy was employed to probe the location of the irradiated and non-irradiated SP and deuterated SPL (SPL-d) species in the PHYT lipid bilayer in excess water or D_2O. The concentration of photochromic in PHYT was 1 mol%. In both SP and SPL-d, and in the absence of any UV light, ^{1}H NMR spectra (Figure 4.9, red lines) showed the presence of SP and a small amount of MC species. The coexistence of the latter species is in accordance with expected amounts at equilibrium. Colouration of the matrix was observed upon UV irradiation. This was accompanied with a decrease in the spiropyran ^{1}H NMR peaks in both the SP and SPL-d (Figure 4.9), which indicates spiro (SP) to merocyanine (MC) photoisomerisation.

However, peaks indicative of MC originally present in the solution (marked with an asterisk) neither increased in intensity nor were any new peaks resolved. This could be attributed to the

restricted movement of the newly formed charged MC species in the bilayer, as a result of strong interaction between the charged species and the lipid hydrophilic head group. This suggests that at equilibrium, the spiropyran headgroups in both the SP and SPL-d moieties were present as freely tumbling groups on the NMR time scale, hence present in a "liquid-like" state. When exposed to UV irradiation, the spiropyran group opens to give the charged MC isomer which becomes present in a "gel-like" state and thus was not able to be observed on the solution NMR time scale, implying that the MC is interacting with the more restricted environment either within or at the interface of the lipid bilayer.

Deuterium NMR was conducted on the SPL-d in order to probe the location of the deuterated tails within the two different liquid crystalline phases. Spectra, shown in Figure 4.10, were recorded at 25ºC and 45ºC, where the matrix displays a $V_{2\ Pn3m}$ and H_2 nanostructure, respectively, shown by the equilibrium SAXS studies in Figure 4.6. As well as being photochromic, spiropyrans are thermotropic compounds which isomerise upon an increase in temperature when in a polar environment[56, 57]. Thus, photolysis of the pyran ring occurs upon heating, and was confirmed on observation of a deep purple at 45ºC. At 25ºC, where the phase is $V_{2\ Pn3m}$ and the SPL-d exists mainly in the spiro form, the d-NMR spectrum showed two peaks, one at 0.8 ppm (sharp) and one at 1.5 ppm (broad isotropic). After increasing the temperature to 45ºC, there was a subsequent decrease in the isotropic peak intensities at 0.8 and 1.5 ppm, and the appearance of a broad underlying feature (from -2 to 4.5 ppm) indicating that the tail groups dwell within a more restricted environment in the H_2 phase. The more restricted environment could be attributed to the constrained packing of lipids within the H_2 phase compared to the $V_{2\ Pn3m}$ phase.

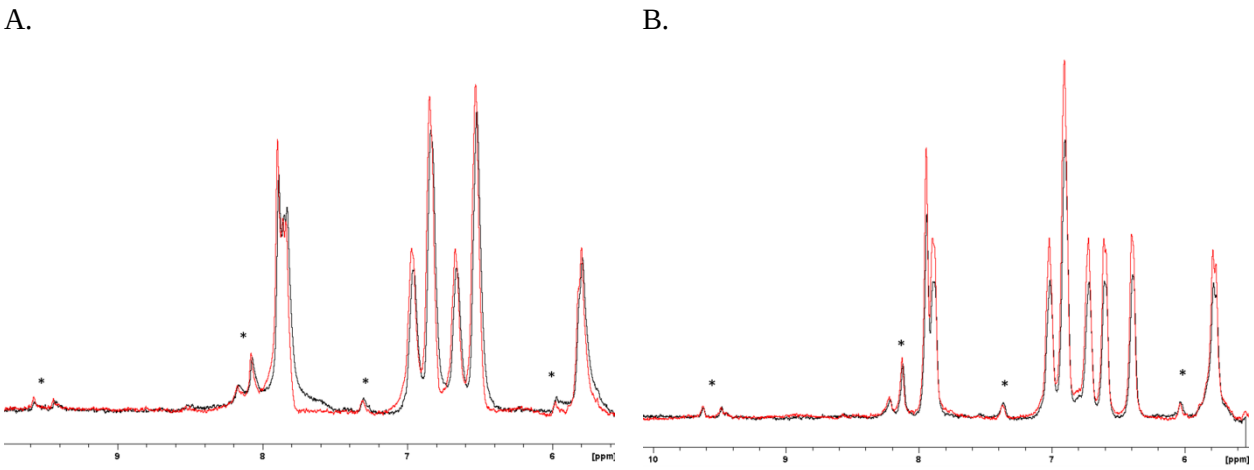

Figure 4.9 – ^{1}H NMR spectra showing the reduction in the spiropyran peak in both the Panel A. 1 mol% SP-PHYT and Panel B. 1 mol% SPL-PHYT liquid crystalline matrices. The red line represents the matrix before UV irradiation, and the black line represents the matrix after 10 min UV irradiation. The MC species is indicated by *. Both matrices are in excess D_2O.

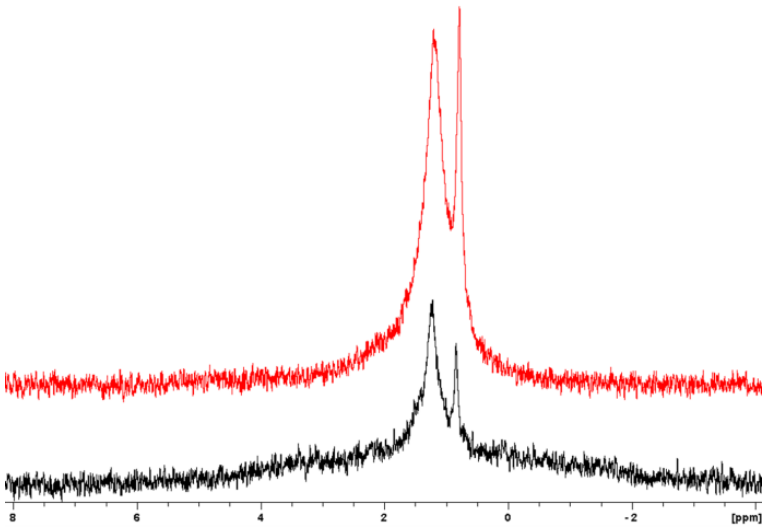

Figure 4.10 – ^{2}H NMR spectra of SPL-d-PHYT liquid crystalline matrix in excess D_2O water at 25ºC and (red line) and 45ºC (black line).

4.5.2.6. *UV Activation of SPL in Cubosomes*

UV sensitive cubosomes were investigated for their ability to respond to light activation. Dispersed PHYT particles containing 2% and 4% SPL were irradiated with UV light and the structure investigated using SAXS (Figure 4.11). The matrices both displayed the $V_{2\ Pn3m}$ phase initially, and during irradiation the peaks shifted to the right; indicating a shrinking of the $V_{2\ Pn3m}$ lattice. Peaks indicative of H_2 phase appeared at 300 s and 50 s for the 2% and 4% SPL-PHYT cubosomes respectively.

A. Irradiation of PHYT + 2% SPL cubosomes B. Irradiation of PHYT + 4% SPL cubosomes

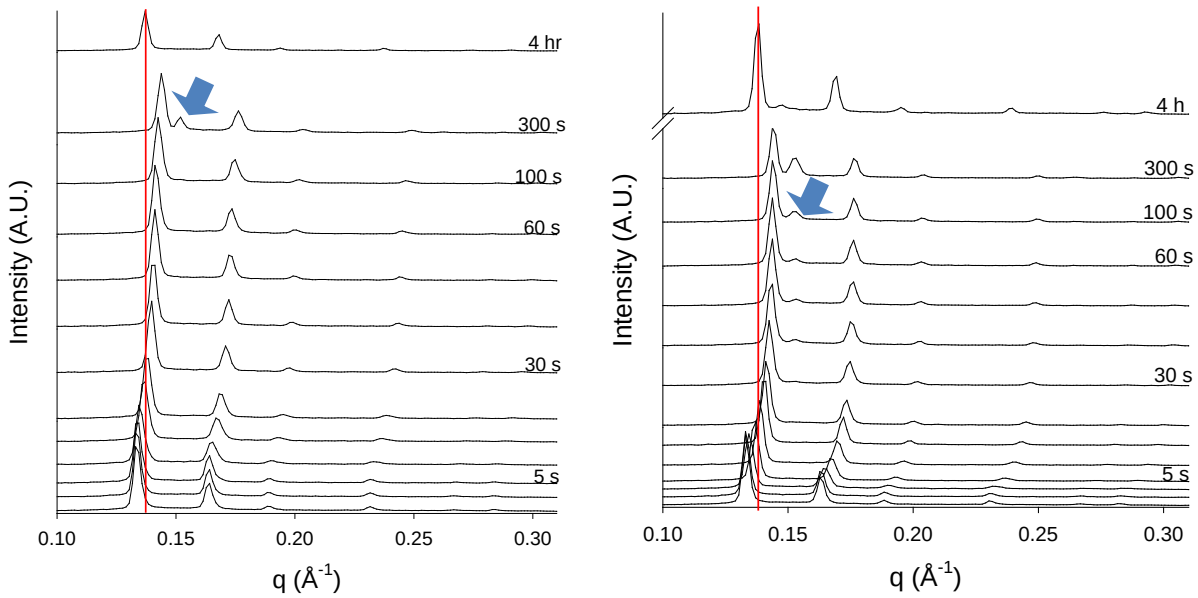

Figure 4.11 – Representative SAXS profiles of the SPL-PHYT cubosomes over time. Panels A. and B. refer to 2 and 4 mol% SPL respectively. Samples were irradiated with UV light (375 nm, 140 mW) for 300 s, then ambient lighting. The red line is intended as a guide to the eye to see the shift in lattice of the nanostructure. Blue arrows indicate the emergence of the first peak for the H_2 phase.

4.5.2.7. *In Vitro* UV Activated Drug Release

The *in vitro* release profiles of ^{14}C-glucose from the PHYT + 1% SPL system is illustrated in Figure 4.12 (left panel). The release rate from the unirradiated matrix was faster than the irradiated

matrix. This release behaviour was attributed to the system being $V_{2\,D}$ at ambient lighting and H_2 upon UV irradiation, analogous to the SAXS data in Figure 4.8. The profiles of percent glucose release against $t^{½}$ were linear in all cases, and the slope of this straight line fitted as a guide to the eye. The release profiles of previous studies using temperature[16] (top right) and pH[58] (bottom right) are also included in Figure 4.12 as a comparison to further highlight the differences in release rate between the $V_{2\,D}$ and H2 nanostructures that can be achieved on application of external stimuli.

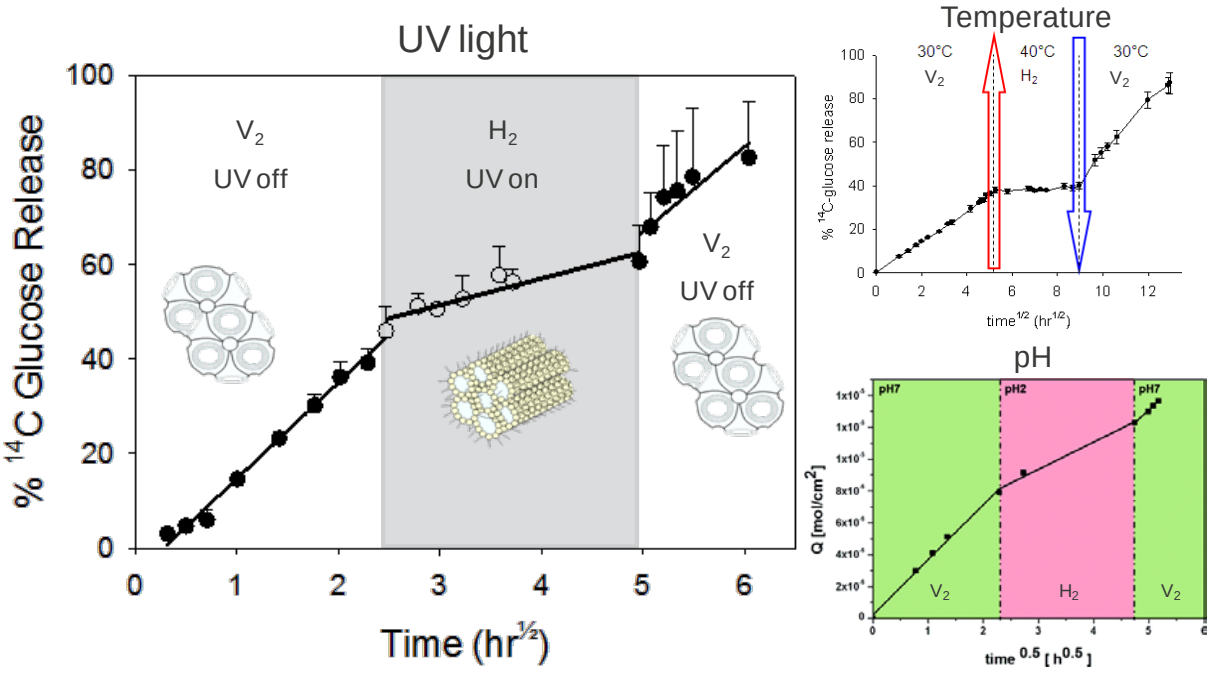

Figure 4.12 – Left: *In vitro* controlled release of a model drug from a SPL-phytantriol LC matrix using a UV light 'switch'. Data are n=2 ± range, pending additional experiments. This UV triggered release study is compared to previous studies using temperature[16] (top right) and pH[58] (bottom right) as *in situ* switches for the modification of drug release. The phase behaviour of the matrices at the different experimental conditions are annotated on the graphs.

4.6. Up-Converting Nanoparticles (UCNP) as an *in situ* UV Switch

Both hydrophobic (OA-UCNP) and hydrophilic (bare-UCNP) nanophosphors were investigated for their ability to trigger an *in situ* phase transition in SPL-PHYT doped matrices. The $NaYF_4$:Yb^{3+},Er^{3+} nanoparticles, similar to those used in this study, have been recognised as one of the most efficient photon up-converting phosphors[59] available. The emission spectrum of the UCNP is shown in Figure 4.13, Panel C. As can be seen, there is strong emission band in the UV region of the spectrum, which overlaps the absorbance spectrum of the SPL (Figure 4.4). Additionally, no emission band is present in the visible wavelengths (~540 nm) which could reverse the isomerism of the spiropyran moiety.

A. B. C.

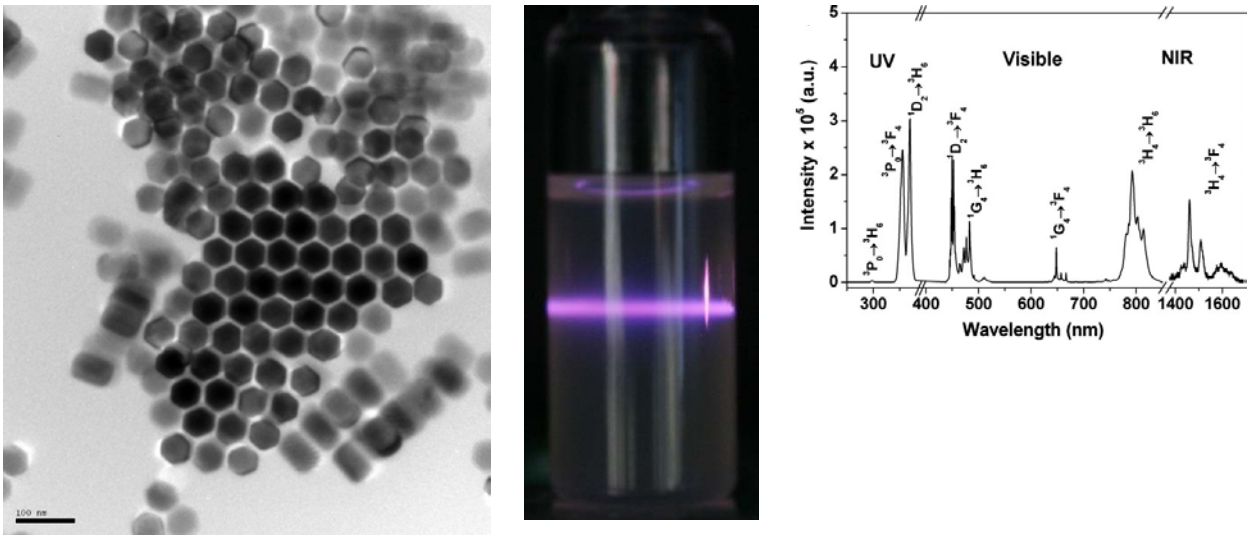

Figure 4.13 – A. TEM image of the synthesised UCNPs, illustrating their uniform size and shape. B. a photograph of the UCNP suspended in hexane under 980 nm continuous wave laser exposure. C. The upconversion emission spectrum of (0.5 mol%) Tm^{3+} (25 mol%) Yb^{3+}-doped $LiYF_4$ nanocrystals spanning the UV to NIR regions used. Adapted from [60].

Both the OA-UCNP and bare-UCNP were incorporated into SPL-PHYT and PHYT cubic phase matrices. These samples were irradiated for 120 s using NIR laser light (980 nm, 150 mW) and the nanostructure followed over time using synchrotron SAXS. The PHYT only matrix (Panel

A.), PHYT + SPL matrix (Panel B.) and PHYT matrices containing UCNP without a photochromic (Panels E. and F.) did not undergo a phase transition upon irradiation. Only the samples containing UCNPs + SPL demonstrated a phase change in response to NIR irradiation. The OA-UCNP and bare-UCNP formulations in Figure 4.14, Panels C. and D. both begin in the $V_{2\ Pn3m}$ configuration and transition to a mixed $V_{2\ Pn3m}$+H_2 phase. Lower concentrations of UCNPs did not produce a response. Higher concentrations of OA-UCNPs incorporated into the liquid crystalline matrix resulted in the modification of the starting phase from $V_{2\ Pn3m}$ to H_2 as shown in Panel E.

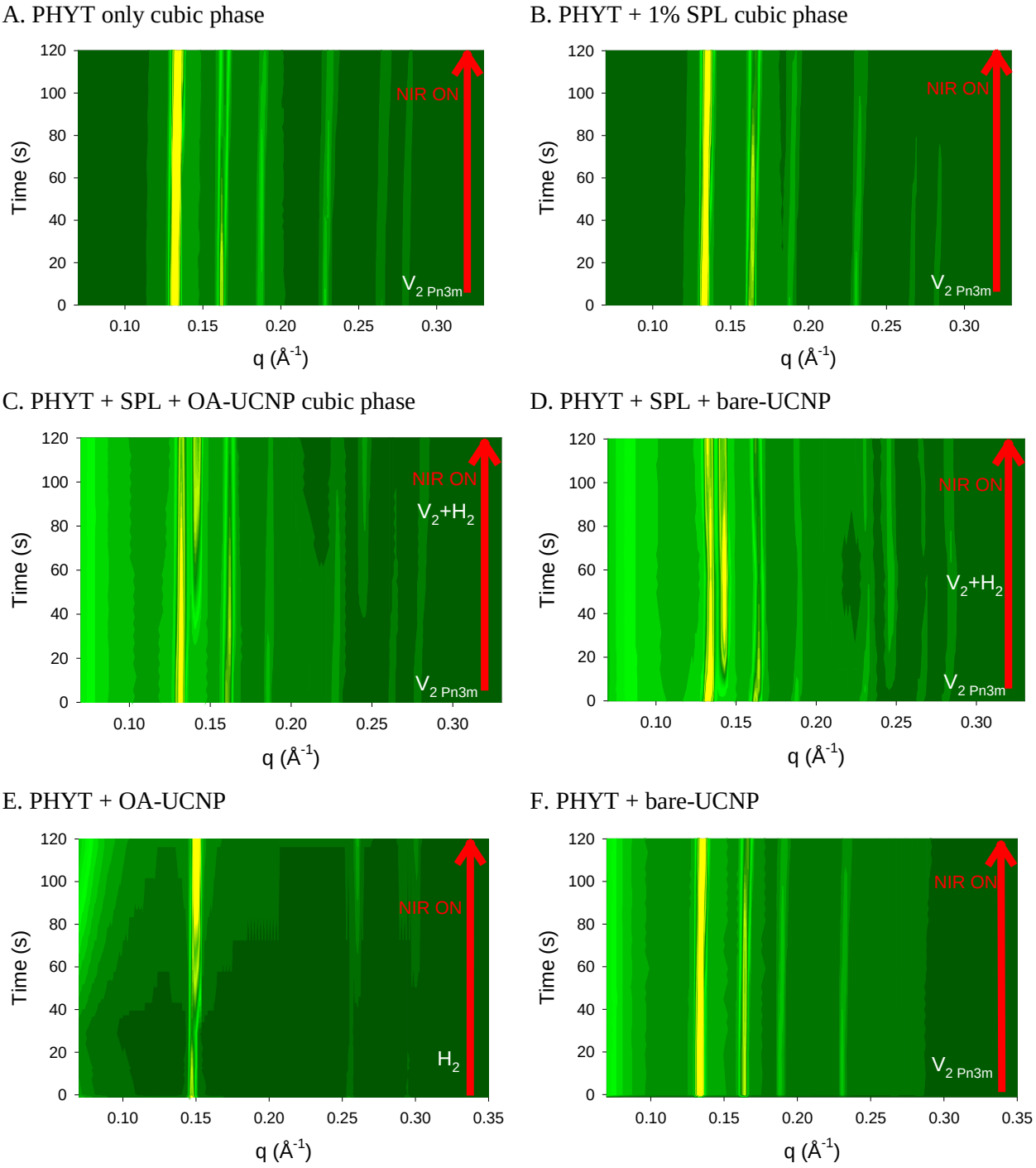

Figure 4.14 – Time-resolved SAXS profiles following the structural evolution of PHYT liquid crystalline matrices containing A. PHYT only, B. 1 mol% SPL, C. 1 mol% SPL + 50 mg/g OA-UCNP, D. 1 mol% SPL + 100 mg/g bare-UCNP, E. PHYT + 100 mg/g OA-UCNP and F. PHYT + 100 mg/g bare-UCNP. All matrices were in excess PBS. Brighter yellow shading indicates greater scattered intensity. Samples were irradiated for 120 s with a 980 nm pen laser (150 mW) as indicated by the red arrow. The liquid crystalline phase transitions are annotated on the right.

4.7. Discussion

The incorporation of both azobenzene and spiropyran photochromics into the lipid bilayer was shown to cause a steric disturbance in the lipid bilayer, and hence a change in liquid crystalline nanostructure. AZO was able to cause a phase transition in the PHYT matrix upon UV irradiation, but the matrix was not able to return to the original phase within an hour after UV exposure. Such a long time for the phase to recover may not be advantageous for pulsatile release. In addition to the steric change in the azo- moiety, the elongated *trans* and bent *cis* forms of azobenzene exhibit different polarities, where the changes in the hydrophilic–hydrophobic balance has been shown to affect the self-assembly of surfactant molecules[61] as well as forming strong intermolecular bonds with polar molecules[62]. The longevity of the *cis*-isomer could thus be attributed to it forming polar intramolecular bonds with the PHYT amphiphiles. In addition, azobenzenes may be unsuitable for pharmaceutical applications due to toxicity issues[63]. As such, they were not pursued further than the initial study presented. The remainder of this discussion focuses on the interaction of spiropyran compounds with the liquid crystalline nanostructure.

In order to exert the greatest effect on lipid packing, photochromic molecules should align themselves in the lipid bilayer near the hydrophilic headgroups of the amphiphiles as shown in Figure 4.15. The NMR studies suggest that at equilibrium, the observable spiro headgroups of both SP and SPL exist in a freely tumbling solution environment, potentially solubilised in the lipidic domains of the liquid crystalline phase. The exact orientation of the molecules are not known, however, spiropyrans will orient themselves within phospholipid bilayers[23] at different angles depending on the polarity of the bilayer interface[64]. Upon photoisomerisation, both SP and SPL move into the interface, however, from this point, it is purported that the behaviour of the two photochromics differs.

The laurate tail on the amphiphilic spiropyran anchors the photochromic into this position, and upon UV irradiation, the zwitterionic planar structure of the open MC form will result in the repositioning of the molecule so that the polar head moves towards the polar head region of the lipid amphiphile, with the non-polar edge pointing inward towards the membrane. The positioning of SPL enhances the disruptive effect of the change in structure on the lipid packing as shown in Figure 4.15, Panel B. In contrast, after photolysis of SP, the small size and charge of the MC form allows the molecule to partition out of the lipid bilayer into the aqueous domain, as shown by the release of the UV-irradiated SP moiety, thereby losing its ability to disrupt the lipid packing and nanostructure (Figure 4.15, Panel A).

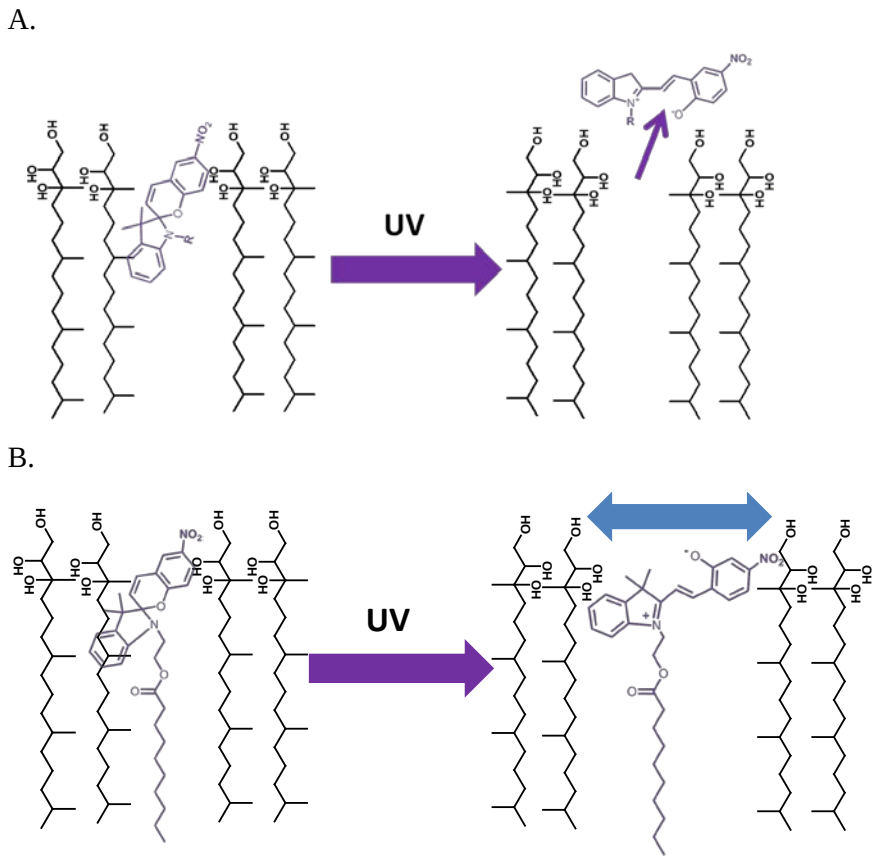

Figure 4.15 – Proposed schematic of the movement of spiropyran compounds within a PHYT lipid bilayer on exposure to UV irradiation. Panel A. The underivatised SP randomly orients within the lipid bilayer and upon isomerisation, the small hydrophilic molecule is free to leave the bilayer. Panel B. The laurate tail of the SPL moiety anchors the molecule in the bilayer where it is able to cause a steric effect on the packing of PHYT molecules at the interface upon UV irradiation.

The reason for the lack of effect on photoisomerisation of SOX is less clear. This small, hydrophobic molecule may preferentially reside in the hydrophobic regions at the intersection on the tails of the phytantriol, and hence its isomerisation does not cause a substantial disruption to lipid packing.

The light-induced phase transition of the SPL-phytantriol-water system was found to be reversible in both bulk and dispersed matrices. Figure 4.7 and Figure 4.8 show the reversible changes in scattering, indicative of changes in nanostructure of the matrix with UV exposure. The UV-induced phase change was also shown to have potential to control the release of actives from within the liquid crystalline material. The rate of reversion of the phase structure back to the original $V_{2\ Pn3m}$ phase on cessation of UV exposure is anticipated to depend on the SPL molecular relaxation rate and the rate of transition of the liquid crystal phase back to the cubic phase. Both of these processes occurred in this system within seconds. SPL preferentially adopts the spiro form in the liquid crystal matrix, evident from the value for k_{2obs} (Table 4.1) and so rapidly reverts back from the MC form when the irradiation ceases. Thus, the rate of liquid crystal structural reversion depends mainly on the speed of phase reversion which has been shown to occur within seconds. The emergence of a non-equilibrium $V_{2\ Ia3d}$ during relaxation was also observed. This was in accordance with previous reports where supercooling and the existence of non-equilibrium structures on transition from H_2 to V_2 phases have been previously shown to occur in phytantriol liquid crystal systems[9, 65, 66].

The success of these nanohybrid materials is dependent on many factors. Careful characterisation of the use of photochromics in functional matrices is required as the photoisomerisation of these dyes are dependent on a balance of environmental properties such as solvent polarity, viscosity, pH and ionic strength[50]. Additionally, aromatic dyes exhibit a blue shift in lipid bilayers due to formation of dimers/aggregates in the anisotropic polar-hydrophobic-polar

environment[67]. Following on from this initial study, a series of alkylated spiropyrans were synthesised and investigated by Tangso *et al.* for their ability to modulate phase transitions and thus optimise the alkyl chain length within the lipid bilayer of self-assembled systems[68].

The NIR triggered partial transition of the UCNP-SPL-PHYT provides a promising alternative to using UV radiation to modify the nanostructure of self-assembled systems. The limited success of this initial study, likely due to poor photon conversion efficiency, at least provides a basis for future research which could involve grafting the photochromic moiety on the surface of the UCNPs[41], which may position itself in association within or in close proximity to the bilayer to ensure the close proximity of the emitted UV light. Thus, by optimising all properties of the individual components in these hybrid nanomaterials – UCNP, photochromic and lipid – the definitive combination these novel technologies may provide a luminous, light activated matrix for on-demand drug delivery that is able to be activated through tissue using NIR light.

4.8. Conclusions

In this chapter, the effect of irradiation of liquid crystalline matrices containing the photochromic dyes azobenzene, spirooxazine, spiropyran and its monolaurate derivative were compared. On irradiation with UV light:

- Azobenzene was able to cause a partially reversible transition from $V_{2\ Pn3m}$ to H_2 phase;
- Spirooxazine and non-alkylated spiropyran had no significant effect on the PHYT liquid crystalline structure. SOX is hypothesised to reside within the alkyl tail region of the lipid bilayer where it cannot efficiently effect a phase transition. SP was shown to partition out of the nanostructure on ionisation, resulting in insignificant disruption to lipid packing.

- Spiropyran laurate induced reversible changes in the nanostructure.
- SPL-PHYT cubosomes demonstrated a reversible partial transition from the $V_{2\ Pn3m}$ to a mixed $V_{2\ Pn3m} + H_2$ phase.

The NIR irradiation of UCNP-SPL-PHYT liquid crystalline matrices affected a partial phase transition and is attributed to the UCNPs acting as an *in situ* UV switch. It is anticipated that UV activation of functionalised spiropyrans within lyotropic liquid crystals can be applied to control changes in drug delivery rate, and hence provide novel, reversible, 'on-demand' drug delivery systems.

5. References

1. Lukyanov BS, Lukyanova MB. Spiropyrans: Synthesis, Properties, and Application. (Review). Chem Heterocycl Compd. 2005 2005/03/01;41(3):281-311.

2. Berkovic G, Krongauz V, Weiss V. Spiropyrans and Spirooxazines for Memories and Switches. Chem Rev. 2000;100(5):1741-54.

3. Tong R, Hemmati HD, Langer R, Kohane DS. Photoswitchable Nanoparticles for Triggered Tissue Penetration and Drug Delivery. Journal of the American Chemical Society. 2012 2012/06/20;134(21):8848-55.

4. Görner H, Chibisov AK. Photoprocesses in Polymethine Dyes: Cyanines and Spiropyrane-Derived Merocyanines. In: Horspool WM, Lenci F, editors. CRC handbook of organic Photochem Photobiol. 2nd ed: CRC Press LLC; 2004.

5. Ercole F, Davis TP, Evans RA. Photo-responsive systems and biomaterials: photochromic polymers, light-triggered self-assembly, surface modification, fluorescence modulation and beyond. Polymer Chemistry. 2010;1(1):37-54.

6. Agasti SS, Chompoosor A, You C-C, Ghosh P, Kim CK, Rotello VM. Photoregulated Release of Caged Anticancer Drugs from Gold Nanoparticles. J Am Chem Soc. 2009;131(16):5728-9.

7. Eastoe J, Vesperinas A. Self-assembly of light-sensitive surfactants. Soft Matter. 2005;1(5):338-47.

8. Eastoe J, Zou A, Espidel Y, Glatter O, Grillo I. Photo-labile lamellar phases. Soft Matter. 2008;4(6):1215-8.

9. Fong W-K, Hanley TL, Thierry B, Kirby N, Boyd BJ. Plasmonic Nanorods Provide Reversible Control over Nanostructure of Self-Assembled Drug Delivery Materials. Langmuir. 2010;26(9):6136-9.

10. Ohya Y, Okuyama Y, Fukunaga A, Ouchi T. Photo-sensitive lipid membrane perturbation by a single chain lipid having terminal spiropyran group. Supramol Sci. 1998;5(1-2):21-9.

11. Bisby RH, Mead C, Mitchell AC, Morgan CG. Fast Laser-Induced Solute Release from Liposomes Sensitized with Photochromic Lipid: Effects of Temperature, Lipid Host, and Sensitizer Concentration. Biochem Biophys Res Comm. 1999;262(2):406-10.

12. Hansen MB, van Gaal E, Minten I, Storm G, van Hest JCM, Löwik DWPM. Constrained and UV-activatable cell-penetrating peptides for intracellular delivery of liposomes. J Controlled Release. 2012 11/28/;164(1):87-94.

13. Amar-Yuli I, Libster D, Aserin A, Garti N. Solubilization of food bioactives within lyotropic liquid crystalline mesophases. Curr Opin Colloid Interface Sci. 2009;14(1):21-32.

14. Clogston J, Caffrey M. Controlling release from the lipidic cubic phase. Amino acids, peptides, proteins and nucleic acids. J Contr Release. 2005;107(1):97-111.

15. Lee KWY, Nguyen T-H, Hanley T, Boyd BJ. Nanostructure of liquid crystalline matrix determines in vitro sustained release and in vivo oral absorption kinetics for hydrophilic model drugs. Int J Pharm. 2009;365(1-2):190-9.

16. Fong W-K, Hanley T, Boyd BJ. Stimuli responsive liquid crystals provide 'on-demand' drug delivery *in vitro* and *in vivo*. J Contr Release. 2009;135(3):218-26.

17. Knoll H. Photoisomerism of Azobenzenes. In: Horspool WM, Lenci F, editors. CRC handbook of organic Photochem Photobiol. 2nd ed: CRC Press LLC; 2004.

18. Merino E, Ribagorda M. Control over molecular motion using the cis-trans photoisomerization of the azo group. Beilstein Journal of Organic Chemistry. 2012;8:1071-90.

19. Chibisov AK, GÃ¶rner H. Photoprocesses in Spiropyran-Derived Merocyanines. J Phys Chem A. 1997;101(24):4305-12.

20. Decker H, Felser H. Cyclic oxonium salts from dicumarketone and spiropyrane derivatives. Berichte Der Deutschen Chemischen Gesellschaft. 1908;41:2997-3007.

21. Tan B-H, Yoshio M, Ichikawa T, Mukai T, Ohno H, Kato T. Spiropyran-based liquid crystals: the formation of columnar phases via acid-induced spiro-merocyanine isomerisation. Chem Comm. 2006;45:4703-5.

22. Seki T, Ichimura K, Ando E. Stable J-aggregate formation of photoinduced merocyanine in bilayer membrane. Langmuir. 1988;4(4):1068-9.

23. Wohl CJ, Kuciauskas D. Isomerization Dynamics of Photochromic Spiropyran Molecular Switches in Phospholipid Bilayers. J Phys Chem B. 2005;109(46):21893-9.

24. Tamai N, Miyasaka H. Ultrafast Dynamics of Photochromic Systems. Chem Rev. 2000;100(5):1875-90.

25. Khairutdinov RF, Hurst JK. Photocontrol of Ion Permeation through Bilayer Membranes Using an Amphiphilic Spiropyran. Langmuir. 2001;17(22):6881-6.

26. Drummond CJ, Albers S, Furlong DN, Wells D. Photocontrol of surface activity and self-assembly with a spirobenzopyran surfactant. Langmuir. 1991 2012/02/19;7(10):2409-11.

27. Drummond CJ, Furlong DN. Photochromism of a surface-active spirobenzopyran moiety in dioxane-water mixtures and self-assembled surfactant aggregates. J Chem Soc, Faraday Trans 1990;86(21):3613-21.

28. Drummond CJ, Furlong DN, Georgaklis G. Comparison of the photochromism of a spirobenzopyran derivative in unilamellar surfactant vesicles and solvent-cast surfactant films. J Chem Soc, Faraday Trans 1990;86(23):3913-8.

29. Such G, Evans RA, Yee LH, Davis TP. Factors Influencing Photochromism of Spiro-Compounds Within Polymeric Matrices. 2003;43(4):547 - 79.

30. InternationalProgrammeOnChemicalSafety. ULTRAVIOLET RADIATION. Geneva: United Nations Environment Programme, International Labour Organisation, World Health Organization, 1994.

31. Sliney DH. Ultraviolet Radiation Exposure Criteria. Radiation Protection Dosimetry. 2000;91(1-3):213-22.

32. Weissleder R. A clearer vision for in vivo imaging. Nat Biotech. 2001;19(4):316-7.

33. Haase M, Schäfer H. Upconverting Nanoparticles. Angewandte Chemie International Edition. 2011;50(26):5808-29.

34. Wang F, Liu X. Recent advances in the chemistry of lanthanide-doped upconversion nanocrystals. Chem Soc Rev. 2009;38(4):976-89.

35. Chatterjee DK, Gnanasammandhan MK, Zhang Y. Small Upconverting Fluorescent Nanoparticles for Biomedical Applications. Small. 2010;6(24):2781-95.

36. Aebischer A, Heer S, Biner D, Krämer K, Haase M, Güdel HU. Visible light emission upon near-infrared excitation in a transparent solution of nanocrystalline β-NaGdF4: Yb3+, Er3+. Chemical Physics Letters. 2005 5/17/;407(1–3):124-8.

37. Krämer KW, Biner D, Frei G, Güdel HU, Hehlen MP, Lüthi SR. Hexagonal Sodium Yttrium Fluoride Based Green and Blue Emitting Upconversion Phosphors. Chemistry of Materials. 2004 2004/04/01;16(7):1244-51.

38. Boyer J-C, Carling C-J, Gates BD, Branda NR. Two-Way Photoswitching Using One Type of Near-Infrared Light, Upconverting Nanoparticles, and Changing Only the Light Intensity. Journal of the American Chemical Society. 2010 2012/03/19;132(44):15766-72.

39. Mader HS, Kele P, Saleh SM, Wolfbeis OS. Upconverting luminescent nanoparticles for use in bioconjugation and bioimaging. Current Opinion in Chemical Biology. 2010;14(5):582-96.

40. Carling C-J, Nourmohammadian F, Boyer J-C, Branda NR. Remote-Control Photorelease of Caged Compounds Using Near-Infrared Light and Upconverting Nanoparticles. Angewandte Chemie International Edition. 2010;49(22):3782-5.

41. Zhang C, Xu C-H, Sun L-D, Yan C-H. Photoswitchable Upconversion Luminescence of Rare-Earth Nanophosphors with Covalently Grafted Spiropyran. Chemistry – An Asian Journal. 2012;7(10):2225-9.

42. Zhang BF, Frigoli M, Angiuli F, Vetrone F, Capobianco JA. Photoswitching of bis-spiropyran using near-infrared excited upconverting nanoparticles. Chemical Communications. 2012.

43. Zhang P, Steelant W, Kumar M, Scholfield M. Versatile Photosensitizers for Photodynamic Therapy at Infrared Excitation. Journal of the American Chemical Society. 2007 2007/04/01;129(15):4526-7.

44. Yan B, Boyer J-C, Habault D, Branda NR, Zhao Y. Near Infrared Light Triggered Release of Biomacromolecules from Hydrogels Loaded with Upconversion Nanoparticles. Journal of the American Chemical Society. 2012 2012/10/10;134(40):16558-61.

45. Dong Y-D, Larson I, Hanley T, Boyd BJ. Bulk and Dispersed Aqueous Phase Behavior of Phytantriol: Effect of Vitamin E Acetate and F127 Polymer on Liquid Crystal Nanostructure. Langmuir 2006;22(23):9512-8.

46. Phan S, Fong W-K, Kirby N, Hanley T, Boyd BJ. Evaluating the link between self-assembled mesophase structure and drug release. Int J Pharm. 2011;421(1):176-82.

47. Hyde S. The Language of shape: the role of curvature in condensed matter--physics, chemistry, and biology. Amsterdam [Netherlands]; New York: Elsevier; 1997.

48. Görner H. Photoprocesses in spiropyrans and their merocyanine isomers: Effects of temperature and viscosity. Chem Phys. 1997;222(2-3):315-29.

49. Darwish TA, Evans RA, Hanley TL. Spiropyran , Chromene and Spirooxazine, Melange á trios: Molecular Logic Systems Through Selective and Reversible Deactivation of Photochromism Mediated by CO2 Gas. *Dyes Pigments*. 2011; *In Press*.

50. Darwish TA, Evans RA, James M, Malic N, Triani G, Hanley TL. CO2 Triggering and Controlling Orthogonally Multiresponsive Photochromic Systems. J Am Chem Soc. 2010;132(31):10748-55.

51. Barauskas J, Landh T. Phase Behavior of the Phytantriol/Water System. Langmuir. 2003;19(23):9562-5.

52. Dong Y-D, Dong AW, Larson I, Rappolt M, Amenitsch H, Hanley T, et al. Impurities in Commercial Phytantriol Significantly Alter Its Lyotropic Liquid-Crystalline Phase Behavior. Langmuir. 2008;24(13):6998-7003.

53. Kholmansky AS, Dumaev KM. Mechanism of the α rupture of the Cspiro-O bond in indolinospiropyrans. Journal of Photochemistry. 1985;31(2–3):307-14.

54. Malkin YN, Krasieva TB, Kuzmin VA. Quantitative study of the photostability of spiropyrans. Journal of Photochemistry and Photobiology A: Chemistry. 1989;49(1–2):75-88.

55. Topchiyev DA. Photochromism of spiropyrans in polymeric media. Some aspects and possibilities of regulating the spectral-kinetic characteristics. Review. Polymer Science USSR. 1990;32(12):2361-83.

56. Shiraishi Y, Inoue T, Sumiya S, Hirai T. Entropy-Driven Thermal Isomerization of Spiropyran in Viscous Media. J Phys Chem A. 2011 2012/03/07;115(33):9083-90.

57. Shiraishi Y, Itoh M, Hirai T. Thermal isomerization of spiropyran to merocyanine in aqueous media and its application to colorimetric temperature indication. Phys Chem Chem Phys. 2010;12(41).

58. Negrini R, Mezzenga R. pH-Responsive Lyotropic Liquid Crystals for Controlled Drug Delivery. Langmuir. 2011:null-null.

59. Heer S, Kömpe K, Güdel HU, Haase M. Highly Efficient Multicolour Upconversion Emission in Transparent Colloids of Lanthanide-Doped NaYF4 Nanocrystals. Advanced Materials. 2004;16(23-24):2102-5.

60. Mahalingam V, Vetrone F, Naccache R, Speghini A, Capobianco JA. Colloidal Tm3+/Yb3+-Doped LiYF4 Nanocrystals: Multiple Luminescence Spanning the UV to NIR Regions via Low-Energy Excitation. Advanced Materials. 2009;21(40):4025-8.

61. Zhao Y. Azobenzene-Containing Block Copolymer Micelles: Toward Light-Controllable Nanocarriers. Smart Light-Responsive Materials: John Wiley & Sons, Inc.; 2008. p. 215-42.

62. Kim S-J, Reneker DH. A mechanochromic smart material. Polymer Bulletin. 1993 1993/09/01;31(3):367-74.

63. Wang X. Azo Polymer Colloidal Spheres: Formation, Two-Dimensional Array, and Photoresponsive Properties. Smart Light-Responsive Materials: John Wiley & Sons, Inc.; 2008. p. 177-213.

64. Jonsson F, Beke-Somfai T, Andréasson J, Nordén B. Interactions of a Photochromic Spiropyran with Liposome Model Membranes. Langmuir. 2013.

65. Dong Y-D, Tilley AJ, Larson I, Lawrence MJ, Amenitsch H, Rappolt M, et al. Nonequilibrium Effects in Self-Assembled Mesophase Materials: Unexpected Supercooling Effects for Cubosomes and Hexosomes. Langmuir. 2010;26(11):9000-10.

66. Salonen A, Muller F, Glatter O. Dispersions of Internally Liquid Crystalline Systems Stabilized by Charged Disklike Particles as Pickering Emulsions: Basic Properties and Time-Resolved Behavior. Langmuir. 2008;24(10):5306-14.

67. Matson M, Carlsson N, Beke-Somfai Ts, Nordén B. Spectral Properties and Orientation of Voltage-Sensitive Dyes in Lipid Membranes. Langmuir. 2012 2012/07/15.

68. Tangso KJ, Fong W-K, Darwish T, Kirby N, Boyd BJ, Hanley T. Novel Spiropyran Derivatives and their Application as Light Responsive Liquid Crystalline Components Soft Matter. 2013;Submitted.

Chapter 5 – *In situ* Laser-Activated Manipulation of Nanostructure in Photothermal Matrices

5. *In situ* Laser-Activated Manipulation of Nanostructure in Photothermal Matrices

5.1. Introduction

The formulation of efficient and biocompatible nanostructured carriers for drug delivery is a key aim towards the development of responsive drug delivery systems. Towards the *in vivo* application of light sensitive hybrid nanostructures, PHYT-GNR samples were investigated for their ability to be activated in subcutaneous tissues and thus control the rate of drug release from the matrix. Although some success was achieved in UV and NIR activation of the photochromic matrices as presented in Chapter 4, these systems were not progressed into *in vivo* studies as further optimisation and characterisation of these systems is required. It is acknowledged that the phase transition in the PHYT-GNR matrix is not ideal as it progresses from $V_{2\,D}$, a phase with a fast release diffusion coefficient, to H_2, a phase with a slow diffusion coefficient. However, as the PHYT matrix provided the most controllable and responsive nanostructure in the initial studies, it was selected as the matrix for this proof-of-concept *in vivo* study. Concurrent studies into systems which provide more appropriate reversible phase transitions e.g. from L_α to V_2 were performed and are reported in Chapter 6.

Gold nanoparticles have been used as a photosensitiser in self-assembled systems for drug delivery in polymeric matrices such as PLGAs[1], hydrogels[2] and liposomes[3, 4]. The *in vitro* selective release of calcein from liposomes was achieved upon UV light activation after internalisation into ARPE-19 cells[5]. The model drug release was attributed to the photothermal phase transition from the lamellar gel phase ($L_{\beta'}$) to the stable ripple phase ($P_{\beta'}$), followed by the formation of the fluid lamellar phase upon constant UV irradiation. Wu et al. also achieved triggered release from liposomes containing hollow gold nanoshells upon irradiation with NIR laser light which was attributed to the occurrence of transient cavitation of the liposome, akin to

ultrasound triggered release[6]. UV-activated pulsatile release was recently achieved by An et al. from gold nanoparticle doped lecithin/cholesterol liposomes, where drug release was attributed to phase transitions within the lipid bilayer, however the structures formed upon irradiation was unknown[7]. Although light activated release has been demonstrated, it is hypothesised that the ability to reversibly and reliably control and quantify the nanostructures formed upon irradiation in self-assembled systems is crucial to the development of liquid crystalline materials as on-demand drug delivery systems.

Investigation into the utilisation of V_2 and H_2 phases in pharmaceutical applications are of particular interest as these phases are thermodynamically stable and determine the rate of active release from within the matrix[8]. They have been proposed as matrices for the delivery of actives that are small and hydrophilic[9], poorly water-soluble[10] as well as nucleic acids, proteins and peptides[11, 12]. The use of bulk and dispersed inverse phases as drug delivery matrices have resulted in the improvement of pharmacokinetic profiles of drugs when employed as oral[10, 13, 14], topical[15-17], ocular[18] and buccal[19] dose forms. Additionally, the release rate of actives from within the liquid crystal nanostructure can be externally manipulated via e.g. a change in temperature[20] or change in pH[21].

Towards light activated drug release, this Chapter presents *ex vivo* and *in vivo* studies into the viability of NIR-activated photothermal systems for on-demand drug delivery. In the first instance, laser penetration through biological tissue was investigated in order to determine the responsiveness of these matrices at subcutaneous depths. This was achieved by *ex vivo* laser activation studies on the SAXS beamline at the Australian Synchrotron using rat skin as the sample tissue. Once the ideal location for dosing was identified on the basis of *ex vivo* through skin activation, matrices were loaded into custom-made implants and inserted into the subcutaneous tissues for investigation into external control of drug release using NIR laser light.

5.2. Hypotheses and Aims

Hypothesis 1

That the liquid crystalline nanostructure of the PHYT-GNR matrix can be manipulated via laser activation through biological tissue.

Hypothesis 2

That the light-activated manipulation of nanostructure of the PHYT-GNR matrix determines the rate of drug release from the matrix, whereby the appearance of drug in plasma is dependent on the liquid crystalline phase formed.

In order to investigate these hypotheses, the following aims will be achieved:

- To determine the ability of NIR laser irradiation to penetrate biological tissue by recording the phase transition kinetics of liquid crystalline materials upon laser activation through *ex vivo* biological tissue using synchrotron SAXS.
- To quantify NIR laser-triggered release behaviour of a model drug from subcutaneously dosed liquid crystalline matrices with and without gold nanorods.

5.3. Materials and Methods

General materials and methods employed are detailed in Chapter 2.

The PHYT-GNR photothermal system was investigated for its ability to control ‘on-demand’ drug release. All experimental procedures involving animals for this project were approved by the Monash Institute of Pharmaceutical Sciences Animal Ethics committee under the project title: “Using externally triggered changes in the nanostructure of liquid crystals to control drug release *in vivo*”, AEC Project Number: VCPA.2009.41 (RBB.3.2009).

5.3.1. Ex vivo Time Resolved Synchrotron SAXS Studies

Ex vivo studies were employed to determine laser penetration through rat skin tissue. Skin samples were taken from blank animals used in studies performed by colleagues in order to minimise the number of animals used. Samples were taken from the back, side, abdomen and hind leg. The experimental SAXS set up is shown in Figure 5.1. Whole shaved skin, hairless skin or sections of skin were placed in between the laser and the liquid crystalline sample in order to assess the attenuation of the NIR laser beam. Depilation of whole skin was achieved by application of Nair® cream (Church & Dwight (Australia) PTY LTD, Brookvale, NSW) for no longer than 5 min then removal via rinsing with warm water.

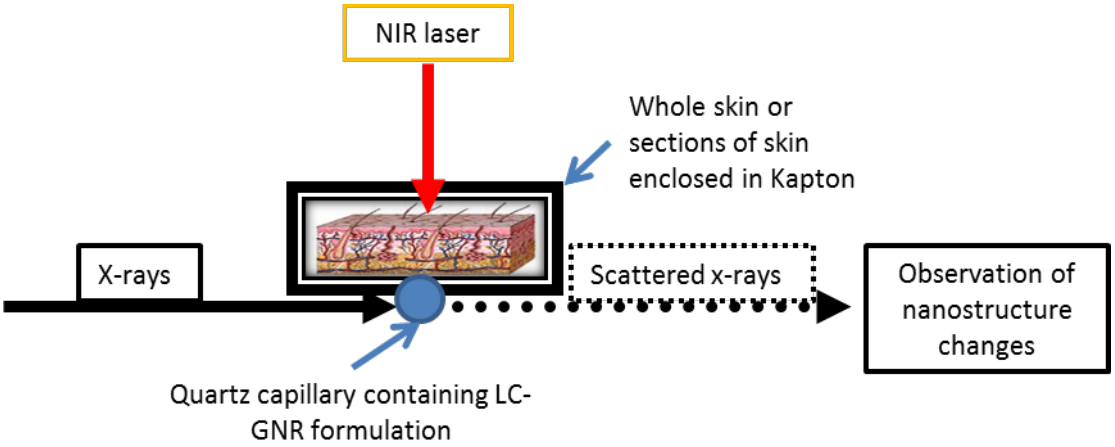

Figure 5.1 – *Ex vivo* experimental set up. LC matrix was loaded into quartz capillaries before placing adjacent to the skin as shown. Skin or skin layers were sandwiched in Kapton tape in order to maintain appropriate hydration of the matrix and integrity of the skin.

5.3.2. In vivo subcutaneous absorption studies

In vivo studies were employed to determine the influence of laser activation of PHYT-based liquid crystalline formulations with and without GNR on the rate of glucose appearance in plasma from a subcutaneous injection.

5.3.2.1. In vivo Materials

Radiolabelled ^{14}C-glucose (262 mCi/mmol) was obtained from Moravek Biochemicals (Brea, California, USA). D-(+)-glucose was purchased from Sigma Aldrich (St. Louis, MO, USA). Heparin Injection BP (1,000 IU/mL) was obtained from Mayne Pharma Pty. Ltd. (Mulgrave, Victoria, Australia). Saline for injection was acquired in 100 mL polyethylene bags from Baxter Healthcare Pty. Ltd. (Toongabbie, NSW, Australia). Acepromazine (acepromazine maleate 10 mg/mL) was purchased from Mavlab (Slacks Creek, Queensland) and Delvet Pty Ltd. (Seven Hills, New South Wales). Xylazine (xylazine hydrochloride 100 mg/mL) was purchased from Troy labs (Smithfield, New South Wales). Parnell Ketamine Injection® (ketamine 100 mg/mL) was purchased from Parnell Laboratories Aust. Pty. Ltd., (Alexandria, New South Wales, Australia). Lethabarb (325 mg/mL pentobarbitone sodium) was purchased from Virbac pty. Ltd. (NSW, Australia). Starscint scintillation cocktail was procured from Perkin Elmer (Boston, MA, USA) and 6 mL and 20 mL polypropylene vials for scintillation counting were obtained from Packard Biosciences (Meriden, CT, USA)

5.3.2.2. Animal Procedures

The absorption studies were conducted using rats (male, Sprague Dawley, 250-330 g). Animals were anesthetised prior to surgery with a subcutaneously-administered anaesthetic cocktail of 37.3% (v/v) ketamine (100 mg/mL), 9.8% (v/v) xylazine (100 mg/mL), 3.9% (v/v) acepromazine (10 mg/mL) and 49.0% (v/v) saline, given at a dose of 1.0 mL/kg. This was followed by a maintenance cocktail consisting of 90.9% (v/v) ketamine (100 mg/mL) and 9.1% (v/v) acepromazine (10 mg/mL) at a dose of 0.44 mg/kg/hr until the termination of the experiment. The anesthetised rats were placed on a heated surface maintained at 37°C and were cannulated via the carotid artery using 0.96 x 0.58 mm polyethylene tubing (Paton Scientific, Victor Harbour, Australia). For the duration of the experiment, the rats were laid on their backs on the 37°C surface.

The subcutaneous site of administration in these studies was located on the left side of the abdomen. Depilation was achieved first by shaving the area, and then by the application of Nair® as described above. A thermocouple thermometer (Digitech Controls, Tamil Nadu, India)), with 0.5% accuracy, was inserted into the subcutaneous pocket adjacent to the implant in order to monitor the subcutaneous temperature during the experiment. At the conclusion of the experiments, animals were sacrificed via infusion of 0.5 mL Lethabarb into the carotid cannula.

5.3.2.3. Formulation Preparation

^{14}C-glucose, a molecule that is readily absorbed *in vivo*, was chosen as the model drug to simplify the analytical aspects of the project. The liquid crystalline formulations were dosed subcutaneously for accessibility to the administration site in terms of sample and laser administration. In the first instance, a subcutaneous dose of a low viscosity lamellar phase (L_α) liquid crystal precursor system was prepared as previous[20]. These precursor systems contain a 12% aqueous component and form V_2 or H_2 on exposure to interstitial fluid[22, 23]. They were prepared in the same manner as described as previous[22, 23]. The aqueous component contained the model hydrophilic drug, ^{14}C-Glucose and glucose. However, as the location and surface area of dose form could not be defined in direct subcutaneous injection of these *in situ* gelling systems, the irradiation of sample was inconsistent as was reflected in the initial results.

Thus, liquid crystalline implants (Figure 5.2) were created to in order to define the surface area and thickness of the dose. Liquid crystalline matrices containing 30% (w/w) aqueous component were prepared for administration. The aqueous component contained approximately 700 mg/mL glucose as a mixture of radiolabelled ^{14}C-glucose and cold glucose. The target dose in terms of radioactivity was 1.5 μCi. These phases were prepared and then equilibrated on a tube roller at 37°C for >48 hr before dosing.

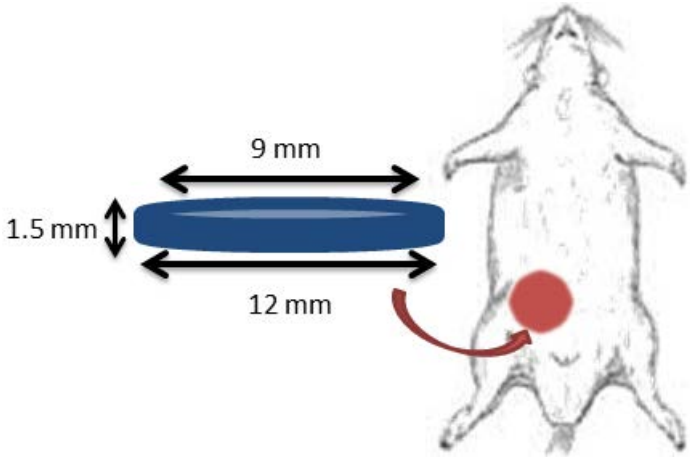

Figure 5.2 – Dimensions of *in vivo* implant and location of dose and laser irradiation. The laser was placed at a distance where the spot size corresponded with the dimensions of the LC implant (2.83 cm^2). The plastic implant was filled with ~100 mg of bulk liquid crystal formulation, and then inserted into the subcutaneous pocket of the skin on the left side of the abdominal region. The implant area was then irradiated with a DPSS NIR laser (572 mW, 2 h).

5.3.2.4. Formulation Administration

The formulations administered were:

1. subcutaneous injection of a glucose solution in saline.
2. subcutaneous insertion of a PHYT V_2 liquid crystal formulation ($PHYTV_2$) containing a 30% aqueous component.
3. subcutaneous insertion of a PHYT + 10% vitamin E acetate H_2 liquid crystal formulation ($PVEH_2$) containing a 30% aqueous component.
4. subcutaneous injection of PHYT + 3 nM GNR (PHYTGNR) liquid crystal formulation containing a 30% aqueous component.

All studies were performed in triplicate. The rats were administered the solution formulations using a 1 mL syringe fitted with 23 gauge needle. The liquid crystal implants were administered into a surgically created subcutaneous pocket, followed by an injection of 0.2 mL saline into the subcutaneous pocket in order to minimise the effect of the liquid crystal imbibing water from surrounding tissue. The formulations contained a nominal dose of 70 mg/kg glucose,

corresponding to an approximate dose of 110 mg of liquid crystal precursor formulation or 300 μL ^{14}C-glucose solution, via subcutaneous injection. The glucose solution and liquid crystalline dose administered were determined by volume and weight respectively.

5.3.2.5. Sampling

Blood samples (0.2 mL) were obtained via the indwelling cannula at t = 1, 6, 20, 40, 60, 90, 120, 140, 160, 180, 240, 300, 387 and 510 min. Cannulas were kept patent by flushing with a small (0.5 mL) volume of 1 IU/mL heparin in saline. Blood samples were placed immediately into a tube containing 10 IU of heparin and plasma was separated by centrifugation for 7 min at 2800 x g. Plasma (100 μL) was removed, to which 2 mL of Starscint scintillation cocktail was added. The sample was then vortexed before analysis by liquid scintillation counting.

5.3.2.6. Sample Analysis and Validation

Data were obtained as disintegrations per minute (DPM) by scintillation counting. The plasma assay was validated for precision (< 10%) and accuracy (< 20%) to establish a limit of quantitation (LOQ) and a linear relationship between volume of ^{14}C-glucose added and DPMs. Blank rat plasma (100 μL) was spiked with 150, 15, 1.5, 0.15, 0.06, 0.05, 0.04 and 0.02 nCi in 6 mL scintillation vials. 2 mL scintillation cocktail was added, and the samples vortexed and counted on a scintillation counter. This was performed in order to determine the LOQ for ^{14}C-glucose and to establish a linear relationship between the volume of glucose added to disintegrations per minute (DPM) counted. Validation data can be found in the Appendix of this chapter.

5.3.2.7. Pharmacokinetic Analysis

The data obtained as disintegrations per minute (DPM) were converted to plasma concentration using the known activity of the glucose used in this study. Plasma concentrations (μg/mL) were normalised to a dose of 50 mg/kg.

Pharmacokinetic parameters, total area under the plasma concentration-time curve (AUC), peak plasma concentration (C_{max}) and time to reach plasma concentration (t_{max}), were calculated for all subcutaneous administrations[24]. Further treatment of the data was performed in order to permit comparison of absorption behaviour between the various formulations through the calculation of the apparent absorption rate constants ($k_{app\ 3\text{-}5}$) of glucose from each system on cessation of NIR laser irradiation. The $k_{app\ 3\text{-}5}$ was calculated as the slope of the three time points of the normalised plasma concentration (μg/mL) vs time curve from t = 3 – 5 h. One way analysis of variance (ANOVA) was performed in order to compare the statistical differences of the calculated pharmacokinetic parameters and $k_{app\ 3\text{-}5}$ of the different systems.

5.4.Results

5.4.1. Ex vivo *synchrotron studies*

5.4.1.1. Impact of skin thickness, location and presence of hair on ex vivo *activation*

Ex vivo laser activation studies were performed in order to determine the ideal location for activation of the subcutaneously administered liquid crystalline matrices. The SAXS profiles displaying kinetics of phase behaviour of the PHYTGNR matrices upon NIR irradiation are shown in Figure 5.3. These profiles are summarised according to the skin type in Table 5.1. With skin attenuating the laser beam, none of the matrices transitioned all the way to the L_2 phase as was seen in the phytantriol + GNR matrices in Chapter 3. In general, it was found that the thicker the skin, the more attenuated the response of the matrix to laser irradiation. Skin removed from the back of the animal appeared to have some pigmentation[25] and could also have added to the minimal response of the matrix to irradiation through the back skin. The presence of hair on the skin also influenced the ability of the laser to penetrate through to the liquid crystal sample.

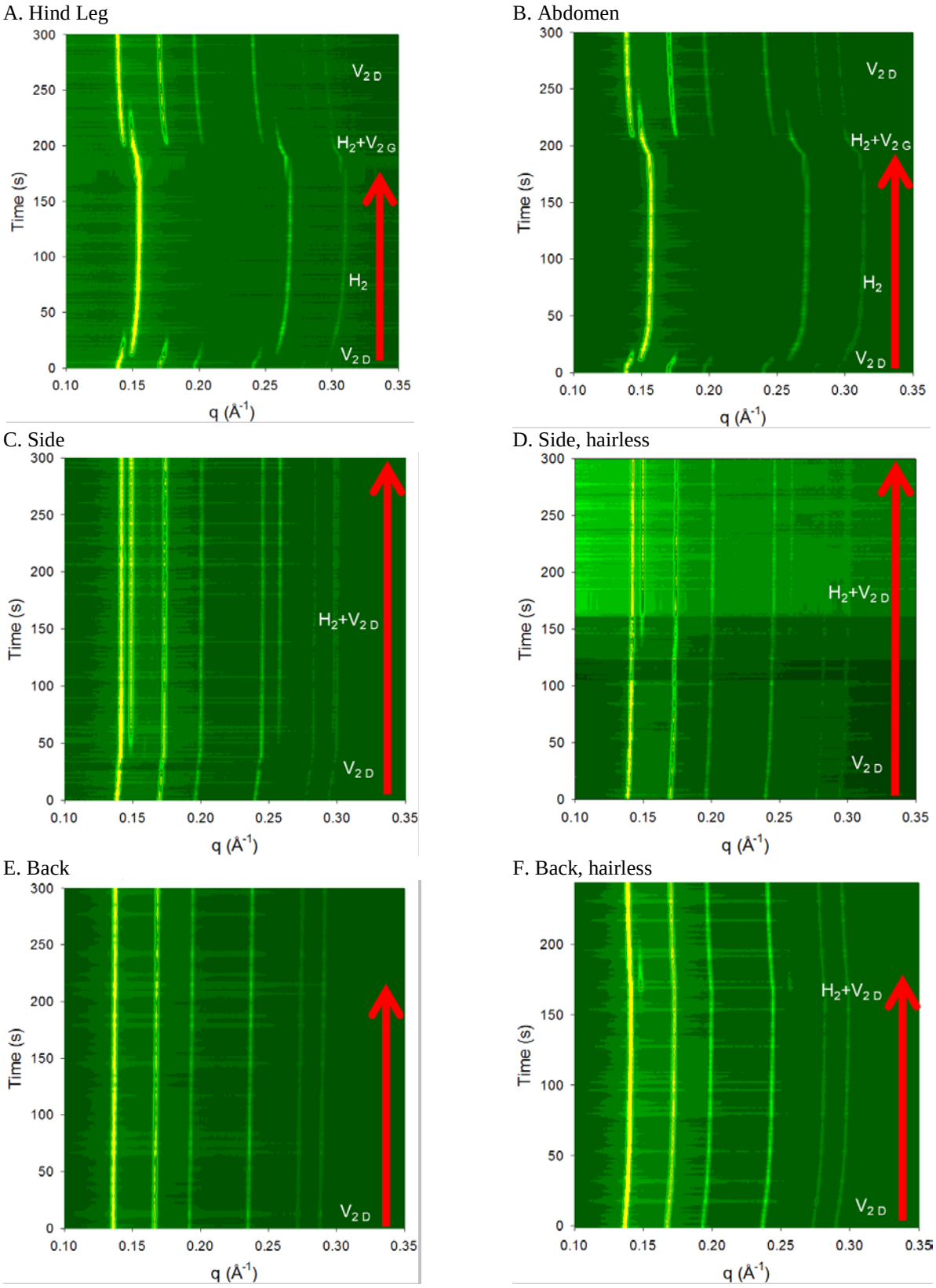

Figure 5.3 – Time resolved SAXS profiles of PHYT + 3 nM GNR upon NIR laser activation through *ex vivo* rat skin taken from: Panel A. Hind Leg, B. Abdomen, C. Side, D. Side, hairless, E. Back and F. Back, hairless. Laser application is indicated by red arrows. Increased colour intensity towards bright yellow indicates increased intensity of signal at that q-value. Annotated phase structures on the right were determined from indexing peaks in intensity vs. q profiles from individual frames.

The data were converted to apparent temperature (T_{app}) experienced by the matrix using the approach outlined in Chapter 2 and employed in Chapter 3. Based on the change in apparent temperature **(**ΔT_{app} (°C)) and the NIR irradiation time required to achieve the maximum apparent temperature (Time to T_{app} max (s)) values tabulated in Table 5.1, the order of maximum matrix response to location of skin was found to be Abdomen > Hind Leg > Side > Back, which broadly reflected the order of skin thickness. The epilation and extra handling of the skin sampled from the side and back of the rat resulted in the thinning of the sample. This resulted in the increased response of the PHYTGNR matrix, however this was still attenuated compared to the response through abdominal skin.

Abdominal skin has a higher permeability to drugs and is thinner than skin sourced from other areas, attributed to a thinner stratum corneum layer and a different composition than in other areas[25]. Thus, although the thickness of skin sourced from the hind leg is thinner than abdominal skin, its composition may have played a part in the reduced matrix response in comparison to the abdominal skin. In addition, the small surface area available for dosing and irradiation on the hind leg would make administration difficult. Consequently, the abdominal region of the rat was chosen as the site for the *in vivo* subcutaneous studies.

Table 5.1 – Summary of the skin thickness (mm), change in apparent temperature **(**ΔT_{app} (°C)), NIR irradiation time required to achieve the maximum apparent temperature (Time to T_{app} max (s)), and the phase formed at T_{app} max.

Location	**Thickness (mm)**	**ΔT_{app} (°C)**	**Time to T_{app} max (s)**	**Phase Formed**
Hind leg	1.01	18.98	164	H_2
Abdomen	1.34	21.27	140	H_2
Side	3.04	6.72	250	$V_{2\,D}$+H_2
Side, hairless	1.96	7.56	250	$V_{2\,D}$+H_2
Back	3.34	3.26	300	$V_{2\,D}$
Back, hairless	1.64	8.73	168	$V_{2\,D}$+H_2

5.4.2. The Effect of Glucose Loading on Phase Transition Behaviour

PHYT formulations containing 20, 40, 60 and 80% (w/w) glucose in the aqueous phase were investigated for the effect of glucose loading on the liquid crystalline nanostructure. Figure 5.4 details the equilibrium phase behaviour of these matrices between 25 – 80ºC. The loading of glucose at these concentrations had little effect on the phase behaviour of the PHYT-water system over this temperature range. This provided confidence that the payload of model drug would not complicate interpretation of structure formation during the *in vivo* studies.

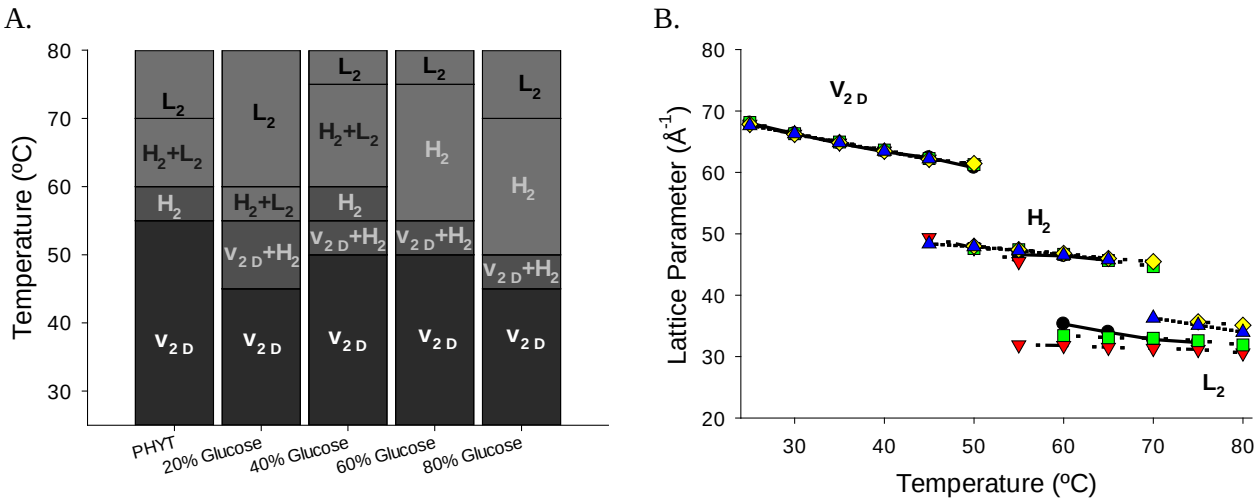

Figure 5.4 – Equilibrium phase behaviour of PHYT in excess water containing 0% glucose, 20% glucose, 40% glucose, 60% glucose, 80% glucose as determined by SAXS.

5.4.3. Subcutaneous Laser Activation Studies

The relative rates of absorption of a model drug, ^{14}C glucose, in these subcutaneous absorption studies were used to indicate differences in release rate during and after laser irradiation of the liquid crystalline matrices *in vivo*. The rate of glucose absorption of ^{14}C-glucose was expected to correlate with the release rate of ^{14}C-glucose from the liquid crystalline matrices, as in past oral and subcutaneous absorption studies from similar systems[8, 20]. The three liquid crystalline formulations comprised of PHYT only ($PHYTV_2$), PHYT + 10% Vitamin E ($PVEH_2$) and PHYT

+ 3 nM GNR (PHYTGNR). The plasma profiles obtained after subcutaneous insertion of liquid crystal formulations containing ^{14}C-glucose loaded into custom made implants, and a subcutaneous injection of an aqueous glucose solution as control formulation, are illustrated in Figure 5.5. The subcutaneously dosed formulations were exposed to NIR laser irradiation for two hours, in order to form the slow releasing H_2 phase in the presence of GNR, or V_2 phase in the absence of GNR, and then the implant was left to release the model drug at ambient temperature and under non-irradiation conditions, where the fast releasing V_2 phase was expected to be present.

Individual plots of normalised plasma concentration over time for each formulation are reported in the Appendix. The summary profiles for the liquid crystalline systems are illustrated in Figure 5.5. The liquid crystal implants demonstrated a sustained release profile in comparison to the subcutaneously dose aqueous solution (Figure 5.5, Panel B.). The absorption profiles of $PHYTV_2$ and $PVEH_2$ in the absence of GNR increased steadily until 4 and 3 h respectively, where the plasma profiles plateaued, resulting in reasonably constant plasma glucose concentrations until the end of the experiment. The calculated pharmacokinetic parameters are tabulated in Table 5.2, and reveal an increase in the T_{max} and C_{max} ($p < 0.05$ for all formulations) compared to the aqueous solution.

Administration of the $PHYTV_2$ matrix released the ^{14}C glucose significantly faster than that of the $PVEH_2$ as expected from previous *in vitro* and *in vivo* studies[20] (Table 5.3). Laser irradiation of the formulations without GNR did not influence the absorption rate of drug into plasma, as the profiles were not discontinuous with and without irradiation. Clearly this was not the case for the PHYGNR formulation discussed further below. The total exposure of the system to model drug (AUCs) for the different formulations were difficult to interpret as the model drug was still being absorbed significantly at the last data point (t = 8.5 h), particularly in the case of the $PHYTV_2$ matrix where the plasma concentration was still slightly increasing, while for $PVEH_2$ the

concentrations were decreasing because the elimination rate had overtaken the absorption rate. Consequently it is not appropriate to compare AUC values for these profiles.

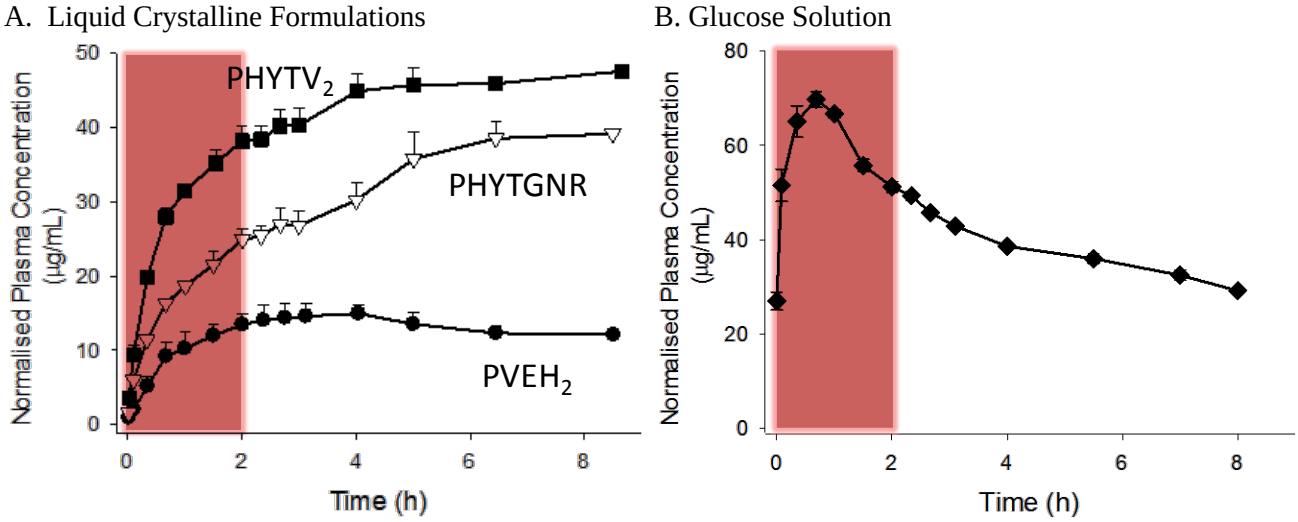

Figure 5.5 – Panel A. – Mean normalised plasma concentration profiles of ^{14}C glucose in rats subcutaneously administered formulations of $PHYTV_2$ (–■–), $PVEH_2$ (–●–) and PHYTGNR (–▽–). Data are mean ± SEM, n=4 except at t=8.5 h, where data is n=1. The red shading indicates the duration of NIR laser irradiation (572 mW, 2 h). Panel B. Mean normalised plasma concentration profiles of ^{14}C glucose in rats administered with a subcutaneous injection of glucose solution. Data are mean ± SEM, n=3 except at t=8.5 h, where data are n=2.

Table 5.2 – Mean pharmacokinetic parameters after subcutaneous administration of glucose in rats. Doses were normalised to a dose of 50 µg/kg glucose dosed per rat. Data expressed as mean ± SEM, n = 4, except *n = 3. AUC values were truncated to the last measurable time point where n ≥ 3.

Formulation	Mean C_{max} (µg/mL)	Mean T_{max} (h)	AUC
Glucose Solution	69.8 ± 1.68*	0.68 ± 0*	69.8 ± 13.9*
$PHYTV_2$	49.3 ± 2.2	5.00 ± 24.5	597.9 ± 22.7
$PVEH_2$	16.1 ± 1.7	3.41 ± 24	217.8 ± 31.9*
PHYTGNR	40.6 ± 0.67*	7.13 ± 35.5*	525.2 ± 92.2*

Figure 5.6 shows the subcutaneous temperature profiles of the three systems over the duration of the experiment. Application of the NIR laser did actually and somewhat unexpectedly increase the subcutaneous temperature by 5 – 6 ºC apparently by non-specific absorption of the NIR irradiation in the systems without GNR present. However, there was no significant difference between the subcutaneous temperature profiles of the three formulations, indicating that the presence of the GNR did not induce significant heating of surrounding tissue above that imparted by the laser alone.

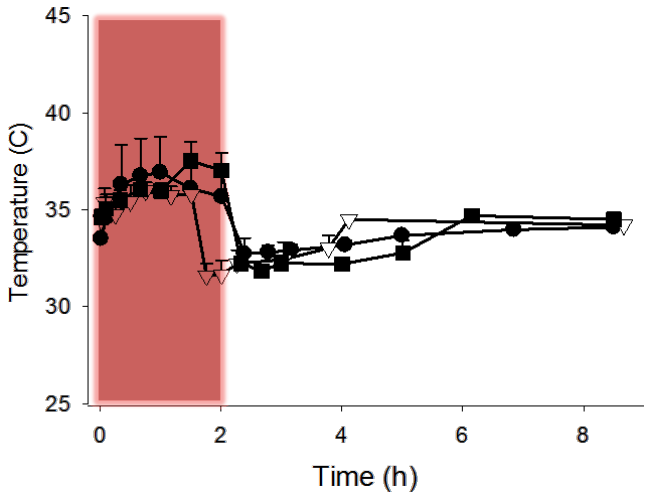

Figure 5.6 –Mean temperatures were recorded adjacent to the implant site of $PHYTV_2$ (–■–), $PVEH_2$ (–●–) and PHYTGNR (–▽–). Data are mean ± SEM, n=4 except at t=8.5 h, where data is n=1. The red shading indicates the duration of NIR laser irradiation (572 mW, 2 h).

Figure 5.7 shows the plasma profile of the PHYTGNR compared to a profile fitted to t = 0 – 3 h data which would be expected to occur if there was no switch in liquid crystalline phase. The plasma concentration profile of PHYTGNR fell between those of the $PHYTV_2$ and $PVEH_2$ profiles between t = 0 – 3 h, and plateaued at ~t = 2.5 hr. At t > 3 h, there was a marked increase in the rate of appearance of the model drug in plasma. This reflected the expected phase transition upon cessation of laser irradiation from H_2, a slower releasing nanostructure, to V_2, a faster

releasing nanostructure. There was a lag period between the end of NIR laser exposure and the spike in plasma concentration which is attributed to the time taken for the faster absorption rate to catch up to the elimination rate, as well as the liquid crystal requiring some time to equilibrate to the V_2 nanostructure. The relatively slow release rate from the irradiated matrix compared to the unirradiated matrix directly echoes previous data using direct cooling as the source of phase transition[20], and a similar change in *in vitro* release rate on pH activation[21].

Table 5.3 compares the apparent absorption rate constants ($k_{app\ 3\text{-}5}$) calculated for the four formulations between t = 3 – 5 h. These time points were chosen as this is the region in which the increase in plasma glucose in the PHYTGNR matrix is the most pronounced. A negative $k_{app\ 3\text{-}5}$ in the glucose solution and $PVEH_2$ formulations are indicative that the rate of elimination being greater than the rate of absorption; there was no increase in the release of glucose on cessation of irradiation. The positive $k_{app\ 3\text{-}5}$ of $PHYTV_2$ and PHYTGNR indicate that the matrices were still releasing glucose at a faster rate than concurrent elimination. The positive $k_{app\ 3\text{-}5}$ of $PHYTV_2$ is attributed to the general release of glucose from the $PHYTV_2$ matrix as these time points occur before the normalised plasma concentrations plateau and there is no distinct spike in plasma concentration. On the other hand, in the PHYTGNR matrix, the spike in plasma concentrations was matched by the significantly higher $k_{app\ 3\text{-}5}$ thus suggesting that a change of phase has occurred after the termination of laser exposure.

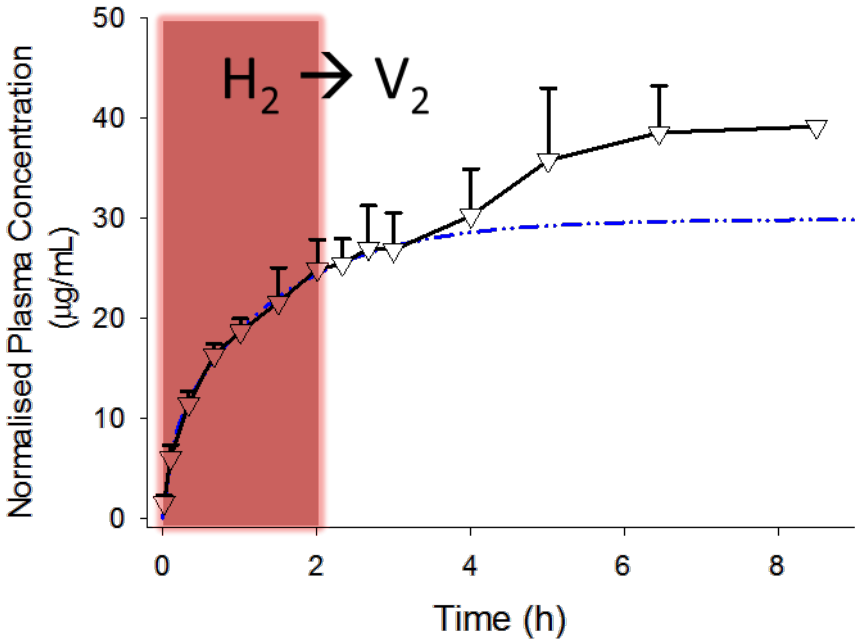

Figure 5.7 – Mean normalised plasma concentration profiles of ^{14}C glucose in rats subcutaneously administered the PHYTGNR matrix compared to a profile fitted to data from t = 0 – 3. The fitted blue line is intended to be guide to the eye and is the release profile that is expected to occur if the matrix did not switch to a faster releasing phase. Data are mean ± SEM, n = 4 except at t = 8.5 h, where data is n=1. The red shading indicates the duration of NIR laser irradiation (572 mW, 2 h). The expected nanostructures formed upon NIR irradiation as determined by SAXS are annotated on the graph.

Table 5.3 – A comparison of the apparent absorption rate constants ($k_{app\ 3\text{-}5}$) of the four formulations investigated (all formulations in comparison to each other were statistically signification $p < 0.05$).

Formulation	**$k_{app\ 3\text{-}5}$**
Glucose Solution	-2.72 ± 0.16
$PVEH_2$	-0.68 ± 0.33
$PHYTV_2$	2.67 ± 0.90
PHYTGNR	4.45 ± 0.93

5.5. Discussion

The defined nanostructures of liquid crystalline matrices provide a unique method of controlling the *in situ* rate of drug release. This proof of concept *in vivo* study demonstrated the ability of the nanostructure of these systems to be manipulated through the application of NIR laser light, as the release of drug from the liquid crystalline phase was in good correlation with the expected phase identified using SAXS. However, there are many issues to be considered with regards to the *in vivo* on-demand manipulation of these systems.

The optical properties of the target tissue will affect the amount of light penetration through the tissue and consequently, to the dose form. The skin thickness and location from which the skin was sourced was the main determinant of matrix response. Laser beam attenuation by the skin tissue could be attributed to non-specific scattering or absorption of the NIR light by components in the skin. In living, non-pigmented tissue, the major NIR absorbers are water, lipids, oxyhemoglobin and deoxyhemoglobin, where the amount of radiation absorbed depends on the molar concentration of each component in the tissue[26]. Thus, although NIR light is able to penetrate relatively deeply into biological tissue[27], its usefulness *in vivo* is limited by the high scattering of living tissue[28]. In order to improve the optical properties of skin, light penetration can be altered through the application of hyperosmotic 'clearing' agents such as glycerol[29]. Additionally, as well as providing triggerable release, light activation may enhance cellular penetration of drugs into cells[30]. Both are methods which may be considered in future experimental procedures.

The use of bulk liquid crystalline materials as drug delivery systems has been hindered by the question of how to dose such viscous materials. As the diffusion of drug from the matrix is dependent on surface area, initial studies employing the subcutaneous injection of low viscosity liquid precursors were unsuccessful as the surface area was hard to define in subcutaneous formulations which likely led to poor alignment of the dose form and the externally applied laser[31].

Thus, to overcome this shortfall, custom-made plastic implants were made to firstly, define the matrix surface area and secondly, contain the matrix within a suitable area which could be irradiated completely and evenly. The use of the implants ensured reproducibility of the plasma profiles which could not be obtained when dosing the formulations as low viscosity matrices through a needle. In this sense this proof of concept study is deficient in that it arguably does not address the practical application of the materials in the strictest sense, nevertheless it has allowed the direct and statistically comparable testing of Hypothesis 2. Further work is required to translate such a system into a viable and robust dose form.

During the period of irradiation, where the PHYTGNR matrix was expected to have the H_2 phase structure, the release rate from the PHYTGNR phase was expected to match that of the $PVEH_2$ formulation. Although the profiles did not match, the release rate of the PHYTGNR upon NIR irradiation was still significantly slower than the $PHYTV_2$ formulation and significantly faster when irradiation was ceased. The initial fast release of glucose from the PHYTGNR matrix is attributed to the system actually starting with the $V_{2\,D}$ nanostructure of the matrix before switching to H_2 upon NIR irradiation; a finite period of time was required after implantation for commencement of NIR irradiation. Through the SAXS experiments, it is known that it takes 140 s for the PHYTGNR phase to switch completely from $V_{2\,D}$ to H_2, which was sufficient time for a detectable amount of glucose to be released from the matrix at the faster rate; however, such subtle differences could not be discerned without further integration of the data. Further modelling of the pharmacokinetic plasma profiles is anticipated to allow the differentiation between the rates of glucose release and elimination in order to gather a clearer picture of subtle differences between the release rates from the V_2 and H_2 nanostructures.

This study highlights the potential utility of these systems as light activated drug delivery systems where the manipulation of non-lamellar liquid crystalline nanostructures controls the rate

of drug release, however further investigation into *in situ* optical and pharmacokinetic interactions are required.

5.6. Conclusions

The liquid crystalline nanostructure of the PHYT-GNR matrix was able to be manipulated via laser activation through biological tissue, where the matrix response depended on skin thickness and location from where the skin was taken. Light-activated manipulation of nanostructure of the PHYT-GNR matrix was shown to determine the rate of drug release from the matrix, whereby the appearance of drug in plasma was dependent on the liquid crystalline phase formed.

References

1. Lee S-M, Park H, Yoo K-H. Synergistic Cancer Therapeutic Effects of Locally Delivered Drug and Heat Using Multifunctional Nanoparticles. Advanced Materials. 2010;22(36):4049-53.

2. Shiotani A, Mori T, Niidome T, Niidome Y, Katayama Y. Stable Incorporation of Gold Nanorods into N-Isopropylacrylamide Hydrogels and Their Rapid Shrinkage Induced by Near-Infrared Laser Irradiation. Langmuir. 2007;23(7):4012-8.

3. Paasonen L, Laaksonen T, Johans C, Yliperttula M, Kontturi K, Urtti A. Gold nanoparticles enable selective light-induced contents release from liposomes. J Contr Release. 2007;122(1):86-93.

4. Park J-H, von Maltzahn G, Ong LL, Centrone A, Hatton TA, Ruoslahti E, et al. Cooperative Nanoparticles for Tumor Detection and Photothermally Triggered Drug Delivery. Advanced Materials. 2010;22(8):880-5.

5. Paasonen L, Sipilä T, Subrizi A, Laurinmäki P, Butcher SJ, Rappolt M, et al. Gold-embedded photosensitive liposomes for drug delivery: Triggering mechanism and intracellular release. J Contr Release. 2010;147(1):136-43.

6. Wu G, Mikhailovsky A, Khant HA, Fu C, Chiu W, Zasadzinski JA. Remotely Triggered Liposome Release by Near-Infrared Light Absorption via Hollow Gold Nanoshells. J Am Chem Soc. 2008;130(26):8175-7.

7. An X, Zhan F, Zhu Y. Smart Photothermal-Triggered Bilayer Phase Transition in AuNPs–Liposomes to Release Drug. Langmuir. 2013 2013/01/29;29(4):1061-8.

8. Lee KWY, Nguyen T-H, Hanley T, Boyd BJ. Nanostructure of liquid crystalline matrix determines in vitro sustained release and in vivo oral absorption kinetics for hydrophilic model drugs. Int J Pharm. 2009;365(1-2):190-9.

9. Costa-Balogh FO, Sparr E, Sousa JJS, Pais AC. Drug release from lipid liquid crystalline phases: relation with phase behavior. Drug Development and Industrial Pharmacy. 2009;0(0):1-12. PubMed PMID: 19848561.

10. Nguyen TH, Hanley T, Porter CJH, Larson I, Boyd BJ. Phytantriol and glyceryl monooleate cubic liquid crystalline phases as sustained-release oral drug delivery systems for poorly water-soluble drugs II. In-vivo evaluation. Journal of Pharmacy and Pharmacology. 2010;62(7):856-65.

11. Clogston J, Caffrey M. Controlling release from the lipidic cubic phase. Amino acids, peptides, proteins and nucleic acids. J Contr Release. 2005;107(1):97-111.

12. Rizwan SB, Boyd BJ, Rades T, Hook S. Bicontinuous cubic liquid crystals as sustained delivery systems for peptides and proteins. Expert Opinion on Drug Delivery. 2010;7(10):1133-44. PubMed PMID: 20858165.

13. Nguyen T-H, Hanley T, Porter CJH, Boyd BJ. Nanostructured liquid crystalline particles provide long duration sustained-release effect for a poorly water soluble drug after oral administration. J Contr Release. 2011;153(2):180-6.

14. Boyd BJ, Whittaker DV, Khoo S-M, Davey G. Hexosomes formed from glycerate surfactants - formulation as a colloidal carrier for irinotecan. Int J Pharm 2006;318(1-2):154-62.

15. Bender J, Ericson MB, Merclin N, Iani V, Rosen A, Engstrom S, et al. Lipid cubic phases for improved topical drug delivery in photodynamic therapy. J Contr Release. 2005;106(3):350-60. PubMed PMID: WOS:000232263200011.

16. Lopes LB, Ferreira DA, de Paula D, Garcia MTJ, Thomazini JA, Fantini MCA, et al. Reverse hexagonal phase nanodispersion of monoolein and oleic acid for topical delivery of peptides: in vitro and in vivo skin penetration of cyclosporin A. Pharmaceutical Research. 2006 Jun;23(6):1332-42. PubMed PMID: 16715364.

17. Esposito E, Cortesi R, Drechsler M, Paccamiccio L, Mariani P, Contado C, et al. Cubosome Dispersions as Delivery Systems for Percutaneous Administration of Indomethacin. Pharmaceutical Research 2005; 22(12):2163-73.

18. Gan L, Han S, Shen J, Zhu J, Zhu C, Zhang X, et al. Self-assembled liquid crystalline nanoparticles as a novel ophthalmic delivery system for dexamethasone: Improving preocular retention and ocular bioavailability. Int J Pharm. 2010;396(1-2):179-87.

19. Swarnakar NK, Jain V, Dubey V, Mishra D, Jain NK. Enhanced Oromucosal Delivery of Progesterone Via Hexosomes. Pharm Res. 2007 2007/12/01;24(12):2223-30. English.

20. Fong W-K, Hanley T, Boyd BJ. Stimuli responsive liquid crystals provide 'on-demand' drug delivery *in vitro* and *in vivo*. J Contr Release. 2009;135(3):218-26.

21. Negrini R, Mezzenga R. pH-Responsive Lyotropic Liquid Crystals for Controlled Drug Delivery. Langmuir. 2011:null-null.

22. Engström S. Cubic phases as drug delivery systems. Polym Preprint. 1990;31:2.

23. Sadhale Y, Shah JC. Biological activity of insulin in GMO gels and the effect of agitation. International Journal of Pharmaceutics. 1999 10 August 1999;191(1):65-74.

24. Shargel L, Yu ABC, Wu-Pong S. Applied biopharmaceutics & pharmacokinetics. 5 ed. New York: McGraw-Hill; 2005.

25. Bronaugh RL, Stewart RF, Congdon ER. Differences in Permeability of Rat Skin Related To Sex and Body Site. J Soc Cosmet Chem. 1983;34(3):127-35. PubMed PMID: WOS:A1983QU52500001. English.

26. Lim YT, Kim S, Nakayama A, Stott NE, Bawendi MG, Frangioni JV. Selection of quantum dot wavelengths for biomedical assays and imaging. Molecular Imaging. 2003 2003;2(1):50-64. PubMed PMID: MEDLINE:12926237. English.

27. Weissleder R. A clearer vision for in vivo imaging. Nat Biotech. 2001;19(4):316-7.

28. Frangioni JV. In vivo near-infrared fluorescence imaging. Current Opinion in Chemical Biology. 2003;7(5):626-34.

29. Matsui A, Lomnes SJ, Frangioni JV. Optical clearing of the skin for near-infrared fluorescence image-guided surgery. Journal of Biomedical Optics. 2009;14(2):024019-.

30. Hansen MB, van Gaal E, Minten I, Storm G, van Hest JCM, Löwik DWPM. Constrained and UV-activatable cell-penetrating peptides for intracellular delivery of liposomes. Journal of Controlled Release. 2012 11/28/;164(1):87-94.

31. Yaghmur A, Rappolt M, Østergaard J, Larsen C, Larsen SW. Characterization of Bupivacaine-Loaded Formulations Based on Liquid Crystalline phases and Microemulsions: The Effect of Lipid Composition. Langmuir. 2012 2012/10/28;28(5):2881-9.

Appendix

Table A1 – *In vivo* ^{14}C-Glucose Validation data

Theoretical nCi	DPM	Average	Precision	Calculated nCi	Average	% Accuracy	Mean % Accuracy
	364816			164.332		109.5544	
150	365306	364240	0.4	164.552	164.07	109.7015	109.4
	362598			163.332		108.8883	
	34334			15.466		103.1051	
15	34699	34364	0.9	15.630	15.48	104.2012	103.2
	34059			15.342		102.2793	
	3216.7			1.449		96.5970	
1.5	3235.3	3226.9	0.3	1.457	1.45	97.1565	96.9
	3228.6			1.454		96.9556	
	304.43			0.137		91.4204	
0.15	327.59	312.63	4.1	0.148	0.14	98.3756	93.9
	305.88			0.138		91.8559	
	134.99			0.061		101.3438	
0.06	139.20	132.97	5.6	0.063	0.06	104.5045	99.8
	124.72			0.056		93.6336	
	116.20			0.052		104.6847	
0.05	95.80	106.32	9.6	0.043	0.05	86.3063	95.8
	106.96			0.048		96.3604	
	75.65			0.034		85.1914	
0.04	77.04	79.53	7.0	0.035	0.04	86.7568	89.6
	85.90			0.039		96.7342	
	43.82			0.020		98.6937	
0.02	41.67	43.84	5.0	0.019	0.02	93.8514	98.7
	46.03			0.021		103.6712	

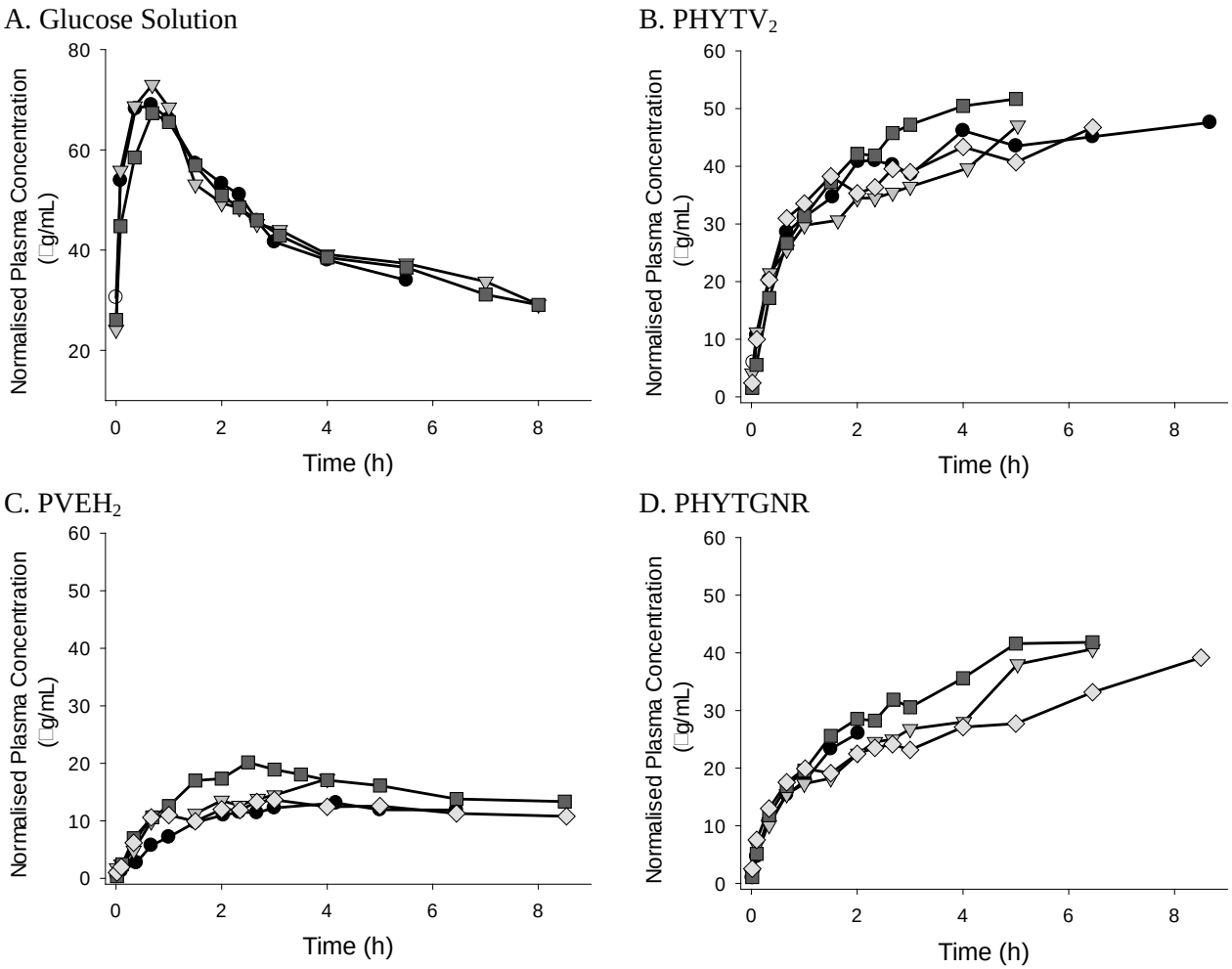

Figure A.1 – Individual plasma profiles of A. subcutaneous injection of glucose solution, B. $PHYTV_2$ implant, C. $PVEH_2$ implant and D. PHYTGNR implant.

Chapter 6 – “Fit-for-Function” Design of Lyotropic Liquid Crystalline Matrices for On-Demand Drug Delivery

6. “Fit-for-Function” Design of Lyotropic Liquid Crystalline Matrices for On-Demand Drug Delivery

6.1. Introduction

In order to create matrices appropriate for its intended function, a resolution of the relationship between structure, composition and function must be achieved. Many amphiphilic lipids and combinations of these self-assemble into liquid crystalline mesophases, most of which were catalogued a decade ago[1], however this list has since been outdated by the discovery and/or synthesis of many novel amphiphiles. This widespread knowledge has been built from the study of lipidomics – the push to understand lipid networks and interactions in biological settings[2] – and their exploitation in applications such as drug delivery[3, 4], food science[5, 6], biosensing[7] and protein crystallisation[8-10].

Lyotropic liquid crystals describe the diverse nanostructures of self-assembling amphiphiles in aqueous environments. However, few amphiphiles form the complex inverse phases: the bicontinuous cubic (V_2) and inverse hexagonal phases (H_2) which have been extensively studied since their designation by Luzzati and colleagues[11, 12]. These mesophases are of interest to drug delivery due to their defined controlled and sustained release capabilities[13, 14], where V_2 phase releases drug at a significantly faster rate than H_2 phase.

Bulk liquid crystal phases can be manipulated through a change in temperature in order to control release[15], and in previous Chapters, the ability to manipulate phase transitions via light activation has been shown. The reversible phase transitions were in the direction from the fast releasing $V_{2\,D}$ phase to the slower releasing H_2 structure in the PHYT and GMO matrices, which is the opposite of that which would be ideal for pulsatile release matrices. However, no lipids are known which follow this transition with an increase in temperature.

Further, it is desirable to control release from a dispersed form of the lipid matrix, as it provides additional versatility in administration compared to a bulk lipid matrix. However, cubosomes and hexosomes, created on dispersion of V_2 and H_2 respectively, are known to exhibit uncontrolled 'burst release' upon administration[3, 16, 17]. In contrast, for hydrophilic drugs as least, liposomes, dispersed lamellar phase (L_α), are known to retain drug in the inner aqueous core due to the lipid membrane providing a poorly permeable barrier not evident in cubosomes and hexosomes. Thus, a potentially useful matrix for on-demand drug delivery is one that provides a slow to fast release transition, such as a L_α to V_2 phase transition upon stimulation, but also has the option of being administered as a dispersible matrix. This would allow for the entrapment of drug within the lamellar phase and then the controlled release of drug from the V_2 phase upon activation.

The driving force for the aggregation of amphiphiles into more energetically favourable liquid crystalline structures is dependent on both the hydrophobicity of its hydrocarbon chain and the level of headgroup hydration as the lipid-water system seeks to minimise chain interaction with the aqueous phase. The aggregates formed are dependent upon the competition between the global packing conditions within the lipid-water systems which is determined by the intrinsic shape of the molecules[18] and the ability of the lipid monolayer to assume a spontaneous radius of curvature[19]. Headgroup hydration determines the amount of hydrogen bonding that occurs between amphiphiles which can determine headgroup-water hydrogen bond networks[20]. The hydrocarbon chain length, alkyl substituents and consequent chain splay are the molecular structure properties which are the hydrophobic variables in the determination of phase behaviour[20-23]. The properties of both the hydrophilic head and the hydrophobic tail groups have been thoroughly investigated with a view to understanding and consequently controlling phase behaviour. A recent review by Fong et al. thoroughly examined amphiphiles which form inverse V_2 and H_2 phases and so have created a

list of rules that summarise the features of amphiphilic moieties which result in the formation of reversed phases upon hydration; these rules are reproduced below in italics[24]:

Hydrophobic portion:

- *The temperature should be above the chain melting temperature such that molten chains are present; and*
- *There should be at least one cis unsaturated bond in a carbon chain of at least 14 carbons at a position at least mid-way along the backbone; or*
- *The carbon backbone should contain at least 12 carbons of which 3 are secondary carbons with methyl branches; and*
- *The molecular weight of the hydrophobe should be at least >200 Daltons.*

Hydrophillic headgroup

- *The headgroup should contain at least three functional groups with minimum hydrophilicity (e.g. hydroxyl);*
- *The headgroup should be able to form headgroup–water hydrogen bond networks; and*
- *The headgroup area should be small relative to the hydrophobe footprint.*

The family of monoacylglycerols are a good demonstration of how slight differences in molecular structure can affect packing of lipid molecules[22]. A comparison between monomyristolein (C14:1c9) and GMO (C18:1c9), where the difference between the two lipids are four methylene groups, resulted in the exclusion of H_2 phase and the stabilisation of L_α phase as the shortened hydrocarbon chain results in a more cylindrical shaped moiety[25]. Additionally, amphiphiles with the highest amount of chain splay are most likely to form inverse phases. Chain splay is influenced by the number and location of double bonds as shown in Figure 6.1, the *trans*

conformation of the double bond in monoelaidin reduces chain splay, whereas the location and number of the *cis* double bond/s determines the chain splay of monovaccenin, GMO and monolinolein respectively. The *cis* double bond nearer to the headgroup makes the GMO molecule more wedge shaped than monovaccenin and the two *cis* double bonds in monolinolein results in the most chain splay and thus the most extreme wedge shape[22].

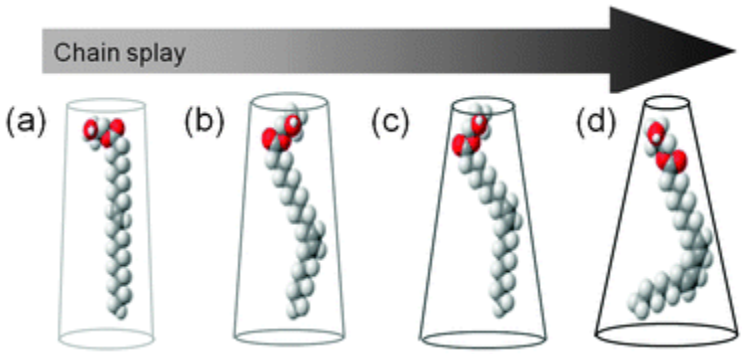

Figure 6.1 – The effect of the location and number of double bonds on chain splay. Chain splay increases from left to right, as indicated by the modification of the wedge shape drawn around the ball and stick models of (a) monoelaidin, (b) monovaccenin, (c) GMO and (d) monolinolein. Figure modified from [22].

Much research has focused on synthesising appropriate amphiphiles that meet the focused needs of the desired application. However, because the global packing constraints required for reverse phase formation can also be achieved using lipid mixtures, this Chapter describes investigation of combinations of readily available lipids which have the potential to display a lamellar to non-lamellar liquid crystalline nanostructure transition in response to moderate temperature changes.

In order to design liquid crystalline matrices which form non-lamellar phases, the interaction of additives with lipid bilayers must be understood as the packing of the complementary shapes of the different components determines the nanostructure formed[26] as well as the spontaneous radius

of curvature[27]. The miscibility of the alkyl chains of the lipids can result in mismatch within the bilayer thickness, thus affecting domain size[28]. The manipulation of liquid crystalline phases through the addition of moieties which affect lipid packing is summarised in Table 6.1 where the shape and charge of the additive determines its ability to modify the membrane curvature.

Table 6.1 – The effect of additives which effect lipid packing on an intermolecular scale, which in turn determines the liquid crystalline phases formed.

Main Lipid	Additive	Effect on phase structure	Justification
GMO	Phospholipids and anionic detergents	$V_{2D} \rightarrow L_{\alpha}$ [8, 29, 30]	Wedge shaped moieties promote a more positive membrane curvature.
	Octyl glucoside	$V_{2D} \rightarrow L_{\alpha \& 1}$ [31]	
GMO	Small hydrophilic protein, cytochrome c	$V_{2D} \rightarrow$ micellar cubic[32]	Increase in interfacial curvature due to interaction of protein with headgroup.
PHYT	Vitamin E acetate	$V_{2D} \rightarrow H_2, L_2$ [33]	The hydrophobic additives promote negative curvature in the lipid packing, inducing the formation of more frustrated phases.
GMO	Fatty acids	$V_{2D} \rightarrow H_2, L_2$ [34, 35]	
	Limonene, Hexadecane & Diacylglycerol	$V_{2D} \rightarrow$ Fd3m, H_2 [14, 36-38]	
Phosphatidylcholine	Cholesterol	$L_{\alpha} \rightarrow$ Fd3m[38]	The hydrophobic additive reduces chain stress in lamellar phases, resulting in the formation of inverse phases.
POPE	Cholesterol	$L_{\alpha} \rightarrow V_{2D}$ [39]	
DOPE/tetradecane	Cholesterol	$L_{\alpha} \rightarrow H_2$ [40]	
DOPC	Phosphatidylinositol	$L_{\alpha} \rightarrow$ Fd3m & H_2 [41]	
DEPE	DMPE(PEG550)	$L_{\alpha} \rightarrow V_{2P}$ & H_2 [42]	
DOPC/DOPE	α-tocopherol	$L_{\alpha} \rightarrow H_2$ [43]	
DOPS/GMO	Decrease in pH	$L_{\alpha} \rightarrow V_{2D}$ [44]	Enhancement of the negative spontaneous curvature of the monolayers with increasing electrostatic interactions.
DOPG/GMO	Ca^{2+}	$L_{\alpha} \rightarrow V_{2D \& P}$ [29, 45, 46]	
GMO/OA	NaCl & decrease in pH	$V_{2D} \rightarrow V_{2P}$ [47]	

The first alternate lipid system studied in this thesis was monoelaidin (ME), introduced in Chapter 3. Following on from that initial study, different lipid formulations were investigated for their ability to exhibit a L_α to V_2 phase transition at a biologically accessible temperature. The molecular structures of the lipids used in this study are shown in Figure 6.2. Systems that exhibited desirable phase transitions i.e. L_α to V_2 were then further investigated for their utility as photothermal matrices via incorporation of GNR and NIR laser irradiation.

Phytantriol (PHYT)

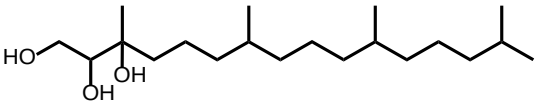

Glyceryl monooleate (GMO)

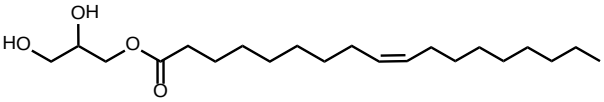

Monoelaidin (ME)

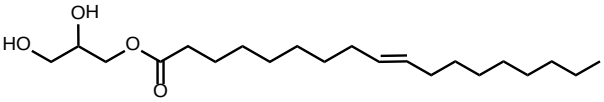

Oleic acid (OA)

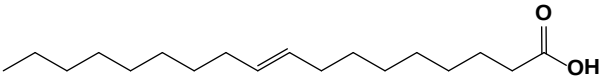

Cholesterol (Ch)

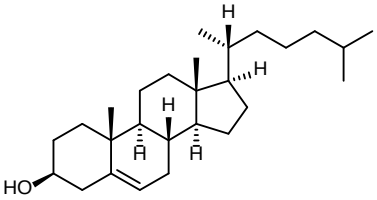

1,2-dioleoyl-sn-glycero-3-phosphocholine (DOPC)

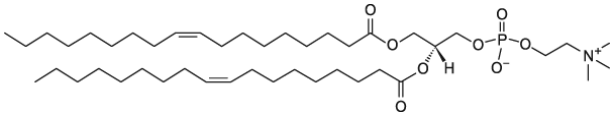

1-oleoyl-2-hydroxy-sn-glycero-3-phosphocholine (lysoPC)

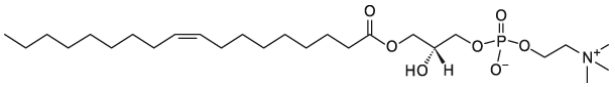

1,2-diphytanoyl-sn-glycero-3-phosphoethanolamine (DPhPE)

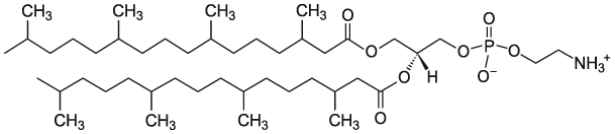

1-Palmitoyl-2-oleoyl-sn-glycero-3-phosphoethanolamine (POPE)

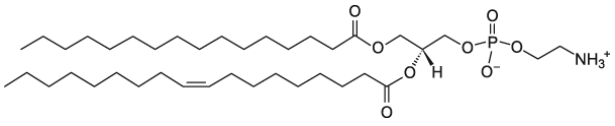

Figure 6.2 – Molecular structures of lipids employed in this study.

6.2. Hypotheses and Aims

Hypothesis 1

That the incorporation of lipids which can promote a more positive spontaneous curvature into PHYT and GMO liquid crystalline matrices will be able to produce a liquid crystalline matrices that demonstrate a lamellar to non-lamellar phase transition on heating.

Hypothesis 2

That these mixed lipid matrices will be able to maintain their nanostructures upon the incorporation of gold nanorods and laser activation of these photosensitised matrices will induce the lamellar to non-lamellar phase transitions observed in equilibrium temperature studies.

In order to address these hypotheses, the following aims will be achieved:

- To determine the effect of increasing concentrations of different amphiphilic additives on liquid crystalline matrices, specifically the effect of increasing concentrations of :
    - DOPC in PHYT and GMO
    - ME in GMO
    - OA in ME
    - lysoPC in PHYT and GMO
    - Cholesterol in POPE
- To investigate the miscibility of gold nanorods in matrices which exhibit a lamellar to non-lamellar phase transition.
- To photothermally activate phase transitions in these mixed lipid matrices using NIR laser irradiation.

6.3.Materials and Methods

General materials and methods can be found in Chapter 2.

6.3.1. Preparation of Lipid Formulations

Lipids were weighed in the appropriate ratios and dissolved in chloroform: methanol 2:1 (v/v). The mixture was then dried under vacuum overnight, then under a stream of nitrogen gas for 3 hr to ensure complete removal of solvent. The lipid mixture was then hydrated in a 1:1 ratio with MilliQ water and thoroughly mixed using gentle heating, vortexing and bath sonication, and allowed to equilibrate on rollers for >48 hr before investigation using SAXS at the Australian Nuclear Science and Technology Organisation (ANSTO) (equilibrium temperature studies) and the Australian Synchrotron (kinetic studies).

6.4.Results

6.4.1. Equilibrium Phase Behaviour

The molecular structures of the lipids investigated in this chapter are shown in Figure 6.2. Mixtures of these lipids were used to modify the thermal phase behaviour of the PHYT and GMO liquid crystalline matrices. The thermal phase behaviour of fully hydrated PHYT and GMO has been established to follow V_2 → H_2 → L_2 upon increase in temperature and ME follows L_α → V_2 → H_2, thus only deviations from this phase behaviour through the addition of other lipids will be elaborated upon.

6.4.1.1. DOPC Addition into PHYT & GMO Matrices

In order to promote a more positive curvature in the liquid crystalline matrix, the phospholipid, DOPC, was incorporated into the PHYT and GMO liquid crystalline matrix. The effect on the equilibrium phase behaviour of the mixtures in excess water was investigated using SAXS. The equilibrium scattering patterns from 25 – 85 ºC, with increasing amounts of DOPC are shown in the Appendix. The reduced phase behaviour data and lattice parameter vs. temperature for each system are collated in Figure 6.3.

The addition of small amounts (<10%) of DOPC into the PHYT and GMO matrices resulted in formation of H_2 phase at a lower temperature and the presence of the H_2 phase over a larger temperature range, as seen previously on incorporation of SPL into these core lipids (Figure 4.6). On addition of moderate amounts of DOPC (~20 – 40 mol%), V_2 was the predominant phase formed and the L_2 phase was no longer observed. An unresolved and unassignable peak appears adjacent to the first peak of the H_2 phase at high temperatures at 9.8 – 22.0 mol% DOPC in PHYT and at 5.4 & 11.0 mol% DOPC in GMO. This was attributed to the formation of long living intermediates which is common in mixed phase systems[48]. Additionally, the lattice parameters of the V_2 phases and to a lesser extent the H_2 phases were larger with increasing amounts of DOPC as

shown in Figure 6.3, which is an indication that the phospholipid increases the hydration, enlarging the interfacial area occupied by the GMO and PHYT headgroups and thus swelling of the water channels of the cubic phase[49, 50]. At ~40 mol% DOPC, both the PHYT and GMO matrices were lamellar phase/vesicles at 25 ºC rather than V_2 phase, a phenomenon which has been previously observed[51], and with increasing temperatures formed the $V_{2\,D}$ phase at 55 ºC and 85 ºC respectively.

The broad peak at q ~1.5 Å underlying the cubic reflections at the high DOPC content may denote an incomplete phase transition. At ~50 mol% the L_α to $V_{2\,D}$ transition was no longer observed for either matrix. Intriguingly, at 62.5 mol% DOPC in PHYT, a sharp peak is formed at ~0.05 Å, which could potentially represent L_α phase. This reflection disappears with an increase in temperature. However, as the second L_α reflection is hidden amongst the vesicle scattering, further integration of the data may be required for confirmation.

Of particular interest were the 43.3 mol% DOPC in PHYT and 45 mol% DOPC in GMO as with increasing temperatures, the matrix underwent a vesicle to $V_{2\,D}$ phase transition. As the PHYT matrix displayed the phase transition in a more accessible temperature, it was further pursued for photothermal investigations (Section 6.4.2.1). It is also acknowledged that this data is far from a complete phase diagram, however as a suitable system was found in this initial study, further ratios were not investigated.

A. PHYT + DOPC

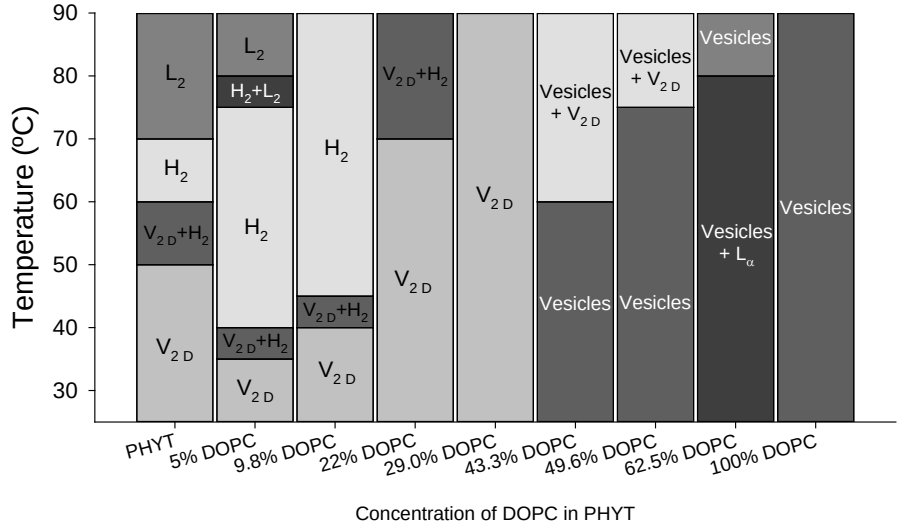

B. GMO + DOPC

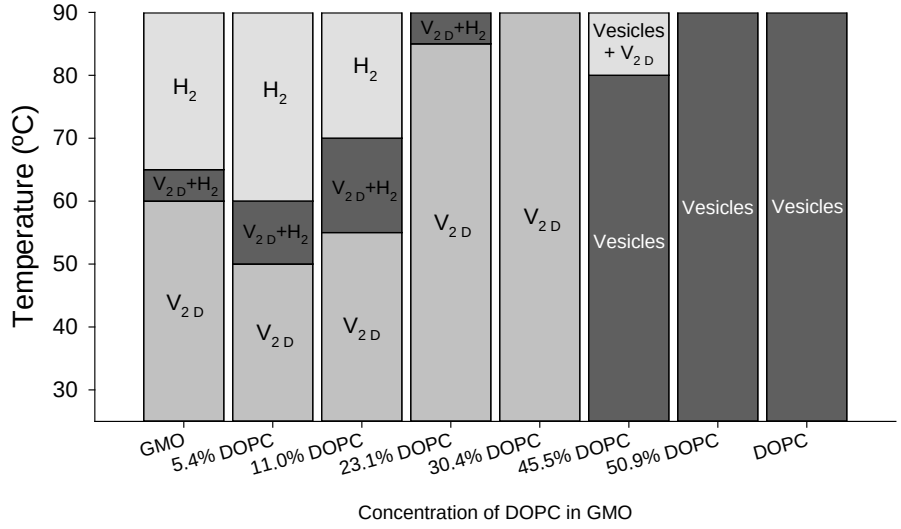

C.

D.

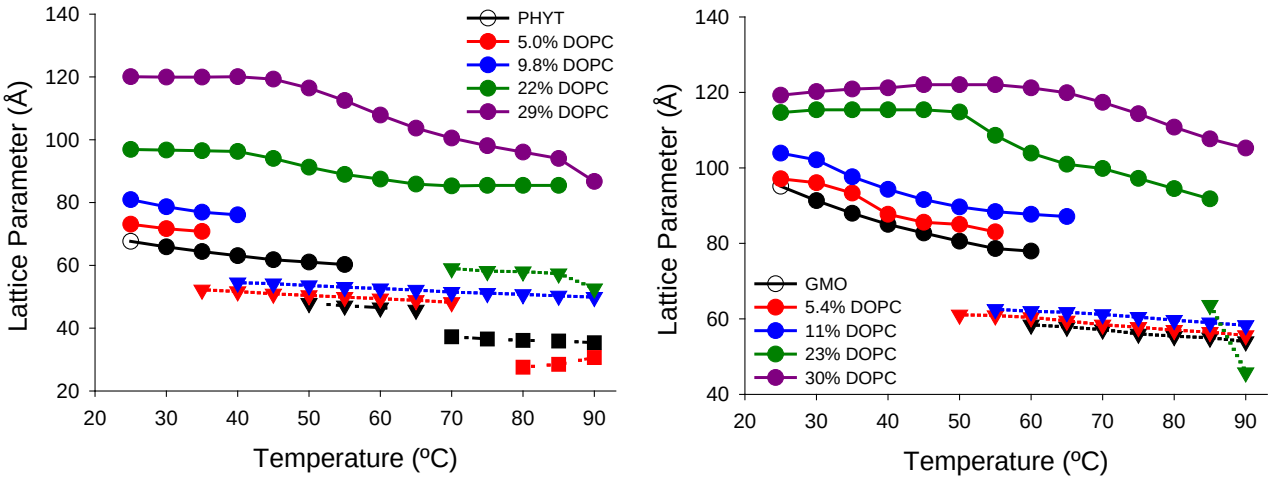

Figure 6.3 – The effect of the addition of DOPC on the equilibrium phase behaviour of A. PHYT and B. GMO. The effect of the addition of DOPC on lattice parameters of Panel C. PHYT + DOPC and Panel D. GMO +DOPC matrices. Circles represent $V_{2\ D}$, triangles represent H_2 and squares represent L_2. With increasing amounts of DOPC, there is an increase in the V_2 lattice parameters observed.

6.4.1.2. Addition of LysoPC into PHYT & GMO Matrices

1-oleoyl-2-hydroxy-sn-glycero-3-phosphocholine (lysoPC) is a zwitterionic single-tailed phospholipid that has been reported to form micellar structures at ambient temperatures[52] and has been shown to form lamellar structures via the addition of cholesterol[26]. The equilibrium temperature scan of hydrated lysoPC (Figure 6.4) indicates that the lipid forms vesicles until 62.5 ºC above which it forms a mixed vesicle + H_2 phase.

The temperature dependent equilibrium phase behaviour on increasing concentration of lysoPC in PHYT cubic phases are presented in Figure 6.4, Panel A. Incorporation of 10.8 mol% lysoPC into the PHYT matrix, caused a left shift in peak positions in q, indicative of an enlargement of lattice parameters in the $V_{2\,D}$ phase. Upon increasing temperature, a $V_{2\,G}$ phase was observed, then H_2 phase. As the infinite periodic minimal surfaces (IPMS) of the three cubic phases $V_{2\,D}$, $V_{2\,G}$ and V_2 are related to each other by the Bonnet transformation[53], the presence of $V_{2\,G}$ was confirmed as the lattice parameter ratio of $V_{2\,D}$:$V_{2\,G}$ was calculated to be 1.548, very close to the reported value of 1.576[53]. At 19.7 mol% lyso PC in PHYT the system was a mixed $V_{2\,G}$ + H_2 phase which, at least according to the scattering data, transitioned to $V_{2\,G}$ between 52.5 – 70 ºC and then returned to the mixed $V_{2\,G}$ and H_2 between 70 – 80 ºC. This anomalous behaviour may be attributed to the two different lipids exerting their influence at the different temperatures. Between 28.3 – 58.5 mol%, the lysoPC + PHYT formulations formed L_α phase throughout the temperature range investigated. At higher concentrations, there was an underlying broad peak which could represent the presence of vesicles.

The equilibrium SAXS scattering patterns for the GMO systems containing increasing concentrations of lysoPC are shown in the appendix, and summary data in Figure 6.4 Panel B. Similar to the PHYT systems, the addition of lysoPC to GMO at low concentrations (11.1 mol%) resulted in the formation of $V_{2\,D}$ with larger lattice parameters for an increased temperature range,

however the $V_{2\,G}$ phase was not observed in the GMO systems. At 19.7 mol% the system exhibited a mixed $V_{2\,D}$ + L_α structure and with an increase in temperature the system transitions to vesicles. As was the case with the PHYT matrices, between 30.0 – 67.5 mol% lysoPC, the lysoPC + GMO formulations formed L_α phase throughout the temperature range investigated, and at higher concentrations, there was an underlying broad peak which could represent the presence of vesicles.

Note that 39.1 – 58.5 mol% lysoPC in PHYT and 38.5 – 67.5 mol% lysoPC in GMO are not included in the summary of phase behaviour for clarity as the phase did not change from L_α for the duration of the temperature scan. As none of the lysoPC formulations investigated demonstrated the L_α to $V_{2\,D}$ phase transition, these formulations were not pursued for further photothermal investigation.

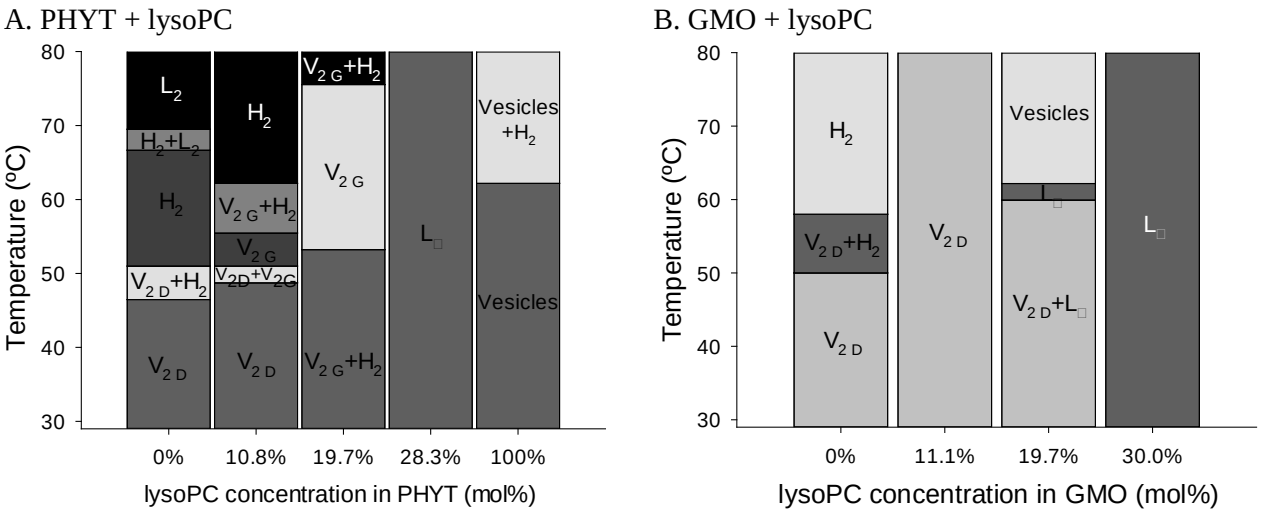

Figure 6.4 – The effect on equilibrium phase behaviour of lysoPC addition into A. PHYT and B. GMO matrices. The phases formed were determined from the integration of individual frames.

6.4.1.3. Mixtures of Structurally Related C18:1 Unsaturated Lipids

Mixtures of GMO and ME: To subtly modify the phase behaviour of GMO in excess water, ME was added and the phase behaviour characterised. Equilibrium SAXS patterns for increasing amounts of ME in GMO in excess water are shown in the Appendix and the phase behaviour is summarised in Figure 6.5. The addition of 5.9%, 10.9% and 26.3% ME into the hydrated GMO phase resulted in the elongation of the temperature range over which the $V_{2\ D}$ phase existed and thus the reduction of the range of existence of the H_2 phase. At 50.1% ME, there appears to be a balance of the phase behaviour of the two pure lipids with coexisting lamellar and cubic phases at ambient temperature.

With increasing amounts of ME above 50.1% the L_α phase appears at ambient temperatures and the phase behaviour was more similar to that of ME than GMO. These matrices transition from L_α+L_2 to $V_{2\ D}$ to L_2. The lipid comprising the major component dominated the phase behaviour of the matrix. This observation is also reflected the trend in lattice parameters for the $V_{2\ D}$ phase with increasing amounts of ME (Figure 6.5, Panel B.). The lattice parameters of the GMO $V_{2\ D}$ matrices (90 – 75 Å) are smaller than those of ME (95 – 85 Å) over the temperature range investigated. With increasing amounts of ME added into the GMO matrix, the lattice parameter increased. The 77.5% ME in GMO matrix would be the most appropriate matrix to further study as it is L_α at ambient temperatures and has a defined $V_{2\ D}$ region at accessible temperatures. Thus, the aim of this study in determining a system exhibiting a L_α to $V_{2\ D}$ transition was achieved, however, as the DOPC + Phyt system provided cleaner transitions it was progressed to photoactivation studies ahead of this system. Given further time, this system would be an interesting one to revisit.

A.

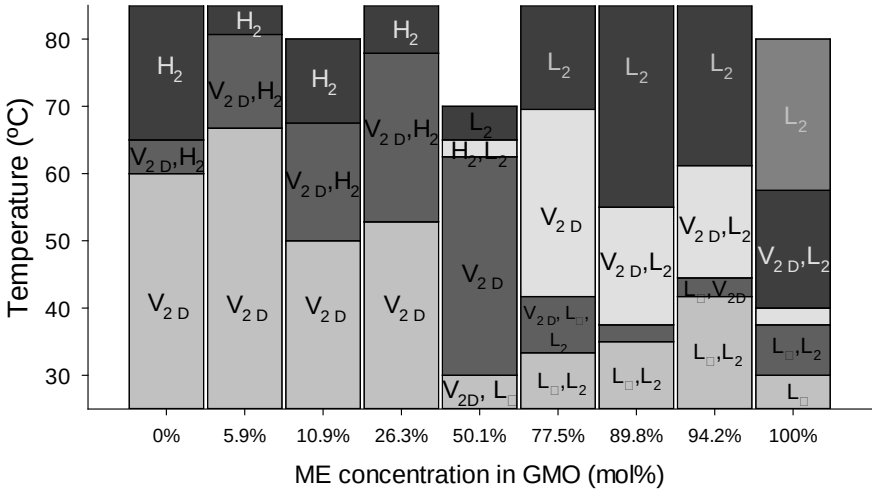

B.

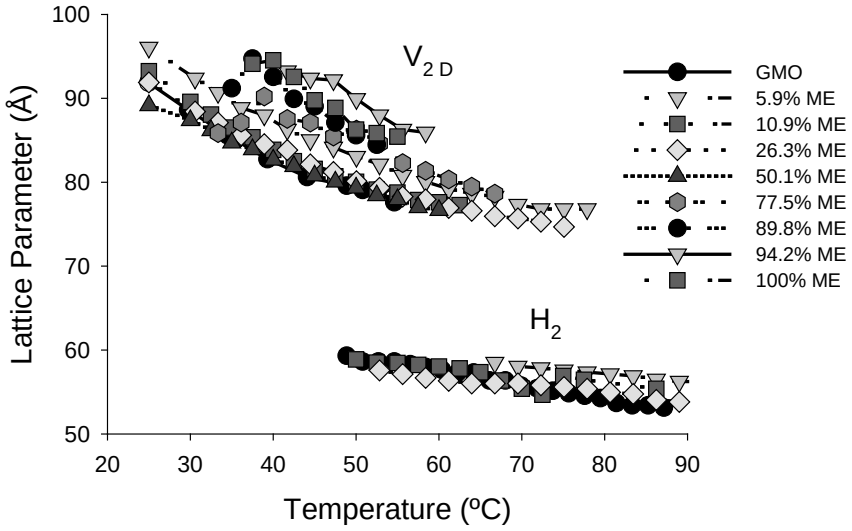

Figure 6.5 – Equilibrium phase behaviour of GMO matrices containing increasing amounts of ME. All matrices are in 50% water. Panel A. details the phase transitions of the matrices between 25 – 85 ºC. Data for the full temperature range was not available for 10.9, 50.1 and 100%. Panel B. displays the lattice parameters of the formulations that displayed $V_{2\,D}$ or H_2 at different concentrations of ME (mol%) in GMO.

Mixtures of oleic acid (OA) and ME: As the effect of addition of OA into the hydrated ME matrix was unknown, OA + ME mixtures were also studied. In contrast to GMO, the addition of OA had a destructive effect on the rich phase behaviour of the ME matrix. Figure 6.6 shows the equilibrium SAXS scattering patterns of the ME matrix containing increasing amounts of OA. The addition of OA resulted in the reduction of the amount of phases that the ME matrix formed, from

four to two namely, L_α and L_2. Increasing amounts of OA also reduced the temperature range at which L_α was observed and at higher temperatures, the system lost structure completely.

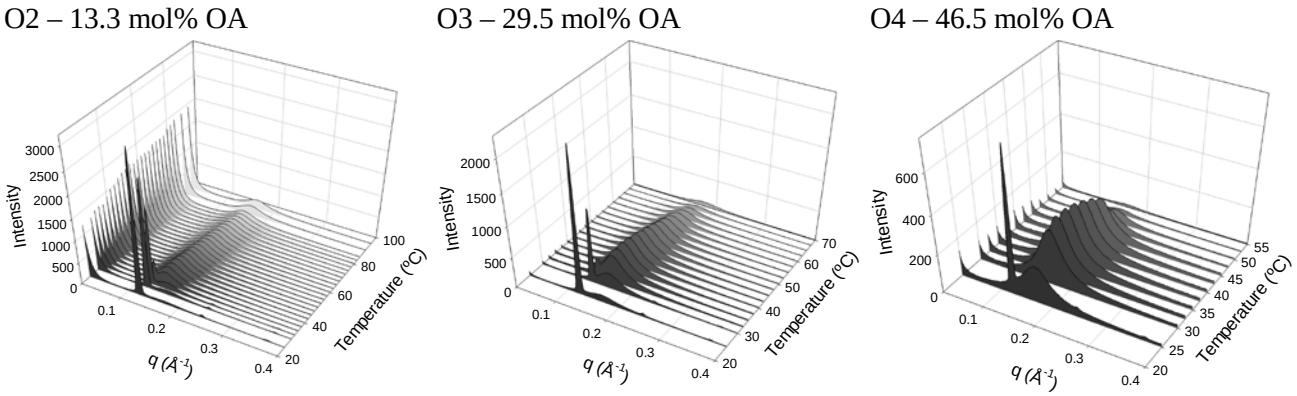

Figure 6.6 – SAXS scattering patterns showing the equilibrium phase behaviour of ME matrices containing increasing amounts of oleic acid.

6.4.1.4. Other Lipids – DPhPE

It was proposed that phytanyl-tailed phospholipids could be used to modify the phase transitions of PHYT in a favourable manner due to the compatibility of the phytanyl chains. Phytanyl-tailed phospholipids are not commonly observed in biological systems and have been synthesised in recent times as novel molecules for the modification of membrane lipids for gene transfection applications[54, 55]. The phase behaviour of hydrated diphytanyl phosphatidyl ethanolamine (DPhPE) has not been previously reported in detail in literature. Anderssen *et al.* investigated phytanyl-tailed phospholipid mixtures; the structurally-related 1,2-diphytanoyl-sn-glycero-3-phosphocholine (DPhPC) was found to form vesicles in aqueous suspension[55, 56], however hydrated DPhPE alone was not studied. Additionally, another structurally-related molecule POPE forms L_α phase, then H_2 phase with increasing temperature[39]. Thus, in this initial study, the phase behaviour of DPhPE was determined.

The equilibrium SAXS scattering patterns of DPhPE are shown in Figure 6.7. Over the temperature range investigated, DPhPE formed H_2 phase. The fluctuation in intensity is attributed to the formulation moving within the sealed capillary in vacuum with the increase in temperature. As the capillary was sealed, a change in hydration of the lipid is not anticipated. The smaller head group of the DPhPE than DPhPC and the increased hydrophobic chain volume compared to POPE resulted in a more wedged shaped molecule, thus encouraging the formation of the inverse H_2 phase instead of lamellar phase.

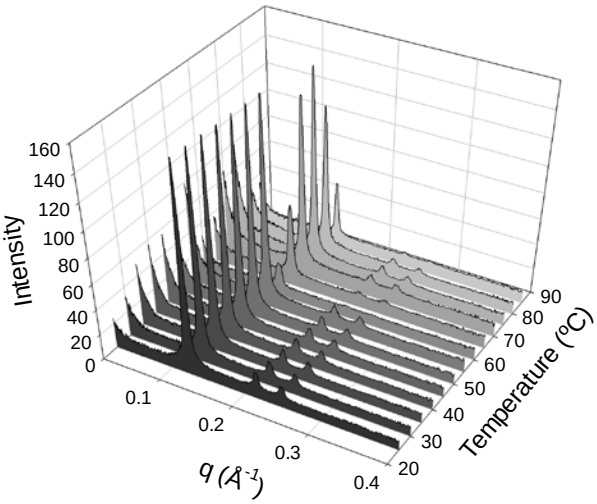

Figure 6.7 – Equilibrium SAXS profiles displaying the thermal phase behaviour of diphytanoylglycerophosphoethanolamine (DPhPE).

6.4.1.5. Other Lipids – POPE + Cholesterol

The L_α to $V_{2\ D}$ phase transition has already been reported in literature in dispersed 1-Palmitoyl-2-oleoyl-sn-glycero-3-phosphoethanolamine (POPE) + cholesterol matrices[39]. The presence of cholesterol in the POPE bilayer induces the formation of a L_α phase which transitions to a cubic phase with an increase in temperature. The published partial phase diagram is reproduced in Figure 6.8, where the blue arrow indicates the molar concentration of cholesterol in POPE chosen for further study in this Chapter.

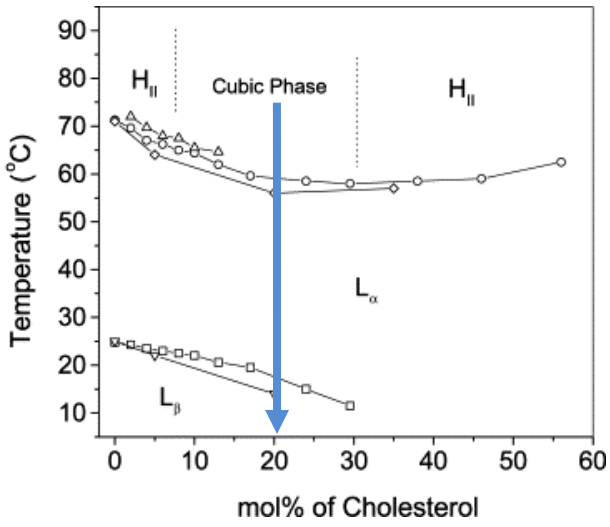

Figure 6.8 – Partial phase diagram of aqueous dispersions of POPE and cholesterol. Symbols ▽ and □ indicate L_β to L_α phase transitions; ◇, ○ and △ indicate lamellar to non-lamellar phase transition. The blue arrow indicates the POPE/cholesterol formulation (20.1 mol% cholesterol) chosen for the photothermal SAXS study. Adapted from [39].

6.4.2. NIR-Triggered Photothermal L_α to $V_{2\ D}$ Phase Transitions

A few select systems that displayed a L_α or vesicle to $V_{2\ D}$ phase transition were available for photothermal investigation, namely, 44.4 mol% DOPC in PHYT (PHYT44DOPC), 20.1 mol% cholesterol in POPE (POPE20Ch) and 77.5% ME in GMO (GMO77ME). However, only

PHYT44DOPC and POPE20Ch were studied with the intention of future study of the GMO77ME system. Gold nanorods (GNR) responsive to NIR irradiation at 810 nm were incorporated into the chosen systems and were then irradiated with a continuous wave NIR laser and changes in their phase behaviour were followed using time-resolved synchrotron SAXS, as performed for the ‘pure’ systems in Chapter 3.

6.4.2.1. 44.4 mol% DOPC in PHYT (PHYT44DOPC)

The equilibrium phase behaviour of the PHYT44DOPC system (Figure 6.9, Panels A. and B.) was in good agreement with the initial study in Section 6.4.1.1 where the matrix transitioned from vesicles to $V_{2\,D}$. However, on addition of GNR, the starting phase changed to $V_{2\,D}$ as the hydrophobic additives may have induced a more negative curvature. Nevertheless the system was still investigated for its ability to respond to photothermal activation as subsequent optimisation studies could potentially reverse the effect of GNR addition by increasing the DOPC content further.

The phase behaviour kinetics upon NIR laser activation (810 nm, 586 mW) of the systems are shown in Figure 6.9, Panels C. and D. In the absence of GNR, as expected, PHYT44DOPC did not transition from the initial $V_{2\,D}$ + vesicles upon laser activation, nor did the lattice change over the duration of NIR irradiation. The photosensitised PHYT44DOPC-GNR matrix, on the other hand, transitioned from $V_{2\,D}$ to $V_{2\,D}$ + H_2 after 7 s of laser irradiation.

Equilibrium phase behaviour on heating

A. PHYT44DOPC, no GNR added

B. PHYT44DOPC + 3 nM GNR

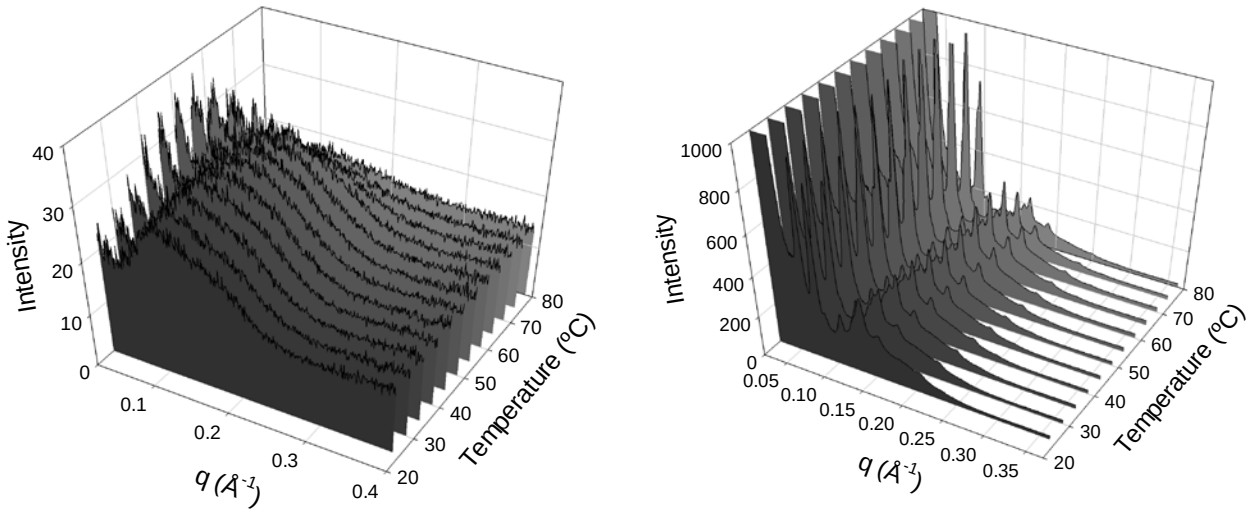

Kinetic phase behaviour on irradiation

C. PHYT44DOPC

D. PHYT44DOPC-GNR

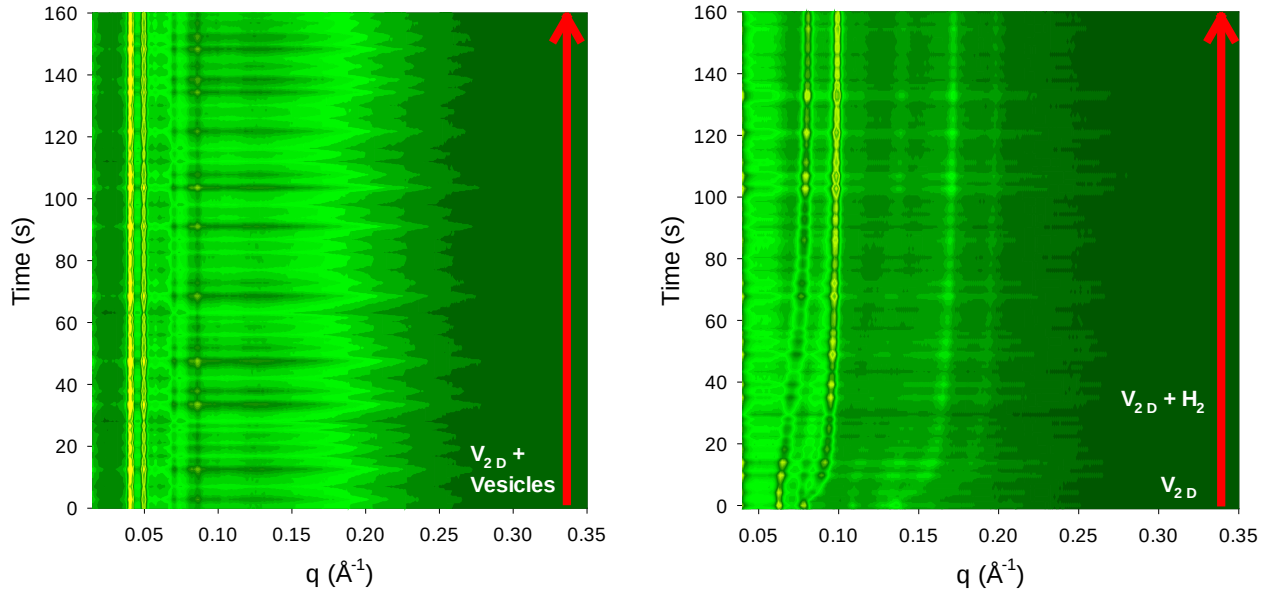

Figure 6.9 – Panels A. and B.: The effect of GNR addition into the PHYT44DOPC matrix. SAXS profiles showing the equilibrium phase behaviour of Panel A. 44.4 mol% DOPC in PHYT (PHYT44DOPC) and Panel B. PHYT44DOPC + 3 nM GNR (PHYT44DOPC-GNR). Panels C. and D: Time resolved SAXS profiles showing the effect of laser irradiation (810 nm, 586 mW) on the phase behaviour of PHYT44DOPC (Panel C.) and PHYT44DOPC-GNR (Panel D.). The phase transitions are annotated on the right and were determined by integration of the individual frames. The red arrow indicates the duration of NIR irradiation (160 s). All matrices are in 50% water. The increased intensity of yellow is indicative of increased scattering.

6.4.2.2. 20.1 mol% Cholesterol in POPE

The phase behaviour of the 20.1 mol% cholesterol in POPE formulation (POPE20Ch) was investigated on incorporation of GNR and the consequent effect of photothermal stimulation. The equilibrium phase behaviour of the POPE20Ch system and POPE20Ch containing 3 nM GNR (POPE20Ch-GNR) are shown in Figure 6.10, Panels A. and B. POPE20Ch in water displays a L_α phase at 25 ºC, and with increasing temperature the system transitioned to L_α + H_2 phase at 45 ºC, then H_2 phase at 60 ºC. Contrary to the previous study by Wang *et al.*[39], POPE20Ch did not exhibit the V_2 phase with increasing temperature. However and more importantly, the POPE20Ch-GNR system *did* exhibit the L_α to $V_{2\ D}$ transition at 55 ºC. The equilibrium phase behaviour of the POPE20Ch-GNR system progressed from L_α to H_2 at 40 ºC, then to a mixed phase of H_2 + $V_{2\ D}$ at 55 ºC to 80 ºC. The featureless scattering in the POPE20Ch-GNR matrix in the early q region is attributed to GNR scattering of the X-rays.

The dynamic phase behaviour of the POPE20Ch and POPE20Ch-GNR matrices upon NIR laser irradiation are illustrated in Figure 6.10, Panels C. and D. respectively. In the absence of GNR, the POPE20Ch system did not transition from L_α phase, nor was a shift in lattice parameter observed over the 160 s of NIR irradiation. In contrast, irradiation of the L_α POPE20ChGNR matrix resulted in the appearance of $V_{2\ D}$ at 26 s, and the transition of the phase to H_2 +$V_{2\ D}$ at 70 s. The photothermal phase transitions are in agreement with the equilibrium phase behaviour. On cessation of irradiation, the $V_{2\ D}$ phase persisted for at least 220 s and then returned to L_α at 500 s.

Equilibrium phase behaviour

A. POPE20Ch, no GNR

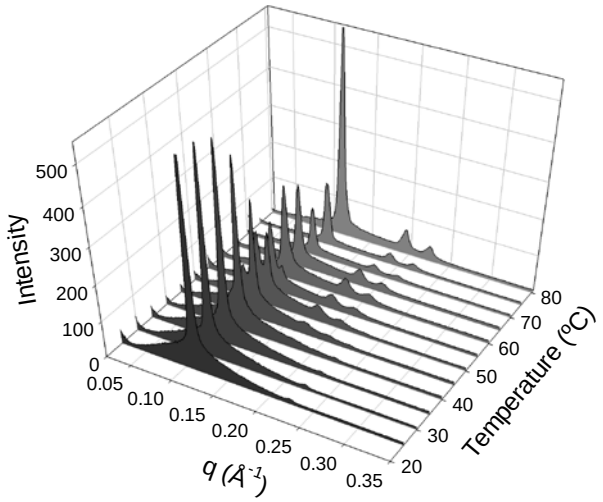

B. POPE20Ch + GNR

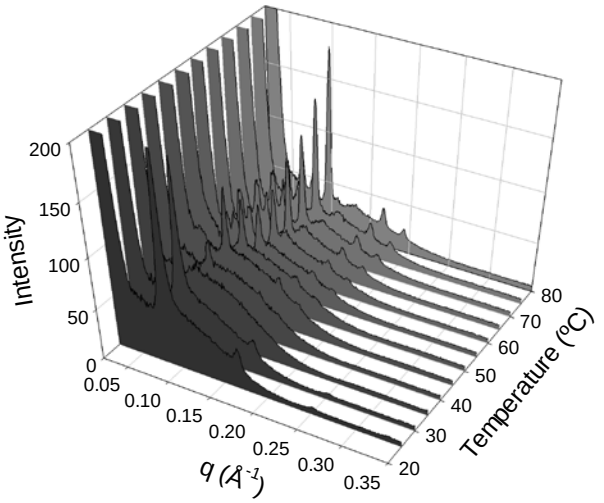

Kinetic phase behaviour on irradiation

C. POPE20Ch, no GNR

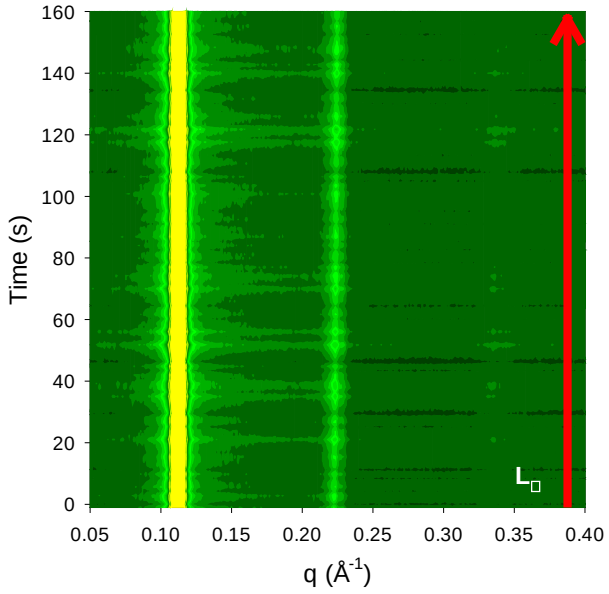

D. POPE20Ch + GNR

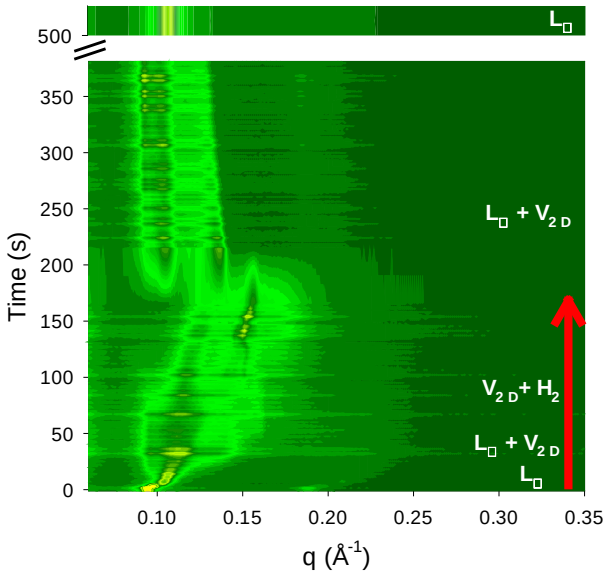

Figure 6.10 – Panels A. and B.: The effect of addition of GNR into the POPE20Ch matrix. SAXS profiles showing the equilibrium phase behaviour of Panel A. 20.1 mol% Cholesterol in POPE (POPE20Ch) and Panel B. POPE20Ch + 3 nM GNR (POPE20Ch-GNR). Panels C. and D: Time resolved SAXS profiles showing the effect of laser irradiation (810 nm, 586 mW) on the phase behaviour of POPE20Ch (Panel C.) and POPE20Ch-GNR (Panel D.). The phase transitions are annotated on the right and were determined by integration of the individual frames. The red arrow indicates the duration of NIR irradiation (160 s). The increased intensity of yellow is indicative of increased scattering. All matrices contained 50% water.

6.5.Discussion

The modification of lipid bilayers through the presence of additives has attracted much attention in the quest to understand the role of different liquid crystalline phases in biomembranes and the competing forces which drive phase transitions. The influence of guest molecules on liquid crystalline nanostructure is related to the degree of their penetration in the membrane as well as to their ability to alter the spontaneous curvature of the lipid bilayer[49, 57]. The purpose of this study was to develop matrices which demonstrate a L_α to V_2 phase transition through the addition of differently shaped amphiphiles.

The formation of inverse bicontinuous cubic phases arises from a frustration between the optimal mean curvature of the interface and the optimal packing of the hydrocarbon chains thus maintaining both a uniform average molecular length (i.e. bilayer thickness) and a uniform mean curvature of the lipid bilayers[58]. Thus, the incorporation of three amphiphiles known to form lamellar phases into the $V_{2\ D}$ matrices formed by PHYT and GMO was proposed to induce a positive influence on the membrane curvature. As introduced in Chapter 1, the packing of lipids can be described by their molecular shapes as determined by their critical packing parameter[59] (CPP) (Equation (1)).

$$CPP = \frac{v}{a\,l} \qquad (1)$$

where *v* is the effective hydrophobic chain volume, *a* is head group area and *l* is hydrophobic chain length. Figure 6.11 exhibits the shapes of the lipids with increasing CPP from left to right. The three additives, lysoPC, DOPC and ME will be discussed in terms of their ability to influence lipid packing in the $V_{2\ D}$ of hydrated PHYT and GMO systems.

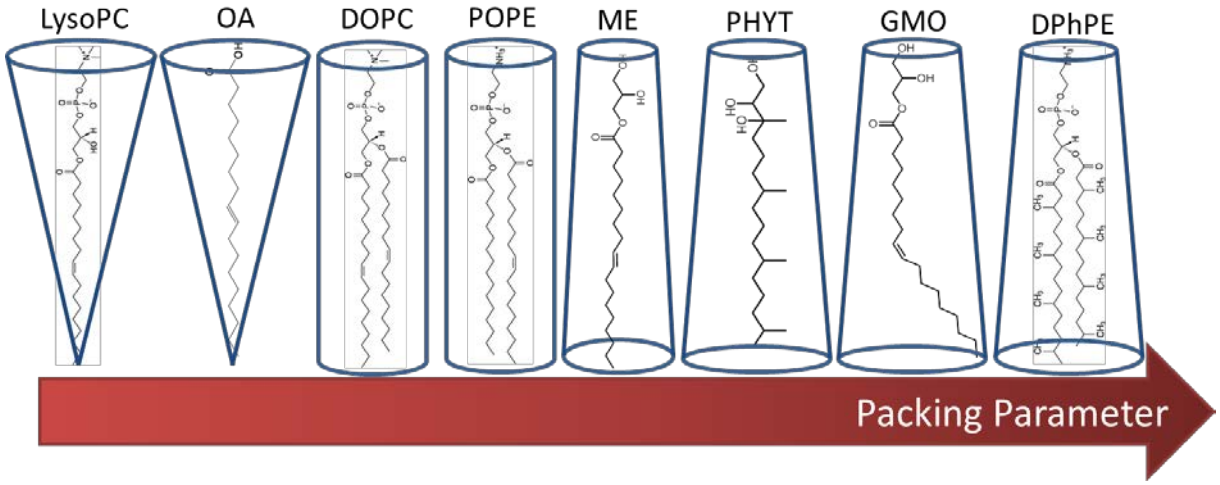

Figure 6.11 – The increasing critical packing parameters of the lipids used in this study as shown by the increasing wedge shapes drawn around the molecular structures. Wedge shaped lipids with CPP ≥ 1 are the lipids most likely to form reversed phases.

The formation of non-lamellar inverse phases in pure hydrated phospholipid systems is uncommon, but the formation of metastable non-lamellar phases has been induced upon thermal cycling[60]. Additives are thus usually required to stabilise the formation of inverse phases in systems containing phospholipids. Some phosphatidylethanolamines, such as POPE and dioleylphosphatidylethanolamine (DOPE) are an exception as they are able to form H_2 in a fully hydrated system, due to their relatively small headgroup compared to its alkyl tail[39, 61]. DOPC is one of the most abundant phospholipids in biological systems. It is a zwitterionic phospholipid which preferentially resides in lipid bilayers as shown by its propensity to diffuse into PHYT and GMO vesicles over time[51]. In terms of CPP, DOPC has larger v and a, giving it a cylindrical shape compared with PHYT and GMO. The addition of phospholipids to GMO and PHYT matrices has been shown to result in the swelling of the $V_{2\ D}$ phase depending on the properties of the phospholipid[62, 63]. In good agreement with previous reports, the addition of small amounts of DOPC to GMO and PHYT stabilised and enlarged the lattice parameters of the phase, which is attributed to the relatively large and more hydrophilic DOPC headgroup increasing the capacity of

the water channels at the lipid-water interface. At higher DOPC concentrations, where the phospholipid dominated the phase behaviour, the insertion of PHYT/GMO into the bilayer was able to reduce the chain stress in lamellar phases and upon increased lipid mobility when heated, resulted in the formation of vesicle + $V_{2\,D}$ phases.

Phosphatidylcholines do not have ideal miscibility in bilayers of high curvatures[64], which can result in the formation of laterally segregated domains comprised of different molecular species on either side of the bilayer[65]. This may have occurred in the DOPC/PHYT and DOPC/GMO phases, however, the use of SAXS alone cannot distinguish between domains in such close proximity. Miscibility issues may be resolved using additional techniques such as electron microscopy[66, 67], molecular probe methods[65, 68] or possibly small angle neutron scattering[69, 70].

LysoPC is a lipid formed by the hydrolysis of phosphatidylcholine by phospholipase A_2. It is a single-chained phospholipid with a relatively large headgroup compared to its C18:1 alkyl chain; as such it is cone-shaped. LysoPC has been shown to promote positive spontaneous splay in phospholipid membranes[71]. The addition of cone-shaped lipids, for example the alkyl glucosides, into the GMO cubic phase in excess water results in the swelling of the cubic phase[69, 72] and at higher concentrations, the formation of L_α phase[50]. This effect was observed in the addition of lysoPC to both GMO and PHYT. A smaller amount of lysoPC (~30 mol%) was required to induce the formation of L_α in comparison to DOPC (~45 mol%) which is attributed to the greater difference in CPP between lysoPC and PHYT/GMO compared with DOPC and PHYT/GMO. Unlike the DOPC mixtures, lysoPC/PHYT and lysoPC/GMO formulations with a L_α starting phase did not exhibit a V_2 phase upon heating at the concentrations investigated. LysoPC is not normally found in cellular membranes but is present in the body to regulate a variety of cellular functions[73, 74]. Additionally, elevated levels of lysoPC in tissues has been indicated in disease states such as cancer[75] as its presence is thought to enhance cellular injury by increasing the permeability of lipid

membranes[76] and inhibits membrane fusion[77]. Thus, the incorporation of lysoPC into the PHYT/GMO bilayer promoted a more positive curvature and thus the formation of L_α, but its presence could not sustain the formation of the $V_{2\,D}$ phase with an increase in temperature.

Monoelaidin (ME), glyceryl monooleate (GMO) and oleic acid (OA) are structurally related unsaturated C18:1 lipids, where GMO and ME have a glycerol backbone, and the double bond in ME and OA have a *trans* confirmation whereas GMO has a *cis* double bond (Figure 6.2). The phase behaviour of OA in fully hydrated GMO matrix has been well studied[47] and results in the formation of H_2 and L_2 phases at lower temperatures, an effect which is not desired in this case. GMO has the ability to form L_α phase at lower water concentrations[53, 78], thus the cylindrically shaped lipid, ME, was added to the GMO matrix in order to induce a L_α to $V_{2\,D}$ phase transition in excess water. The lipid comprising the major component, either ME or GMO, was found to dominate the phase behaviour of the matrix.

The phase behaviour of fully hydrated ME and GMO were established in Chapter 3, however, it is noted that the phase behaviour of the ME used in this series of experiments differs to the material used in Chapter 3 as well as literature values[79, 80] which could be attributed to the batch of lipid. The presence of impurities in the source material is known to effect the phase behaviour of liquid crystalline materials[81], thus the difference in phase behaviour could be attributed to the source material. Yaghmur *et al.* recently reported the phase behaviour of fully hydrated ME/GMO/OA systems[82], in which the studies were conducted on a similar time frame to the experiments in the present study. In agreement with the results presented in this Chapter, the 1:1 ME:GMO system resulted in the existence of the $V_{2\,D}$ phase over a greater temperature range and the formation of the H_2 phase at temperatures above 60 ºC. On the other hand, the rich phase behaviour of the ME/OA system identified by Yagmur et al. was not observed. This could be attributed to the oil dissolving the ME instead of incorporating into the interface, thus causing the

formation of the inverse micelles, and again, it could also be attributed to the different source material used possibly containing differing proportions of free fatty acids.

The ability to create fit-for-function lipid systems is a balance of the influence of each component in the mixture[83]. In each of the lipid mixtures investigated where the lipid additive was cylindrically shaped (CPP = 1), namely ME and DOPC, the equilibrium thermal phase behaviour of the system favoured the lipid which was in the majority. These additives promoted bilayer curvature at the interface thereby stabilising the $V_{2\,D}$ structure, thus the formation of the $V_{2\,D}$ was observed in these systems with an increase in temperature. On the other hand, cone shaped moieties (CPP $\leq$1) lysoPC and OA, reduced the number of phases observed, which was attributed to the disruptive effect on lipid packing.

Photothermal lamellar to non-lamellar phase transitions were demonstrated through the NIR laser activation of POPE20Ch and PHYT44DOPC matrices containing GNR as summarised in Figure 6.12. Similar to the photothermal phase transitions observed in Chapter 3, the non-lamellar phase transition of the PHYT44DOPC-GNR required less irradiation time, and thus photothermal energy, than the L_α to $V_{2\,D}$ of the POPE20Ch-GNR matrix. Phothermal drug release from liposomes has previously been demonstrated using UV irradiation as the light source, where drug release was attributed to the phase transition from the gel to the ripple phase[84, 85]. Yet, the L_α to $V_{2\,D}$ phase transition could provide a matrix with a more defined geometry and therefore a more predictable release pattern. Additionally the use of NIR radiation may be more applicable for *in vivo* applications as UV light has its limitations as discussed in Chapter 5. This study gives rise to further potential controlled release materials, where the reversible L_α to $V_{2\,D}$ phase transition provides an ideal ‘off-on’ switch, as opposed to the ‘on-off’ behaviour of the systems in Chapter 3, for practical pulsatile drug delivery.

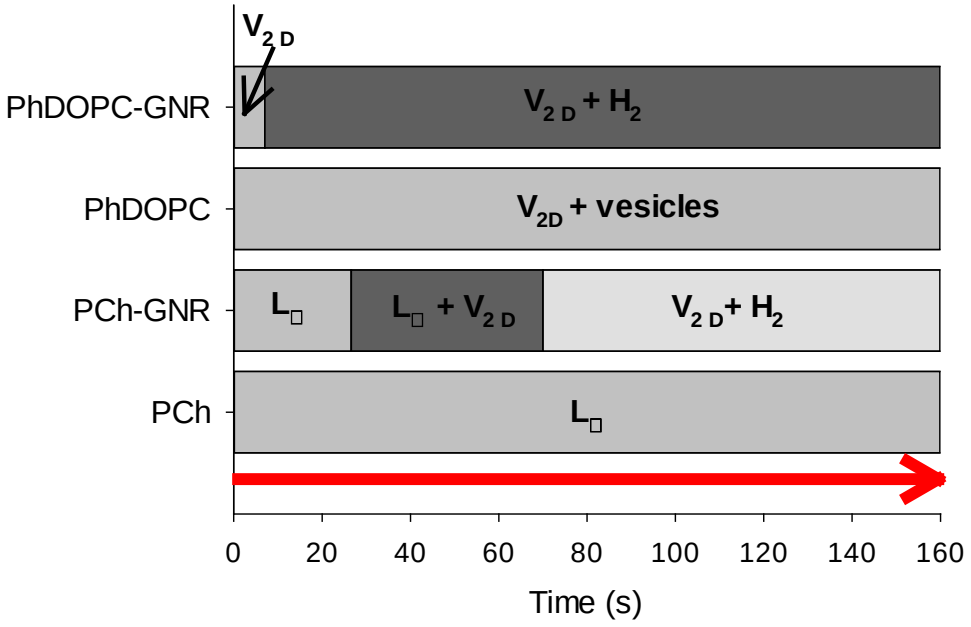

Figure 6.12 – Summary of the effect of laser irradiation (810 nm, 586 mW) on the phase behaviour of the PHYT44DOPC-GNR, PHYT44DOPC, POPE20Ch-GNR and POPE20Ch systems. The red arrow indicates the duration of irradiation (160 s). As expected, only the matrices containing GNR exhibited laser triggered phase transitions.

6.6. Conclusions

The partial phase diagrams of PHYT/GMO containing DOPC, lysoPC and ME were reported and the phase behaviours of the hydrated lipid mixtures were found to be a consequence of the ability of each lipid component to influence the lipid packing. The addition of lipids with a CPP = 1 allowed for the formation of the bicontinuous cubic or reversed hexagonal phases upon heating, whereas lipids with a CPP < 1 did not.

The L_α to $V_{2\,D}$ phase transition was photothermally induced in a system containing POPE and cholesterol. It is anticipated that photothermally induced phase transitions in self assembled systems will provide potential triggerable systems for drug delivery and other bioapplications.

References

1. Koynova R, Caffrey M. An index of lipid phase diagrams. Chemistry and Physics of Lipids. 2002;115(1-2):107-219.

2. Wolf C, Quinn PJ. Lipidomics: Practical aspects and applications. Progress in Lipid Research. 2008;47(1):15-36.

3. Shah JC, Sadhale Y, Chilukuri DM. Cubic phase gels as drug delivery systems. Adv Drug Deliv Rev 2001;47(2-3):229-50.

4. Drummond CJ, Fong C. Surfactant self-assembly objects as novel drug delivery vehicles. Curr Opin Colloid Interface Sci. 1999;4(6):449-56.

5. Amar-Yuli I, Libster D, Aserin A, Garti N. Solubilization of food bioactives within lyotropic liquid crystalline mesophases. Curr Opin Colloid Interface Sci. 2009;14(1):21-32.

6. Larsson K. Lyotropic liquid crystals and their dispersions relevant in foods. Curr Opin Colloid Interface Sci. 2009 Feb;14(1):16-20.

7. Nazaruk E, Bilewicz R, Lindblom G, Lindholm-Sethson B. Cubic phases in biosensing systems. Anal Bioanal Chem. 2008;391(5):1569-78.

8. Cherezov V, Clogston J, Misquitta Y, Abdel-Gawad W, Caffrey M. Membrane Protein Crystallization In Meso: Lipid Type-Tailoring of the Cubic Phase. Biophys J. 2002;83(6):3393-407.

9. Kulkarni CV, Ales I. In Cubo Crystallization of Membrane Proteins. Advances in Planar Lipid Bilayers and Liposomes. Volume 12: Academic Press; 2010. p. 237-72.

10. Landau EM, Rosenbusch JP. Lipidic cubic phases: A novel concept for the crystallization of membrane proteins. Proceedings of the National Academy of Sciences. 1996 December 10, 1996;93(25):14532-5.

11. Luzzati V, Tardieu A, Gulik-Krzywicki T, Rivas E, Reiss-Husson F. Structure of the Cubic Phases of Lipid-Water Systems. Nature. 1968;220(5166):485-8.

12. Mariani P, Luzzati V, Delacroix H. Cubic phases of lipid-containing systems : Structure analysis and biological implications. Journal of Molecular Biology. 1988;204(1):165-89.

13. Lee KWY, Nguyen T-H, Hanley T, Boyd BJ. Nanostructure of liquid crystalline matrix determines in vitro sustained release and in vivo oral absorption kinetics for hydrophilic model drugs. Int J Pharm. 2009;365(1-2):190-9.

14. Phan S, Fong W-K, Kirby N, Hanley T, Boyd BJ. Evaluating the link between self-assembled mesophase structure and drug release. Int J Pharm. 2011;421(1):176-82.

15. Fong W-K, Hanley T, Boyd BJ. Stimuli responsive liquid crystals provide 'on-demand' drug delivery *in vitro* and *in vivo*. J Contr Release. 2009;135(3):218-26.

16. Boyd BJ. Characterisation of drug release from cubosomes using the pressure ultrafiltration method. Int J Pharm. 2003 Jul;260(2):239-47.

17. Chang CM, Bodmeier R. Swelling of and drug release from monoglyceride-based drug delivery systems. J Pharm Sci. 1997;86(6):747-52.

18. Hyde S. The Language of shape: the role of curvature in condensed matter--physics, chemistry, and biology. Amsterdam [Netherlands]; New York: Elsevier; 1997.

19. Kirk GL, Gruner SM, Stein DL. A thermodynamic model of the lamellar to inverse hexagonal phase transition of lipid membrane-water systems. Biochemistry. 1984 1984/03/01;23(6):1093-102.

20. Boyd BJ, Drummond CJ, Krodkiewska I, Grieser F. How chain length, headgroup polymerization, and anomeric configuration govern the thermotropic and lyotropic liquid crystalline phase behavior and the air-water interfacial adsorption of glucose-based surfactants. Langmuir. 2000 Sep;16(19):7359-67.

21. Seddon JM, Cevc G, Kaye RD, Marsh D. X-ray-Diffraction Study of the Polymorphism of Hydrated Diacylphosphatidylethanolamine and Dialkylphosphatidylethanolamine. Biochemistry. 1984;23(12):2634-44.

22. Kulkarni CV, Tang T-Y, Seddon AM, Seddon JM, Ces O, Templer RH. Engineering bicontinuous cubic structures at the nanoscale-the role of chain splay. Soft Matter. 2010;6(14):3191-4.

23. Lewis RN, McElhaney RN, Harper PE, Turner DC, Gruner SM. Studies of the thermotropic phase behavior of phosphatidylcholines containing 2-alkyl substituted fatty acyl chains: a new class of phosphatidylcholines forming inverted nonlamellar phases. Biophys J. 1994;66(4):1088-103.

24. Fong C, Le T, Drummond CJ. Lyotropic liquid crystal engineering-ordered nanostructured small molecule amphiphile self-assembly materials by design. Chem Soc Rev. 2012;41(3):1297-322.

25. Briggs J, Caffrey M. The Temperature-Composition Phase-Diagram of Monomyristolein in Water: Equilibrium and Metastability Aspects. Biophys J. 1994 Mar;66(3):573-87.

26. Kumar VV. Complementary molecular shapes and additivity of the packing parameter of lipids. Proceedings of the National Academy of Sciences. 1991 January 15, 1991;88(2):444-8.

27. Shyamsunder E, Gruner SM, Tate MW, Turner DC, So PTC, Tilcock CPS. Observation of inverted cubic phase in hydrated dioleoylphosphatidylethanolamine membranes. Biochemistry. 1988;27(7):2332-6.

28. Heberle FA, Petruzielo RS, Pan J, Drazba P, Kučerka N, Standaert RF, et al. Bilayer Thickness Mismatch Controls Domain Size in Model Membranes. Journal of the American Chemical Society. 2013.

29. Awad TS, Okamoto Y, Masum SM, Yamazaki M. Formation of Cubic Phases from Large Unilamellar Vesicles of Dioleoylphosphatidylglycerol/Monoolein Membranes Induced by Low Concentrations of Ca2+. Langmuir 2005;21(25):11556-61.

30. Borne J, Nylander T, Khan A. Phase Behavior and Aggregate Formation for the Aqueous Monoolein System Mixed with Sodium Oleate and Oleic Acid. Langmuir. 2001;17(25):7742-51.

31. Persson G, Edlund H, Amenitsch H, Laggner P, Lindblom G. The 1-Monooleoyl-rac-glycerol/n-Octyl-β-d-Glucoside/Water System. Phase Diagram and Phase Structures Determined by NMR and X-ray Diffraction. Langmuir. 2003;19(14):5813-22.

32. Kraineva J, Narayanan RA, Kondrashkina E, Thiyagarajan P, Winter R. Kinetics of Lamellar-to-Cubic and Intercubic Phase Transitions of Pure and Cytochrome c Containing Monoolein Dispersions Monitored by Time-Resolved Small-Angle X-ray Diffraction. Langmuir. 2005;21(8):3559-71.

33. Dong Y-D, Larson I, Hanley T, Boyd BJ. Bulk and Dispersed Aqueous Phase Behavior of Phytantriol: Effect of Vitamin E Acetate and F127 Polymer on Liquid Crystal Nanostructure. Langmuir 2006;22(23):9512-8.

34. Engström S, Nordén TP, Nyquist H. Cubic phases for studies of drug partition into lipid bilayers. European Journal of Pharmaceutical Sciences. 1999;8(4):243-54.

35. Engblom J, Engström S, Fontell K. The effect of the skin penetration enhancer Azone® on fatty acid-sodium soap-water mixtures. J Contr Release. 1995;33(2):299-305.

36. Pouzot M, Mezzenga R, Leser M, Sagalowicz L, Guillot S, Glatter O. Structural and Rheological Investigation of Fd3m Inverse Micellar Cubic Phases. Langmuir. 2007;23(19):9618-28.

37. Yaghmur A, Kriechbaum M, Amenitsch H, Steinhart M, Laggner P, Rappolt M. Effects of Pressure and Temperature on the Self-Assembled Fully Hydrated Nanostructures of Monoolein-Oil Systems. Langmuir. 2009;26(2):1177-85.

38. Seddon JM. An inverse face-centered cubic phase formed by diacylglycerol-phosphatidylcholine mixtures. Biochemistry. 1990;29(34):7997-8002.

39. Wang X, Quinn PJ. Cubic phase is induced by cholesterol in the dispersion of 1-palmitoyl-2-oleoyl-phosphatidylethanolamine. Biochimica et Biophysica Acta (BBA) - Biomembranes. 2002;1564(1):66-72.

40. Chen Z, Rand RP. The influence of cholesterol on phospholipid membrane curvature and bending elasticity. Biophys J. 1997;73(1):267-76.

41. Mulet X, Templer RH, Woscholski R, Ces O. Evidence That Phosphatidylinositol Promotes Curved Membrane Interfaces. Langmuir. 2008 2012/04/23;24(16):8443-7.

42. Koynova R, Tenchov B, Rapp G. Low amounts of PEG-lipid induce cubic phase in phosphatidylethanolamine dispersions. Biochim Biophys Acta Biomembr. 1997;1326(2):167-70.

43. Wang X, Quinn PJ. The distribution of α-tocopherol in mixed aqueous dispersions of phosphatidylcholine and phosphatidylethanolamine. Biochimica et Biophysica Acta (BBA) - Biomembranes. 2000 12/20/;1509(1–2):361-72.

44. Okamoto Y, Masum SM, Miyazawa H, Yamazaki M. Low-pH-Induced Transformation of Bilayer Membrane into Bicontinuous Cubic Phase in Dioleoylphosphatidylserine/Monoolein Membranes. Langmuir. 2008;24(7):3400-6.

45. Yaghmur A, Laggner P, Sartori B, Rappolt M. Calcium Triggered L-alpha-H-2 Phase Transition Monitored by Combined Rapid Mixing and Time-Resolved Synchrotron SAXS. PLoS ONE. 2008 Apr;3(4):11.

46. Yaghmur A, Sartori B, Rappolt M. The role of calcium in membrane condensation and spontaneous curvature variations in model lipidic systems. Phys Chem Chem Phys. 2011;13(8):3115-25.

47. Aota-Nakano Y, Li SJ, Yamazaki M. Effects of electrostatic interaction on the phase stability and structures of cubic phases of monoolein/oleic acid mixture membranes. Biochim Biophys Acta Biomembr. 1999;1461(1):96-102.

48. Angelov B, Angelova A, Vainio U, Garamus VM, Lesieur S, Willumeit R, et al. Long-Living Intermediates during a Lamellar to a Diamond-Cubic Lipid Phase Transition: A Small-Angle X-Ray Scattering Investigation. Langmuir. 2009;25(6):3734-42.

49. Kulkarni CV, Wachter W, Iglesias-Salto G, Engelskirchen S, Ahualli S. Monoolein: a magic lipid? Phys Chem Chem Phys. 2011;13(8):3004-21.

50. Misquitta Y, Caffrey M. Detergents Destabilize the Cubic Phase of Monoolein: Implications for Membrane Protein Crystallization. Biophysical Journal. 2003;85(5):3084-96.

51. Vandoolaeghe P, Barauskas J, Johnsson M, Tiberg F, Nylander T. Interaction between Lamellar (Vesicles) and Nonlamellar Lipid Liquid-Crystalline Nanoparticles as Studied by Time-Resolved Small-Angle X-ray Diffractionâ€ Langmuir. 2009;25(7):3999-4008.

52. Wu WG, Huang CH, Conley TG, Martin RB, Levin IW. Lamellar-micellar transition of 1-stearoyllysophosphatidylcholine assemblies in excess water. Biochemistry. 1982 1982/11/01;21(23):5957-61.

53. Hyde ST, Andersson S, Ericsson B, Larsson Kr. A cubic structure consisting of a lipid bilayer forming an infinite periodic minimum surface of the gyroid type in the glycerolmonooleat-water system. Z Krist. 1984 2011/03/28;168(1-4):213-9.

54. Dal-Maso AD, Dellacasagrande J, Legendre F, Tiraby G, Blonski C, Hoffmann P. Synthesis and evaluation of new phosphonolipid compounds for gene delivery. European Journal of Medicinal Chemistry. 2008;43(8):1758-66.

55. Marshall J, Nietupski JB, Lee ER, Siegel CS, Rafter PW, Rudginsky SA, et al. Cationic Lipid Structure and Formulation Considerations for Optimal Gene Transfection of the Lung. Journal of Drug Targeting. 2000;7(6):453-69.

56. Andersson M, Jackman J, Wilson D, Jarvoll P, Alfredsson V, Okeyo G, et al. Vesicle and bilayer formation of diphytanoylphosphatidylcholine (DPhPC) and diphytanoylphosphatidylethanolamine (DPhPE) mixtures and their bilayers’ electrical stability. Colloids and Surfaces B: Biointerfaces. 2011;82(2):550-61.

57. Barauskas J, Johnsson M, Joabsson F, Tiberg F. Cubic Phase Nanoparticles (Cubosome): Principles for Controlling Size, Structure, and Stability. Langmuir. 2005;21(6):2569-77.

58. Gruner SM. Stability of lyotropic phases with curved interfaces. The Journal of Physical Chemistry. 1989 1989/11/01;93(22):7562-70.

59. Israelachvili JN, Mitchell DJ, Ninham BW. Theory of self-assembly of lipid bilayers and vesicles. Biochim Biophys Acta Biomembr. 1977;470(2):185-201.

60. Erbes J, Czeslik C, Hahn W, Winter R, Rappolt M. On The Existence of Bicontinuous Cubic Phases in Dioleoylphosphatidylethanolamine. Berichte der Bunsengesellschaft für Physikalische Chemie. 1994;98(10):1287-93.

61. Toombes GES, Finnefrock AC, Tate MW, Gruner SM. Determination of L[alpha]-HII Phase Transition Temperature for 1,2-Dioleoyl-sn-Glycero-3-Phosphatidylethanolamine. Biophys J. 2002;82(5):2504-10.

62. Chupin V, Killian JA, de Kruijff B. Effect of Phospholipids and a Transmembrane Peptide on the Stability of the Cubic Phase of Monoolein: Implication for Protein Crystalization from a Cubic Phase. Biophysical Journal. 2003;84(4):2373-81.

63. Wadsten-Hindrichsen P, Bender J, Unga J, Engström S. Aqueous self-assembly of phytantriol in ternary systems: Effect of monoolein, distearoylphosphatidylglycerol and three water-miscible solvents. J Colloid Interface Sci. 2007;315(2):701-13.

64. Quinn PJ. Lipid–lipid interactions in bilayer membranes: Married couples and casual liaisons. Progress in Lipid Research. 2012 7//;51(3):179-98.

65. Lentz BR, Barenholz Y, Thompson TE. Fluorescence depolarization studies of phase transitions and fluidity in phospholipid bilayers. 2. Two-component phosphatidylcholine liposomes. Biochemistry. 1976 1976/10/01;15(20):4529-37.

66. Zasadzinski JA. Transmission electron microscopy observations of sonication-induced changes in liposome structure. Biophys J. 1986;49(6):1119-30.

67. Rizwan SB, Dong YD, Boyd BJ, Rades T, Hook S. Characterisation of bicontinuous cubic liquid crystalline systems of phytantriol and water using cryo field emission scanning electron microscopy (cryo FESEM). Micron. 2007;38(5):478-85.

68. Rowinski P, Korytkowska A, Bilewicz R. Diffusion of hydrophilic probes in bicontinuous lipidic cubic phase. Chemistry and Physics of Lipids. 2003;124(2):147-56.

69. Angelov B, Angelova A, Garamus VM, Lebas Gv, Lesieur S, Ollivon M, et al. Small-Angle Neutron and X-ray Scattering from Amphiphilic Stimuli-Responsive Diamond-Type Bicontinuous Cubic Phase. J Am Chem Soc. 2007;129(44):13474-9.

70. Lee CT, Smith KA, Hatton TA. Small-Angle Neutron Scattering Study of the Micellization of Photosensitive Surfactants in Solution and in the Presence of a Hydrophobically Modified Polyelectrolyteâ€ Langmuir. 2009;25(24):13784-94.

71. Fuller N, Rand RP. The Influence of Lysolipids on the Spontaneous Curvature and Bending Elasticity of Phospholipid Membranes. Biophysical Journal. 2001 7//;81(1):243-54.

72. Mezzenga R, Grigorov M, Zhang Z, Servais C, Sagalowicz L, Romoscanu AI, et al. Polysaccharide-Induced Order-to-Order Transitions in Lyotropic Liquid Crystals. Langmuir. 2005;21(14):6165-9.

73. Chai Y-C, Howe PH, DiCorleto PE, Chisolm GM. Oxidized Low Density Lipoprotein and Lysophosphatidylcholine Stimulate Cell Cycle Entry in Vascular Smooth Muscle Cells: EVIDENCE FOR RELEASE OF FIBROBLAST GROWTH FACTOR-2. J Biol Chem. 1996 July 26, 1996;271(30):17791-7.

74. Hirata K-i, Miki N, Kuroda Y, Sakoda T, Kawashima S, Yokoyama M. Low Concentration of Oxidized Low-Density Lipoprotein and Lysophosphatidylcholine Upregulate Constitutive Nitric Oxide Synthase mRNA Expression in Bovine Aortic Endothelial Cells. Circulation Research. 1995 June 1, 1995;76(6):958-62.

75. Okita M, Gaudette DC, Mills GB, Holub BJ. Elevated levels and altered fatty acid composition of plasma lysophosphatidlycholine(lysoPC) in ovarian cancer patients. International Journal of Cancer. 1997;71(1):31-4.

76. Colles SM, Chisolm GM. Lysophosphatidylcholine-induced cellular injury in cultured fibroblasts involves oxidative events. Journal of Lipid Research. 2000 August 1, 2000;41(8):1188-98.

77. Chernomordik LV, Kozlov MM, Melikyan GB, Abidor IG, Markin VS, Chizmadzhev YA. The shape of lipid molecules and monolayer membrane fusion. Biochimica et Biophysica Acta (BBA) - Biomembranes. 1985 2/14/;812(3):643-55.

78. Engström S, Lindahl L, Wallin R, Engblom J. A study of polar lipid drug systems undergoing a thermoreversible lamellar-to-cubic phase transition. Int J Pharm. 1992;86(2-3):137-45.

79. Chung H, Caffrey M. Polymorphism, mesomorphism, and metastability of monoelaidin in excess water. Biophys J. 1995 Nov;69(5):1951-63.

80. Kulkarni CV. Nanostructural Studies on Monoelaidinâ€“Water Systems at Low Temperatures. Langmuir. 2011 2012/10/18;27(19):11790-800.

81. Dong Y-D, Dong AW, Larson I, Rappolt M, Amenitsch H, Hanley T, et al. Impurities in Commercial Phytantriol Significantly Alter Its Lyotropic Liquid-Crystalline Phase Behavior. Langmuir. 2008;24(13):6998-7003.

82. Yaghmur A, Sartori B, Rappolt M. Self-Assembled Nanostructures of Fully Hydrated Monoelaidin-Elaidic Acid and Monoelaidin-Oleic Acid Systems. Langmuir. 2012 2012/07/03;28(26):10105-19.

83. Yaghmur A, Laggner P, Zhang S, Rappolt M. Tuning Curvature and Stability of Monoolein Bilayers by Designer Lipid-Like Peptide Surfactants. PLoS ONE. 2007;2(5):e479.

84. Paasonen L, Laaksonen T, Johans C, Yliperttula M, Kontturi K, Urtti A. Gold nanoparticles enable selective light-induced contents release from liposomes. J Contr Release. 2007;122(1):86-93.

85. Paasonen L, Sipilä T, Subrizi A, Laurinmäki P, Butcher SJ, Rappolt M, et al. Gold-embedded photosensitive liposomes for drug delivery: Triggering mechanism and intracellular release. J Contr Release. 2010;147(1):136-43.

Appendix

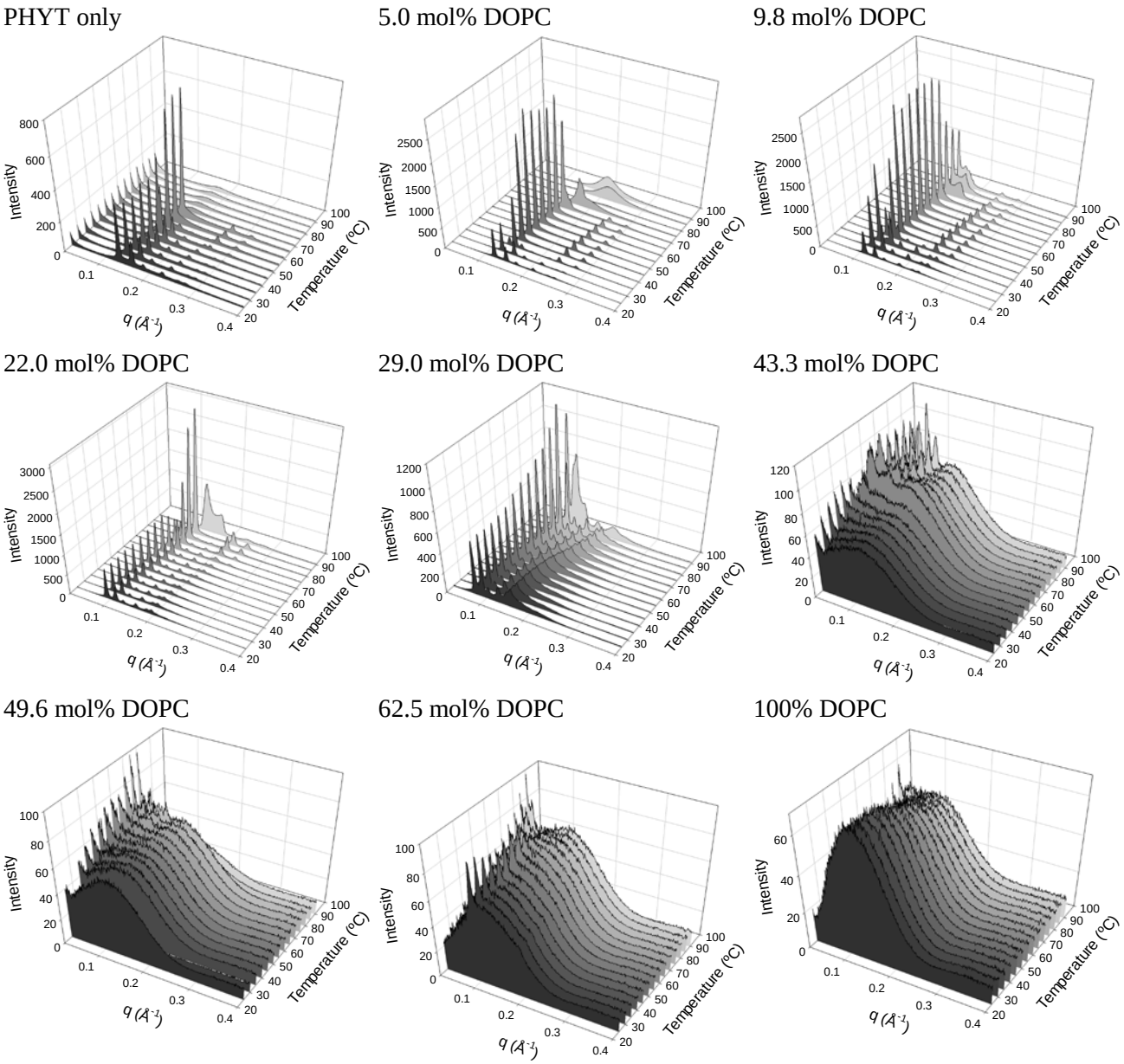

Figure A1 – Equilibrium SAXS scattering patterns displaying the effect of increasing amounts of DOPC addition on the thermal phase behaviour of PHYT matrices. The molar concentrations of DOPC addition into PHYT in each system are annotated on the graph. All matrices contain lipid mixture:MilliQ water 1:1 (w/w).

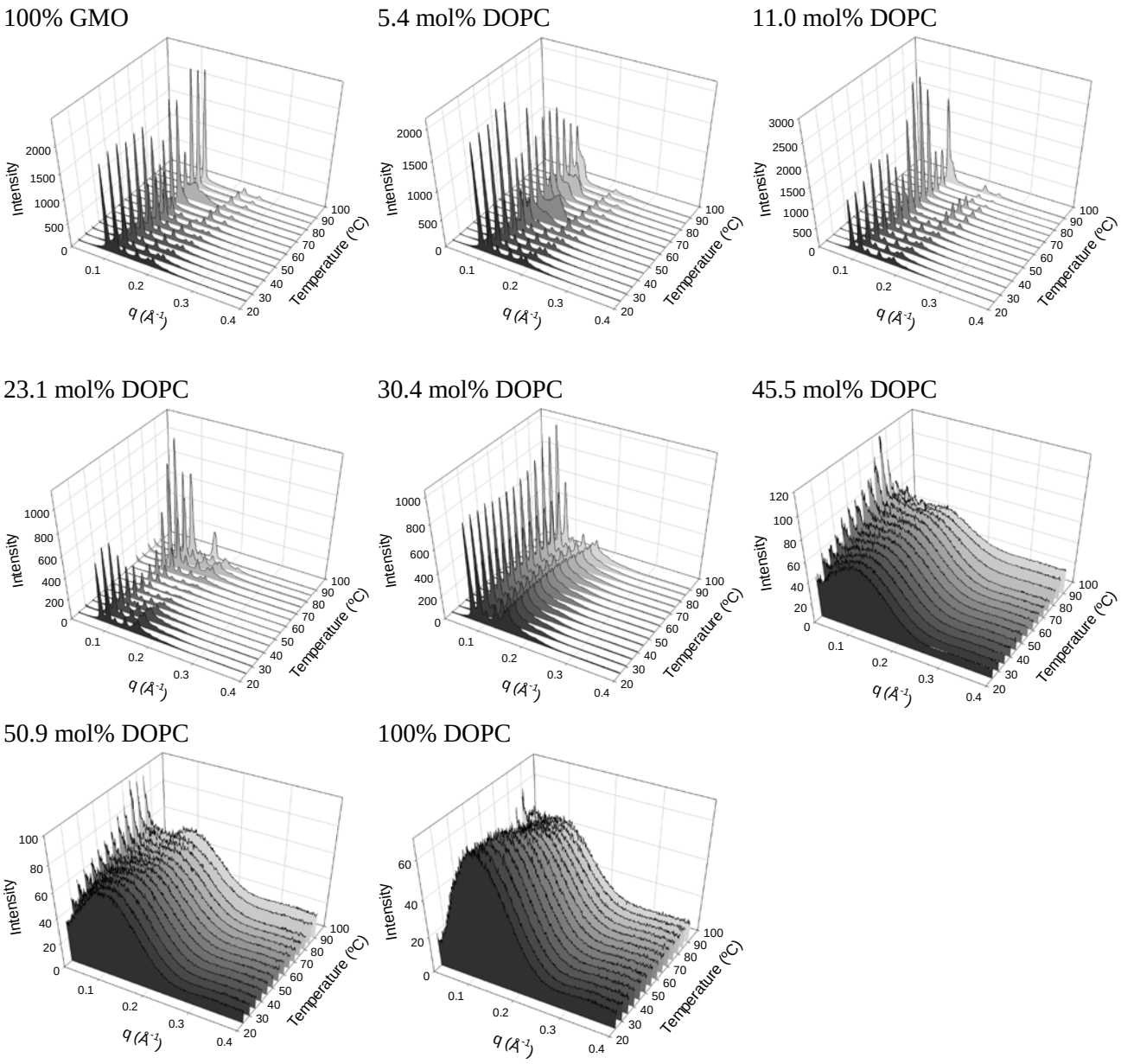

Figure A2 – Equilibrium SAXS scattering patterns displaying the effect of increasing amounts of DOPC addition on the thermal phase behaviour of GMO matrices. All matrices contain lipid mixture: MilliQ water 1:1 (w/w).

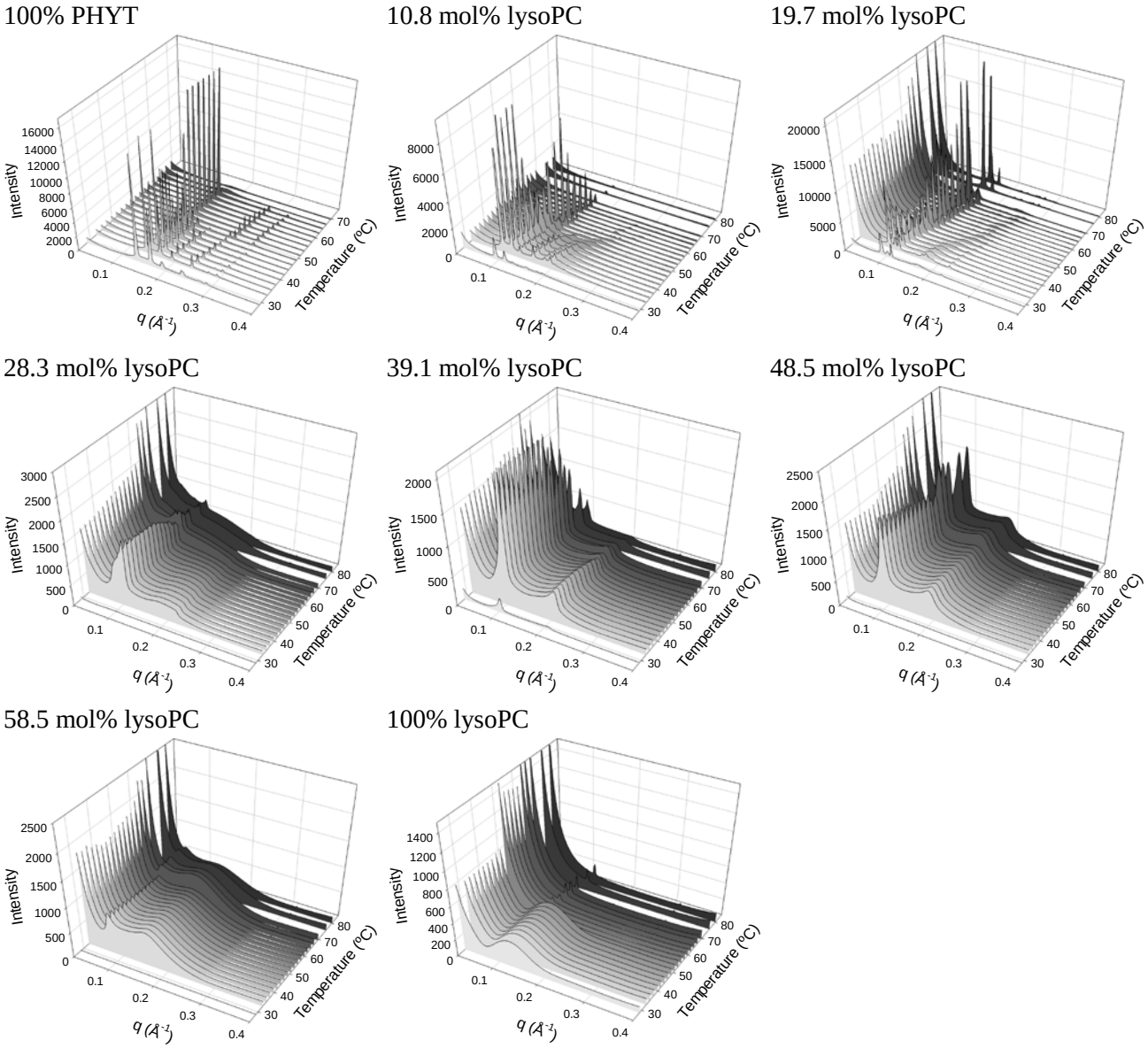

Figure A3 – Equilibrium SAXS scattering patterns displaying the effect of increasing amounts of LysoPC added to the PHYT cubic phase as determined by SAXS. All matrices contained 50% water (w/w).

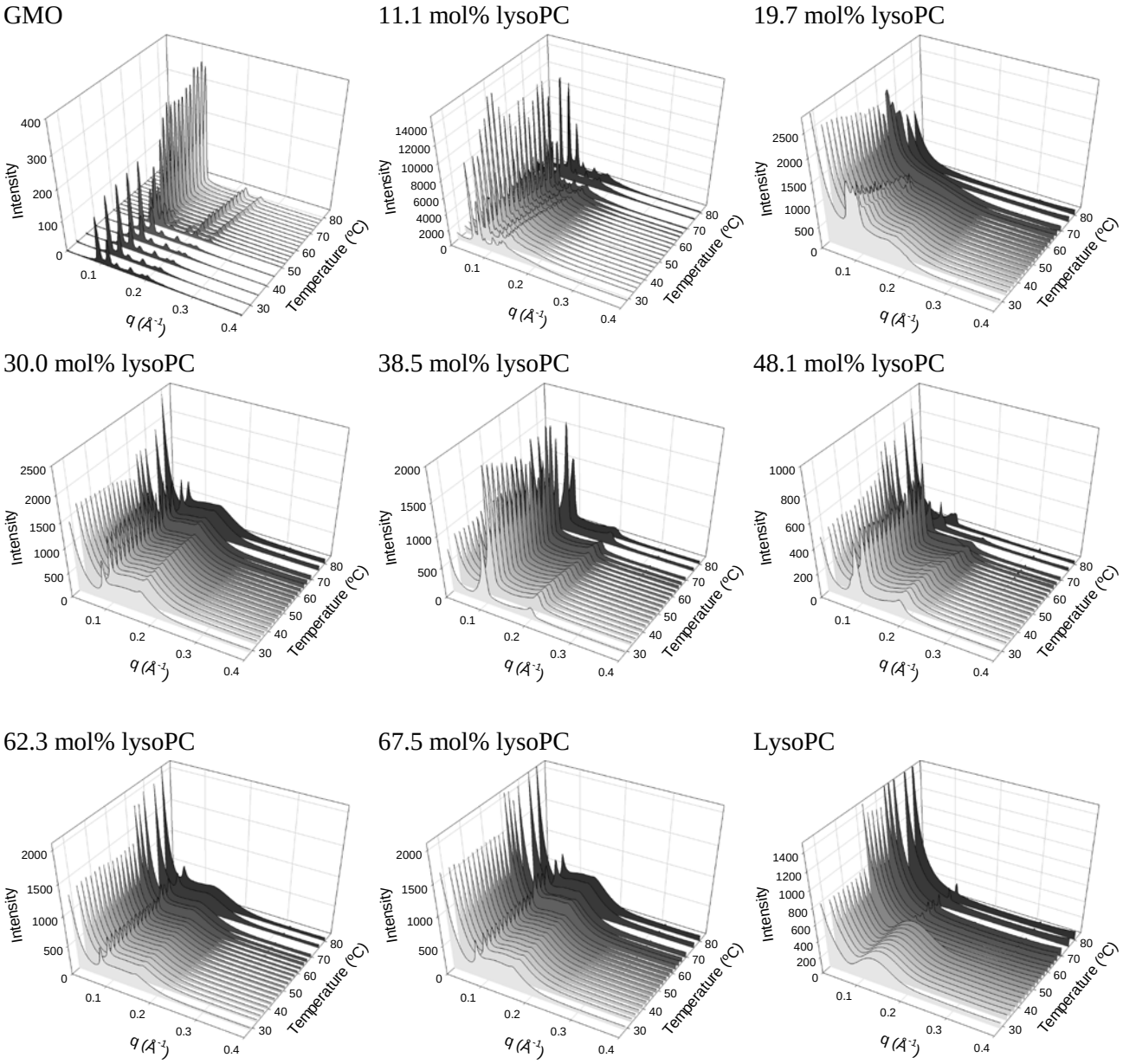

Figure A4 – Equilibrium SAXS scattering patterns displaying the effect of increasing amounts of LysoPC on GMO as determined by SAXS. All matrices contained 50% water (w/w).

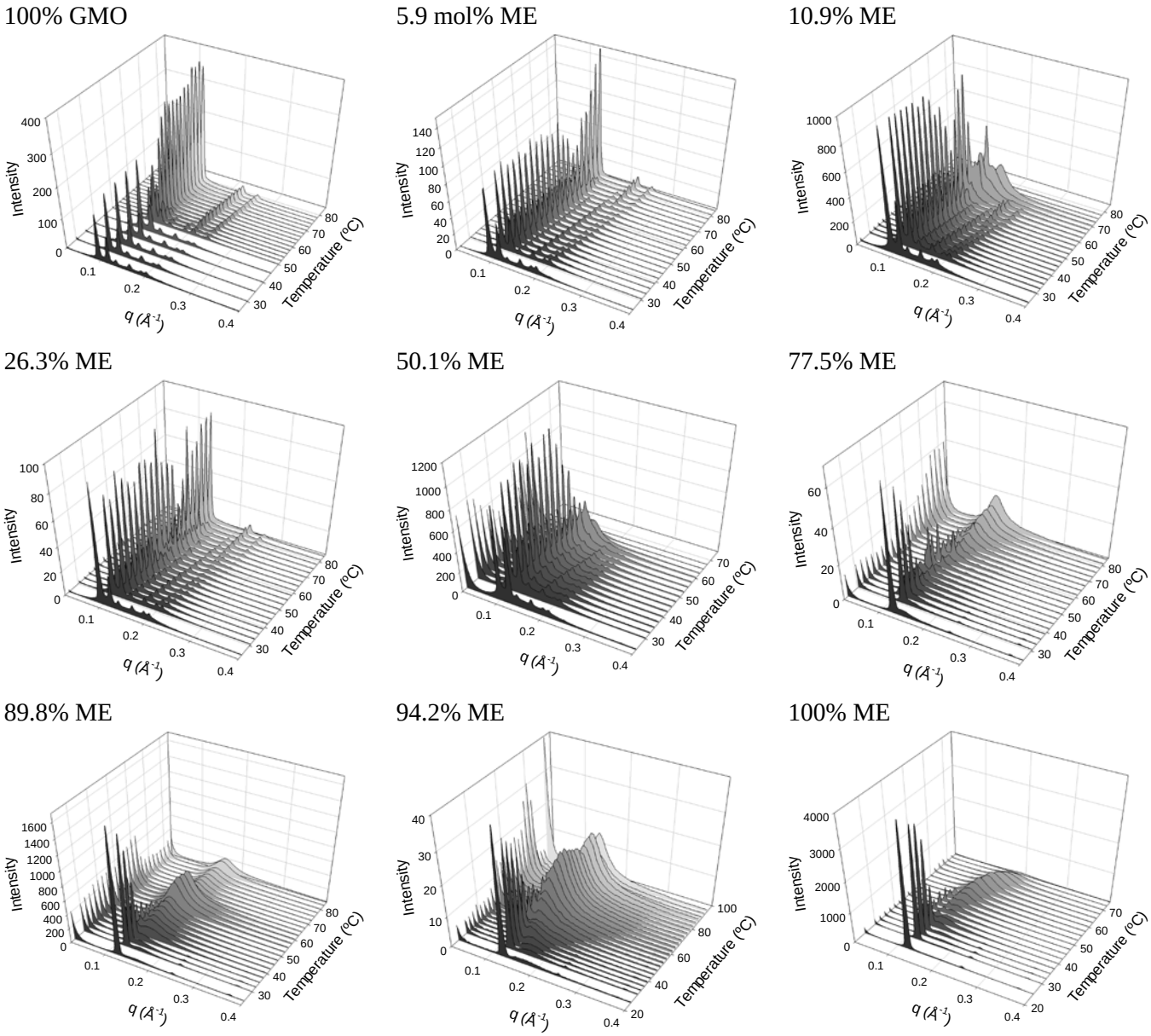

Figure A5 – SAXS scattering patterns showing the equilibrium phase behaviour of fully hydrated GMO matrices containing increasing amounts of ME.

Chapter 7 – Summary, Implications and Future Directions

7. Summary, Implications and Future Directions

7.1. Summary of Findings

Lipid based liquid crystalline materials (LC) provide the ideal matrix for triggerable drug delivery as drug release is controlled by liquid crystalline nanostructure, where changes in nanostructure can be externally manipulated as required in order to activate the 'on-off' drug release switch. This thesis presents approaches to light-responsive lipid-based liquid crystalline matrices by the incorporation of light-responsive additives that change the nanostructure of the matrix upon both near infrared and UV irradiation. The overarching hypotheses governing the studies were:

1. That the internal nanostructure of bulk liquid crystal systems can be rendered light sensitive through inclusion of light sensitive materials into the matrix.
2. That light-activated changes in liquid crystalline nanostructure are reversible and depend on three main factors: the quantity and properties of additive incorporated in to the matrix, the interplay between the light responsive moiety and the liquid crystalline nanostructure, and thirdly, the nature of the irradiation source.
3. That dispersed particles of light responsive liquid crystalline materials exhibit similar photoresponsive behaviour to the bulk, non-dispersed material.
4. That bulk light-responsive liquid crystal systems act as a sustained release drug depot which can be switched on/off through external optical activation *in vitro* and *in vivo*.

On the whole, the hypotheses were well supported by the conclusions reported in this thesis. Some subtle differences between the equilibrium and dynamic phase behaviour was observed, such as supercooling and formation of non-equilibrium structures, but in general, the behaviour of the systems studied agreed with that expected from the equilibrium temperature dependent phase behaviour.

Two different approaches were taken in order to fulfil the first three hypotheses. Firstly, in studies detailed primarily in Chapter 3, a photothermal approach where gold nanorods (GNR) embedded into the LC matrix were activated by near infrared laser irradiation to heat the matrix which then activated the nanostructure 'switch'. The gold nanorods embedded in the liquid crystalline matrix essentially acted as *in situ* nanoheaters. The photothermal manipulation of nanostructure was found to be dependent on the properties of the liquid crystalline matrix, the gold nanorods as well as the properties of the NIR light. All of these factors can potentially be tailored in order to create a system which has the optimal, desired response.

Chapter 4 describes the second approach which involved the incorporation of photochromics into the liquid crystalline nanostructure, where the switch in nanostructure was caused through a steric disturbance within the bilayer upon UV irradiation. A reversible light-induced change in a phytantriol (PHYT)-water nanostructure was most efficient in the system which contained spiropyran laurate (SPL). The alkylation of the spiropyran moiety with a laurate tail anchored the photochromic into the lipid bilayer where it could exert the maximum steric effect.

In order to extend the potential applicability of the UV activated systems to potentially allow *in vivo* application, it was necessary to find a method of indirect UV exposure of the matrix to avoid absorption of UV by healthy tissue. Upconverting nanoparticles, which absorb NIR light and emit light of UV wavelengths, were employed as an *in situ* UV source to activate the

photochromic systems, providing a potential avenue to circumvent penetration and safety issues associated with the use of UV radiation.

The fourth hypothesis was addressed by *in vitro* and *in vivo* studies of photosensitised bulk systems. In both the UV and NIR triggered systems, the release rate of the model drug matched the phase behaviour as identified by SAXS. Chapter 5 describes the external NIR activation of a subcutaneously implanted PHYT-GNR cubic phase, which resulted in the modification of the appearance of the model drug *in vivo*. As the subcutaneous administration of drug delivery systems is unpredictable in terms of surface area and exact location, the use of a plastic implant was required which is not ideal in terms of biocompatibility and long term use. Perhaps the use of a more biodegradable material, for example, starch in order to contain the liquid crystalline implant would be a more favourable approach.

The external UV activation of an SPL-PHYT matrix resulted in the modification of the release behaviour of a model drug *in vitro* as described in Chapter 4. Although this data was limited, the general trend was shown to agree well with previous direct heat and pH activated release behaviour in similar systems. The practical use of UV responsive systems is limited by radiation absorption by healthy tissue and consequently, the lack of penetration of UV radiation. The development of alternative delivery strategies such as intradermal dosing using microneedles or as transdermal patches may provide an alternate avenue for use of UV activated matrices for drug delivery as the location of administration for these systems are more easily accessible. In addition, LC formulations are hypothesised to enhance transdermal drug penetration through interaction with the intracellular lipid packing of the stratum corneum[1]. Thus, a potential avenue for the use of optically responsive liquid crystalline materials may be as drug delivery systems to dermal and subdermal tissues.

Synchrotron SAXS is likely play a definitive role in understanding changes in structure of both the delivery system and skin if liquid crystalline materials are used to deliver drugs across the skin. Although not part of this thesis, the liquid crystalline structure of rat skin was also investigated using SAXS in order to visualise any self-assembled structures within the tissue. The SAXS patterns were not shown, but the scattering patterns revealed a fascinating plethora of structures in the tissue, which has been previously observed in human stratum corneum[2]. As cellular function is related to the organisation of lipids into domains, differences in normal and diseased tissue have been shown using SAXS and offers a promising alternative for the fast diagnosis of diseased soft tissues[3-5] as well as a means to investigate the interaction of materials with dermal tissues on a nanoscale[6].

The major aim of this thesis was to determine methods of rendering non-lamellar systems light responsive. Practical application as pulsatile release systems requires reversible conversion from a closed or slow releasing structure to a fast releasing structure under stimulation. The light activated systems identified and characterised in the earlier part of the thesis contradicts this statement; it transitioned from the fast releasing bicontinuous cubic phase, to the slow releasing inverse hexagonal phase. Consequently, in the final aspects of the thesis, systems with potential for light activation from a slow to fast releasing matrix were investigated. The strategy involved manipulation of packing parameters of lipids in a rational manner to determine appropriate systems to render light active. The effect of the addition of differently shaped lipids into the self-assembled matrix was therefore explored and reported in Chapter 6. Systems that exhibit lamellar to cubic phase transformations were identified through the incorporation of other amphiphilic lipids. A highly biocompatible system comprised of POPE and cholesterol was rendered light active on incorporation of GNR, and underwent the desired reversible phase transitions on irradiation. It is anticipated that more research will follow on from this work to extend this system

into *in vitro* release and *in vivo* proof of concept as a light-activated pulsatile drug delivery systems.

7.2. Future Directions

Stimuli-responsive drug delivery systems have the potential to optimise and streamline pharmaceutical therapies by simplifying treatment regimens and give health professionals, and even the patients themselves, personalised control over their treatments. Light-activated drug delivery systems provide a selective and non-invasive approach to accessing tissues that are not amenable to direct treatment, for instance in the posterior section of the eye or in cancerous tissues. External activation of previously dosed drug delivery matrices may help to avoid complications, infections and poor compliance associated with treatments that require frequent administration by injection, such as treatments for diabetes and macular degeneration, and pain management or hormone treatments. It is recognised that further development is required to translate stimuli responsive delivery systems such as those proposed in this thesis into actual products, however, the identification of photosensitive, biocompatible systems is a necessary first step towards viable on demand drug delivery products.

To progress the current studies towards actual products, the following next stages of work are suggested. The balance between concentration of photoresponsive additive in the matrix and the laser radiation dose could be further optimised. Although low concentrations of gold nanorods and photochromics were used in this study, the duration of NIR and UV irradiation employed to enact a phase change can be considered to be high. The most effective approach may be to change the radiation source from a continuous wave to a higher power, pulsed laser source. In addition, a deeper understanding into the role that self-assembled nanostructure plays in both the release of drug, as well as the processes that occur upon contact with relevant biological components, is

required. As these light responsive systems are proposed for the treatment of macular degeneration, interaction of these systems with the eye tissues will be the crucial next step towards making them viable drug delivery matrices.

The development of novel nanomaterials for drug delivery has been extensive and spans many fields. Limited lipid-based drug delivery systems designed to improve pharmacological and therapeutic properties, have become viable products on the market[7]. These nanomedicines include Doxil® (liposomal doxorubicin), LipoDox® (PEGylated liposomal doxorubicin) and more recently, Marqibo® (vincristine sulfate liposome injection) with many more in clinical trials[8], however, there are no stimuli responsive systems available on the market to date. There is a controlled release formulation available on the market which relies on the diffusion of drug from the inverse hexagonal phase – Elyzol. Although not strictly stimuli responsive, it comprises of an injectable low viscosity lamellar precursor which forms a gel on exposure to biological fluid. The application of nanoparticles and nanostructured systems in drug delivery is promising, but is limited by compliance with regulatory restrictions, which are still under development as this field is so new.

The regulatory approval processes for stimuli responsive drug delivery systems will be even more involved. Their effective use relies on controllable variables and each aspect must be carefully investigated not only for miscibility with other components in the system, but also for biocompatibility and toxicity. The implications of misuse, accidental activation, prolonged activation etc. will need to be evaluated before they can be deployed as approvable medicines. Although many physicochemical variables were considered in this study, there are still many unknown factors which are essential for their translation as viable drug delivery products. The incorporation of drugs and additives of different charges and sizes into self-assembled systems can alter the phase behaviour of the liquid crystalline matrix[9]. For example, the interaction between encapsulated DNA and a cationic liquid crystalline matrix prevented its release due to a strong confinement of the DNA at the water channels/lipid interface and an increase in water channel

diameter[10]. The phase behaviour upon the intentional and/or unintentional release of additives into the matrix must also be determined; in particular, that of amphiphilic components, as they may partition out of the interface, potentially leading to a change in phase behaviour as was observed with the spiropyran component in the photochromic systems.

Although many of the lipids and stimuli responsive elements which are used in the creation of responsive systems designed for *in vivo* use are biocompatible, the combination of many biocompatible elements may result in changes in activity and stability upon storage. For example, sodium polystyrenesulfonate-stabilised gold nanorods are not cytotoxic when freshly prepared, but became cytotoxic after three months of storage[11]. As the use of liquid crystalline materials as novel drug delivery systems is still at an early stage, research into their compatibility with biological tissue as well as into the determination of phase behaviour *in vivo* are currently being investigated.

There has been study into understanding the interaction of dispersed non-lamellar phases with biological membranes[12]. However, when associated with plasma components, cubosomes have been found to be unstable[13]. This has led to the development of novel stabilisers[14], however, as mentioned in Chapter 6, an alternate strategy may be to dose the nanomedicines, that is drug and delivery system, as a dispersed lamellar phase (L_α) and induce a phase change *in situ* through the application of an external stimulus. In so doing, stability issues associated with cubosomes will be avoided, but the benefits of nanostructure-controlled release will be maintained. Additionally, the process of dispersing non-lamellar phases is quite energy intensive in comparison to the dispersion of liposomes. The scalable production of liposomes over cubosomes may thus be an easier feat to achieve. Thus, lamellar matrices which have nanostructures that can be switched, on demand, presents an opportunity for developing a better method for the production and administration of nanomedicines for stimuli responsive controlled release.

In conclusion, the merging of technologies in the development of stimuli responsive drug delivery is a rapidly expanding field of research which may yet revolutionise pharmaceutical treatments. The understanding of these materials on a nano-scale is fundamental to their eventual use in practice. Future research into these materials will be of great fascination to observe, and of great excitement to be a part of.

References

1. Otto A, Wiechers JW, Kelly CL, Dederen JC, Hadgraft J, du Plessis J. Effect of Emulsifiers and Their Liquid Crystalline Structures in Emulsions on Dermal and Transdermal Delivery of Hydroquinone, Salicylic Acid and Octadecenedioic Acid. Skin Pharmacology and Physiology. 2010;23(5):273-82.

2. Bouwstra JA, Gooris GS, Vanderspek JA, Bras W. Structural Investigations of Human Stratum-Corneum by Small-Angle X-ray-Scattering. J Invest Dermatol. 1991 Dec;97(6):1005-12. PubMed PMID: WOS:A1991GQ45000008. English.

3. Ziblat R, Leiserowitz L, Addadi L. Crystalline Lipid Domains: Characterization by X-Ray Diffraction and their Relation to Biology. Angewandte Chemie International Edition. 2011;50(16):3620-9.

4. Sidhu S, Falzon G, Hart SA, Fox JG, Lewis RA, Siu KKW. Classification of breast tissue using a laboratory system for small-angle x-ray scattering (SAXS). Physics in Medicine and Biology. 2011;56(21):6779.

5. Theodorakou C, Farquharson MJ. Human soft tissue analysis using x-ray or gamma-ray techniques. Physics in Medicine and Biology. 2008;53(11):R111.

6. Torin Huzil J, Sivaloganathan S, Kohandel M, Foldvari M. Drug delivery through the skin: molecular simulations of barrier lipids to design more effective noninvasive dermal and transdermal delivery systems for small molecules, biologics, and cosmetics. Wiley Interdisciplinary Reviews: Nanomedicine and Nanobiotechnology. 2011;3(5):449-62.

7. Allen TM, Cullis PR. Drug Delivery Systems: Entering the Mainstream. Science. 2004 March 19, 2004;303(5665):1818-22.

8. Wei A, Mehtala JG, Patri AK. Challenges and opportunities in the advancement of nanomedicines. J Controlled Release. 2012 12/10/;164(2):236-46.

9. Amar-Yuli I, Libster D, Aserin A, Garti N. Solubilization of food bioactives within lyotropic liquid crystalline mesophases. Curr Opin Colloid Interface Sci. 2009;14(1):21-32.

10. Amar-Yuli I, Adamcik J, Blau S, Aserin A, Garti N, Mezzenga R. Controlled embedment and release of DNA from lipidic reverse columnar hexagonal mesophases. Soft Matter. 2011;7(18):8162-8.

11. Leonov AP, Zheng J, Clogston JD, Stern ST, Patri AK, Wei A. Detoxification of Gold Nanorods by Treatment with Polystyrenesulfonate. ACS Nano. 2008 2008/12/23;2(12):2481-8.

12. Vandoolaeghe P, Barauskas J, Johnsson M, Tiberg F, Nylander T. Interaction between Lamellar (Vesicles) and Nonlamellar Lipid Liquid-Crystalline Nanoparticles as Studied by Time-Resolved Small-Angle X-ray Diffractionâ€ Langmuir. 2009;25(7):3999-4008.

13. Leesajakul W, Nakano M, Taniguchi A, Handa T. Interaction of cubosomes with plasma components resulting in the destabilization of cubosomes in plasma. Colloids Surf, B. 2004;34(4):253-8.

14. Chong JYT, Mulet X, Waddington LJ, Boyd BJ, Drummond CJ. Steric stabilisation of self-assembled cubic lyotropic liquid crystalline nanoparticles: high throughput evaluation of triblock polyethylene oxide-polypropylene oxide-polyethylene oxide copolymers. Soft Matter. 2011;7(10):4768-77.

...ad infinitum